ABSTRACT

Title of Document:	Efficiency Enhancement for Natural Gas Liquefaction with CO_2 Capture and Sequestration through Cycles Innovation and Process Optimization
	Abdullah Alabdulkarem, Doctor of Philosophy, 2014
Directed By:	Professor, Reinhard Radermacher, Mechanical Engineering

Liquefied natural gas (LNG) plants are energy intensive. As a result, the power plants operating these LNG plants emit high amounts of CO_2. To mitigate global warming that is caused by the increase in atmospheric CO_2, CO_2 capture and sequestration (CCS) using amine absorption is proposed. However, the major challenge of implementing this CCS system is the associated power requirement, increasing power consumption by about 15-25%. Therefore, the main scope of this work is to tackle this challenge by minimizing CCS power consumption as well as that of the entire LNG plant though system integration and rigorous optimization.

The power consumption of the LNG plant was reduced through improving the process of liquefaction itself. In this work, a genetic algorithm (GA) was used to optimize a propane pre-cooled mixed-refrigerant (C3-MR) LNG plant modeled using HYSYS software. An optimization platform coupling Matlab with HYSYS was developed. New refrigerant mixtures were found, with savings in power consumption as high as 13%. LNG plants optimization with variable natural gas feed compositions

was addressed and the solution was proposed through applying robust optimization techniques, resulting in a robust refrigerant which can liquefy a range of natural gas feeds.

The second approach for reducing the power consumption is through process integration and waste heat utilization in the integrated CCS system. Four waste heat sources and six potential uses were uncovered and evaluated using HYSYS software. The developed models were verified against experimental data from the literature with good agreement. Net available power enhancement in one of the proposed CCS configuration is 16% more than the conventional CCS configuration.

To reduce the CO_2 pressurization power into a well for enhanced oil recovery (EOR) applications, five CO_2 pressurization methods were explored. New CO_2 liquefaction cycles were developed and modeled using HYSYS software. One of the developed liquefaction cycles using NH_3 as a refrigerant resulted in 5% less power consumption than the conventional multi-stage compression cycle.

Finally, a new concept of providing the CO_2 regeneration heat is proposed. The proposed concept is using a heat pump to provide the regeneration heat as well as process heat and CO_2 liquefaction heat. Seven configurations of heat pumps integrated with CCS were developed. One of the heat pumps consumes 24% less power than the conventional system or 59% less total equivalent power demand than the conventional system with steam extraction and CO_2 compression.

EFFICIENCY ENHANCEMENT FOR NATURAL GAS LIQUEFACTION WITH CO_2 CAPTURE AND SEQUESTRATION THROUGH CYCLES INNOVATION AND PROCESS OPTIMIZATION

By
Abdullah Alabdulkarem

Dissertation submitted to the Faculty of the Graduate School of the
University of Maryland, College Park, in partial fulfillment
of the requirements for the degree of
Doctor of Philosophy
2014

Advisory Committee:

Professor Reinhard Radermacher, Chair

Associate professor Bao Yang

Professor Michael Ohadi

Associate professor Peter Sunderland, Dean's representative

Associate professor Yunho Hwang

DEDICATION

To my grandfather, who always believed in me and inspired me to pursue the field of energy.

ACKNOWLEDGEMENTS

First and foremost, I would like to thank Allah who created me from nothing and provided me with everything I needed to complete my PhD study. I would also like to express my sincere thanks and gratitude to my parents, my grandfather and my wife for all the support, encouragement, wishes, sacrifice and patience they provided.

I am forever thankful to my adviser, Prof. Radermacher, who gave me a life opportunity to work in his research group, the Center of Environmental Energy Engineering (CEEE). Prof. Radermacher was not only an academic adviser who guided me patiently during my research, but I also learned from him several skills such as proposal writing, research, teaching, interaction between research and industry as well as interacting with sponsors. Prof. Radermacher was very generous in giving me the chance to work in three consortia in his group where I learned both experimental work and simulation. I am also very grateful for his generous financial support.

I am forever thankful to the Associate Director of CEEE, Prof. Hwang, for his generous support and guidance. Prof. Hwang was always there when I needed anything and I am always inspired by his dedication to research and publication. I also would like to thank the committee members, Prof. Ohadi, Prof. Sunderland and Prof. Yang, for their valuable suggestions and reviews which improved my thesis.

I met many people in CEEE from whom I learned something or made a friendship. I would like to thank them all especially Jan Muehlbauer, Dr. Amir

Mortazavi, Dr. Ali Alalili, Dr. Khaled Saleh, Dr. Vikrant Aute, Dr. Xu Xing, Dr. Kyle Gluesencamp. I would like also to thank Mary Baugher for her kindness.

I would like to thank the King Saud University, Riyadh, Saudi Arabia, for giving me the scholarship to pursue my study. I also would like to thank the Petroleum Institute, Abu Dhabi, UAE, for sponsoring part of this project. Last but not least, I would like to thank my son, Abdulmohsen, who made me feel the urge to graduate and who patiently listened to my thesis presentation dry runs when he was four months old.

Table of Contents

List of Tables

List of Figures

Chapter 1: Introduction

1.1 Overview

Liquefied natural gas (LNG) plants are increasing in number due to the growing demand for natural gas. Natural gas (NG) is the cleanest fossil fuel and has higher heating value than other fossil energy resources [2]. The International Energy Agency (IEA) projects that LNG trade will experience substantial growth in the coming years, as shown in Figure 1 [3].

NG is transported in either pipelines or in LNG carriers. LNG is produced from the liquefaction of NG by cooling it from the atmospheric temperature to -160^{o}C. This liquefaction process is energy intensive, and a typical LNG plant consumes about 5.5 to 6 kWh energy per kmol of LNG produced [4]. An LNG plant typically requires about 10% of the heating value contained in the NG to be consumed as fuel for the liquefaction process [5]. Since LNG plants emit high amount of CO_2 at plants' site and mostly located near oil or gas reservoirs, they are suitable for CO_2 capture and sequestration.

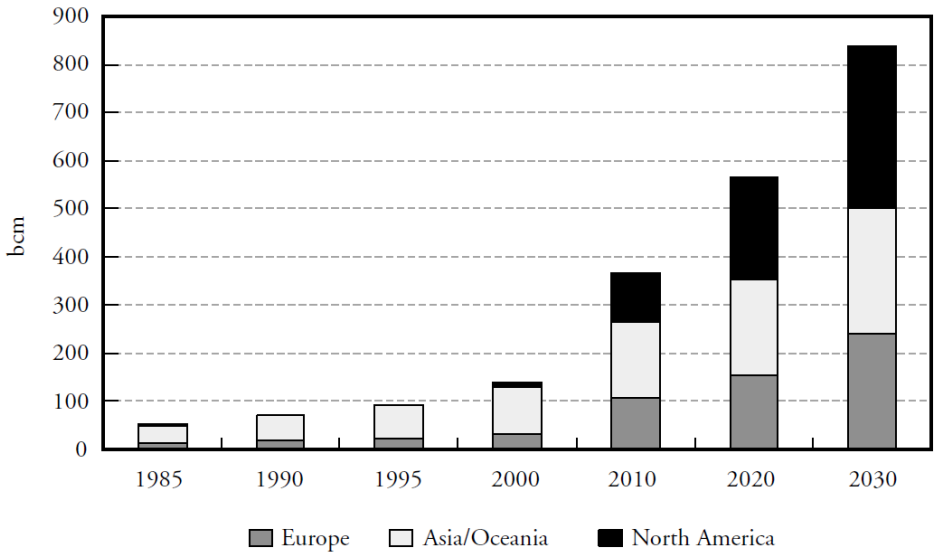

Figure 1: International LNG trade, evolution and outlook [3].

The growth of LNG production is associated with increase in CO_2 emission. CO_2, Methane and Nitrous Oxide are considered greenhouse gases. CO_2 emission from fossil fuel combustion in power generation has the highest global warming effect according to Figure 2. In the Intergovernmental Panel on Climate Change (IPCC) Fourth Assessment Report [6], they concluded: "Most of the observed increase in global average temperatures since the mid-20th century is very likely due to the observed increase in anthropogenic greenhouse-gas concentrations".

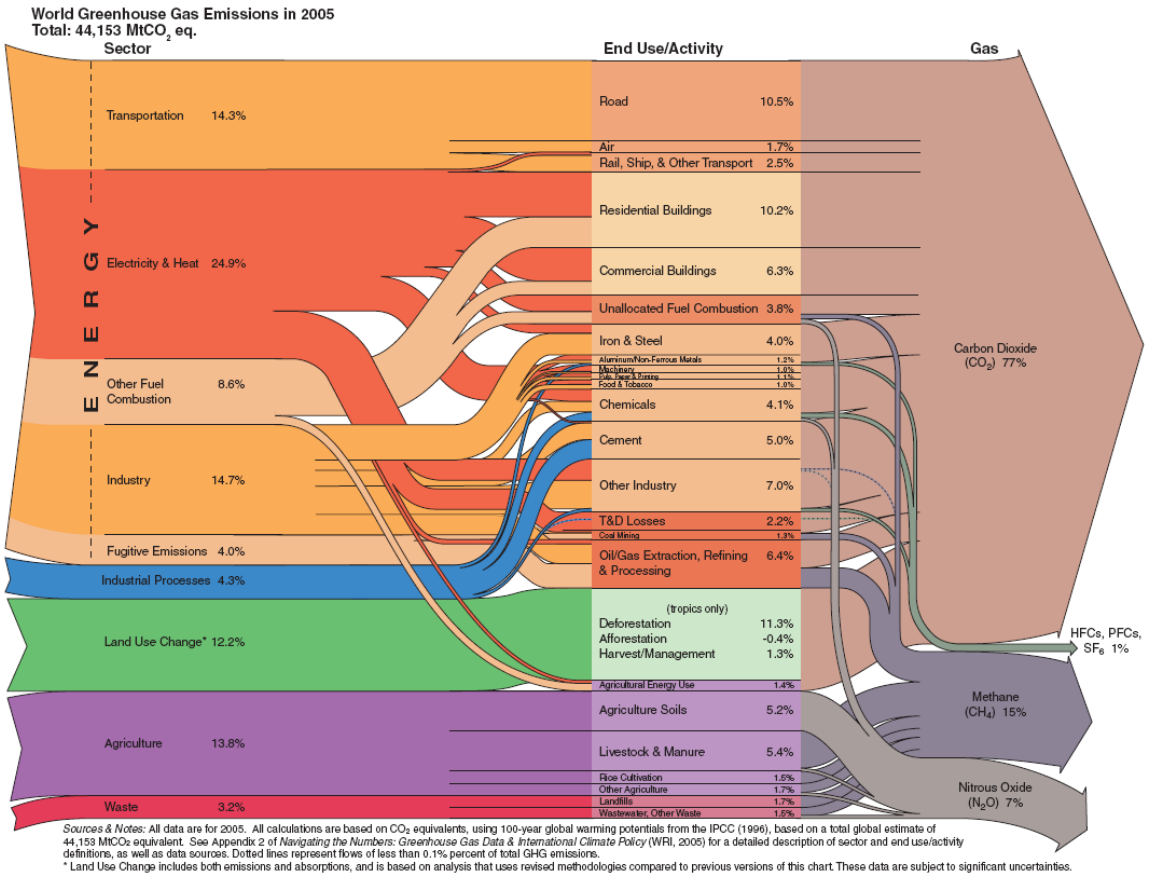

Figure 2: World greenhouse gas emissions in 2005 [7].

The accumulation of anthropogenic greenhouse gases in the atmosphere produce net global warming by strengthening the natural "greenhouse effect"[8]. CO_2 concentration in the atmosphere was at steady level in the preindustrial era (about 280 ppmv). The CO_2 concentration has been increasing with the global average temperature over the years as shown in Figure 3.

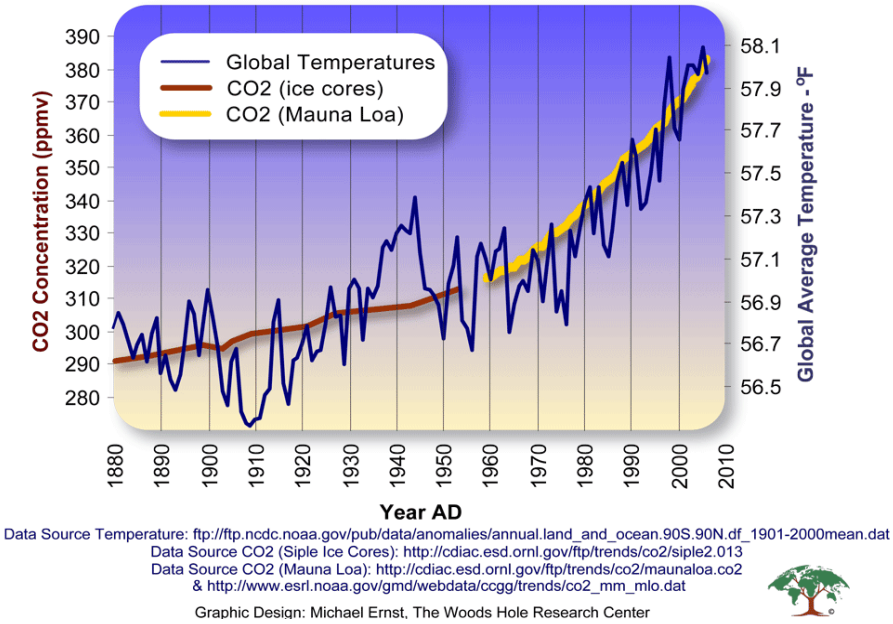

Figure 3: Global temperature and CO_2 concentration since 1880 [9].

1.2 CO_2 Capturing and Sequestration

In order to mitigate the global warming, CO_2 is captured from stationary sources and sequestered in geological formation. Since about one third of all CO_2 emissions from fossil fuel energy sources come from electric power plants, which have the highest density of CO_2 emissions in terms of mass per area per time [10], they provide an appropriate target in the attempt to mitigate the global warming.

White *et al.*'s review [11] concluded that it is practical and feasible to: (1) separate CO_2 from other exhaust gases released by fossil-fuel combustion in stationary sources; (2) capture the CO_2 in gas, solid, or liquid forms; (3) transport the CO_2 with negligible escape to appropriate geological formations; (4) inject the CO_2 into the formations; (5) safely maintain the CO_2 in formations for hundreds of years with negligible leakage back to the atmosphere; and (6) monitor for public safety and leakage.

1.3 Methods

There are three different methods for capturing the CO_2 from a power plant and four storage options (Figure 4). The capturing methods are post-combustion, pre-combustion and oxy-combustion. The storage options are injection in gas or oil well to enhance well recovery (EOR), injection in depleted wells, injection in coal bed and injection in saline formation.

In post-combustion, CO_2 is captured after combustion occurred by using chemical or physical absorption or other methods. Flue gas is at atmospheric pressure and typically has a CO_2 concentration of less than 15%. Therefore, the thermodynamic driving force for CO_2 capture from flue gas is low. Nevertheless, post-combustion CO_2 capture is seen as having the greatest near-term potential for reducing CO_2 emissions since it can be retrofitted to existing power plants that generate two-thirds of the CO_2 emissions in the power sector [12].

In pre-combustion method, the fuel and air is reacted in a steam reformer to produce H_2 and CO_2. Hydrogen, the fuel, is separated from the CO_2 and then the CO_2 is captured. In the oxy-combustion method, the combustion uses pure O_2 instead of air which requires modification to the combustion chambers. The CO_2 is captured after combustion.

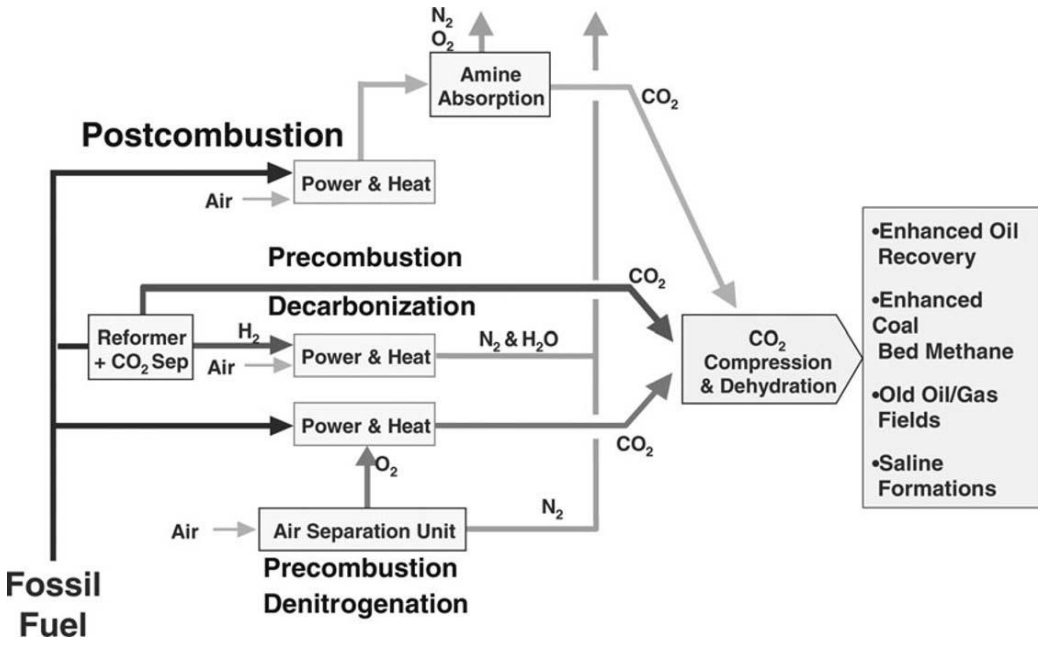

Figure 4: Main CO_2 capturing technologies and storage options [13].

Because post-combustion concepts based on absorption of CO_2 in aqueous amine solutions are considered the most mature and common technologies for CO_2 capture from power plants (9), absorption of CO_2 in aqueous amine solutions was chosen in this thesis. It is the state-of-the-art technology for the capture of CO_2 from fossil fuel power plants [14]. Further, it can be implemented to existing fossil fuel power plants. The proposed sequestration method is injection into oil and gas wells for EOR because it stores the CO_2 permanently and enhances wells production.

1.3.1 CO_2 Removal by Amine Absorption

The CO_2 removal by amine absorption process configuration is shown in Figure 5. Flue gas stream is cooled in a direct contact cooler. Then it is fed to the bottom of an absorption column and is sweetened by the counter-currently flowing

amine solvent. The sweet gas, i.e., with no CO_2, exits the top of the absorber and the CO_2 rich solvent is pumped to the stripper column.

In the stripper, the CO_2 rich amine is regenerated using steam where the CO_2 and some water leave the stripper. This water is cooled and condensed in the overhead condenser. The condensed water is recirculated back to the process and the CO_2 is sent to compressors. The CO_2 is compressed to the required storage pressure. The regenerated amine, lean amine, is sent to lean-rich amine heat exchanger where it heats the rich amine before it goes to the stripper column.

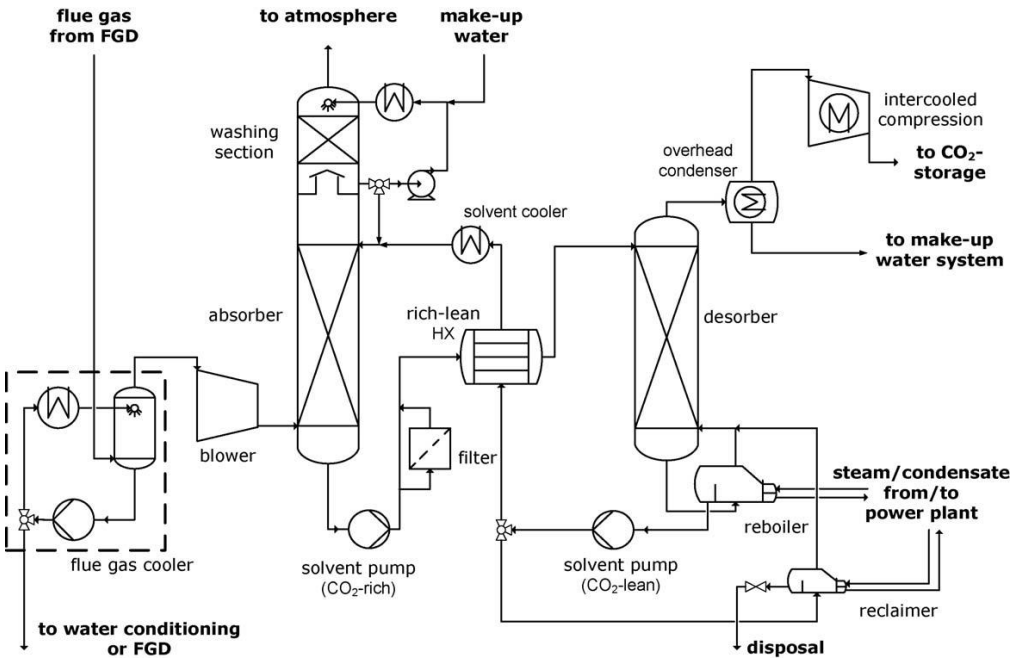

Figure 5: Configuration of CO_2 Removal by Amine Absorption [15].

The absorption of CO_2 by aqueous monoethanolamine (MEA) solutions involves the following six reactions [16].

Kinetically controlled reversible reactions:

$$CO_2 + MEAH + H_2O \leftrightarrow MEACOO^- + H_3O^+ \quad \text{R1}$$

$$CO_2 + OH^- \leftrightarrow HCO^- \quad \text{R2}$$

Instantaneous reversible reactions:

$$HCO_3^- + H_2O \leftrightarrow CO_3^{2-} + H_3O^+ \quad \text{R3}$$

$$MEAH + H_3O^+ \leftrightarrow MEAH_2^+ + H_2O \quad \text{R4}$$

$$MEAH + HCO_3^- \leftrightarrow MEACOO^- + H_2O \quad \text{R5}$$

$$2H_2O \leftrightarrow HO^- + H_3O^+ \quad \text{R6}$$

1.4 Literature Review

CO_2 removal by amine absorption is energy-intensive and has been applied to CO_2 removal from natural gas and flue gas streams. According to one year evaluation on CO_2 removal pilot plant from MEA solvent done by Knudsen *et al*. [17], the average steam requirement for MEA solvent regeneration was approximately 3.7 GJ/ton CO_2 and the MEA consumption due to degradation was 1.4-2.4 kg/ton CO_2. The required amount of steam, which is extracted from a steam turbine, results in a drop in plant efficiency and net power produced. For example, Desideri *et al*. [18] modeled 320.9 MW power plants (44.3% efficiency) without CO_2 removal using ASPEN Plus software. They modeled the net power with the steam extraction for CO_2 regeneration to be 267.2 MW for the natural gas power plant (36.9% efficiency) and 237.3 MW for the coal power plant (32.7% efficiency). They also simulated the liquefaction cycle (Hampson–Linde cycle) power consumption to be 17.3 MW for the natural gas power plant and 28.4 MW for the coal power plant. According to another

study on a coal power plant, energy efficiency was reduced by up to 16%-points due to steam extraction, excluding the compression of CO_2 which accounts for an additional drop of 3–4%-points [19].

Wide topics of research related to CO_2 removal from power plants are being pursued in the literature. Rao *et al*. [20] sent a questionnaire and interviewed a dozen leading experts working in the area of amine-based CO_2 capture for fossil fuel power plants so that they identify the research priorities in possible improvements in some of the key underlying parameters that govern the performance and cost of the amine absorption technology. The experts agreed on the following four items as the top R&D priority issues:

- To develop sorbents with lower regeneration energy requirements.
- To develop less expensive technologies for CO_2 storage/disposal.
- To improve heat integration within the power plants (to reduce the energy penalty due to steam extraction for sorbent regeneration).
- To develop more efficient power plants.

In order to develop and evaluate solvents that have less energy penalty than MEA solvent, many papers in the open literature pursued experimental and modeling work about CO_2 absorption in different solvents. Other papers concentrated on developing new column configurations or better heat integration that can reduce the energy penalty of CO_2 removal by MEA solvent. An overview of different attempts to reduce the energy penalty of CO_2 removal by amine absorption is presented in this review. Further, the developed models and the available experimental or simulation

work in the literature are also briefly mentioned. The main focus is on enhancement of CO_2 absorption in MEA solvent and processes integration. According to Salem [21] and Figueroa *et al.* [12], major research should be directed to evaluate the potential savings in deeper integration of the capture plant with the rest of the power plant. The efficiency penalty for CO_2 capture for coal power plant with flue gas scrubbing using amine solvents can be reduced to about 20% (from 28%) with improved thermodynamic integration and lower-energy solvents [22]. Since one way to reduce the power demand is to reduce the power consumption of the LNG plant itself which can be reduced by process optimization and waste heat utilization within the LNG plant. Part of the literature review also covers LNG plant enhancement and optimization.

1.4.1 Experimental Work

Many papers in the open literature presented experimental work about CO_2 absorption in amine. For example, Dugas [23] investigated CO_2 absorption in MEA solvent in a pilot plant. He also developed an ASPEN Plus model for CO_2 absorption in MEA solvent. Dugas *et al.* [24] experimentally compared CO_2 absorption in Piperazine (PZ) solvent against MEA solvent. They found that 8 m PZ has about a 75% greater CO_2 capacity than 7 m MEA and CO_2 absorption and desorption is 2–3 times faster with PZ than with MEA at equivalent CO_2 partial pressure.

Idem *et al*. [25] compared mixed MEA/methyldiethanolamine (MDEA) solvent against MEA solvent in a pilot plant. They found that the mixed MEA/MDEA requires less regeneration heat than MEA but the mixed MEA/MDEA has higher degradation rate than the MEA. Choi *et al*. [26] experimentally compared mixed

MEA/ 2-amino-2-methyl-1-propanol (AMP) solvent against MEA solvent and AMP solvent. They discovered that the mixed MEA/AMP solvent has a higher CO_2 loading than MEA and a higher reaction rate than AMP.

Mangalapally *et al*. [27] conducted experimental study on MEA and on new solvents they developed: CASTOR1 and CASTOR2. According to their experiments, the new solvents could have less regeneration energy than MEA in higher absorber column height. Ogawa *et al*. [28] developed a new solvent and tested it in a pilot plant. They claim that their solvent has only 60% CO_2 regeneration energy of the MEA solvent.

Experiments were done to compare NH_3 and MEA for capturing CO_2 by several authors ([29], [30] and [31]). They found that regeneration energy for NH_3 solvent is less than that for the regeneration of MEA solvent. They also found that NH_3 has higher removal efficiency than MEA at their testing conditions. However, the absorption temperature in NH_3 is less than MEA solvent. Darde *et al*. [32] calculated the regeneration energy requirements using NH_3 to be 2 MJ/kg of CO_2. Choi *et al*. [33] experimentally compared mixed AMP/NH_3 solvent against MEA solvent and AMP solvent. They found the addition of NH_3 into aqueous AMP solution increased the absorption rate and loading ratio of CO_2. Gabrielsen *et al*. [34] carried out experimental study on CO_2 absorption in AMP solvent.

Cullinane *et al*. [35] showed that PZ is an effective promoter in potassium carbonate (K_2CO_3). Chen [36] carried out experimental evaluation of CO_2 absorption in K_2CO_3/PZ. Bryngelsson *et al*. [37] presented pilot plant data for CO_2 removal

using K_2CO_3/PZ solvent from a CHP plant. They were able to capture 98% of the emitted CO_2 with 3.25-3.7 MJ/kg of CO_2.

Lee *et al*. [38] presented pilot plant data for CO_2 removal using different amine from an LNG plant. They compared different amines and found that MEA has the highest CO_2 recovery. Feron [39] compared the potential energy savings using enhanced chemical sorbents.

1.4.2 Developed Models

CO_2 absorption in MEA solvent models were also developed and validated against experimental data by several authors (Zhang *et al*. [40], Mores *et al*. [41], Pintola *et al*. [42] and Tobiesen *et al*. [43]). Kucka[16] also developed a thermodynamic model of CO_2 absorption in MEA. Dynamic models for CO_2 absorption in MEA solvent were also developed by several authors (Kvamsdal *et al*. [44], Ziaii *et al*. [45], Lawal *et al*. [46], and Gáspár *et al*. [47])

Dey *et al*. [48] developed a correlation for CO_2 mass transfer coefficient in an MEA-AMP blend. Aboudheir *et al*. [49] developed CO_2 absorption in aqueous AMP solutions and validated it against experimental data. Suenson *et al*. [50] developed a dynamic model for CO_2 absorption and stripping in diethanolamine solvent. Mathias *et al*. [51] developed a model for CO_2 absorption and stripping in NH_3.

Cullinane *et al*. [52] developed a thermodynamic model for predicting CO_2 absorption in K_2CO_3/PZ. Oyenekan *et al*. [53] developed a CO_2 stripper model from K_2CO_3/PZ solution. Sanyal *et al*. [54] developed a CO_2 absorption model in K_2CO_3/PZ solution. Thiele *et al*. [55] developed a thermodynamic model for CO_2

absorption and stripping in K_2CO_3 solvent and they validated it with experiments. They also optimized the process parameters (e.g., mass flow rates, temperatures) using ChemCAD software. Their objective function was based on annualized costs comprising both investment and operating costs.

1.4.3 Simulation Work

Desideri *et al*. [18] used ASPEN Plus software to model a CO_2 removal plant using MEA solvent. They also modeled a steam power cycle and Hampson cycle for CO_2 liquefaction. They investigated the overall performance of the integrated system using either natural gas or coal as fuel. Aboudheir *et al*. [56] used ProMax simulation software to compare HTC solvent against 30% (by weight) MEA solvent in capturing CO_2 from the flue gas of a natural gas fueled combined heat and power plant with 3.5 mol. % CO_2. They also conducted a parametric study on the CO_2 removal efficiency and found that 85% is an optimum CO_2 removal efficiency. They concluded that the HTC solvent performance is superior over MEA.

Bernier *et al*. [57] used GA to optimize CO_2 absorption cycle in MEA solvent modeled in ASPEN Plus. The power cycle is a natural gas combined cycle with partial flue gas recirculation. Their objective functions were the levelized cost of electricity and its life cycle global warming potential. Dugas *et al*. [58] modeled a CO_2 absorber in MEA using ASPEN Plus and validated with experimental data. Khan *et al*. [59] modeled a CO_2 absorber in MEA using ASPEN Plus and validated with experimental data. Aliabad *et al*. [60] used HYSYS and ASPEN Plus software to compare MDEA and diethanolamine (DEA) solvents in removing CO_2 and H_2S from flue gas. Kim *et al*. [61] used ASPEN Plus to model MEA absorption. Abuzahra *et al*.

[62] used ASPEN plus to conduct parametric studies on a CO_2 removal plant. Luo *et al*. [63] compared four software and two in-house simulation codes against 16 experimental datasets. They found that all the simulators are capable of giving reasonable predictions on overall performance. However, the boiler duties, concentration and temperature profiles are less well predicted.

Sanpasertparnich *et al*. [64] used ProMax software to model a CO_2 removal plant using MEA solvent from a coal power plant. They modeled a coal power plant and a CO_2 compression plant using in-house code. They studied part-load performance and full-load performance without any validation. They also conducted a parametric study on the effect of the extracted steam pressure on the power degradation. Another simulation study on the part-load performance was done by Moller *et al*. [65].

Amrollahi *et al*. [66] conducted an exergy analysis on a CO_2 removal plant using MEA solvent from a Natural Gas Combined Cycle (NGCC) power plant. They modeled the CO_2 removal plant using UniSim software and they used GT PRO software for modeling the NGCC power plant the CO_2 compression plant. They found that the exergy efficiency of the CO_2 capture plant is 21.2%, and the total exergy efficiency of CO_2 capture and compression plants is 31.6%. They also found that adding a CO_2 capture and compression unit to a NGCC power plant caused an energy efficiency penalty of 7.1% points.

Erik [67] and Genova *et al*. [68] used HYSYS software to model a NGCC power plant integrated with a CO_2 removal plant using MEA solvent. They

investigated the different CO_2 removal plant parameters' effect on the regeneration heat and removal efficiency. Oexmann *et al*. [15] used ASPEN Plus to compare the performance of MEA and K_2CO_3/PZ solvents at different desorber pressures. Oexmann *et al*. [69] used ASPEN Plus and Ebsilon Professional to model a CO_2 removal plant that uses K_2CO_3/PZ solvent and a coal power plant with CO_2 compression plant. They carried out a sensitivity analysis of lean loading, desorber pressure and CO_2 capture rate for various solvent compositions to reduce the overall energy consumption.

1.4.4 Performance Enhancement of CO_2 Removal Cycle

Many authors in the open literature suggested new CO_2 absorption/stripping cycle configurations that minimize CO_2 regeneration energy. The energy requirement is minimized at the expense of increased capital cost and process complexity [70]. For example, Rahimpour *et al*. [71] developed a model for CO_2 absorption in a split-flow absorber using DEA solvent. In a split-flow absorber, a portion of lean solution from the stripper is cooled and fed into the top of the absorber while the major portion is added at a point some distance below the top without any change in temperature. According to Rahimpour *et al*., this modification improves the purity of the product gas by decreasing the equilibrium vapor pressure of the CO_2 over the portion of solution last contacted by the gas. Chang *et al*. [72] modeled a split flow absorber and an absorber with intercooler configurations using ASPEN Plus software, and then optimized them using the logical search plan optimization method. Absorber intercooler configuration allows a greater solute build-up in the rich solvent, and thereby reducing the total solvent circulation rate.

Oyenekan *et al*. [14] used Aspen Custom Modeler (ACM) to evaluate the performance of three stripper configurations: a simple stripper operating at 160 kPa, a multipressure stripper operating at three pressures (330/230/160 kPa), and a vacuum stripper (30 kPa). In the multipressure stripper, the vapor from a lower-pressure stage in the stripper is compressed and used to regenerate the solution in the stripper. The condenser water latent heat is recovered in the stripper. This leads to lower reboiler duties, and CO_2 is produced at a greater pressure than with the simple stripper. Since some water vapor is compressed with the CO_2, the compression work is greater than that of the simple stripper. They found that the multipressure stripper has the least regeneration heat for MEA solvent.

Oyenekanet *et al*. [70] used ACM to evaluate four new stripper configurations (matrix, internal exchange, flashing feed, and multipressure with split feed) with different solvents and a generic solvent model they developed. The four configurations are shown in Figure 6. Their description can be found in Oyenekan *et al*. [70]. The performance ranking of the alternative configurations is (1) matrix, (2) internal exchange, and (3) multipressure with split feed then flashing feed. Similarly, Fisher *et al*. [73] modeled three stripper configurations (CO_2 vapor recompression heat recovery, and multipressure stripping with and without vapor recompression heat recovery). They found the multipressure stripping with CO_2 heat recovery, shown in Figure 7, to be the least energy consuming configuration. According to Fisher *et al*., the power reduction was reduced from 38.1% to 34.4%, or 17 MW power savings, when using the multipressure stripping with CO_2 heat recovery on a 500 MW coal power plant. Romeo *et al*. [74] optimized CO_2 compression process with heat

recovery in heating the water of the steam cycle. Nagashima *et al.* [75] conducted life cycle analysis and compared heat integration on a power plant with CCS where the stripper heat can be either from a separate boiler or from steam extracted from the steam cycle. Gibbins *et al.* [22] investigated recovering compressor and stripper condenser heats in heating the feedwater to the HRSG as well as using lower regeneration energy solvents.

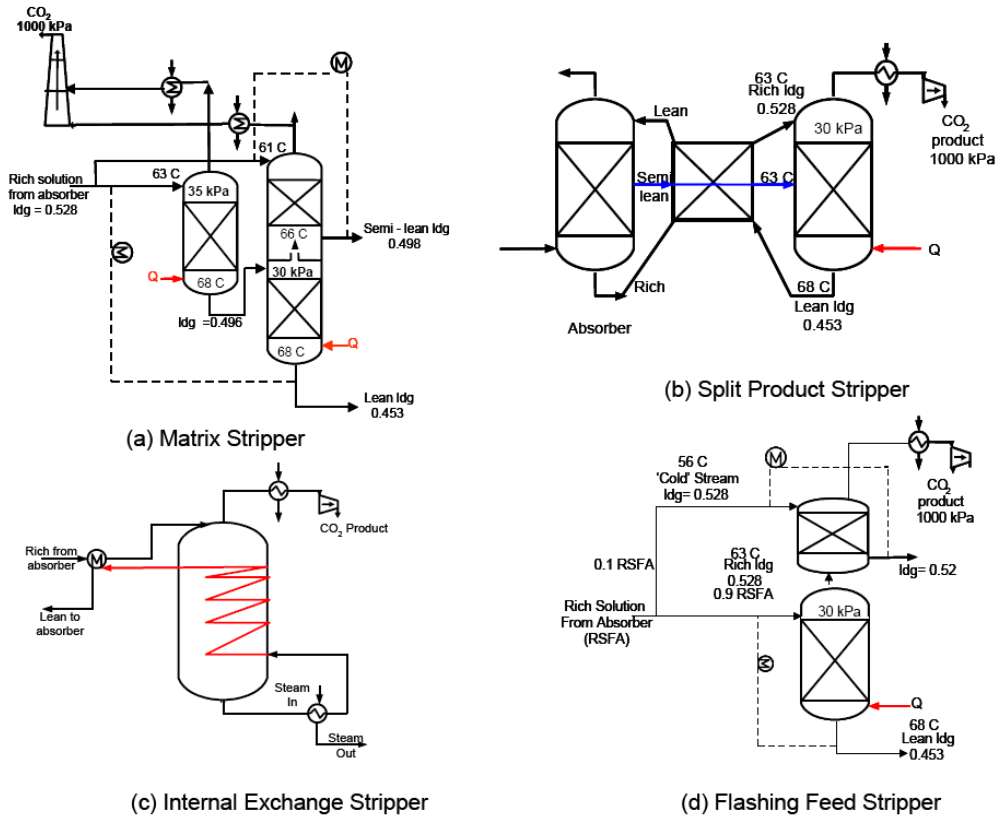

Figure 6: Alternative stripper configurations studied by Oyenekanet *et al*. [70]

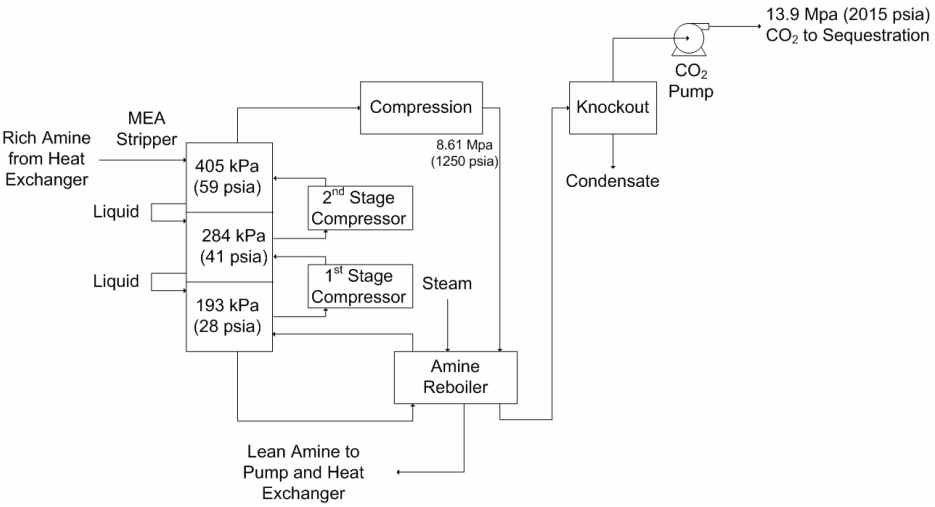

Figure 7: Multipressure stripping with heat recovery studied by Fisher *et al*. [73]

Pellegrini *et al*. [76] used ASPEN Plus to model a CO_2 removal cycle using MEA. They validated their model with Dugas's data. They investigated two CO_2 stripping methods that have energy savings. The first method is a modified version of the double column configuration proposed by Oyenekan *et al*. [14]. The modification was introducing recycled stream from the first absorber column to the desorber. The second method is the original multipressure column, which was suggested by Oyenekan *et al*. [14]. Pellegrini *et al*. compared the performance of these configurations using the boiler duty and the equivalent work, which is based on the Carnot cycle. According to Pellegrini *et al*.'s calculations, the savings in the equivalent work is 25.3% for the modified double column configuration and 13.7% for the multipressure column configuration.

Chinn *et al*. [77] simulated a CO_2 removal cycle using MEA from 392 MW NGCC power plants. They suggested flashing the lean amine and then compressing it using an ejector before the stripper. They claimed that this improvement reduced the

boiler duty which resulted in increasing the plant efficiency from 47.3% to 48.8%. They also suggested recycling 50% of the NGCC exhaust back to the front-end air compressor, which increased the feed CO_2 content (4.0 to 8.5 vol.%) of the gas entering the amine plant. They claimed that this improvement reduced the boiler duty, which resulted in increasing the plant efficiency from 47.3% to 50.6%.

Fluor [78] developed a lean vapor flash configuration, shown in Figure 8, in which the hot lean solvent from the stripper is flashed at low-pressure in a flash drum. The flashed vapor, which is mainly steam and some water and solvent, is compressed and returned to the stripper where it contributes to CO_2 stripping from the rich solvent. With this improvement, the boiler steam requirement is reduced but additional steam compression power is required.

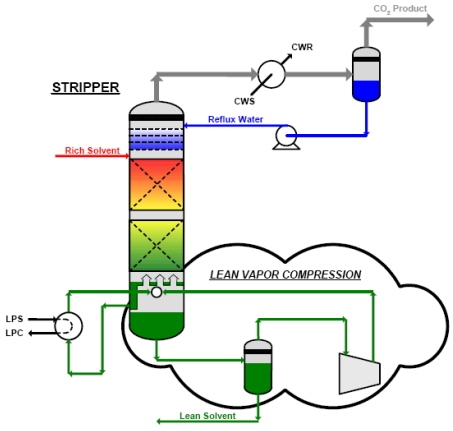

Figure 8: Lean vapor compression configuration [78].

Pfaff *et al*. [79] used ASPEN Plus software to model a CO_2 removal cycle using MEA solvent and EBSILON software to model a coal power plant and a CO_2 compression plant. They investigated using the CO_2 compressor intercoolers heat and the stripper condenser heat in order to heat the condensate steam in the steam cycle,

and/or heat the compressed air before combustion. Their best option, when all heat sources are utilized, resulted in an efficiency gain of approximately 1.02% points. Moser *et al*. [80] optimized a CO_2 removal plant using CHEMASIM software. They found that the optimum plant has the least flue gas temperature. Shooshtari *et al.* [81] proposed and tested an absorber with microchannel contactors. Microchannel technology was used to enhance the mass transfer rate by increasing surface-to-volume ratio and improving the thermal controllability of the absorption process. They also developed a correlation between electric conductivity and the amount of absorbed CO_2.

1.4.5 Processes Integration with CO_2 Removal Cycle

Harkin *et al*. [82]-[83] used pinch analysis, a heat and process integration technique, to determine the potential for reductions in capture cost by minimizing the energy penalty associated with the addition of the CCS. They estimated that the energy penalty from CO_2 removal using amine absorption could be reduced from 39% for a CCS plant with no heat integration to 24% for a plant with effective heat integration. Harkin *et al*. did not design the heat exchangers network that is required for pinch analysis.

Romeo *et al*. [84] compared three options for providing CO_2 regeneration energy using MEA solvent, modeled in ASPEN Plus. The options are natural gas auxiliary boiler, integrating the absorption process into the original power plant, and auxiliary gas turbine. They found that steam extraction from the low-pressure turbine and mixing with condensate re-injection from boiler is the most efficient option. It resulted in about 3.6% point higher efficiency than simple steam extraction.

Aroonwilas *et al*. [85] developed an integrated code for modeling CO_2 removal plant and coal power plant. They studied the effect of the split type absorber configuration and found that it lowered energy penalty by 6.4% point. They also found that using MEA mixed with MDEA solvent reduced the energy penalty ranging from 6 to 12% when compared to MEA solvent only. They carried out a similar study with MEA mixed with AMP solvent [86]. Botero *et al*. [87] suggested integrating the amine boiler to the heat recovery steam generator (HRSG) and partial flue gas recirculation in NGCC power plant. According to their simulation, 1% point increase in the plant efficiency can be achieved using their improvement.

Cifre *et al*. [19] used EBSILON and CHEMASIM software to model a CO_2 removal plant using MEA and a coal power plant, respectively. They also conducted a parametric study on the CO_2 removal plant. They suggested several options for reducing the energy penalty. The first one was liquefying the CO_2 above the critical pressure, which lead to a reduction of 0.2%-points of efficiency loss. The second one used the heat in the compressed CO_2 to heat the water in the steam cycle after the condenser, which resulted in a plant efficiency increase of 0.1%-points. The third one used the extracted steam to heat the condensate water after the boiler, which increased net plant efficiency of 0.3 up to 0.4%-points. Jonshagen *et al*. [88] used IPSEPRO software to model a CO_2 removal plant using MEA and NGCC power plant. They suggested using pressurized hot water instead of steam to regenerate the CO_2 in the stripper. According to Jonshagen *et al*., this allowed the flue gas utilization temperature to be 95.3^{o}C which increased the plant efficiency from 51.99% to 52.12%.

Most of the presented literature used multi-pressure compression with intercooling. Few authors looked at different compression strategies. Aspelund *et al*. [89]-[90] studied CO_2 liquefaction for ship transport. They considered three liquefaction pressures (20, 55 or 95 bars) where CO_2 is liquefied after compression by either seawater or using an open cooling cycle that they patented. Moore *et al*. [91] carried out similar study. According to Moore *et al*.'s preliminary analysis, a 35% reduction in power is possible when liquefying the CO_2 using absorption chillers and pumping the CO_2 instead of compressing it. Botero *et al*. [92] compared different compression strategies for CO_2 compression using HYSYS software. They investigated using absorption chillers and cold seawater for CO_2 liquefaction at three liquefaction pressures.

Proprietary CO_2 liquefaction processes are available in some applications such as in the food and beverage industries. However, such applications of CO_2 liquefaction differ from power plant in terms of quantity and quality of feed gas and product gas. Several liquefaction cycles exist for natural gas liquefaction but they differ significantly from CO_2 liquefaction in terms of liquefaction temperature and cooling curves. While absorption chillers are a mature technology and many manufacturers exist, they have low efficiency and are considered complex and expensive [93].

1.4.6 LNG Process Efficiency Enhancement

Since this thesis focuses on enhancing the energy efficiency of LNG plants with CCS, it is necessary to cover enhancing the energy efficiency of LNG plants itself. Although there are many publications in the literature on the analysis and

enhancement of LNG plants (e.g. [99]-[100]), only a few exist regarding their design optimization. Designing an LNG plant is very complex and involves many variables. Optimization techniques could be employed to assure optimal designs if robust models were developed [101]. An optimal LNG plant is categorized by having low initial cost as well as low energy consumption.

Several papers in the open literature reported optimization studies on LNG plants. Lee *et al.* [95] conducted an optimization study on a Prico cycle [102], the simplest LNG mixed-refrigerant liquefaction cycle, using non-linear programming (NLP). Their approach was to optimize the refrigerant mixture composition of C1-C4 and N_2 at given pressures and mass flow rates. If there is no temperature cross across the heat exchanger, they propose new refrigerant mass flow rate and pressure levels based on heuristics, judgment, or optimization. Lee *et al.* also compared three different forms of objective function: minimization of the crossover, minimization of the sum of the crossovers, and minimization of the compressor power. Aspelund *et al.* [103] modeled Prico cycle using HYSYS and optimized it using a Tabu Search (TS) method combined with the Nelder-Mead Downhill Simplex (NMDS) methods [104]. The reason for combining the global TS with the NMDS local search according to Aspelund *et al.* is that the local search, i.e. NMDS, usually converges to the best solution in the TS-detected area more rapidly than the TS would on its own.

Nogal *et al.* [105] developed a thermodynamic model for a mixed refrigerant cycle and optimized it using GA. Their refrigerant mixture composition was C1-C4 and N_2. Jensen *et al.* [106] modeled and optimized Mixed Fluid Cascade (MFC) process using gPROMS software [107]. Vaidyaraman *et al.* [108] also used NLP to

minimize the power consumption of a cascade MR cycle. Their optimization variables were refrigerant composition (C1, C2, C3 and n-butane), vaporization fraction in flash tanks and compressor pressure ratios. Their modeling formulation, however, only considered temperature cross at the ends of heat exchangers, and so does not guarantee that the Second Law of thermodynamics was not violated by having a temperature cross in the middle of heat exchangers.

Paradowski *et al.* [98] carried out a parametric study on a C3-MR cycle. They varied MCR refrigerant composition, propane cycle pressures, pre-cooling temperature and propane cycle compressor speed. Their aim was to show that the C3-MR cycle could be adapted to even larger plants than those already built, thus maintaining its position as the first choice liquefaction cycle. Venkatarathnam [109] performed an optimization study on a C3-MR cycle using the Sequential Quadratic Programming (SQP) method [101], available in the ASPEN Plus optimization tool. He varied refrigerant composition and compressor pressure ratios to maximize the cycle exergy efficiency.

Xu *et al.* [138] optimized a Prico cycle, the simplest LNG mixed-refrigerant liquefaction cycle, with different ambient temperatures using GA and ASPEN Plus software. Their results show that when ambient temperature increases, the concentrations of methane, ethylene and propane should decrease whereas i-pentane should increase. Shirazi *et al*. [139] optimized SMR cycle using a model developed in Matlab. Wang *et al.* [140] applied mixed-integer nonlinear programming (MINLP) in GAMS software to minimize the C3-MR cycle power consumption

1.4.7 Summary of Literature Review

Referring back to Rao *et al.*'s investigation for top R&D issues in the area of amine-based CO_2 capture for fossil fuel power plants and the presented literature review, it can be seen that many researchers are working on developing solvents that could have less regeneration energy than MEA solvent. Many thermodynamic models were developed and validated against experimental data by several authors. Other researchers have developed innovative absorber/stripper column configurations that have some energy savings according to their models. Optimization and exergy analysis study were carried out by a number of authors to reduce power demand associated with CCS.

Although some authors simulated integrated power cycle with CCS, there is a lack of literature in this area (one of the top R&D issues according to Rao *et al.*'s investigation). There has been no research done on integrating an LNG plant with power cycle and CCS, with comprehensive waste heat evaluation, along with uses that will result in power savings with any solvents used to capture the CO_2. In addition, no author has carried out a comprehensive study on whether liquefying and pumping CO_2 for injection consumes less power than multistage CO_2 compression, and then designed several CO_2 liquefaction cycles (cascade and single-refrigerant). Further, there has been no research done on optimizing the CO_2 liquefaction pressure, and none of the authors have suggested a way to enhance the CO_2 removal efficiency independently from the CO_2 removal plant. Moreover, no one has suggested using regeneration sources other than using steam extracted or compressed CO_2 to regenerate the CO_2. In addition, no author applied global optimization on C3-MR

cycle and investigated the effect of cryogenic heat exchanger performance. Last but not least, no author considered the effect of uncertainty in feed gas compositions on the performance of C3-MR cycle and developed a refrigerant which can handle a range of natural gas feeds.

1.5 Research objectives

The overall objective of the thesis is to develop an optimum CCS for LNG plants by (1) enhancing the natural gas liquefaction process, (2) reducing the energy consumption associated with CCS and enhancing the CO_2 removal efficiency, (3) developing new CO_2 pressurization concepts, and (4) developing new concepts of regeneration heat. Therefore, this thesis has four research thrusts, as shown in Figure 9.

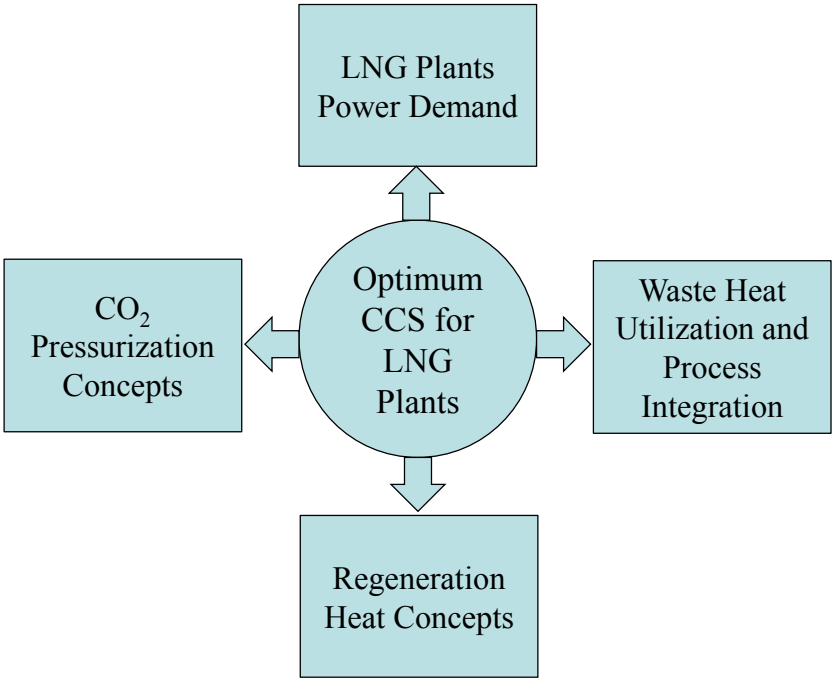

Figure 9: Research thrusts of the thesis.

In order to meet the objective of the thesis, the following approach was proposed:

1. *Enhancing the natural gas liquefaction process*

   1.1. Reduce the power demand of natural gas liquefaction process

   - Optimize refrigerant mixture compositions and their operating variables against different type of heat exchangers
   - Optimize the propane cycle operating variables
   - Develop a platform capable of handling complex process optimization

   1.2. Develop a robust refrigerant for natural gas liquefaction

   - Identify the challenge in natural gas liquefaction with uncertainty in natural gas field
   - Optimize refrigerant mixture compositions with uncertainty in natural gas field

2. *Reducing the energy consumption associated with CCS and enhancing the CO_2 removal efficiency*

   2.1. Establish new CCS configurations that integrate the APCI LNG plant with the power cycle, CO_2 removal cycle and CO_2 compression cycle

   - Reduce the power demand thorough process integration and waste heat utilization
   - Develop an approach for enhancing the CO_2 removal efficiency using MEA solution

   2.2. Compare the proposed integrated CCS configuration with the conventional CCS configuration

- Design and model CO_2 removal cycle, steam cycles, and CO_2 compression cycle using HYSYS software
- Validate the developed models with the available data from the literature

2.3. Comprehensive evaluation of waste heat sources and propose uses for them in the integrated CCS system

- Evaluate the proposed three power cycles concept (combined cycle and ORC power cycle)
- Identify waste heat sources in the integrated CCS system
- Use Pinch Analysis to compare the proposed and the conventional CCS systems

3. Developing new CO_2 pressurization concepts

3.1. Design and model CO_2 liquefaction cycles using HYSYS software

- Investigate several CO_2 liquefaction cycles
- Optimize CO_2 liquefaction pressure
- Compare CO_2 liquefaction and pumping against conventional CO_2 compression
- Evaluate the performance of the open CO_2 liquefaction cycle
- Validate the developed models with the available data from the literature

4. Developing new concepts of providing regeneration heat

4.1. Develop a new concept for providing the CO_2 regeneration heat that will result in less power demand than the available options

- Develop several heat pumps that provide the CO_2 regeneration heat
- Investigate working fluids for the developed heat pumps

- Develop heat pumps that provide the CO_2 regeneration heat as well as CO_2 liquefaction heat
- Compare the developed heat pumps against the conventional CCS system

Chapter 2: Optimization of Propane Pre-cooled Mixed Refrigerant LNG Plant

2.1 Introduction

Different natural gas (NG) liquefaction cycles exist that use either pure refrigerant in cascade cycles, multi-pressure cycles, or mixed refrigerant cycles. Pure refrigerant cycles have a constant evaporating temperature that is a function of the saturation pressure (Figure 10, left). Mixed refrigerant cycles, on the other hand, do not maintain a constant evaporating temperature at a given pressure. Their evaporating temperature range, called temperature glide, is a function of their pressure and composition (Figure 10, right). Refrigerant composition, e.g., a mixture of hydrocarbons and nitrogen, is chosen so that it has an evaporation curve that matches the cooling curve of the NG with the minimum temperature difference. Small temperature difference reduces entropy generation and, thus, improves thermodynamic efficiency and reduces power consumption [94].

Due to the high complexity of MCR cycles design, their refrigerant compositions selection has been done by trial-and-error and guided only by heuristics [95]. Patents were registered for compositions of refrigerant mixtures for certain cooling processes[96], [97].

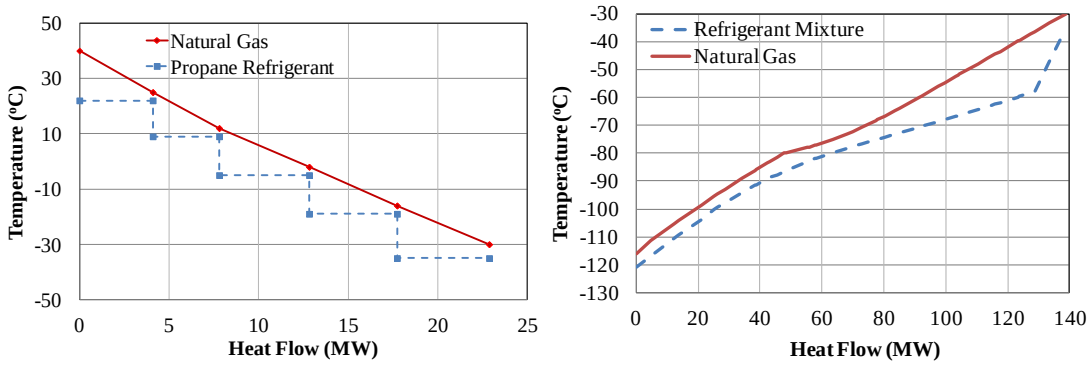

Figure 10: Temperature profile in single refrigerant heat exchangers (left) and in a mixed refrigerant heat exchanger with 3 K pinch temperature (right).

Among all available cycles, APCI LNG cycle, developed by Air Products and Chemicals Inc., is the most predominant cycle in the LNG industry [98]. It has a multi-pressure propane cycle and a mixed-refrigerants cycle that uses a mixture of C1-C3 and N_2 as a refrigerant.

In this chapter, a HYSYS model was developed for the APCI LNG plant that was modeled by Mortazavi *et al*. [1]. The APCI LNG plant HYSYS model was verified with the Mortazavi *et al.*'s ASPEN Plus model, with discrepancies of less than 3.2%. Both software products, HYSYS and ASPEN Plus [110], are well known in the process simulation field. They include varieties of built-in equation of states and components such as heat exchanger models and compressor models. Matlab software [111] is well known in its optimization capabilities.

The use of HYSYS as the thermodynamic model and Matlab as the optimizer (using its GA method) is explored in this thesis, in order to optimize the verified APCI LNG plant model. The optimization is very comprehensive and includes finding the optimum refrigerant mixture composition, mass flow rates, working

pressures, and temperatures that will have the minimum power consumption with the same LNG and LPG production.

Furthermore, the effect of different pinch temperatures of cryogenic heat exchangers on the power consumption was investigated. Different pinch temperatures are equivalent to different heat exchangers that vary in their cost and performance. In addition, two HYSYS-APCI models that use Venkatarathnam and Paradowski's optimized refrigerant mixture were also developed and compared with the obtained refrigerant mixtures. The effect of changes in the natural gas feeds on the performance of the APCI LNG plant is identified and solved in this thesis.

2.2 Gas Turbine Model

APCI LNG Plant compressors driver was modeled by Mortazavi *et al.* using ASPEN Plus software. The compressors are driven by a gas turbine that has a rated a rated capacity of 130 MW. Their ASPEN Plus model is shown in Figure 11. They modeled compressor and the turbine using the compressor and turbine blocks of ASPEN software. They modeled the combustion chamber using RGIBBS block, which minimizes the Gibbs free energy of outlet streams to the combustion chamber. They also verified their model results against vendor's data as shown in Table 1. The maximum discrepancy of the modeling results from the data is about 1.16%.

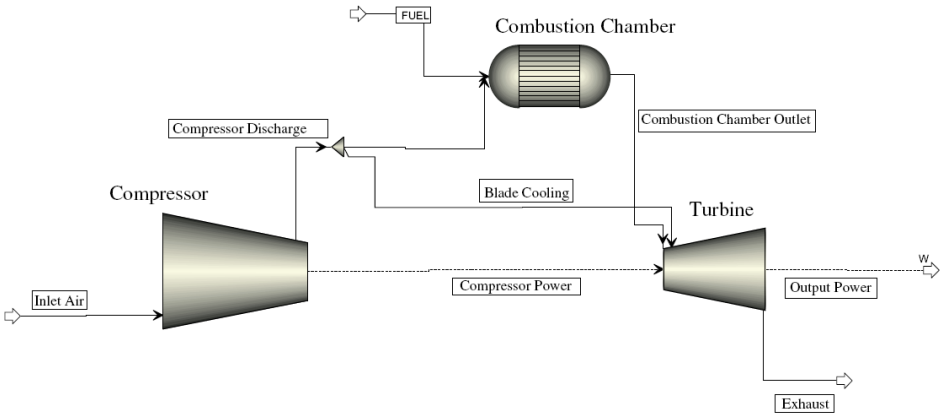

Figure 11: Gas turbine cycle modeled with ASPEN [1].

Table 1: Comparison of gas turbine simulation results with vender's data at ISO condition [1]

Parameter	ISO Rated Power (MW)	Efficiency (%)	Exhaust Temperature (^{o}C)
Actual Gas Turbine	130.1	34.6	540
ASPEN Model	130.103	35	540.4
Discrepancy	0.003	0.4	0.4

2.3 Baseline LNG Plant

2.3.1 APCI Natural Gas Liquefaction Process

The dominant LNG liquefaction cycle is the APCI LNG cycle [112]. As shown in Figure 12, the feed gas is processed through the gas sweetening plant for the removal of sulfur, carbon dioxide and mercury. As it passes through the pre-cooler and cold box, its temperature decreases to approximately -30^{o}C and some components are condensed at the same time. In the separator, the remaining gas and condensate are separated. The condensate is then sent to the fractionation unit, where it is separated into propane, butane, pentane, and heavier hydrocarbons. The remaining gas is further cooled in the cryogenic column to below -160^{o}C and is liquefied. Its pressure is then reduced to atmospheric pressure by passing through the LNG expansion valve. There are two refrigeration cycles utilized in this whole process: the

propane cycle and the MCR cycle. The first cycle provides the required cooling to the pre-cooler, cold box and fractionation unit. The second cycle supplies the cooling needed in the cryogenic column.

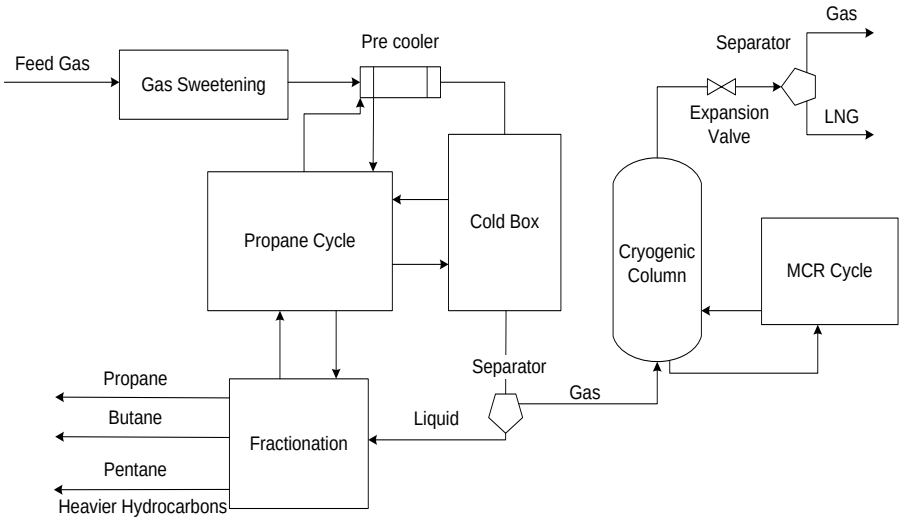

Figure 12: Schematic diagram of APCI LNG production process [1].

2.3.2 Model Development

Mortazavi *et al.* [1] designed their APCI LNG plant model based on some industrial data and modeling assumptions. They used ASPEN Plus software, which is steady-state process modeling software [110]. ASPEN Plus has an optimization tool. However, it does not have GA methods available and we were not able to connect it with Matlab, which has GA as well as different optimization methods. HYSYS, a steady state and transient process modeling software [110], does not have a GA either but I was able to connect it with Matlab and utilize its optimization capabilities. Therefore, a model was developed using HYSYS for the APCI LNG plant with the same inputs and assumptions as the model in ASPEN Plus which was developed by Mortazavi *et al.* [1]. A detailed modeling parameter can be found in the Mortazavi *et*

al. [1]. In summary, the Peng-Robinson equation of state was selected for modeling the property of substances. All HYSYS model convergence tolerances for the relative residuals were set to be $1x10^{-4}$. Gas sweetening units were not modeled for simplification purposes and the feed gas was assumed to be after the sweetening units with composition shown in Table 2. Centrifugal and axial type compressors were used for the propane and MCR cycles, respectively.

The two sections of SWHX were modeled using segmented UA method so that the cooling curve inside the SWHX is calculated more accurately. The first section of the SPWH has 53 segments and the second section has 38 segments. All condensers and inter-coolers were assumed to have been cooled by seawater. It was assumed that the propane cycle would have five stages of cooling. The MCR cycle has a two-stage compressor with an intercooler. The main assumptions are summarized in Table 3.

Table 2: Gas composition after gas sweetening [1]

Component	Mole Fraction (%)
Nitrogen	0.100
Carbon Dioxide	0.005
Methane	85.995
Ethane	7.500
Propane	3.500
i-Butane	1.000
n- Butane	1.000
i-Pentane	0.300
n-Pentane	0.200
Hexane Plus	0.400
Total	100

Table 3: Modeling assumptions for APCI base cycle [1]

Axial compressor isentropic efficiency	0.86
Centrifugal compressor isentropic efficiency	0.83
Pinch temperature	3 K
Sea water temperature	35°C
Refrigerant temperature at condenser or super heater exit	40°C
LNG temperature at the exit of cryogenic column	-160°C
Degree of superheating in propane cycle	10 K
LNG expander exit pressure	101.3 kPa

Simulation results from models in HYSYS and ASPEN Plus are tabulated in Table 4. It can be seen that there is a perfect agreement between the two software models. Furthermore, the components level, e.g. state points in compressors, was also compared, but not presented here, with discrepancy of less than 0.12%. The reason for the discrepancies is that the binary coefficients of the equation of state in HYSYS and ASPEN Plus are slightly different between the two software. The schematic of the APCI LNG plant HYSYS model is shown in Figure 13. There is a break point in the process flow sheet, which is required for HYSYS and ASPEN Plus model convergence. However, inside the Matlab code the two sides at the break point are set to be identical to each other.

Table 4: Simulation results of APCI base cycle model in ASPEN Plus and HYSYS

	Model in ASPEN Plus	Model in HYSYS	Discrepancy (%)
Propane compressor power (MW)	43.651	43.698	-0.1
Mixed refrigerant compressor power (MW)	66.534	66.48	0.08
Propane cycle cooling capacity (MW)	115.469	115.733	-0.22
Mixed refrigerant cycle cooling capacity (MW)	67.635	67.508	0.18
Propane cycle COP	2.645	2.648	-0.13
LNG vapor fraction after expansion valve (%)	1.4	1.43	-2.14
LNG production (kg/s)	98.83	98.89	-0.06
LPG (propane, butane, pentane and heavier hydrocarbons) (kg/s)	11	10.97	0.27
Flash gas flow rate after LNG expansion valve (kg/s)	1.28	1.24	3.13

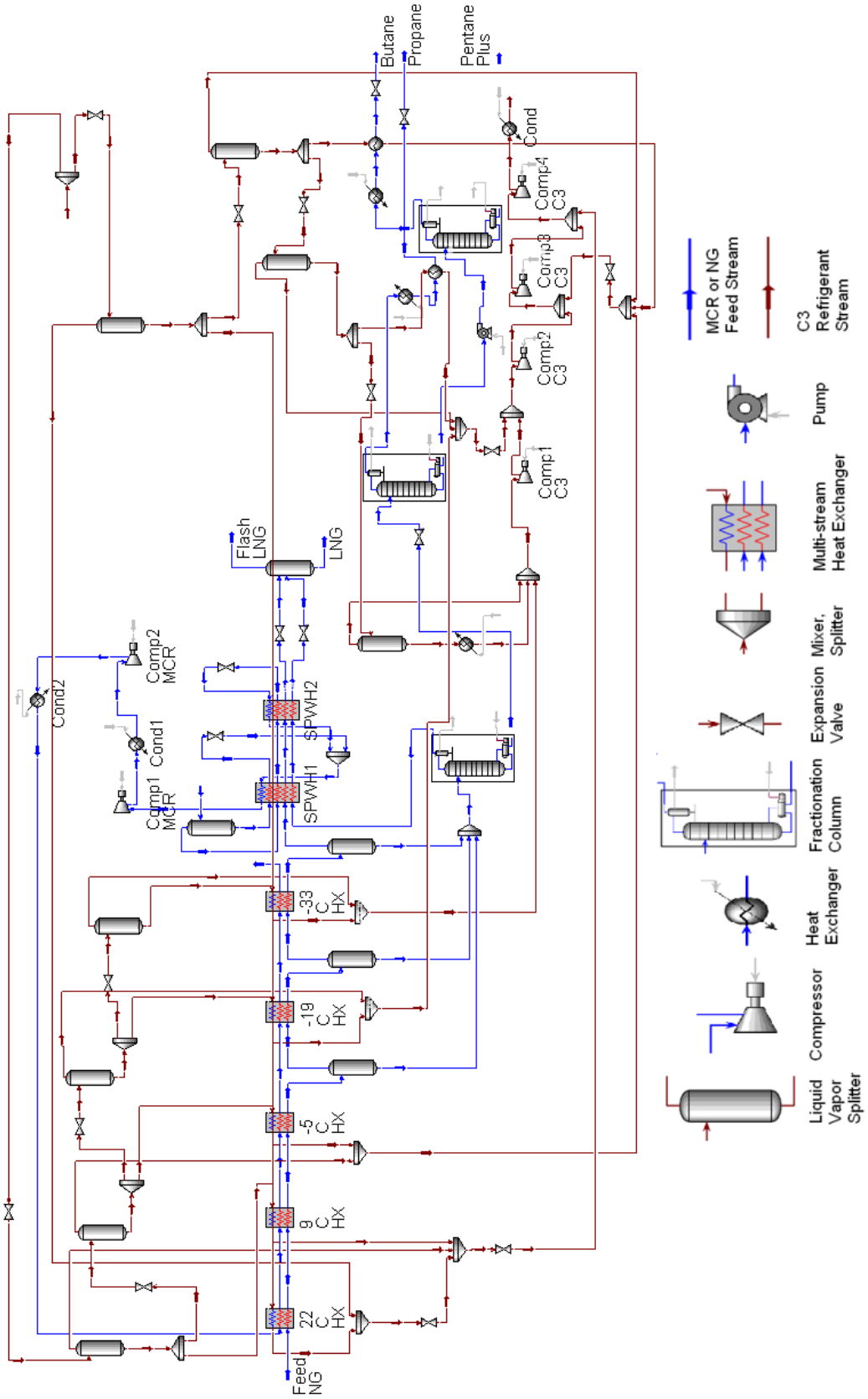

Figure 13: APCI LNG plant HYSYS model.

2.4 Optimization of the APCI LNG Plant

2.4.1 Optimization Approach

Since there are many variables involved in designing the APCI LNG plant, the optimization problem is computationally very expensive. Thus, the optimization was carried out in two stages as shown in Figure 14. First, the MCR cycle was optimized, and then the propane cycle was optimized. The only effect of separating the two cycles is that the propane cycle pre-cools the MCR cycle. This pre-cooling load changes with refrigerant mixture composition, temperature/pressure and mass flow rate. This effect was considered as the optimization constraint.

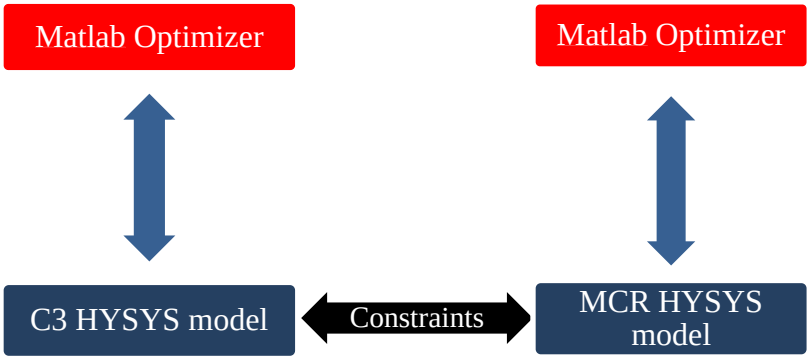

Figure 14: APCI LNG plant optimization approach.

Matlab has a powerful optimization tool [111]. It has different methods such as gradient-based and Genetic Algorithm (GA). GA was used because it works for discrete as well as continuous functions. Additionally, it has the potential of reaching a global optimum, especially in the design of an LNG plant that is a highly nonlinear problem with many local optima. Different methods, e.g. gradient-based or pattern

search [101], from Matlab as well as from the HYSYS and ASPEN optimization tool were used. However, the most optimum results, i.e., minimum power consumption, were found with the GA method. For instance, the pattern search optimization method resulted in 7.16% savings in MCR power consumption whereas GA resulted in 13.28% savings in MCR power consumption with an identical optimization problem. HYSYS object is created in Matlab codes to access HYSYS Component Object Model (COM) functionality. The Matlab *actxserver* command is used to create the HYSYS COM server. Then instances are created in the Matlab code to read HYSYS simulation variables and adjust them based on the GA runs. All HYSYS model convergence tolerances for the relative residuals were set to be $1x10^{-4}$. All initial populations were based on the baseline values.

The number of design variables for the MCR cycle is 8, compared with 14 for the propane cycle. Each cycle takes between 16 and 24 hours to solve on an Intel Core 2 Duo processor (2.83 GHz) with 1.96 GB of RAM. Typical GA tuning parameters used in the optimization are listed in Table 5.

Table 5: Typical GA tuning parameters

Tuning parameters	Value
Population size	20 x number of design variables
Reproduction count	50% of the population size
Maximum number of generations	100
crossover fraction	0.8
Selection method	Tournament
Tournament size	8
Fitness scaling method	Top
Number of crossover points	1
Mutation method	Adaptive feasible

The objective function of the MCR cycle optimization and propane cycle optimization is to reduce the total power consumption of the APCI LNG plant. The power consumption comes from the compressors and seawater pumps, as calculated by HYSYS software. The model in HYSYS is treated as a black box in this optimization study. The variables of the MCR optimization are listed in Table 6. The range of the optimization variables is taken to be ±20% of the baseline values. The MCR optimization's seven constraints with limits taken from the baseline model are listed as follow:

1) Temperature of the LNG ≤ -160^{o}C
2) LNG mass flow rate = 98.89 kg/s
3) Pre-cooling load of the propane cycle ≤ 88.22 MW
4) Two compressors vapor quality ≥ 0.99
5) Two heat exchangers pinch temperatures ≥ 3 K

Table 6: List of MCR cycle optimization variables.

Variable	Baseline Value
Refrigerant mass flow rate (kg/s)	270
Four refrigerant composition mass fractions(N_2/C1/C2/C3)	0.0971/0.2225/0.5445/0.1359
Evaporating pressure (kPa)	420
Intercooling pressure (kPa)	2,300
Condensing pressure (kPa)	4,000

The propane cycle optimization variables are listed in Table 7. The range of the optimization variables is also taken to be ±20% of the baseline values except for the condensing temperature, which was varied from 40 to 45^{o}C according to the available seawater temperature. The condensing temperature was included as an optimization variable in the propane cycle optimization but not in the MCR cycle optimization because the real plant operational data used by Mortazavi *et al.* has a

43°C condensing temperature for the propane cycle and a 40°C condensing temperature for the MCR cycle. Sub-cooling of the propane cycle would increase its cooling capacity and it would also increase seawater pumping power consumption. Changing an intermediate compressor outlet pressure is equivalent to changing a corresponding evaporation temperature because each heat exchanger, evaporator, is connected to a compressor outlet. The propane cycle optimization's 17 constraints with limits taken from the baseline model are listed as follow:

1) Three LPG produced vapor quality ≤ 0.01
2) Propane fuel production = 2.95 kg/s
3) Pentane Plus fuel production = 5.1 kg/s
4) Butane fuel production = 2.92 kg/s
5) Condensing load of the fractionation unit = 5.07 MW
6) Four compressors vapor quality ≥ 0.99
7) Six heat exchangers pinch temperatures ≥ 3 K

Table 7: List of propane cycle optimization variables.

Variable	Baseline Value
Refrigerant mass flow rate (kg/s), x_1	447
Condensing temperature (°C), x_2	43
Compressor 1 outlet pressure (kPa), x_3	253
Compressor 2 outlet pressure (kPa), x_4	406
Compressor 3 outlet pressure (kPa), x_5	618
Compressor 4 outlet pressure (kPa), x_6	1,540
22 C Heat exchanger pressure (kPa), x_7	882
Ref. mass splitter to the -19°C HX split ratio, x_8	0.465
Ref. mass splitter to the -5°C HX split ratio, x_9	0.758
Ref. mass splitter to the 9°C HX split ratio, x_{10}	0.143
Ref. mass splitter to the 16°C HX split ratio, x_{11}	0.886
Ref. mass splitter to the 22°C HX split ratio, x_{12}	0.705
Ref. mass splitter to liquefy the propane produced, x_{13}	0.909
Ref. mass splitter to liquefy the butane produced, x_{14}	0.938

2.5 Optimization Results

2.5.1 MCR Cycle Optimization

The optimized MCR cycle has a power consumption of 63.63 MW, which is 4.48% less than the baseline power consumption. The optimized MCR cycle has lower refrigerant mass flow rate and lower overall compression ratio than the baseline cycle as shown in Table 8. Nitrogen and propane mass fraction increased while the methane and ethane decreased. Since nitrogen has the lowest boiling temperature, it lowers the lowest refrigeration temperature. On the other hand, propane has the highest boiling temperature, which increases the refrigeration capacity of the refrigerant.

Table 8: MCR cycle optimization results

Cycle	Variables								Objective function
	$\dot{m}$ (kg/s)	x_{N2}	x_{C1}	x_{C2}	x_{C3}	P_i (kPa)	P_H (kPa)	P_{Ex} (kPa)	Power Cons. (MW)
Baseline	270	0.0971	0.2225	0.5445	0.1359	2300	4000	420	66.62
Optimized	267	0.1027	0.218	0.5306	0.1487	2346	4137	451	63.63

A plot of the cooling curves for the optimized and baseline MCR cycles is shown in Figure 15. The spiral-wound heat exchanger (SWHX) has two sections with log mean temperature difference (LMTD) for the optimized cycle of 5.24^{o}C and 4.91^{o}C, whereas the baseline cycle the LMTDs are 7.12^{o}C and 5.17^{o}C. Figure 15 and the LMTD values show that the cold curve in the optimized cycle is closer to the hot curve than the baseline cycle, which means more efficient heat transfer or less entropy generation in the heat exchanger.

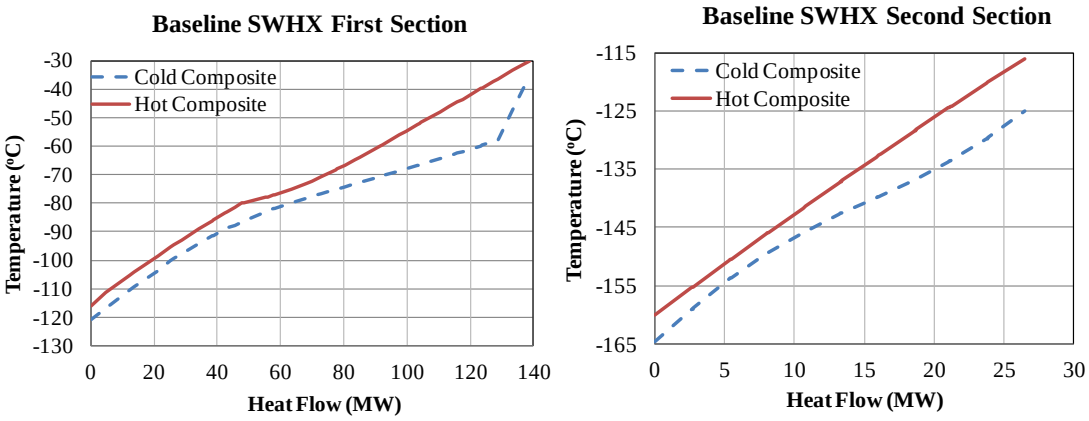

(a)

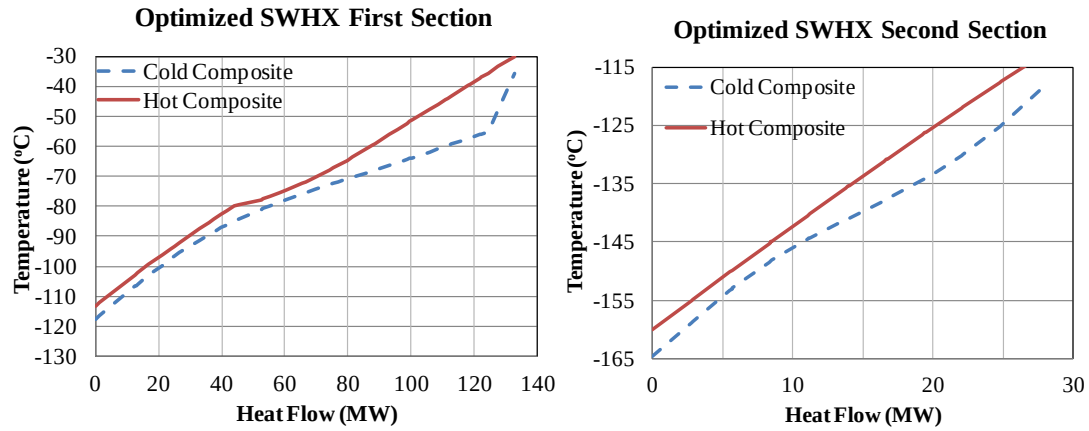

(b)

Figure 15: Cooling curves in SWHX of the baseline (a) and optimized (b) MCR cycles. The cooling curves are closer to the heating curves in the optimized cycle than the baseline cycle at equivalent pinch temperature of 3 K.

2.5.2 Propane Cycle Optimization

The optimized propane cycle has a power consumption of 37.15 MW, which is 15.98% less than the baseline power consumption. The optimized propane cycle has a higher refrigerant mass flow rate, maximum sub-cooling and slightly lower overall compression ratio than the baseline cycle as shown in Table 9. Split ratios, x_8 and x_9, are reduced so that an optimized amount of refrigerant is provided to lower temperature heat exchangers, -19°C and -33°C, respectively, which has lower

expansion pressure that requires more compression power. The other split ratios, x_{11}, x_{13} and x_{14}, were adjusted by the optimizer to meet the change in the total mass flow rate. In order to know how much power savings were obtained due to lower condensing temperature, 40°C condensing temperature was applied on the baseline model which resulted in 0.817 MW power reductions from the total baseline cycle power consumption. Therefore, the optimized cycle power savings is mainly due to the optimized mass distributions and pressure levels.

Table 9: Propane cycle optimization results.

Cycle	Variables							
	$\dot{m}$ (kg/s)	T_c (°C)	Pressures (kPa)					
	x_1	x_2	x_3	x_4	x_5	x_6	x_7	
Baseline	447	43	253	406	618	882	1540	
Optimized	465	40	240	406	758	847	1433	
Cycle	Variables							Obj. func.
	Split Ratios							Power Cons. (MW)
	x_8	x_9	x_{10}	x_{11}	x_{12}	x_{13}	x_{14}	
Baseline	0.465	0.758	0.143	0.886	0.705	0.909	0.938	44.22
Optimized	0.449	0.7	0.143	0.905	0.705	0.911	0.902	37.15

2.6 Second Law Efficiency

The Second Law efficiency, Eq. 1, is used to compare a thermodynamic cycle to an ideal reversible cycle. The minimum reversible compressors power required for LNG and LPGs productions was calculated from Eq. 2 to be 50.36 MW.

$$\eta_{II} = \dot{W}_{Minimum} / \dot{W}_{Calculated} \quad (1)$$

$$\dot{W}_{Minimum} = \dot{m}\Delta ex = \dot{m}\,(\Delta h - T_o \Delta s) \quad (2)$$

Where Δex is the exergy difference between the feed gas and the LNG and LPGs produced.

The total power consumption of the baseline cycle, as well as that of the optimized cycle, was calculated by the model in HYSYS to be 110.84 MW and 100.78 MW, respectively. This resulted in a Second Law efficiency of 45.43% for the baseline cycle and 49.97% for the optimized cycle. The baseline LNG plant model consumes 5.66 kWh energy per kmol of LNG produced whereas the optimized plant consumes 5.14 kWh energy per kmol of LNG produced.

2.7 Effect of Pinch Temperature

Multi-stream heat exchangers that are used in LNG industry offer high flexibility in the flow arrangement, which in turn minimizes the heat-transfer area. They are usually associated with large heat transfer at temperature differences as small as 1-3 K at the cold ends, in order to enhance efficiency [113].

APCI LNG plant uses SWHX, which is a proprietary heat exchanger, developed by Linde Inc. [114]. This expensive heat exchanger is used in the cryogenic column and it has a low pinch temperature, with a range that goes as low as 3 K [115]. The other type of less expensive heat exchanger that is used for liquefying NG is a plate fin heat exchanger [102].

The effect of pinch temperature on the LNG plant power consumption was investigated as shown in Table 10. The optimizer, coupled by HYSYS, was run with four pinch temperatures: 0.01, 1, 3 and 5 K. Different pinch temperatures represent the performance of different heat exchangers. Low pinch temperatures (0.01 K) represent extremely large and efficient, high UA value heat exchangers that do not exist and is an ideal heat exchanger. As shown in Figure 16, the savings in power consumption increases with the decrease in the pinch temperature. This savings can

be translated to operating cost and then compared with initial cost for economic evaluation of different LNG plants selection. Eq. 3 fits the resulting optimized MCR power for different pinch temperatures.

$$P_{MCR} = 1.538\,TP^2 - 3.316\,TP + 59.453 \quad (3)$$

Where, P_{MCR} optimized MCR power consumption (MW)

TP, pinch temperature (K)

Table 10: LNG plant optimization results with different pinch temperatures.

Cycle	Variables								Obj. function	LMTDs (K)
	$\dot{m}$ (kg/s)	x_{N2}	x_{C1}	x_{C2}	x_{C3}	P_i (kPa)	P_H (kPa)	P_{Ex} (kPa)	MCR Power Cons. (MW)	
Baseline	270	0.0971	0.2225	0.5445	0.1359	2300	4000	420	66.62	7.12/5.17
Optimized TP≥0.01 K	268	0.1072	0.2101	0.5308	0.1519	2700	3880	506	57.77 (13.28% Saving)	0.74/3.9
Optimized TP≥1 K	268	0.0978	0.2186	0.5376	0.146	2870	4003	501	58.68 (11.91% Saving)	2.86/3.06
Optimized TP≥3 K	267	0.1027	0.218	0.5306	0.1487	2346	4137	451	63.63 (4.48% Saving)	5.24/4.91
Optimized TP≥5 K	267	0.1175	0.2132	0.5287	0.1407	2137	4458	399	70.69 (6.61% More power cons.)	7.9/7.39

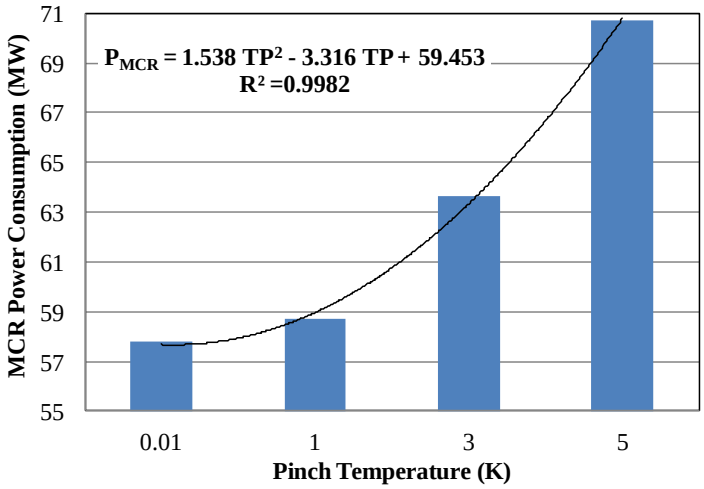

Figure 16: Optimized MCR power consumption at different heat exchanger pinch temperatures.

2.8 Optimized MCR Refrigerant Mixture versus Optimized MCR Refrigerant Mixture in Literature

Venkatarathnam [109] and Paradowski *et al.* [98] have published their optimized refrigerant mixtures for an MCR cycle in an APCI LNG plant. They did not use GA methods to obtain their refrigerant mixtures compositions (refer to literature review section). Venkatarathnam and Paradowski used similar NG feed, shown in Table 11, which is different than this work NG gas feed.

Table 11: Gas composition used in Venkatarathnam [109] and Paradowski *et al.* [98] models.

Component	Mole Fraction (%)
Nitrogen	4
Methane	87.5
Ethane	5.5
Propane	2.1
i-Butane	0.3
n- Butane	0.5
i-Pentane	0.1

In order to compare our optimization approach against the optimization approach of Venkatarathnam and Paradowski *et al.*, the MCR optimization was done

with similar NG feed, pre-cooling temperature and liquefaction temperature as Venkatarathnam and Paradowski *et al.* used. The resulting optimized MCR cycle is shown in Table 12. Two models were developed in HYSYS that use refrigerant mixtures discussed by Venkatarathnam and Paradowski *et al.*, which are then optimized for the same objective function, variables (except the refrigerant mixture composition), and constraints as described in the MCR optimization section. The optimized power consumption for the models in HYSYS that use refrigerant mixtures discussed by Venkatarathnam and Paradowski *et al.* is 6.98% and 13.6% higher than the optimized power consumption of this work as shown in Figure 17. Their LMTDs for the two sections in SWHX are also higher than the optimized cycle LMTDs as shown in Table 12. This shows the superiority of the refrigerant mixture composition obtained by using GA than the mixtures obtained by other methods.

Table 12: Comparison between this work results and results from the optimized HYSYS models that use refrigerant mixtures optimized by Venkatarathnam and Paradowski *et al.*

Cycle	Variables								Objective function	LMTDs (K)
	$\dot{m}$ (kg/s)	x_{N2}	x_{C1}	x_{C2}	x_{C3}	P_i (kPa)	P_H (kPa)	P_{Ex} (kPa)	MCR Power Cons. (MW)	
Optimized, TP≥3 K	232.8	0.0731	0.2506	0.5291	0.1472	2259	3967	511	51.67	5.55/5.9
Venkatarathnam Optimized, TP≥3 K	217.97	0.0725	0.2479	0.3324	0.3472	2900	4665	337	58.7 (13.6% More power consumption)	6.14/12.24
Paradowski *et al.* Optimized, TP≥3 K	222.11	0.0488	0.2701	0.4422	0.2389	2284	4446	420	55.28 (6.98% More power consumption)	7.99/6.04

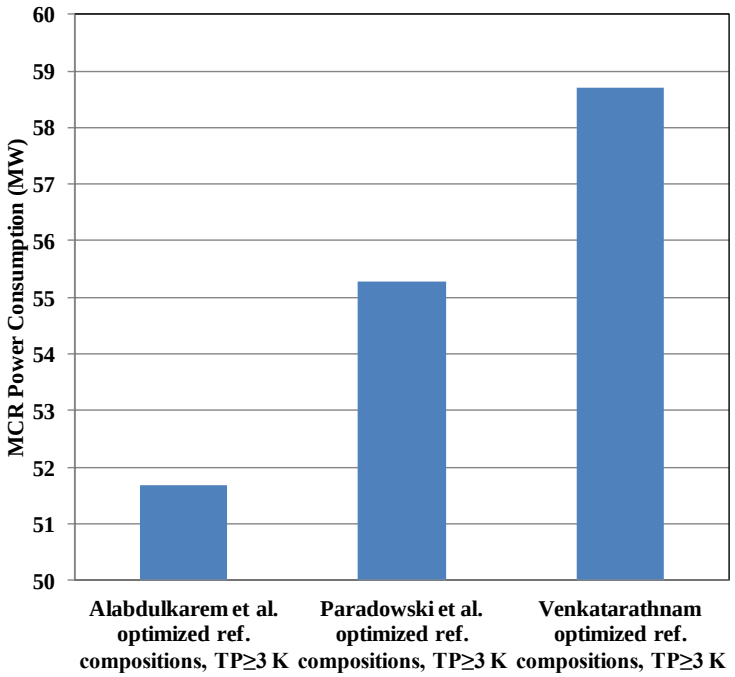

Figure 17: Optimized MCR power consumption that this work optimized refrigerant mixtures against the optimized refrigerant mixtures of Venkatarathnam and Paradowski, *et al*.

2.9 APCI Optimization with Uncertainty in Natural Gas Compositions

2.9.1 Introduction

It was observed that optimizing the APCI cycle for different natural gas feed compositions results in different refrigerant mixture and different operating variables as shown in Table 13. The results in the table are for applying identical optimization approach for two different natural gas fields with equivalent total mass flow rate as described in Section 2.5.1 and Section 2.8.

Although the difference in the methane content, which is the main component in the natural gas feed compositions, is only 2%, the optimum refrigerant mixture composition differs by 28.8% and the power consumption differs by 18.8%. Therefore, it is necessary to apply optimization to each natural gas field individually

when designing a new LNG plant. Each natural gas feed needs certain refrigerant compositions that match the liquefaction cooling curve (i.e., matches the boiling temperature and liquefaction load). However, in certain cases natural gas plants serves several gas reservoirs or there is an uncertainty of a single gas reservoir's compositions which could also change with time.

Table 13: Comparison between optimization results for two different natural gas feeds.

Cycle	Variables								Objective function	LMTDs (K)
	$\dot{m}$ (kg/s)	x_{N2}	x_{C1}	x_{C2}	x_{C3}	P_i (kPa)	P_H (kPa)	P_{Ex} (kPa)	MCR Power Cons. (MW)	
Optimized, TP≥3 K, NG Feed in Table 2	267	0.1027	0.218	0.5306	0.1487	2346	4137	451	63.63	5.24/4.91
Optimized, TP≥3 K, NG Feed Gas in Table 11	232.8	0.0731	0.2506	0.5291	0.1472	2259	3967	511	51.67	5.55/5.9
Differences (%)	-12.8	-28.8	15.0	-0.3	-1.0	-3.7	-4.1	13.3	-18.8	5.9/20.2

In order to handle this type of optimization problems (i.e., APCI optimization with uncertainty in natural gas fields), robust optimization methods were proposed to be used to solve this type of problems. Robust optimization methods, unlike conventional optimization methods, are capable of dealing with optimization problems that involve uncertainty in design variables and parameters.

After the problem was defined and the solution methodology was identified, the corresponding APCI model, the generic HYSYS-Matlab platform and the optimization approach for the robust refrigerant problem were developed in

collaboration with DDSL. A robust optimization method was developed by Mortazavi *et al.* [141] called Gradient Assisted Robust Optimization (GARO) method. The method was used to solve several engineering problems with uncertainty. GARO was used to optimize the APCI cycle with uncertainty in natural gas feed [142].

2.9.2 Optimization Approach

Since the robust optimization methods are more computationally expensive that conventional optimization methods, it was necessary to simplify the APCI cycle model and enable variable gas feed to the model as shown in Figure 18. The model calculates the propane cycle power consumption using the propane cycle COP from the detailed model. Thus, the propane cycle power consumption can be calculated by knowing the propane cycle load for each cooling stage.

The optimization objective function and design variables are similar to the ones in Section 2.4.1 and Table 6, respectively with limit shown in Table 14. The uncertain parameters are the feed natural gas compositions with uncertainty shown in

Table **15**. Heavy hydrocarbons uncertainties were not considered because they condense in the propane cycle, and, thus don't affect the performance of the MCR cycle. The robust refrigerant optimization's four constraints (g_1..g_4) with limits taken from the baseline model are listed as follow:

1) First and Second MCR evaporator heat exchangers pinch temperatures $\geq$ 3 K (g_1 and g_2)
2) First and Second MCR compressor vapor quality $\geq$ 1 (g_3 and g_4)

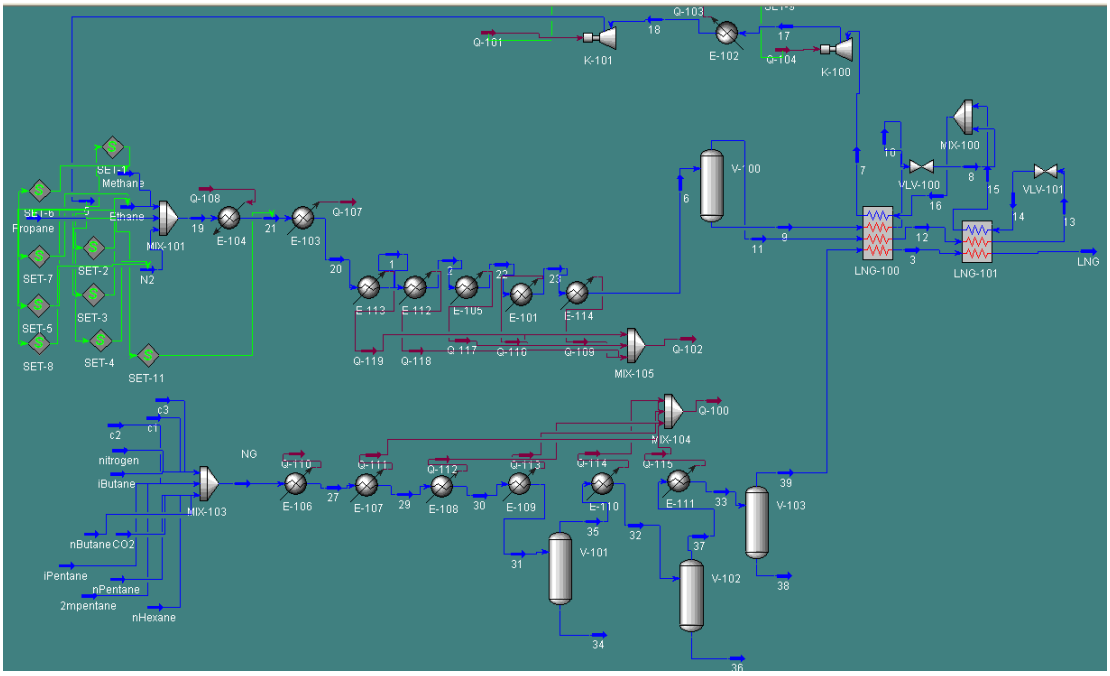

Figure 18: Simplified HYSYS model for APCI cycle.

Table 14: Design variable range for robust refrigerant optimization problem.

Variable	Range
$\dot{m}_{N_2}$ (kg/s)	9-50
$\dot{m}_{C1}$ (kg/s)	30-110
$\dot{m}_{C2}$ (kg/s)	90-180
$\dot{m}_{C3}$ (kg/s)	5-70
P_{Ex} (kPa)	90-900
P_i (kPa)	900-3000
P_H (kPa)	2900-6000

Table 15: Feed gas compositions with uncertainity.

Component	Nominal Mass Fraction	Uncertainty Range (%)
Ethane	0.1157	48%
Propane	0.0792	51%
Nitrogen	0.0014	50%
i- Butane	0.0298	50%
n- Butane	0.0298	50%
Methane	0.7441	17%

2.9.3 Results

The optimization resulted in robust refrigerant which consumes 35.19 MW more than Alabdulkarem *et al.* #1 refrigerant for liquefying the nominal feed gas as shown in Table 16 and Figure 19. Applying robust optimization will always result in less optimal value if it was compared with deterministic optimization without uncertainty. However, robust optimization will result in a design that is relatively insensitive to uncertainty. In other words, the robust refrigerant can be used to liquefy a range of natural gas feeds.

Table 16: Robust refrigerant design values versus refrigerant mixtures from the literatures.

Refrigerant	Power (MW)	$\dot{m}$ (kg/s)	x_{N2}	x_{C1}	x_{C2}	x_{C3}	P_i (kPa)	P_H (kPa)	P_{Ex} (kPa)
Robust	138.841	291	0.1072	0.2753	0.5833	0.0343	1292	4877	368
Mortazavi *et al.*	113.328	289	0.0971	0.2225	0.5445	0.1359	2300	4000	420
Alabdulkarem *et al.* #1	103.652	262	0.1027	0.218	0.5306	0.1487	2346	4137	451
Alabdulkarem *et al.* #2	121.552	279	0.0731	0.2506	0.5291	0.1472	2259	3967	333
Venkatarathnam	105.398	235	0.0725	0.2479	0.3324	0.3472	2900	4665	302
Paradowski *et al.*	122.170	242	0.0488	0.2701	0.4422	0.2389	2284	4446	239

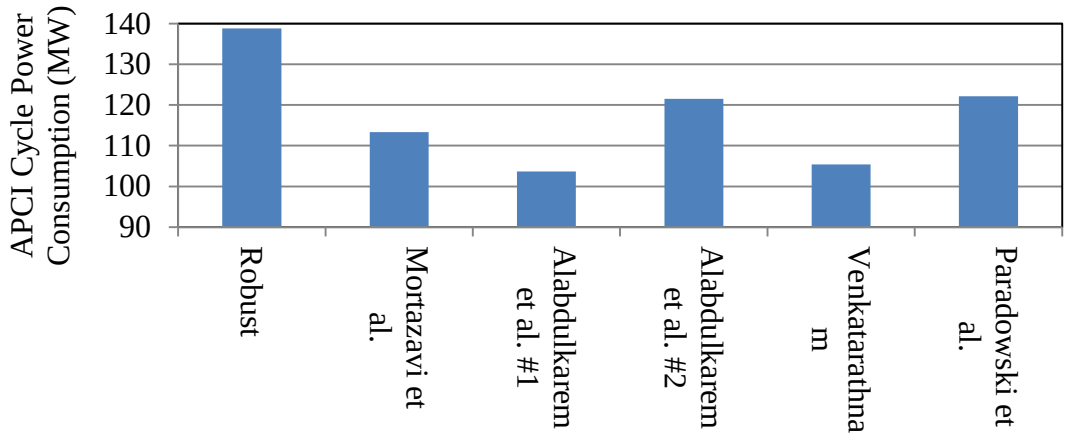

Figure 19: Power consumption using different optimization results for liquefying the nominal feed gas.

In order to compare the robust refrigerant against the other refrigerant, the natural gas feed was divided into 10 subsets within the uncertainty range as shown in Table 17. The power consumption for liquefying the ten feed gas using the different refrigerants are listed in Table 18. Since some refrigerants cannot liquefy some of the natural gas feed, constraints violated (e.g. pinch temperature) are listed instead of the power consumption. The robust refrigerant is the only refrigerant which was able to handle all 10 natural gas feeds. However, its power consumption is higher than the other refrigerants when they don't violate any constraint. The least power consuming refrigerants are sensitive to the change in feed gas compositions uncertainty because they have small approach temperature inside the MCR heat exchangers and they have lower suction superheat which make temperature crossing possible with changes in feed gas boiling temperature and latent load.

Table 17: Natural mixtures corresponding to the natural gas uncertainty subsets.

Gas mixture	x_{Ethane}	$x_{Propane}$	x_{N2}	$x_{i\text{- Butane}}$	$x_{n\text{- Butane}}$	$x_{Methane}$
1	0.0553	0.04	0.0007	0.015	0.015	0.874
2	0.0698	0.0499	0.0009	0.0187	0.0187	0.842
3	0.0842	0.0598	0.001	0.0224	0.0224	0.8102
4	0.0987	0.0697	0.0012	0.0262	0.0262	0.778
5	0.1132	0.0796	0.0014	0.0299	0.0299	0.746
6 (Nominal)	0.1157	0.0792	0.0014	0.0298	0.0298	0.7441
7	0.1276	0.0895	0.0016	0.0336	0.0336	0.7141
8	0.1421	0.0994	0.0017	0.0374	0.0374	0.682
9	0.1565	0.1093	0.0019	0.0411	0.0411	0.6501
10	0.171	0.1192	0.0021	0.0448	0.0448	0.6181

Table 18: Power consumption using different optimization results for liquefying different feed gas mixtures.

Liquefaction Cycle Power Demand (MW)										
Natural Gas Mixture	1	2	3	4	5	6	7	8	9	10
Robust	140.7	140.3	139.9	139.4	138.9	138.8	138.2	137.5	136.6	135.7
Mortazavi *et al.*	g1	115.5	114.9	114.2	113.3	113.3	g3	g3	g3	g3
Alabdulkarem *et al.* #1	g1,g2	g1,g2	g1	g1	103.7	103.7	102.8	g3	g3	g3
Alabdulkarem *et al.* #2	g2	g2	g2	g2	121.6	121.6	120.5	g3	g3	g3
Venkatarathnam	g1	g1	g1	g1	g1	105.4	g3	g3	g3	g3
Paradowski *et al.*	g2	g2	g2	g2	122.2	122.2	120.9	119.4	g3	g3

Since methane has the highest mass flow rate in the feed gas and is the component of the LNG, it has prominent effect on the APCI cycle power consumption. The APCI cycle power consumption increased with increasing the methane content as shown in Figure 20.

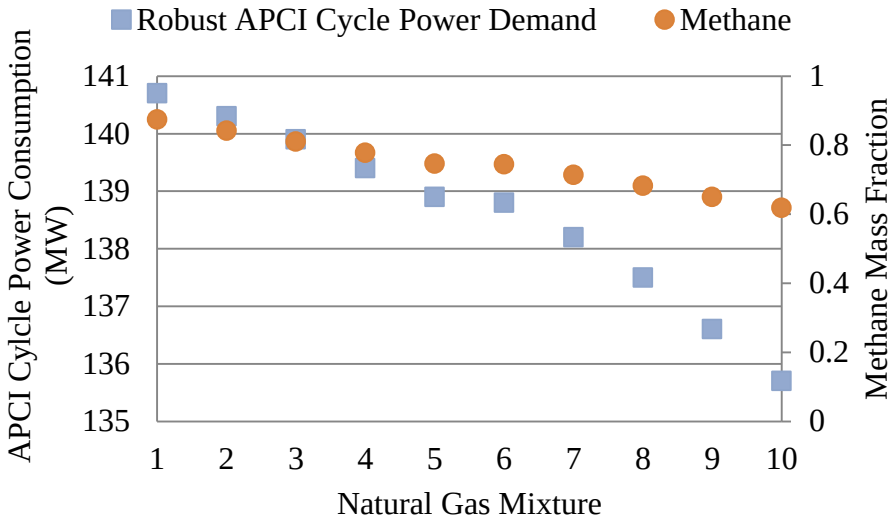

Figure 20: Effect of methane content in feed gas on the robust APCI cycle power consumption.

2.10 Conclusions

An APCI LNG plant was modeled in HYSYS and verified with Mortazavi *et al.*'s ASPEN Plus model, with good agreements. Although the approach of coupling a comprehensive modeling software, HYSYS, with a powerful optimization software tool, GA in Matlab, is time consuming, it provides greater confidence in reaching a global optimal.

Optimized refrigerant mixture and system variables were obtained. Total power consumption was reduced by 9.08%. The effect of the pinch temperatures on power consumption was also investigated. The savings in power consumption from using heat exchangers with 1 K pinch temperature in the cryogenic column is 17% lower than using heat exchangers with 5 K pinch temperature.

The obtained optimum composition of refrigerant mixtures for this work was compared with two optimized compositions of refrigerant mixtures from the open literature. Results show that the current work has achieved better refrigerant compositions than the literature ones. The method used in this work can be implemented in optimizing any processes modeled with HYSYS software.

The effect of uncertainty in natural gas feed was identified, and a robust refrigerant was developed. The natural gas liquefaction load and temperature changes with the natural gas feed compositions. The robust refrigerant can handle several natural gas feeds consumes 35.19 MW more than the refrigerant that was developed using deterministic optimization. However, this refrigerant was very sensitive to variation in natural gas feeds.

Chapter 3: Energy Consumption Reduction in CO_2 Capturing and Sequestration of an LNG Plant through Process Integration and Waste Heat Utilization

3.1 Introduction

The high energy consumption in natural gas driven LNG plants with CO_2 capturing makes them produce high amount of waste heat such as heat in the flue gas or in condensed steam. The amount of the waste heat in a NGCC power plant is about the capacity of the NGCC power plant (i.e., the power plant efficiency is 50%). Several waste heat utilization technologies such as absorption cycles or Organic Rankine Cycle (ORC) that utilize the waste heat which would otherwise be dumped to the ambient. However, optimum process integration is essential in reducing LNG plants power loss with CCS.

Although some authors simulated integrated power cycle with CCS (refer to literature review section), there is a lack of literature in this area (one of the top research issues according to Rao *et al.*'s investigation). There has been no research done on integrating an LNG plant with power cycle and CCS using experimentally validated models, with comprehensive waste heat evaluation, along with uses that will result in power savings with any solvents used to capture the CO_2. Further, no authors have suggested a way to enhance the CO_2 capture efficiency independently from the CO_2 capture plant.

The objectives of this chapter are to reduce the power loss in an LNG plant with a CCS and to enhance the CO_2 capture efficiency through process integration

and waste heat utilization. The work is carried out by the development of several models in HYSYS software with models validation against experimental data. Several steam cycles with steam extraction configuration were also investigated. Further, Pinch Analysis technology was used to compare the conventional integrated CCS and the proposed integrated CCS.

3.2 Conventional CO_2 Capturing Configuration

In the conventional post-capture CCS configuration using CO_2 absorption in amine solution shown in Figure 21, exhaust gases exiting a power plant are cooled by seawater before CO_2 capture. Exhaust gas temperature out of the steam cycle is a function of sulfur content in the fuel so that no sulfur condenses on the heat exchanger material. For natural gas fuel, exhaust gas temperature is typically 140°C and could be as low as 80°C. In case of high sulfur flue gas, corrosion resistance heat exchangers such as stainless steel heat exchangers can be used to utilize the low grade heat [116]. The cooling temperature of the flue gas is a function of the available seawater temperature, which is assumed to be 35°C.

The captured CO_2 is regenerated in the stripper column with steam, at a temperature around 130°C. The steam is extracted from the steam cycle, resulting in 12.11% power loss in the NGCC power as shown in Figure 22. The evaporated solution containing CO_2, MEA and water is condensed to 40°C, using seawater. The condensed solution is recirculated to the stripper column, and the vapor (around 90% CO_2 and 10% water by weight) is compressed in multistage compressors from atmospheric pressure to the required well injection pressure, resulting in 3.15% power loss in the NGCC power.

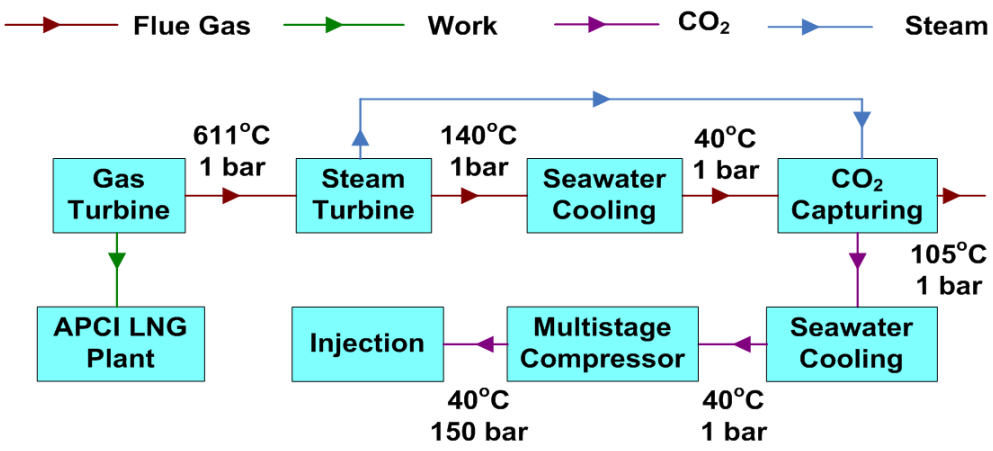

Figure 21: Conventional CO_2 capturing configuration.

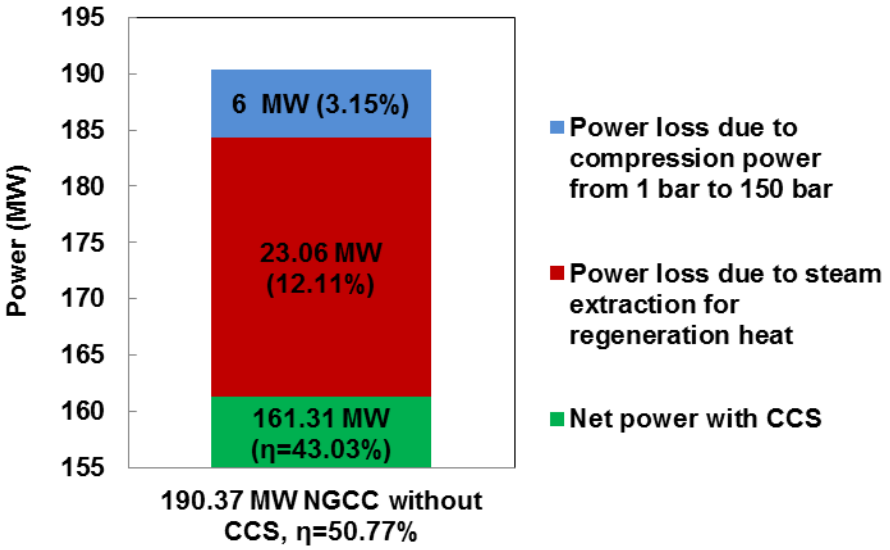

Figure 22: Power loss brakedown in conventional CCS due to CO_2 regeneration heat and CO_2 compression power.

3.3 Proposed CO_2 Capturing Configuration

In order to improve the CO_2 removal, a new configuration is proposed. A careful observation of the experimental results obtained by Dugas *et al*. [24] that shows the CO_2 loading versus the CO_2 partial pressure in the flue gas in the absorber,

Figure 23, reveals that as we lower the flue gas temperature, we can obtain higher CO_2 removal at a given flue gas pressure. This observation was the basis for proposing to cool the flue gas before absorption, through the use of absorption chillers.

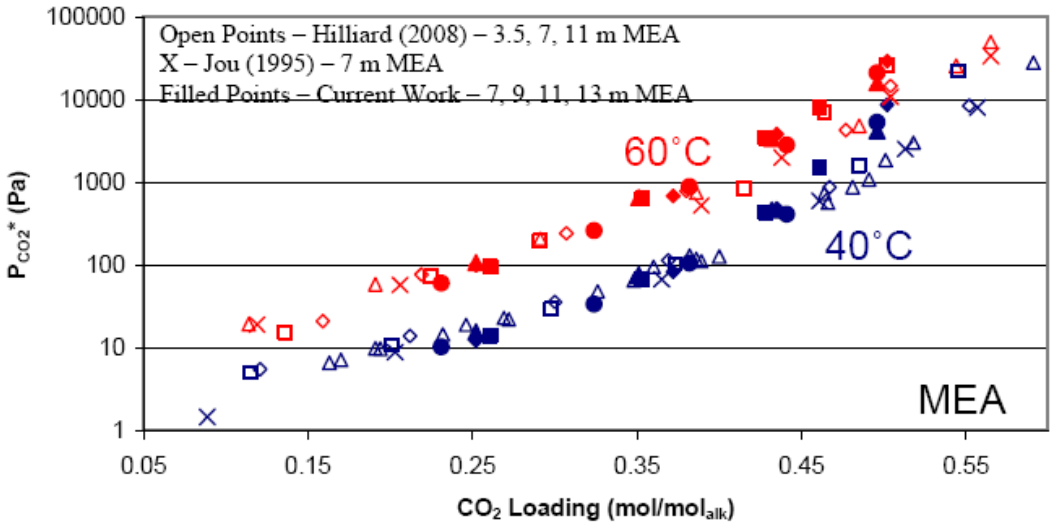

Figure 23: CO_2 partial pressure data for MEA solutions at 40 and 60^{o}C [24].

Since the exhaust gas is cooled from 140°C to 40°C using seawater, there is waste heat lost in this process that can be utilized through absorption chillers. Thus, a single-effect desorber and half-effect desorber, or organic Rankine cycle (ORC) power cycle are proposed to utilize the waste heat of the flue gas from 140°C to 80°C. Furthermore, it is proposed to place another half-effect desorber or ORC power cycle between the stripper column and the CO_2 condenser to utilize the waste heat from 110°C to 80°C. The proposed configuration is shown in Figure 24.

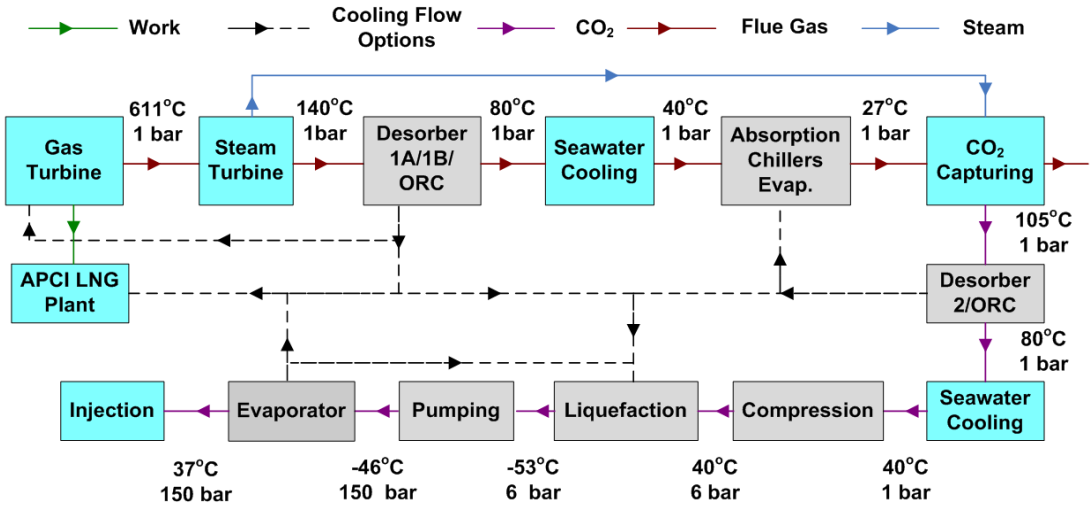

Figure 24: Proposed CO_2 capturing configuration.

The obtained cooling from the absorption chillers is proposed to be used for cooling the flue gas so that it reaches a temperature that is lower than the one obtained by seawater cooling. Therefore, the CO_2 removal will increase due to the increase in the CO_2 mass transfer coefficient in the amine solvent. The CO_2 mass transfer flux, N_i, is given in Eq. 4 and the CO_2 mass transfer coefficient, K_{tot,CO_2}, is given in Eq. 5 (Kvamsdal *et al* .[44]).

$$N_i = K_{tot,CO_2}(P_{CO_2}^{eq,*} - P_{CO_2}^{g}) \quad (4)$$

$$K_{tot,CO_2} = \frac{1}{\frac{RT_g}{k_{CO_2}^{g}} + \frac{H_{E,CO_2}}{k_{CO_2}^{l} E_{CO_2}}} \quad (5)$$

Where,

$P_{CO_2}^{eq,*}$: CO_2 equilibrium pressure

$P_{CO_2}^{g}$: CO_2 partial pressure in flue gas

T_g : Flue gas temperature

H_{E,CO_2}: Henry's Law constant

$k_{CO_2}^{l}$: Liquid mass transfer coefficient for CO_2

E_{CO_2}: Enhancement factor

The captured CO_2 is proposed to be liquefied and pumped instead of undergoing compression. The pressurized liquid CO_2 is cooled, and this cooling is proposed to be recovered through cooling the natural gas in the APCI cycle or in cooling the CO_2 itself. This will reduce the power consumption of the APCI cycle or the CO_2 liquefaction cycle.

3.4 Waste Heat Visualization Graph

In order to visualize that there is available waste heat in a cooling process that could be utilized in another process, or that there is free cooling available in a heating process, a waste heat visualization diagram is developed as shown in Figure 25. The horizontal axis represents the amount of heat that is rejected or gained in heat exchangers. The amount of the heat is the stream mass flow rate times the enthalpy change across a heat exchanger. The vertical axis represents the change in the stream temperature during heating or cooling processes.

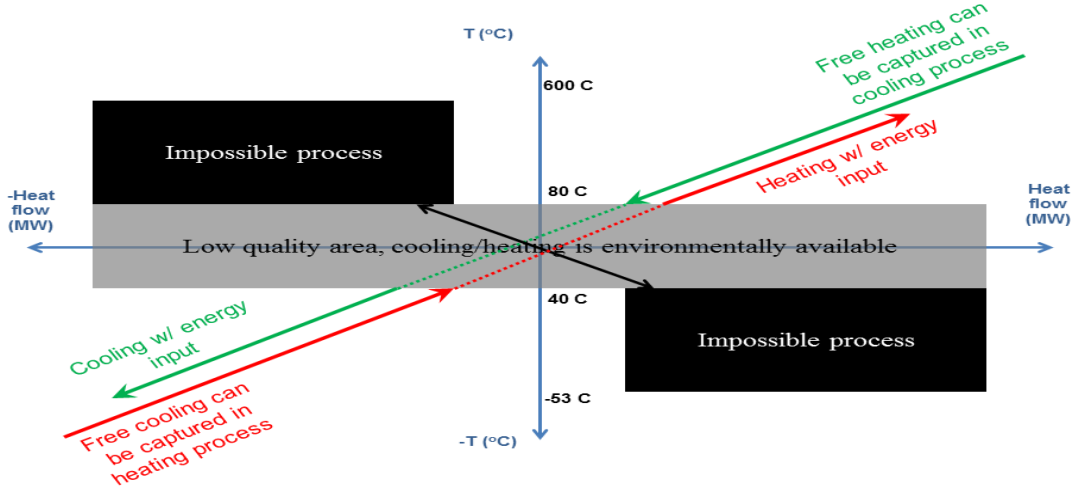

Figure 25: The developed waste heat visualization graph.

In order not to violate the First Law of thermodynamics, a cooling process follows a line that is heading to the 3rd quarter of the graph. The green line in the graph represents a stream cooling line where the temperature and enthalpy are reduced. Any cooling process that happened to occur in the 1st quarter of the graph has utilizable waste heat. For example, waste heat can be captured in cooling the flue gas from 120°C to 80°C in absorption chillers. However, no waste heat can be captured in a cooling process that is in the 3rd quarter of the graph which starts at the ambient temperature, 40°C. This cooling process requires energy input via cooling cycle. The gray box in the graph represents the low quality area where it is feasible for cooling to be done by an environment such as seawater cooling. No waste heat can be captured in the gray box area.

Similarly, a heating process follows a line that is heading to the 1st quarter of the graph. The red line in the graph represents a stream heating line where the temperature and enthalpy increases. Any heating process that happened to be in the

2nd quarter of the graph has a utilizable cooling. For example, free cooling can be captured in heating the liquefied CO_2 from -53°C to 40°C. Heating in the 1st quarter requires energy input. On the other hand, heating in the low quality area (40 to 80°C) could be done by process integration such as using heat from compressor intercooling.

Further, no heating process that follows the black arrows to the 2nd quarter, which represents increasing the stream temperature while reducing the enthalpy at content pressure, is thermodynamically possible. Likewise, no cooling process that follows the black arrows to the 4th quarter, which represents decreasing the stream temperature while increasing the enthalpy at the same time, is thermodynamically possible.

3.4.1 Waste Heat Visualization Graph Example 1

The developed graph was plotted for the flue gas of the developed system in Figure 26. The red circles represent heat exchangers. For example, the flue gas is cooled from 140°C to 40°C in the flue gas cooler before the CO_2 absorber. The graph shows that this process direction is heading to the 3rd quarter from the 1st quarter in Figure 25. Thus, there is utilizable waste heat in this process from 140°C to 80°C. However, the process crosses the low quality area from 80°C to 40°C which is done by environmentally available cooling (seawater cooling). Further, part of the CO_2 heating in the stripper falls also in the low quality area from 80°C to 40°C. Therefore, this portion of heating is accomplished by environmentally available heating which comes from the lean solution in the solution-to-solution heat exchanger (Figure 5). The rest of the CO_2 heating in the stripper is in the 1st quarter heading to the 3rd

quarter which requires energy for heating from 80°C to 120°C. This heating comes from the boiler.

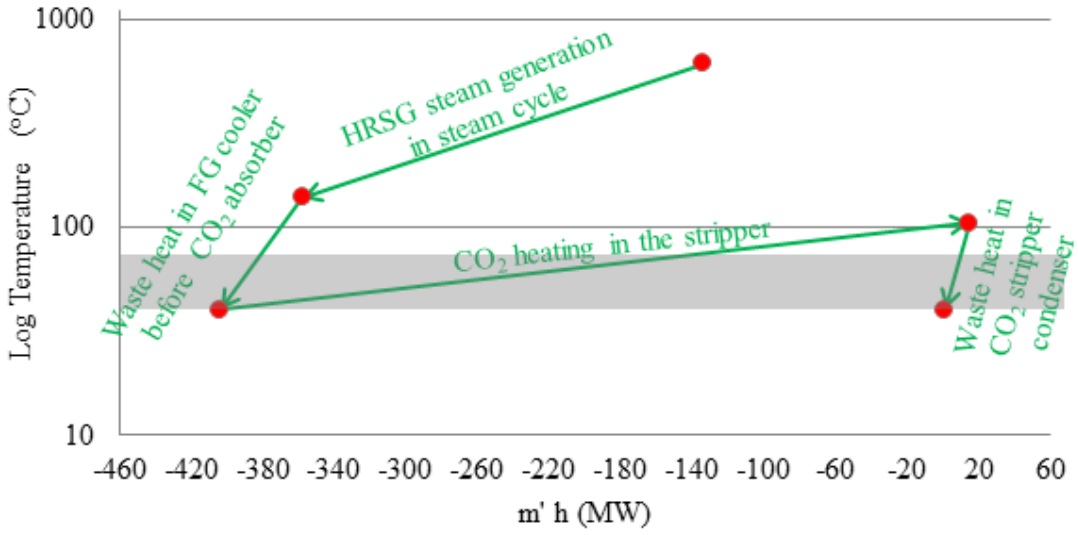

Figure 26: Flue gas energy visualization diagram.

3.4.2 Waste Heat Visualization Graph Example 2

The developed graph was also plotted for the captured CO_2 of the developed system in Figure 27. The CO_2 intercooling is cooled from 90°C to 40°C which is mostly in the low quality area. On the other hand, the CO_2 heating process is in the 3rd quarter region heading to the first quarter in Figure 25. Thus, there is a free cooling in this process that can be utilized from -53°C to 40°C.

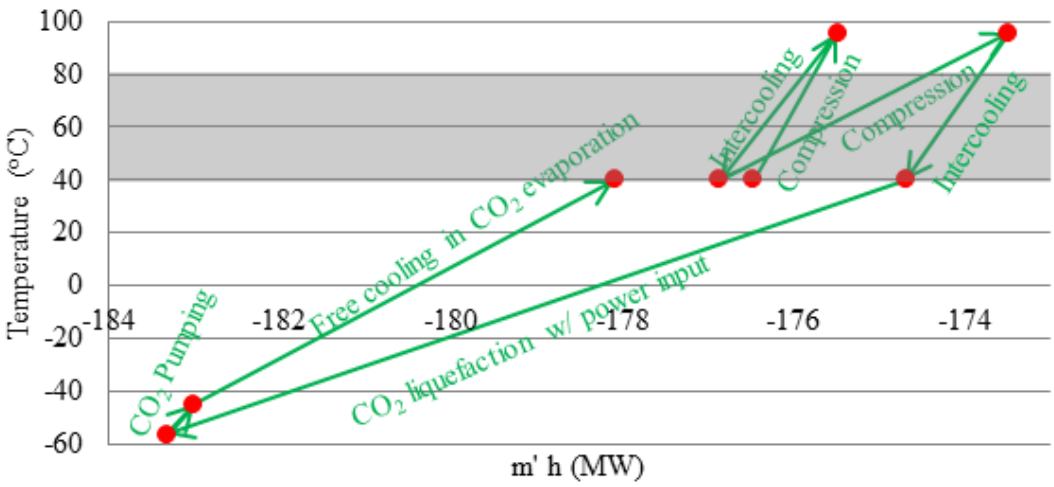

Figure 27: CO_2 energy visualization diagram.

3.5 CCS Waste Heat Sources and Uses Evaluation

Four waste heat sources in the integrated CCS system were identified. The first one is the waste heat in the flue gas after the combined cycle. The second one is the waste heat in the regenerated CO_2 stream. The third one is the remaining low pressure steam that was used to regenerate the CO_2. The fourth one is the wasted cooling in the liquefied and pressurized CO_2.

Many options were proposed for using the available waste heat as shown in Figure 28. The proposed uses are cooling flue gas, cooling CO_2 in CO_2 liquefaction cycle, cooling natural gas (NG) in the APCI LNG cycle, cooling inlet air of the gas turbine, power generation using Organic Rankine Cycle (ORC) or preheating the condensed water before it goes to the HRSG. These uses can be seen in Figure 24. Detailed evaluation through modeling these uses for a specified amount of waste heat is necessary to find the potential savings in power consumption of the integrated system.

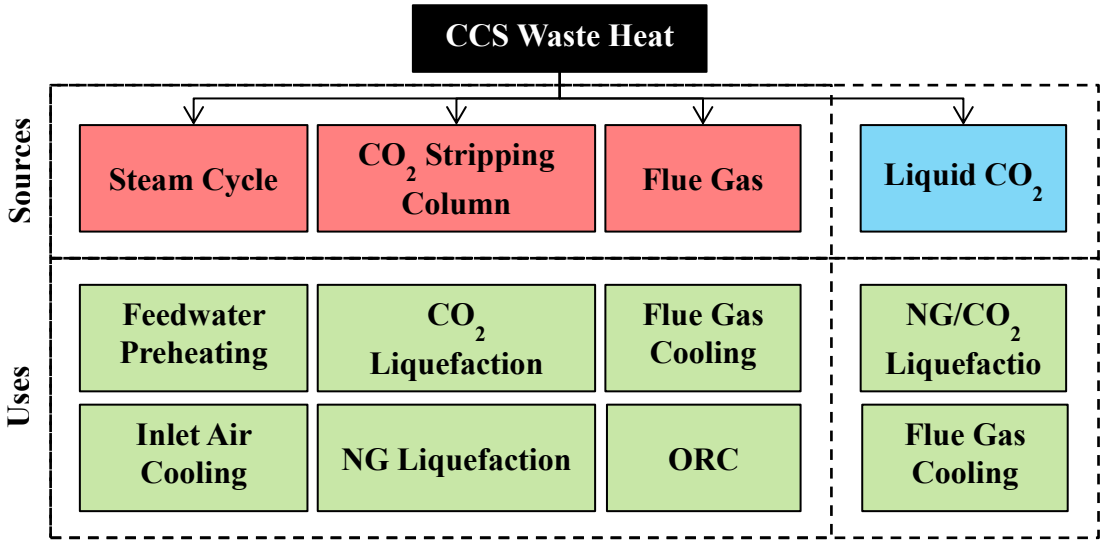

Figure 28: CCS waste heat classifications, Red: waste heat sources. Blue: cold sources, Green: potential uses for waste heat.

3.6 Component Modeling

This section describes the conventional CCS and the proposed CCS components modeling. The CO_2 liquefaction and compression cycles are addressed in Chapter 4. The components were modeled using HYSYS software. HYSYS is well known in the process simulation field. It includes varieties of built-in equation of states and components such as heat exchanger models and compressor models.

The equation of state that is used in all of these thesis models is the Peng-Robinson equation of state, as it is well known for its accuracy, and it is recommended by the HYSYS equation of state recommendation tool [110]. The assumptions of the modeling work are listed in Table 19.

Table 19: Modeling assumptions used in HYSYS models

Centrifugal compressor isentropic efficiency	80%
Pump isentropic efficiency	75%
Heat exchanger pinch temperature	3 K
Heat exchanger pressure drop	10 kPa
Sea water temperature	35°C

3.6.1 Steam Power Cycles

Steam cycles with steam extraction combined with the gas turbine model were developed. Steam is generated in a heat recovery steam generator (HRSG) using the gas turbine flue gas exhaust that enters the HRSG at a temperature of 610^{o}C. The temperature of the exhaust gas after the HRSG, e.g. the utilization temperature of the fuel, is kept at 140^{o}C. The HRSG is a counter flow heat exchanger that is composed of three heat exchangers. The first one from the right is the economizer, where the water is heated until it reaches saturated water conditions. The middle one is the boiler, where the water is evaporated. The third one is the superheater, where the water vapor is superheated.

To regenerate the CO_2 in the stripper column, the 70.42 MW of steam is extracted from the steam turbine at a temperature of 130^{o}C. Different steam cycle configurations were developed that differ in their steam extraction location. These configurations are described in the following sections.

3.6.1.1 Partial Steam Extraction Configuration

This configuration, shown in Figure 29, extracts part of the steam flow in a single steam turbine with two stages. The extracted steam goes to the boiler of the stripper and the rest goes to the second stage of the steam turbine. The extracted steam flow rate is 43% of the flow rate in Lars Erik's configuration. Therefore, this

configuration has less pressure drop. The resulting net power output with this configuration is 162.81 MW.

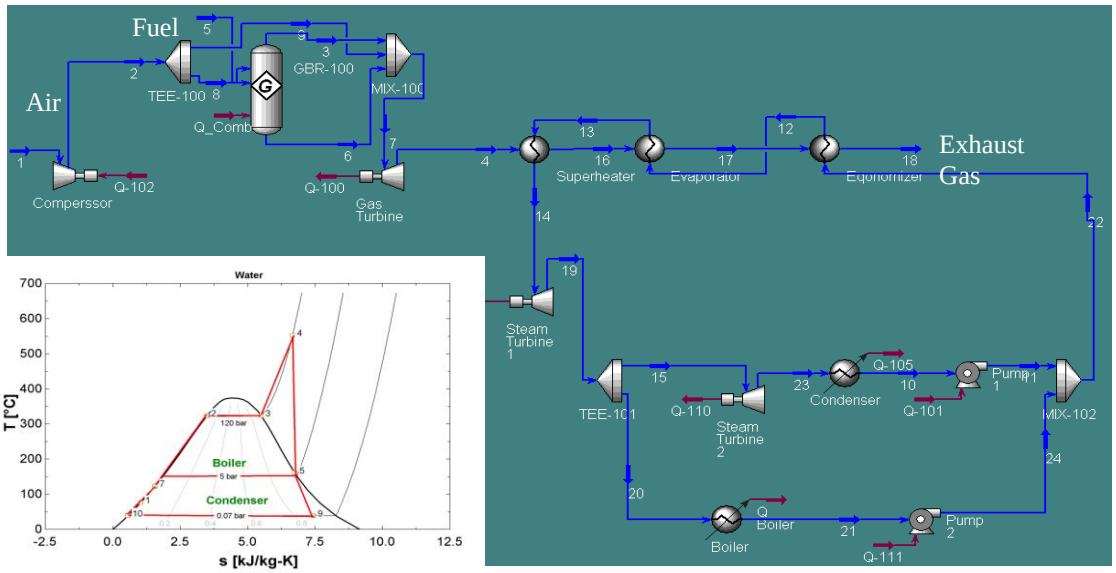

Figure 29: HYSYS model for combined cycle with partial steam extraction configuration and its T-s diagram.

3.6.1.2 The High Temperature Condenser Configuration

This configuration, shown in Figure 30, is for high sulfur content fuel where the waste heat in the flue gas will not be utilized from 140^{o}C to 80^{o}C in absorption chillers. This configuration has a high condensing temperature (134^{o}C). The steam condenser was replaced by a 70.42 MW boiler and the rest, 85.97 MW, is used in a desorber of single-effect water/LiBr absorption chillers. The resulting net power output with this configuration is 162 MW.

If the flue gas is to be utilized from 140^{o}C to 80^{o}C in absorption chillers, this configuration will have a net power of 155.63 MW and 92.33 MW waste heat in the steam cycle desorber. The reason why this case has lower net power is due to the absorption chillers' desorbers, where there is a higher pressure drop in the flue gas.

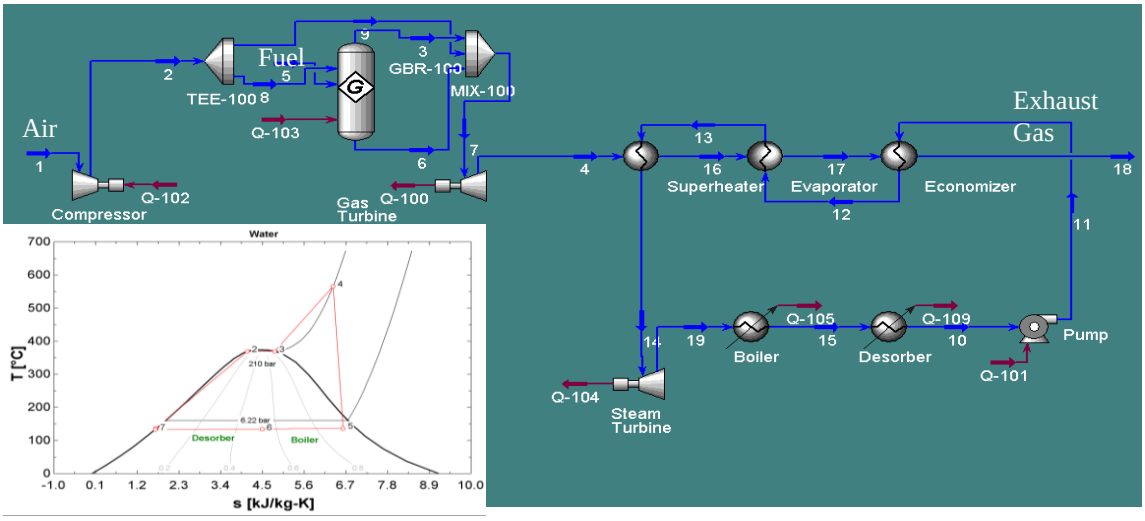

Figure 30: HYSYS model for combined cycle with the High Temperature Condenser Configuration and its T-s diagram

3.6.1.3 Diverting the Entire Steam Flow Configuration

This configuration, shown in Figure 31, depicts Lars Erik's configuration where the entire steam mass flow rate is sent from the high pressure steam turbine to the stripper boiler, then it is returned to the low pressure stream turbine. Sending a higher steam flow will have a higher pressure drop than extracting portion of the steam flow. The resulting net power output with this configuration is 162.81 MW.

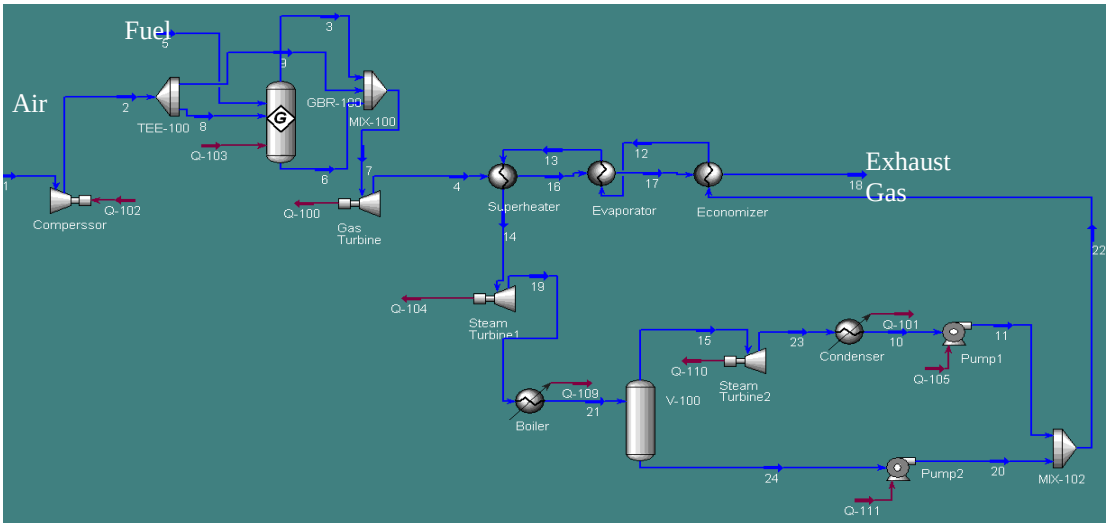

Figure 31: HYSYS model for combined cycle with entire steam diverted configuration.

3.6.1.4 Parallel Steam Turbines Configuration

This configuration, shown in Figure 32, has two steam turbines in parallel. One of them has a high condensing temperature that serves the boiler of the stripper. The other one has atmospheric condensing temperature. The resulting net power output with this configuration is 164.7 MW.

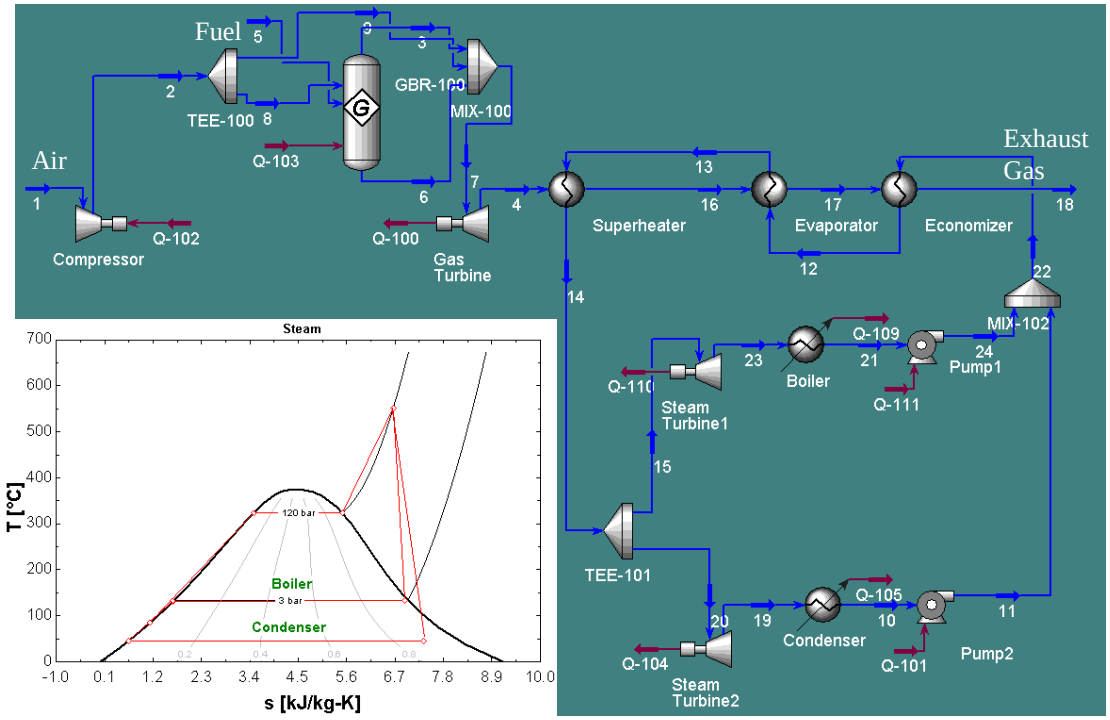

Figure 32: HYSYS model for combined cycle with parallel steam turbines configuration and its T-s diagram.

3.6.1.5 Exhaust Gas Fired Stripper Configuration

This configuration, shown in Figure 33, uses the flue gas to regenerate the CO_2 in the stripper. The resulting net power output with this configuration is 148.3 MW. Since the exhaust gas temperature is 140^{o}C and the stripper boiler load is 70.42 MW, this creates a high quality of heat in the flue gas at a temperature of 290^{o}C lost in regenerating the CO_2 in the stripper which requires a hot fluid temperature around 130^{o}C only. This explains why this configuration has the least net power generated compared to the other configurations.

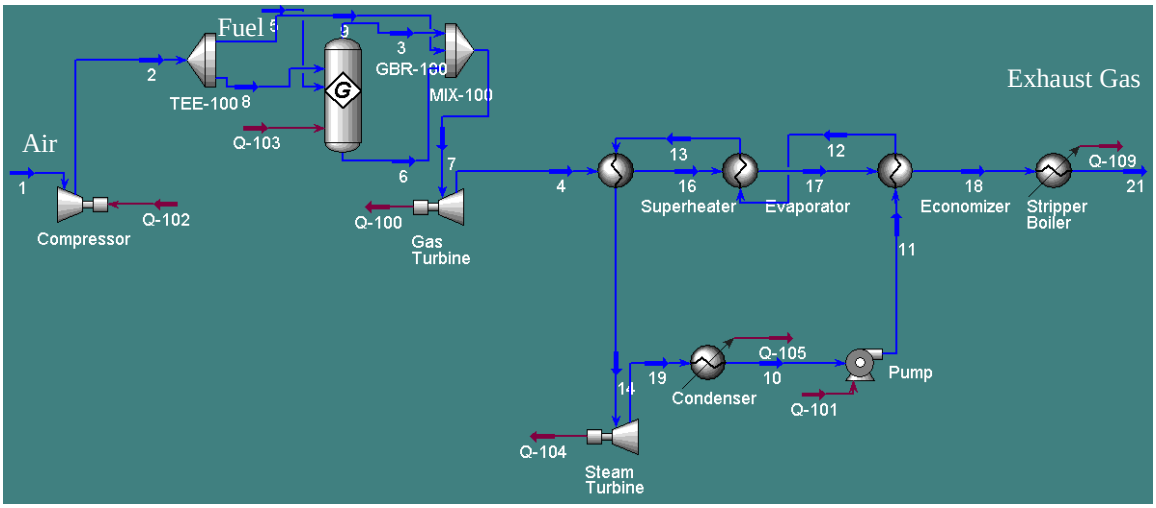

Figure 33: HYSYS model for combined cycle with exhaust gas fired stripper configuration

3.6.1.6 Steam Cycle Verification

The High Temperature Condenser configuration model in HYSYS was verified against EES with discrepancy of less than 3%. The verification results are shown in Table 20.

Table 20: Verification results for the steam cycle model.

	EES	HYSYS	Discrepancy (%)
W_{Pump} (MW)	2.3	2.4	2.7
$W_{Turbine}$ (MW)	64.2	63.3	-1.3
Efficiency (%)	38.2	37.4	-2.0
Steam mass flow (kg/s)	78.8	79.4	0.7
Condenser load (MW)	161.9	162.8	0.5

3.6.1.7 Steam Cycle Optimization

The developed steam cycle configurations were optimized using GA of Matlab optimization toolbox. The GA tuning parameters are listed in Table 5. The objective function of the optimization is to increase power production of the steam cycles. The variables of the optimization are (1) steam mass flow rate, (2) steam superheat temperature, (3) steam pressure, and (4) steam split ratio in case of steam splitting configurations (partial steam extraction and parallel steam turbines

configurations). The range of the optimization variables is taken to be ±20% of the baseline values except for the steam pressure where it was limited to just below the critical point pressure. The optimization's seven constraints with limits taken from the baseline model are listed as follow:

1) Temperature of the exhaust gas after HRSG ≥ 140^{o}C
2) Extracted steam pressure ≥ 3 bar
3) Extracted steam load = 70.42 MW
4) Turbines outlet vapor quality ≥ 0.87
5) Economizer, evaporator, and superheater heat exchanger pinch temp. ≥ 3 K

The results of the optimization are listed in Table 21 and plotted in Figure 34. The difference in the gas turbine power is due to different back pressure. The exhaust gas in configurations with CCS needs to be at a higher pressure to overcome the pressure drop resulted from the exhaust gas cooling heat exchangers and CO_2 absorber column. For example, the assumed exhaust pressure after the gas turbine is 1.55 bar for Diverting the Entire Steam Flow configuration whereas it is 1.16 bar for baseline NGCC without CCS configuration. Higher exhaust pressure resulted in higher exhaust temperature leaving the gas turbine. Thus, higher heat is available in the HRSG which made steam cycles with CCS produces more power than steam cycles without CCS but the total NGCC power consumption is different. The optimization resulted in steam cycle power increase from 1.88% to 7.96%. In all configurations the optimum boiler pressure and superheat temperature were increased as expected from Carnot cycle efficiency. The highest NGCC power producing configuration is the Parallel Steam Turbines configuration, producing 169.18 MW

power. Then the second one is the Diverting the Entire Steam Flow configuration, producing 168.23 MW NGCC power.

Table 21: Optimization results of the developed configurations.

		Baseline					
Configuration	GT Power (MW)	ST Power (MW)	m_{steam} (kg/s)	T_{sh} (^oC)	P_{boiler} (bar)	Split Ratio	NGCC Power (MW)
BS NO CCS	119	70.09	61.11	540	120	-	189.09
Diverting the Entire Steam Flow	94.7	68.11	71.65	552	120	-	162.81
Partial Steam Extraction	94.7	68.11	70.94	552	120	0.44	162.81
Parallel Steam Turbines	94.7	69.96	71.75	552	120	0.453	164.66
Exhaust Gas Fired Stripper	93.57	54.73	46.81	556.7	120	-	148.3
High Temp. Condenser (Higher T_{FG})	106.6	55.41	79.39	510.3	200	-	162.01
High Temp. Condenser	94.7	60.93	79.39	565.9	210	-	155.63
	Optimum						
	ST Power (MW)	m_{steam} (kg/s)	T_{sh} (^oC)	P_{boiler} (bar)	Split Ratio	CC Enh-ancement (MW)	CC Enh-ancement (%)	NGCC Power (MW)
BS NO CCS	71.37	60.712	559.01	140.95	-	1.27	1.82	190.37
Diverting the Entire Steam Flow	73.53	71.25	608.26	219.96	-	5.42	7.96	168.23
Partial Steam Extraction	72.61	70	592.9	141	0.46	4.498	6.6	167.31
Parallel Steam Turbines	74.48	70.46	608.26	192.26	0.468	4.52	6.46	169.18
Exhaust Gas Fired Stripper	57.53	46.07	610.53	194.6	-	2.8	5.12	151.1
High Temp. Condenser (Higher T_{FG})	58.62	74.09	584.16	220	-	3.21	5.78	165.22
High Temp. Condenser	62.85	76.44	608.26	220	-	1.92	3.15	157.55

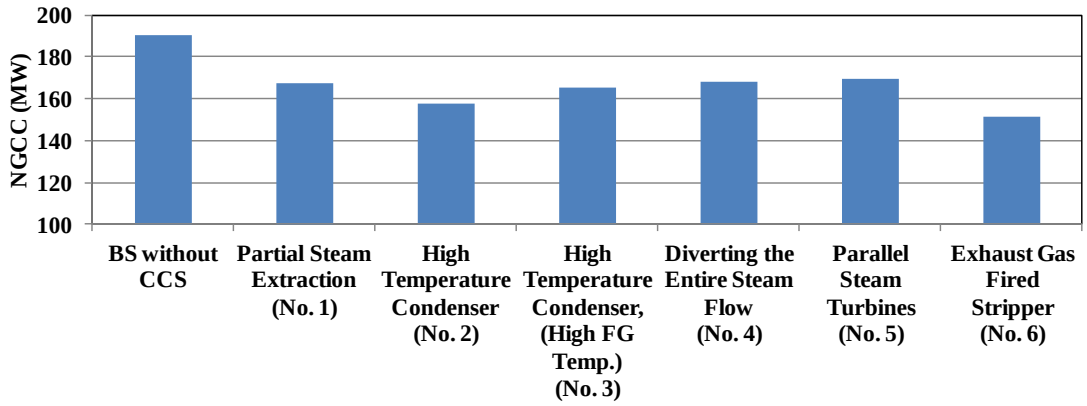

Figure 34: Optimized NGCC power for the developed configurations.

3.6.2 CO_2 Removal Cycle

CO_2 capturing cycle based on CO_2 absorption in amine solvent was developed in HYSYS software. Aspen Tech, the developer of HYSYS software, has implemented an Amine Package which contains thermodynamic models developed by D.B. Robinson & Associates for their proprietary amine plant simulator, AMSIM. Aspen Tech has validated this Amine Package in HYSYS software against experimental data [110].

The developed CO_2 absorption model is based on MEA solvent. The model, shown in Figure 35, consists of an absorption column and a stripping column. There is a liquid-to-liquid heat exchanger that preheats the rich solution through the use of the waste heat from the lean solution. The Q condenser represents the seawater condenser whereas the Q boiler represents the steam that comes from the steam power cycle for regenerating the CO_2.

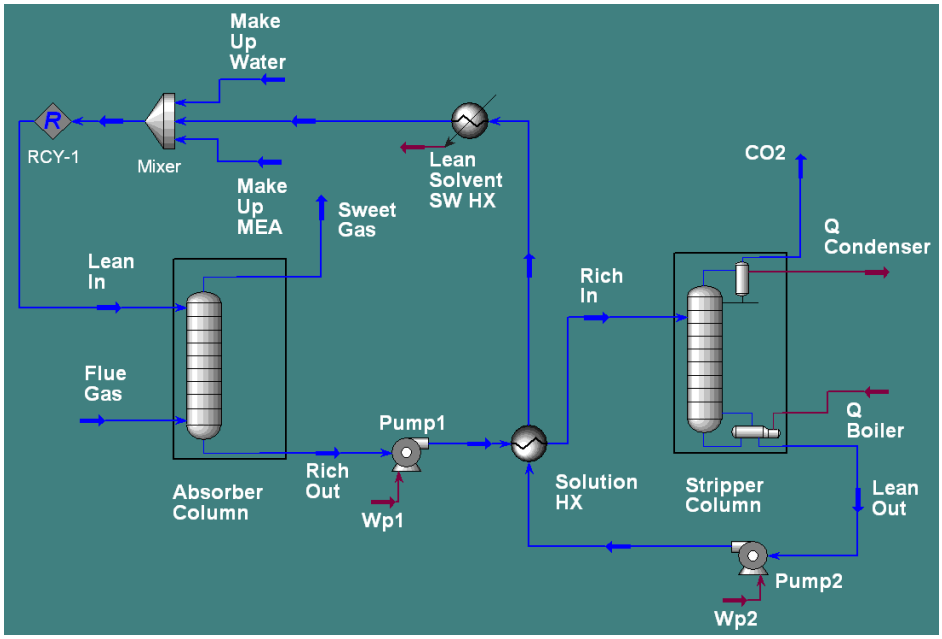

Figure 35: CO_2 removal cycle HYSYS model

The rich out/in stream is a liquid stream that is rich in CO_2. The opposite is true for the lean out/in stream. The sweet gas stream is a gas stream that does not contain CO_2 (mainly N_2, O_2, and NO). The CO_2 stream is a stream that has mainly CO_2 and H_2O. Some make up water and MEA are introduced to the cycle in the mixer component to account for the losses in the process and to maintain a specified solution concentration (e.g. 30% MEA by weight).

3.6.2.1 CO_2 Removal Cycle Model Validation

Since AspenTech has not published their validation results for the HYSYS Amine Package, validation for the developed CO_2 capturing cycle model was carried out against two experimental cases from a series of experiments done by Dugas [23]. Dugas's experiments were based on a close-looped absorption/stripping pilot plant with 42.7 cm ID columns, which were used to capture CO_2 using an 32.5 wt% aqueous MEA solution. Both the absorber and stripper contained 6.1 m. of packing.

The packing type for the absorber and stripper columns is IMTP #40 and Flexipac 1Y, respectively. The number of stages of both columns is 20.

Table **22** lists the developed HYSYS model results against experiments (Case 47) and simulation results from ASPEN Plus model that was developed by AspenTech [110]. This work results from the HYSYS model predicted the measurements more accurately than did the ASPEN Plus model. The temperature profiles in the absorber and stripper columns are shown in Figure 36 and Figure 37, respectively.

The temperature profiles, stream loadings and CO_2 absorption were predicted with good agreements but not the condenser and boiler loads. The reasons for the discrepancy in the condenser and boiler loads as follow: first, Dugas used an electric heater instead of the solution heat exchanger to provide part of the sensible heat component, which ranged from 10% to 64% of the total heat duty. According to Dugas, the electric heater, which is responsible for part of the sensible heat, was undersized. Therefore, more steam is required to heat the solution (sensible and latent heat) in the stripper boiler of the HYSYS model. The second source of error, according to Dugas, is the estimated heat loss of the stripping column, which ranged from 5% to 35% of the total heat duty. Dugas used an empirical equation for estimating the heat loss of a distillation column. The equation was previously developed with distillation testing.

Table 22: CO_2 removal cycle model validation against Case 47 from Dugas's experiments and ASPEN Plus model by AspenTech.

	This work HYSYS model	Measurement (Case 47)	ASPEN Plus model by AspenTech
Pure CO_2 (kg/h)	94.6	92	98.2
Q Boiler (MJ/hr)	325	738	-
Q Condenser (MJ/hr)	28.9	445	-
CO_2 Removal (%)	63.4	69	65.53
CO_2 Loading of Rich In, MolCO_2/MolMEA	0.501	0.539	0.473
CO_2 Loading of Lean In, MolCO_2/MolMEA	0.281	0.281	0.281
CO_2 Loading of Lean Out, MolCO_2/MolMEA	0.314	0.286	0.28
Absorbed CO_2 (kg/hr)	110	104	-

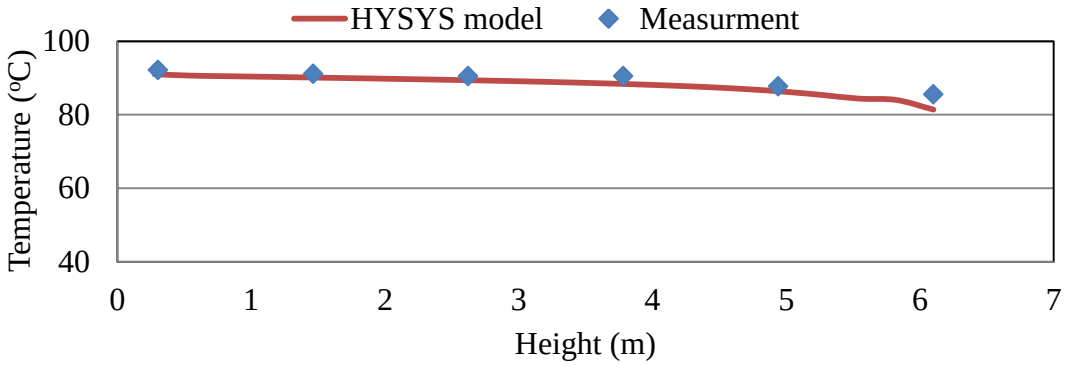

Figure 36: Stripper temperature profile from the HYSYS model and experiments (Case 47).

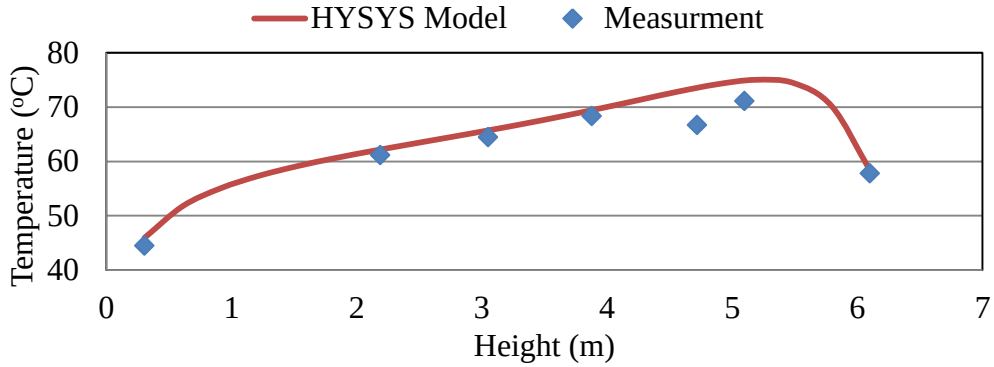

Figure 37: Absorber temperature profile from the HYSYS model and experiments (Case 47).

A second case was also validated from the same pilot plant. The validation results are shown against experiments (Case 36) and simulation results from an ASPEN Plus model that was developed by Dugas. The model matched the experimental data very well, with a maximum error of 3.32%, except in the condenser heat. The reason why the condenser heat has a high error is that the CO_2/H_2O temperature in the experiment after the condenser is unknown. If this temperature was known, the condenser heat would have been predicted more accurately.

Table 23: CO_2 removal cycle model validation against Case 36 from Dugas's experiments and ASPEN Plus model.

	This work HYSYS model	Measurement (Case 36)	ASPEN by Douglas
Q Boiler (MJ/hr)	540.4	559	-
Q Condenser (MJ/hr)	104	144	-
CO_2 Removal (%)	97.8	95	95
CO_2 Loading of Rich In, $MolCO_2/MolMEA$	0.411	0.425	0.425
CO_2 Loading of Lean In, $MolCO_2/MolMEA$	0.284	0.284	0.284
CO_2 Loading of Lean Out, $MolCO_2/MolMEA$	0.284	0.279	-
Absorbed CO_2 (kg/hr)	79.24	77	-

The absorber temperature profile from the HYSYS model and the experiments of Case 36 are shown in Figure 38. The developed HYSYS model predicted the absorber temperature profile more accurately than Douglas ASPEN Plus model as shown in Figure 39.

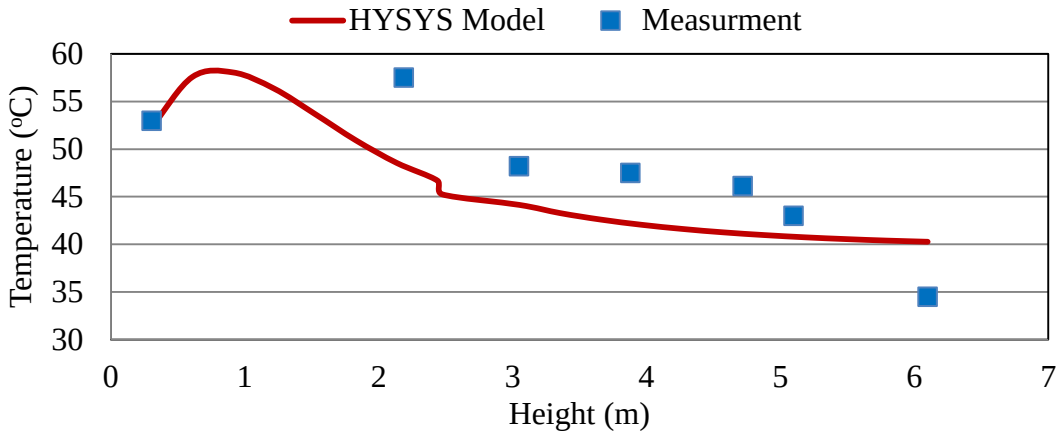

Figure 38: Absorber temperature profile from the HYSYS model and experiments (Case 36).

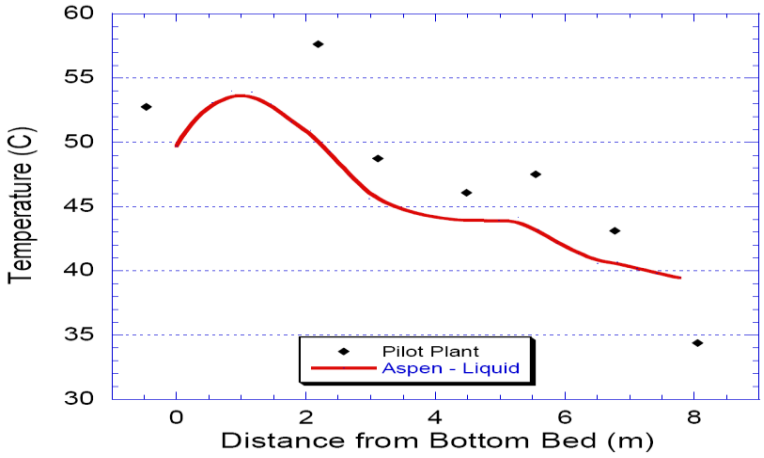

Figure 39: Absorber temperature profile from Dugas ASPEN Plus model and experiments (Case 36) [23].

3.6.2.2 CO_2 Removal Cycle Model Verification

Another CO_2 removal cycle was developed using HYSYS software. The model was verified against Lars Erik's HYSYS model, where he developed a CO_2 absorption cycle for a 500 MW combined cycle power plant [67]. The CO_2 solvent for his model is 29% MEA by mass. His absorber and stripper columns have 10 and 6 stages, respectively. The verification was done on five points that represent the

variations of the CO_2 removal efficiency and energy consumption per kg of CO_2 against flue gas temperature as shown in Figure 40. The developed model matched Lars Erik's model adequately with a maximum discrepancy of 1.56%.

Figure 40 also shows that the Amine property package in HYSYS was able to predict the improvements in the CO_2 removal efficiency as the flue gas temperature decreases as was predicted from Eq. 5. According to Figure 40, about 5.5% more CO_2 is captured at 30°C as compared to 50°C.

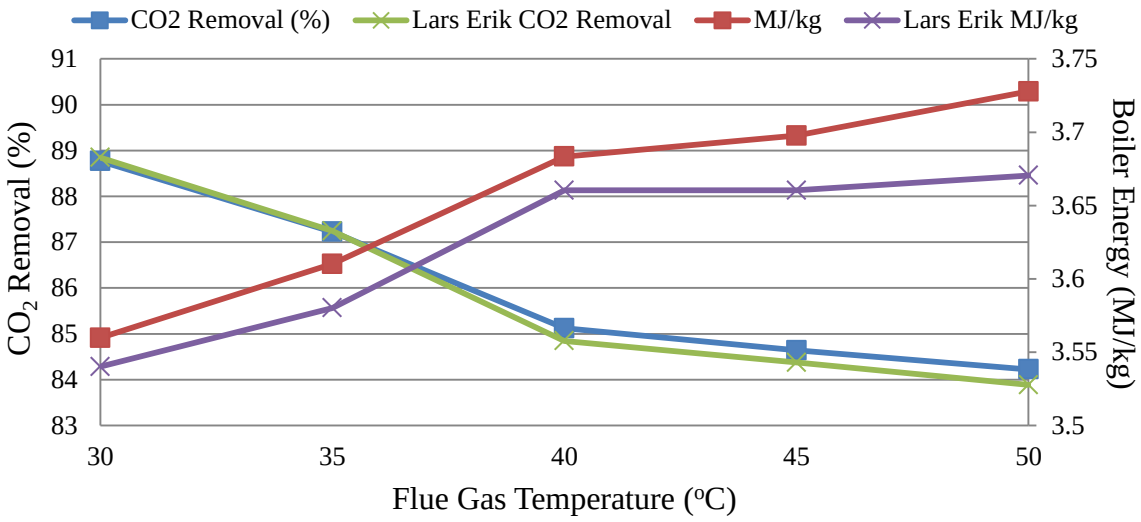

Figure 40: CO_2 removal cycle model against Lars Erik's model. This graph shows the performance of the CO_2 removal cycle at different flue gas temperatures.

3.6.2.3 CO_2 Removal Cycle Model for the APCI LNG Plant Gas Turbine Driver

CO_2 removal cycle based on CO_2 absorption in MEA solvent was developed for the APCI LNG plant gas turbine driver. When the gas turbine is coupled with a steam cycle, net power produced is 189.1 MW. The exhaust gas contains 74 Tons of CO_2/hr, and its compositions are listed in Table 24.

Table 24: Exhaust Gas compositions of the APCI LNG plant gas turbine driver

Component	Mass fraction
O_2	1.57e-01
N_2	7.53e-01
CO_2	4.88e-02
H_2O	4.00e-02
NO_2	1.91e-05
NO	6.06e-04

The developed CO_2 removal cycle using HYSYS software, shown in Figure 35, has columns parameters similar to Lars Erik's model. The columns parameters are listed in Table 25. In order to capture 93.59% of the 74 tons of CO_2 emitted per hour at a 40^oC flue gas temperature, the CO_2 removal model estimated that 70.42 MW of steam is needed in the boiler of the stripper.

Table 25: Absorber and stripper columns parameters of the CO_2 removal cycle

Lean amine temperature	40^oC
Lean amine pressure	1 bar
Liquid/gas ratio in the absorber	0.942
MEA content in lean amine	28.3% mass
CO_2 in lean amine	5.3% mass
Number of stages in absorber	10
Column packing type	Sieve packing
Column height/diameter	6.1/1.5 m
Rich amine pump pressure	2.2 bar
Lean amine pump pressure	2.2 bar
Heated rich amine temperature	105^oC
Number of stages in stripper	6
Reboiler temperature	119^oC
Lean amine pump pressure	2.2 bar

3.7 Efficiency Enhancement Options

This section describes the energy efficiency enhancement options proposed in Figure 24.

3.7.1 Using Waste Heat to Preheat the Water before HRSG

One of the proposed uses of the waste heat (Figure 28) was to preheat the water before HRSG which will make the HRSG generates more steam for equivalent heat. A preheater heat exchanger that uses a portion of the stripper condenser heat (23 MW at 105^{o}C to 80^{o}C) was placed between the HRSG and the pumps to preheat the water to 102^{o}C in all configurations except High Temperature Condenser Configuration because the condensed water temperature is at 133^{o}C. The results show, Table 26, that the highest power increase was 7.65% in the Exhaust Gas Fired Stripper Configuration because this configuration has the lowest condensing temperature (45^{o}C) or feed water temperature to the HRSG without the preheater. In order to compare different waste heat utilization options, the power gain from waste heat ratio (defined in Eq. 6) was calculated for feedwater preheating and found to vary from 0.31 to 0.37 MW of power/MW of waste heat.

$$\text{Ratio of power gain to waste heat} = \frac{\text{Net power gain}}{\text{Amount of waste heat used}} \quad (6)$$

Table 26: Steam cycles power using preheater before HRSG.

Configurations	Power w/o Preheater (MW)	Preheater Heat (MW)	Power w/ Preheater (MW)	Power Increase (MW)	Power Increase (%)	NGCC Power (MW)
Diverting the Entire Steam Flow	73.53	4.56	75.21	1.68	2.28	169.91
Parallel Steam Turbines	74.48	4.66	76.02	1.55	2.08	170.72
Partial Steam Extraction	72.61	7.53	74.98	2.37	3.26	169.67
Exhaust Gas Fired Stripper	57.53	11.79	61.93	4.4	7.65	155.5

3.7.2 Using Absorption Chillers to Cool the Feed Gas to the Absorber

An absorption chiller is a heat-driven device which provides cooling in the evaporator by using heat in the desorber as the primary energy source different from the case of vapor compression cycles (VCCs) using electricity. When waste heat is used to operate the absorption chillers, the cooling provided is essentially "free" cooling. Detailed description about modeling of absorption chillers can be found in Somers *et al.* [117]. A simple schematic diagram of a single-effect absorption chiller is shown in Figure 41.

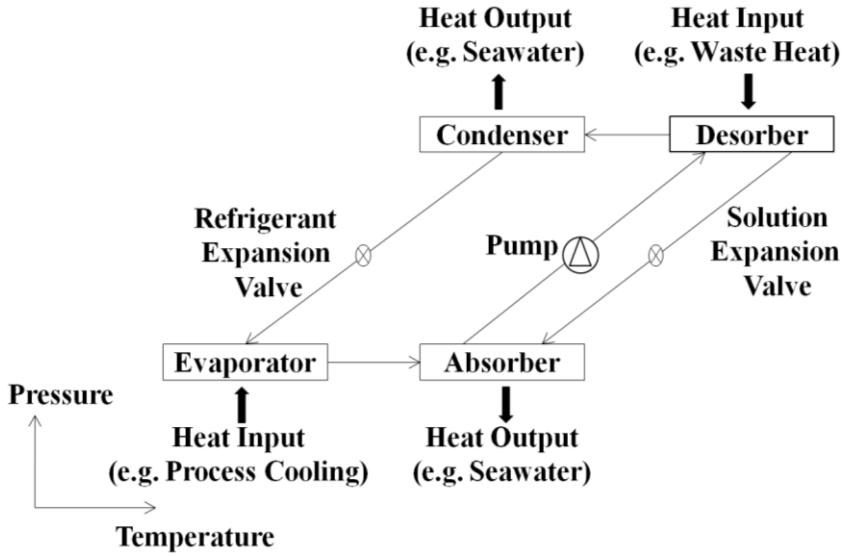

Figure 41: Schematic diagram of a single-effect absorption chiller.

According to the proposed CCS configuration in Figure 24, two absorption chillers were introduced upstream from the CO_2 removal cycle. One absorption chiller is single-effect water/LiBr, which has a typical COP of about 0.75 and it utilizes the waste heat from 140 to 105^{o}C. The second absorption chiller is half-effect

water/LiBr which has a typical COP of about 0.37 and it utilizes the waste heat from 105 to 80°C. The COP of absorption chillers is defined as follows:

$$COP\ of\ absorption\ chillers\ = \frac{Evaporator\ cooling\ output}{Heat\ input\ to\ Desorber} \quad (7)$$

The absorption chillers cool the flue gas from 40°C (sea water cooling temperature) to 27°C. The configuration of the chillers capacity estimation HYSYS model is shown in Figure 42. The estimated absorption chillers capacities are tabulated in Table 27.

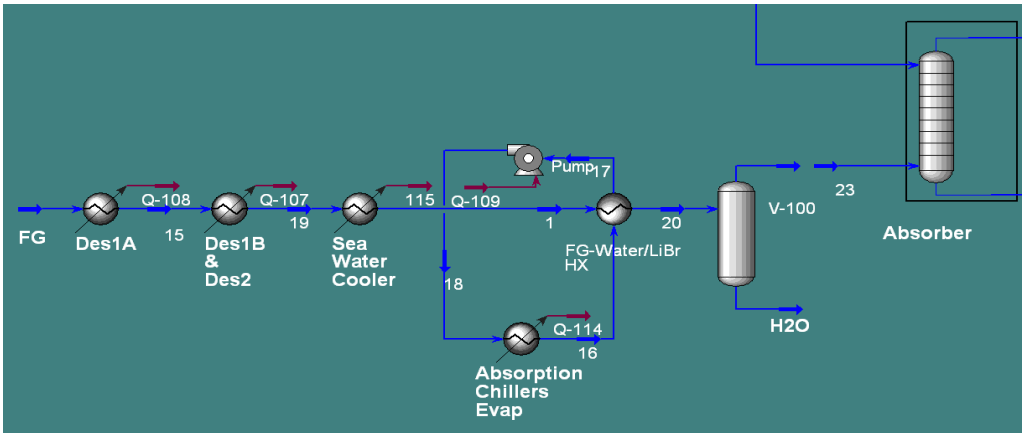

Figure 42: Absorption chillers configuration.

Table 27: Estimated absorption chillers capacities.

Absorption Chillers	Capacity
Abs. chillers 1A, (140-105°C), COP=0.75	15.76 MW
Abs. chillers 1B, (105-80°C), COP=0.37	
Abs. chillers 2, (105-80°C), COP=0.37	8.51 MW

3.7.3 Using Waste Heat to Cool Inlet Air to Gas Turbine Using Absorption Chillers

One of the proposed uses of the waste heat (Figure 28) was to use absorption chillers powered by waste heat for cooling the inlet air to the gas turbine. Inlet air

cooling reduces the air density which allows the combustor to take more air mass flow rate. At a fixed air volume flow rate of 20,320 m^3/minute and air-fuel mass ratio of 18.12%, the effect of air cooling was investigated on the High Temperature Condenser configuration and the results are tabulated in Table 28.

The results, Figure 43, show that 0.507 MW or 0.33% NGCC power loss for every degree temperature increase. Considering the gas turbine only, 0.46 MW or 0.49% power is lost for every degree temperature increase. The ratio of power gain to waste heat was calculated to be 0.89 MW of power/MW of waste heat. The increase in fuel consumption rate is the reason why only a slight increase in the overall efficiency was observed. It is to be noted that using gas turbine inlet air cooling increases the amount of the CO_2 to be captured and pressurized because the increase in amount of consumed fuel.

Table 28: Effect of gas turbine inlet air cooling on configuration 5. $Q_{desorper}$ is the heat available in the condenser after the stripper boiler.

T_{air} (^oC)	m_{air} (kg/s)	$Q_{Cooling}$ (MW)	W_{GT} (MW)	$Q_{Desorper}$ (MW)	W_{ST} (MW)	$W_{GT}+W_{ST}$ (MW)	Efficiency (%)
50	368.59	0	78.87	88.01	59.32	138.19	41.35
45	374.4	1.9	80.92	88.56	59.52	140.44	41.37
40	380.39	3.87	83.03	89.14	59.74	142.77	41.40
35	386.58	5.89	85.21	89.37	59.96	145.17	41.42
30	392.98	7.98	87.47	90.35	60.18	147.65	41.44
25	399.59	10.14	89.8	90.98	60.42	150.22	41.47
20	406.43	12.37	92.21	91.64	60.67	152.88	41.49
15	413.51	14.67	94.7	92.33	60.93	155.63	41.51
10	420.83	17.05	97.29	93.03	61.19	158.48	41.54

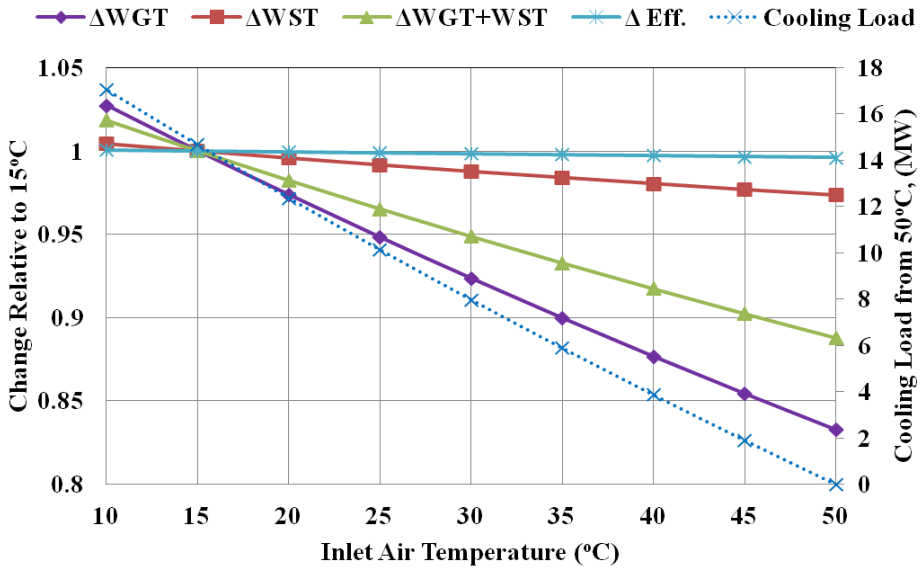

Figure 43: Change in gas turbine and steam turbine efficiencies with inlet air temperature.

Pressure drop in inlet air cooler was assumed to be negligible in Figure 43. A pressure drop of 0.24 kPa only was considered in a vendor's data [118]. High pressure drop in inlet air cooler could result in power loss with the addition of inlet air cooler, as shown in Figure 44 where a constant power line divides the figure into two regions. If the intercooler has low pressure drop at a given cooling temperature, power would be gained from the addition of the intercooler (Bottom region in Figure 43) and vice versa.

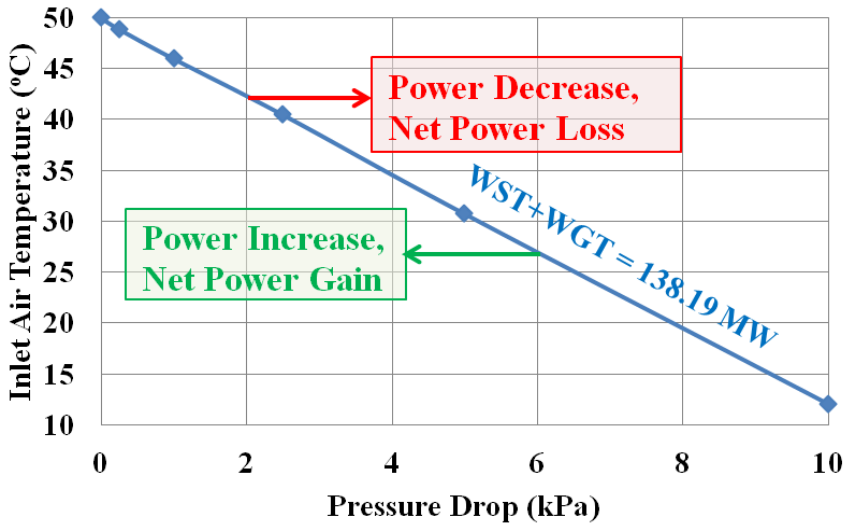

Figure 44: Effect of pressure drop in inlet air cooler on NGCC power output.

3.7.4 Using Waste Heat to Power an Organic Rankine Cycle

One of the proposed uses of the waste heat (Figure 28) was to run an ORC. ORC is a power producing cycle which can run by a waste heat. An ORC model was developed using HYSYS software as shown in Figure 45. The working fluid is evaporated to a high temperature, e.g., 130^{o}C, in a boiler and then expanded in a turbine. The expanded fluid then condenses in a condenser and then pumped in a pump to the boiler pressure.

The developed model was validated against experimental data from Quoilin *et al.* [119]. The working fluid used is R123. The equation of state used in this model is the Peng-Robinson equation of state. The experimental setup is shown in Figure 46. The validation results are tabulated Table 29 and plotted in Figure 47.

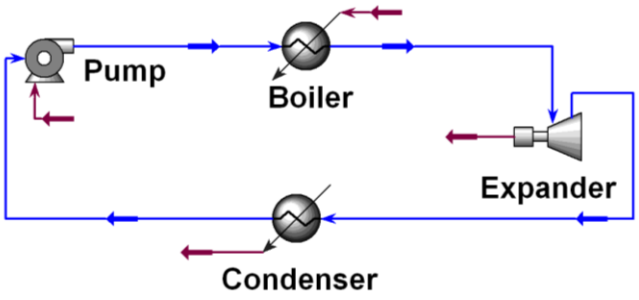

Figure 45: HYSYS Organic Rankine Cycle model.

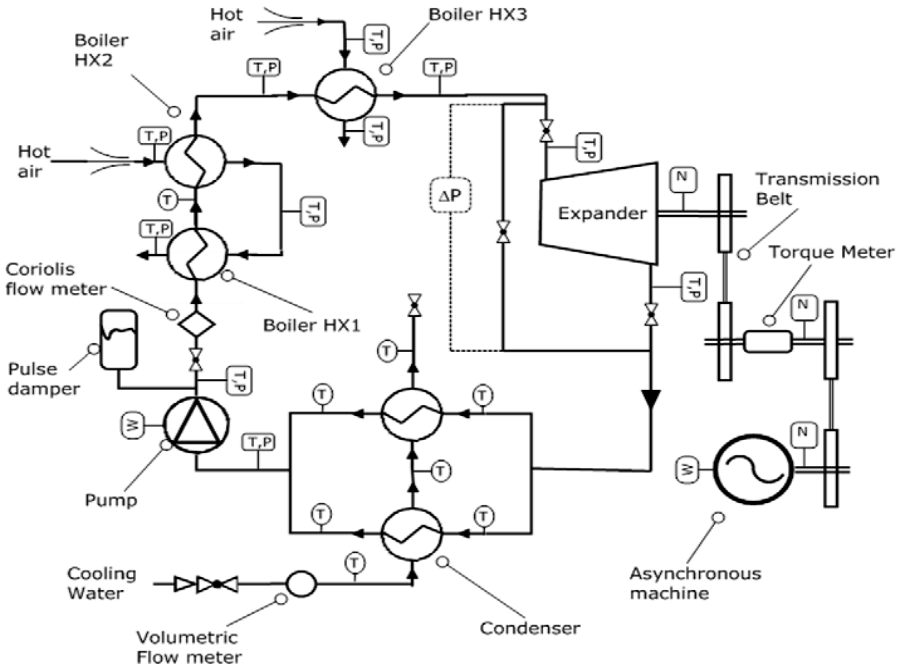

Figure 46: Organic Rankine Cycle model experimental setup Quoilin *et al.* [119].

Table 29: ORC HYSYS model validation results.

Test Case	061107 A		061031 B		061110 A		061108 A		061110 B	
	Experimental Data	HYSYS Model	Experimental Data	HYSYS Model	Experimental Data	HYSYS Model	Experimental Data	HYSYS Model	Experimental Data	HYSYS Model
Superheating (K)	36.01	34.6	31.26	29.72	61.29	58.728	62.52	60.343	44.38	41.98
Expander Power (W)	1034	1018.3	1067	1047.7	1015	991.2	708.7	703.4	780.7	768.9
Cycle Efficiency	4.9	5.343	5.4	5.402	6.1	6.26	4	4.22	5.5	5.63

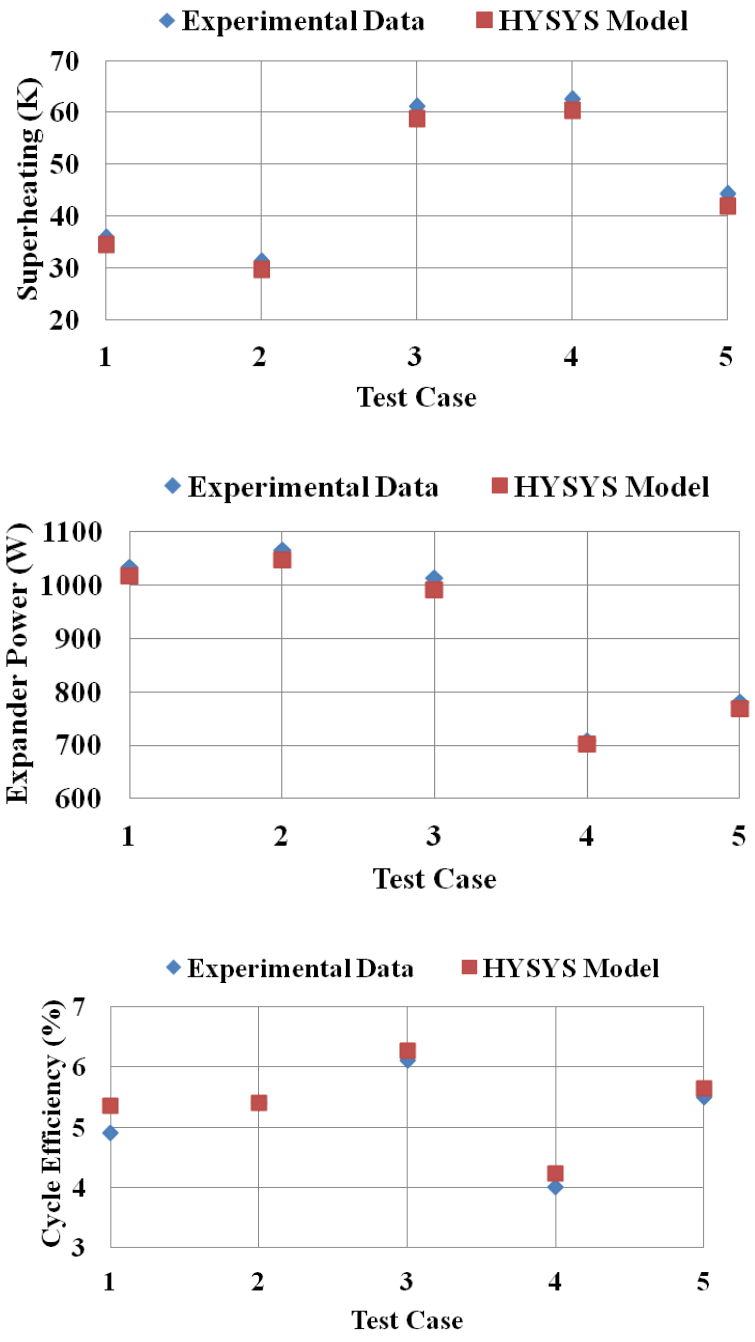

Figure 47: ORC HYSYS model validation results.

Twenty four working fluids were investigated for the ORC that run by a 92.33 MW waste heat at 133°C and 40°C condensing temperature. The investigated refrigerants were proposed in the literature [120], [121] and [122]. The results show that R11 and R141b resulted in the highest efficiency with an efficiency of 15.5% and

14.93%, respectively. From the efficiency of Rankine power cycle, working fluids with smaller latent heat ratios are expected to have higher efficiency. The results are shown in Table 30 and in Figure 48.

$$\eta = 1 - \frac{Q_{condenser}}{Q_{boiler}} \quad (8)$$

Table 30: Different working fluids investigated for the ORC.

Working Fluids	Expander Power (MW)	Boiler Heat (MW)	Pump Power (MW)	Efficiency (%)
R134a	13.43	92.33	3.57	10.67
N-Pentane	13.24	92.33	0.40	13.91
C_7H_8	9.12	92.33	0.04	9.83
N-Butane	13.86	92.33	1.13	13.8
Benzene	12.99	92.33	0.09	13.96
N-Hexane	12.40	92.33	0.17	13.24
I-Butane	13.93	92.33	1.13	13.86
R113	12.99	92.33	0.31	13.74
R245fa	13.78	92.33	5.04	9.47
i-Pentane	13.05	92.33	0.49	13.6
R-152a	12.85	92.33	2.10	11.64
R-143a	17.73	92.33	7.97	10.57
Hexamethyldisiloxane	9.91	92.33	0.10	10.63
R12	11.94	92.33	1.50	11.3
Water	13.36	92.33	0.01	14.46
R112A	12.69	92.33	0.10	13.64
R1270	13.65	92.33	3.52	10.97
Cyclohexane	13.16	92.33	0.11	14.14
N-heptane	11.22	92.33	0.08	12.06
N-Propylbenzene	6.09	92.33	0.01	6.59
Ethylbenzene	8.90	92.33	0.02	9.61
R123	14.03	92.33	0.527	14.62
R141b	14.20	92.33	0.412	14.93
R11	14.84	92.33	0.531	15.5

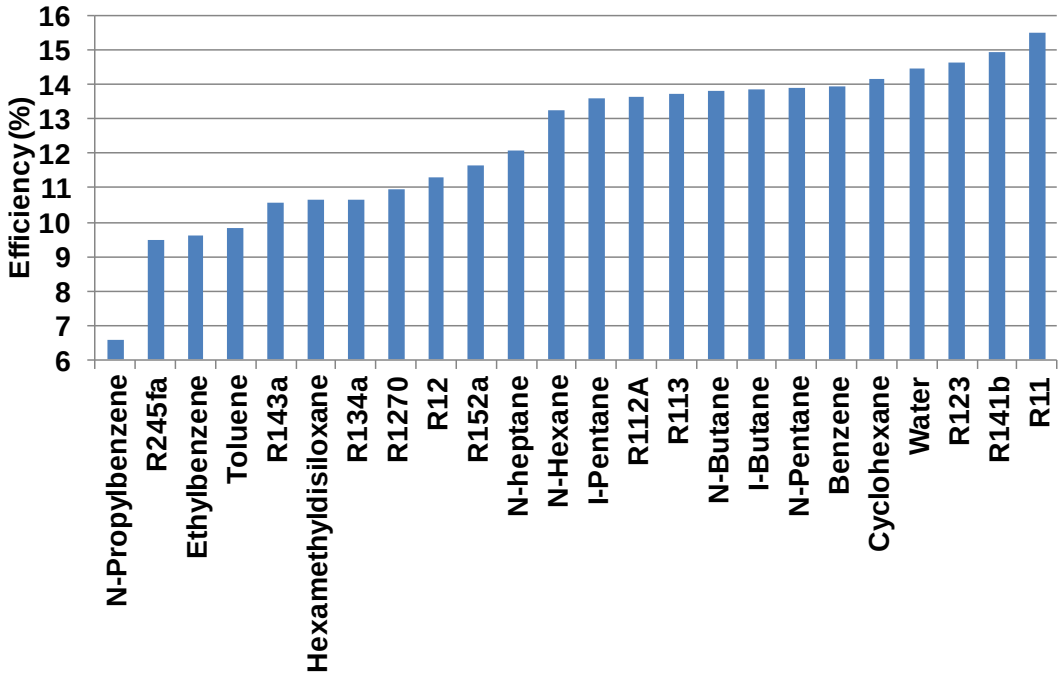

Figure 48: ORC efficiencies for different working fluids.

An ORC can be modified by introducing a recuperator heat exchanger to preheat the refrigerant before it goes to the boiler using the expanded fluid leaving the expander, as shown in Figure 49. Adding a recupator resulted in increasing the efficiency as shown in Table 31. This is due to the shape of the T-s diagram where a recupator is applicable with working fluid that has an inclined T-s diagram towards the superheated region. That is, a working fluid with larger specific heat (more complex molecule), has a T-s diagram skewed to the right [123]. Such working fluids experience larger entropy increase with temperature change. The T-s diagram for on ORC with R123 is shown in Figure 50. The power cycle shown in Figure 49 is a triple power cycle which would outperform the conventional NGCC if the low pressure steam cycle has lower efficiency than the ORC which is about 15%.

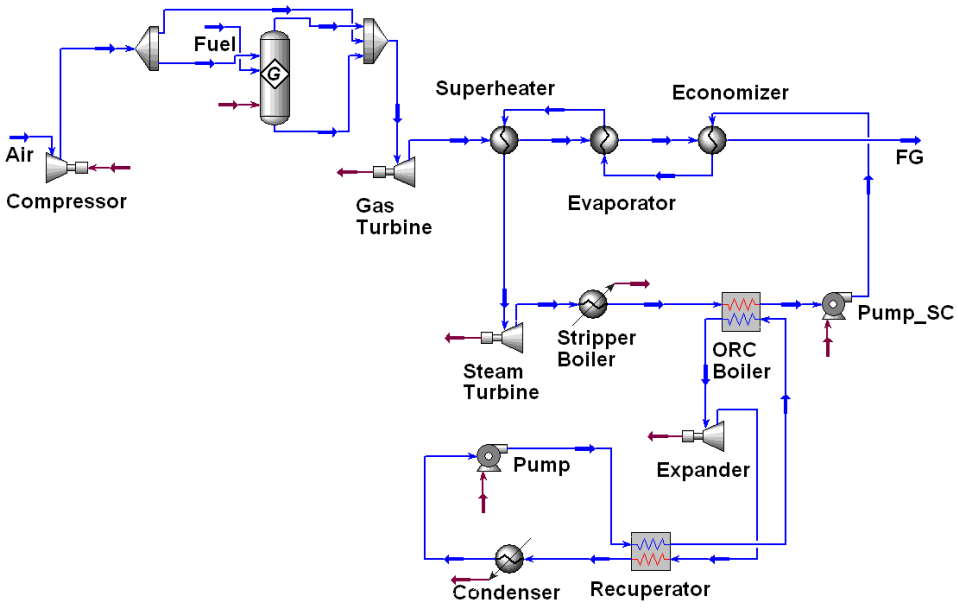

Figure 49: ORC with a recupator HX integrated with NGCC.

Table 31: Different working fluids investigated for the ORC with a recupator HX.

Working Fluids	Expander Power (MW)	Boiler Heat (MW)	Pump Power (MW)	Efficiency (%)
R123	14.72	92.33	0.570	15.331
R141b	14.65	92.33	0.447	15.381
R11	14.88	92.33	0.549	15.522
R113	14.94	92.33	0.364	15.787

The ORC model with a recupator heat exchanger was verified against EES, as shown in Table 32. The T-s diagram is shown in Figure 50.

Table 32: ORC with a recupator HX model verification.

Model	Expander Power (MW)	Boiler Heat (MW)	Expander Power (MW)	Pump Power (MW)	Efficiency (%)	Discrepancy Power	Discrepancy Efficiency
HYSYS	R123	14.72	92.33	0.570	15.33	-	-
EES	R123	15.02	92.33	0.576	15.64	2.0%	2.04%

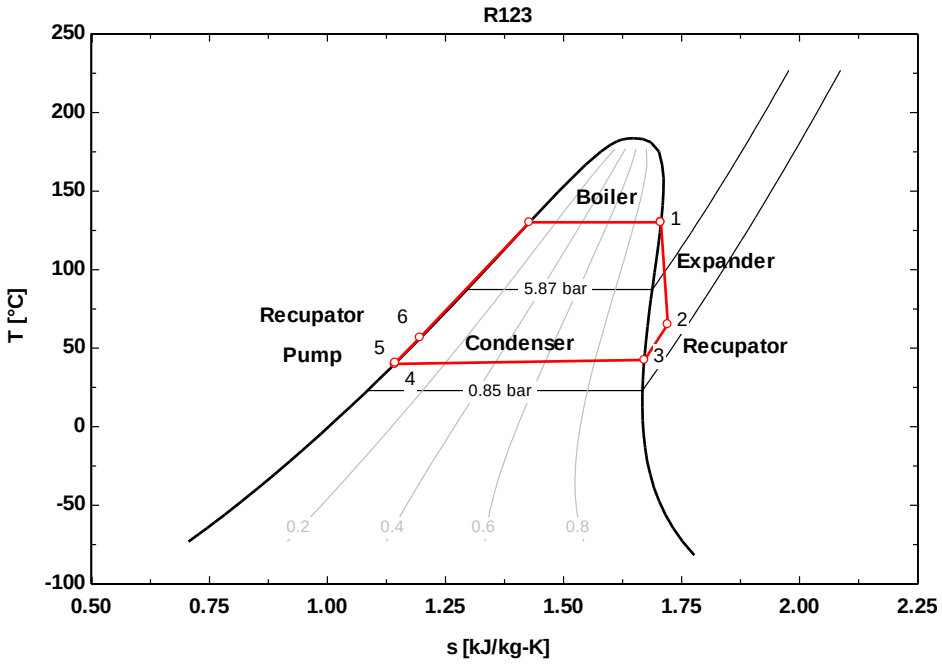

Figure 50: T-s Diagram for R123 ORC with a recupator HX.

3.7.5 Using Waste Heat to Reduce the APCI LNG Plant Power Consumption

Since the propane cycle in the APCI LNG plants cools the NG and the MCRs from atmospheric temperature to -30°C in five heat exchangers, one application is to eliminate some of the propane cycle evaporators by absorption chillers. Therefore, the liquefaction load of the APCI LNG plant or the power consumption is reduced. Detailed studies on absorption chillers integration with LNG plants can be found in Mortazavi et al. [1] or Kalinowski et al. [124].

3.7.5.1 Replacement of the 22°C, 9°C and -5°C Evaporators in the APCI LNG Plant by Absorption Chillers

The available waste heat in the combined cycle with a High Temperature Condenser configuration (Figure 30), which does not utilize the waste heat in the flue gas from 140°C to 80°C, is 85.97 MW. Part of this waste heat, 26.68 MW, is used to

cool the flue gas to 27^{o}C. The rest is used to cool the NG and MCR in the APCI LNG Plant to -2^{o}C by using absorption chillers. In other words, the 22^{o}C and 9^{o}C Evaporators were replaced by absorption chillers and the -5^{o}C Evaporator load was reduced by absorption chillers (Figure 13). Therefore, the propane cycle load was reduced. As a result, the power consumption of the propane cycle was reduced from 43.7 MW to 35.12 MW which is 8.58 MW or 19.63% power savings.

3.7.5.2 Replacement of the 22^{o}C and 9^{o}C Evaporators in the APCI LNG Plant by Absorption Chillers and Subcooling the Propane Cycle to 15^{o}C by Absorption Chillers

The available waste heat in the Combined Cycle with a High Temperature Condenser configuration (Figure 30) that does not utilizes the waste heat in the flue gas from 140^{o}C to 80^{o}C is 85.97 MW. Part of this waste heat, 26.68 MW, is used to cool the flue gas to 27^{o}C. The rest is used to subcool the propane refrigerant to 15^{o}C and cools the NG and MCR in the APCI LNG Plant to 12^{o}C by using absorption chillers. In other words, the 22^{o}C and 9^{o}C Evaporators were replaced by absorption chillers. Therefore, the propane cycle load was reduced. As a result, the power consumption of the propane cycle was reduced from 43.7 MW to 32 MW, which is 11.7 MW or 26.77% power savings.

3.7.5.3 Replacement of the 22^{o}C and 9^{o}C Evaporators by Absorption Chillers and Subcooling the Propane Cycle to 5^{o}C.

The available waste heat in the Combined Cycle with a High Temperature Condenser configuration (Figure 30) that also utilizes the waste heat in the flue gas from 140^{o}C to 80^{o}C is 116.6 MW. Part of this waste heat, 26.68 MW, is used to cool

the flue gas to 27°C. Other part, 78.97 MW, is used to subcool the propane refrigerant to 5°C and cools the NG and MCR in the APCI LNG Plant to 5°C by using absorption chillers. In other words, the 22°C and 9°C Evaporators were replaced by absorption chillers and the -5°C Evaporator load was reduced by absorption chillers. Therefore, the propane cycle load was reduced. As a result, the power consumption of the propane cycle was reduced from 43.7 MW to 28.69 MW, which is 15.01 MW or 34.29% power savings.

3.7.6 Using Liquefied and Pressurized CO_2 to Reduce the APCI LNG Plant Power Consumption

The proposed idea of using the cold CO_2 in natural gas liquefaction and MCR subcooling was investigated and modeled using HYSYS software as shown in Figure 51. The basic idea is that the cold CO_2 (at -48°C after liquefaction and pumping to injection pressure) will reduce the cooling load of the propane cycle. The resulting savings in power consumption is 1.32 MW or 3.02%. The reason why this savings is not big is because that the flow rate of the CO_2 is very small compared to the mass flow rate of the propane (mass flow ratio is 7.32%).

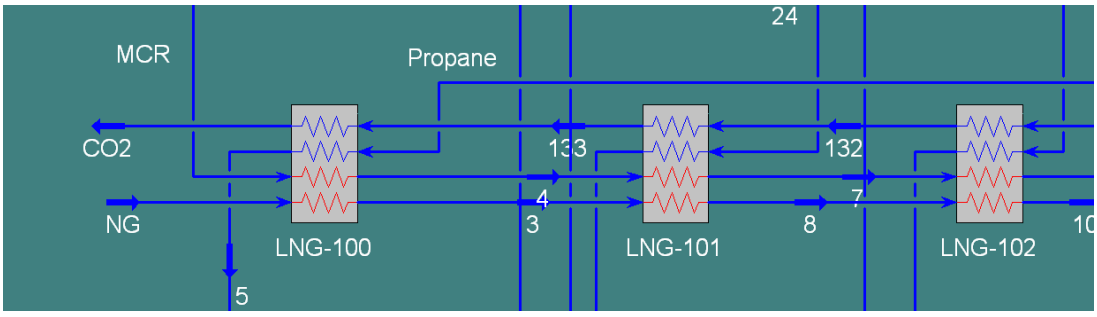

Figure 51: APCI LNG plant integration with the cold CO_2. Three out of five heat exchangers is shown in the Figure 13.

3.8 Performance Comparison

The identified waste heat sources and uses were evaluated. Using different applications for the waste heat resulted in different power gains as shown in Table 33 and Figure 52. The highest value was for using the waste heat for inlet-air cooling and then feedwater preheating but they can only utilize a fraction of the available waste heat so that no temperature cross occurs inside the heat exchanger.

Table 33: Maximum power gain from waste heat ratio for different waste heat application.

Waste Heat Application	Ratio of Power Gain to Waste Heat (Eq. 6)
Preheat Feed Water to HRSG	0.37
Precool the NG and MCR Using Absorption Chillers	0.19
Precool the NG and MCR Using Liquid CO_2	0.35
Subcooling and Precooling the CO_2 VCC Using Liquid CO_2	0.52
Cool Inlet-Air to the Gas Turbine Using Absorption Chillers	0.89
Power an Organic Rankine Cycle	0.16

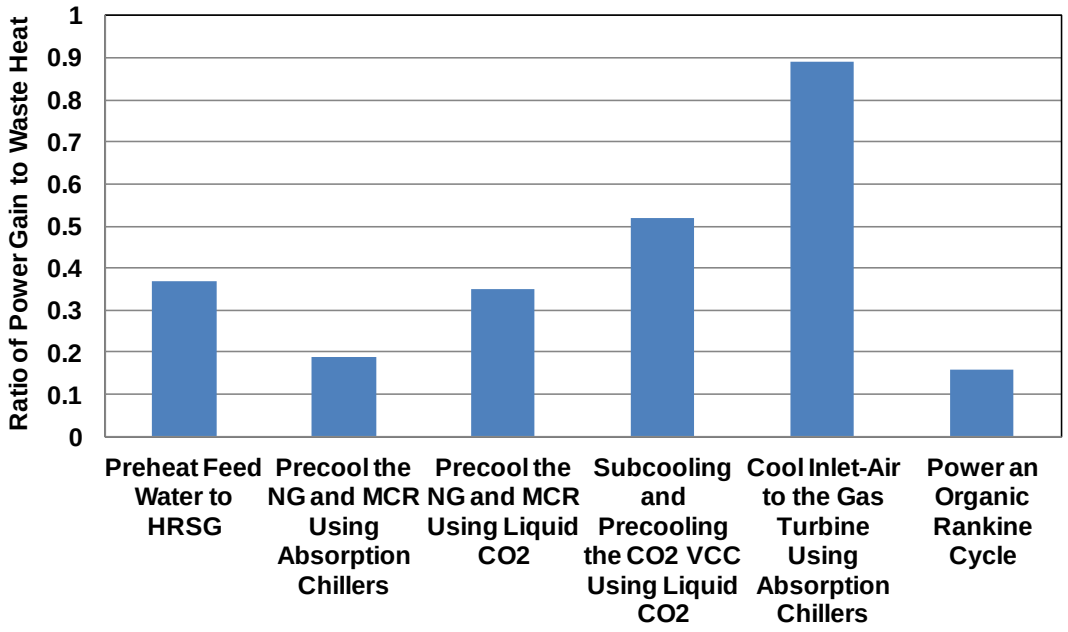

Figure 52: Maximum power gain from waste heat ratio for different waste heat application.

The summary of integrated CCS systems with nine waste heat utilization scenarios is shown in Table 34 and Figure 53. The details of utilizing the liquid CO_2 and CO_2 pressurization options can be found in Chapter 4. The table shows the performance of proposed CCS configurations with and without CO_2 capture enhancement via flue gas cooling against the conventional CCS. The power loss increases with enhancing the CO_2 capture efficiency because large portion of the waste heat (Table 27) was used to cool the flue gas before the absorber. As a result, the CO_2 capture efficiency increased from 93.59% to 97.87% or 4.3 tons of CO_2/hr more capturing. The available waste heat in the NGCC configuration 2 is higher than the other NGCC configurations because the remaining low pressure steam in the steam cycle condenser.

The other NGCC configurations utilized this low pressure steam to produce power in a low pressure steam turbine. In CCS with CO_2 capture enhancement, using the waste heat in inlet air cooling and the "excess waste heat, Table 28" in ORC resulted in the highest power gain. The net available power was found to be 179.33 MW, which is 11.17% more power than the conventional CCS. The enhancement in the CO_2 capture efficiency resulted in 2.92% or 5.39 MW reductions in the net available power.

In CCS without CO_2 capture enhancement, using the waste heat in inlet air cooling, ORC, CO_2 liquefaction and NG and MCR cooling resulted in the highest power gain. The net available power was found to be 187.61 MW, which is 16.31% more power than the conventional CCS configuration. All proposed CCS configurations that have excess waste heat in the steam cycle condenser (NGCC

configuration 2) outperformed proposed CCS configurations without excess waste heat in the steam cycle condenser (e.g. NGCC configuration 1).

Table 34: Performance of several proposed CCS configurations against the conventional CCS configuration.

CCS Configuration	Conventional	Proposed CCS w/o CO_2 Capture Enhancement				Proposed CCS w/ CO_2 Capture Enhancement				
Case	1	2	3	4	5	6	7	8	9	10
NGCC Configuration No.	1	3	2	2	1	2	2	2	2	1
Waste Heat Application	-	ORC, Inlet Air Cooling	ORC, Inlet Air Cooling, CO_2 Liq., NG and MCR Cooling	ORC, Inlet Air Cooling	ORC, Inlet Air Cooling, CO_2 Liq., Feedwater Prehating	ORC	ORC, Inlet Air Cooling	NG and MCR Cooling, and CO_2 Liq.	ORC, CO_2 Liq.	Feedwater Prehating
Waste Heat (MW)	48.98	105.69	142	142	49.68	142	142	142	142	49.68
Power Gain (MW)	-	31.04	38.08	36.77	23.33	14.58	31.39	15.01	12.47	2.37
Net NGCC Power (MW)	167.31	192.69	192.06	190.67	188.14	172.13	185.37	172.56	170.02	169.67
CO_2 Capture Efficiency (%)	93.59	93.59	93.59	93.59	93.59	97.87	97.87	97.87	97.87	97.87
Enhancement in CO_2 Capture Efficiency (%)	-	-	-	-	-	4.57	4.57	4.57	4.57	4.57
CO_2 Pressurization Power (MW)	6.00	6.04	4.45	6.04	4.45	5.93	6.04	4.37	4.37	5.93
Net Available Power (MW)	161.31	186.65	187.61	184.72	183.69	166.2	179.33	168.19	165.65	163.74
Enhancement in Net Available Power (%)	-	15.71	16.31	14.51	13.87	3.03	11.17	4.27	2.69	1.51
Net Available Power Efficiency (%)	43.03	48.92	49.17	48.41	48.14	44.33	47	44.86	44.18	43.67

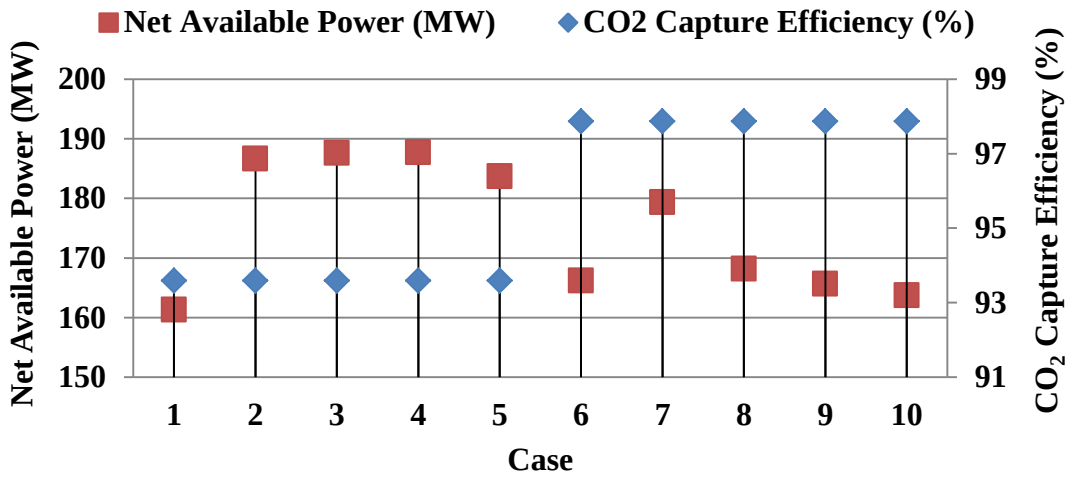

Figure 53: Performance of several proposed CCS configurations against the conventional CCS configuration (Case 1).

3.9 Pinch Analysis

Pinch analysis is a heat and process integration method based on thermodynamics principles. It can be used to determine the potential in energy consumption reductions by enhancing heat exchangers network. The pinch analysis was developed by Linnhoff and Hindmarsh [125]. Few authors introduced extensions on the original pinch analysis method by combining it with exergy analysis [126] [127] . Relevant literature review is presented in literature review section.

The objective of using pinch analysis here is to investigate the minimum utility cooling or heating is needed in the proposed CCS configuration as well as the conventional CCS configuration. In order to find the minimum possible utility cooling or heating or "energy targets", the problem table algorithm is used which requires each stream supply and target temperatures, heat capacity and mass flow rate [125]. A pinch analysis spreadsheet tool was developed by Kemp [128] and it was used in this work.

3.9.1 Pinch Analysis on the APCI LNG Plant

The problem table algorithm for the APCI LNG plant is shown in Table 35. Hot streams are stream which require cooling whereas cold streams are streams which require heating.

Table 35: Streams in the APCI LNG Plant.

Stream Name	Supply Temp. (°C)	Target Temp. (°C)	Mass Flow Rate (kg/s)	Enthalpy Change (kJ/kg)	Heat Flow (MW)	Stream Type
NG feed to -5°C HX	40.0	-2.0	111.1	-116.0	12.89	Hot
NG -5°C to -19°C HX	-2.0	-16.0	106.2	46.4	4.93	Hot
NG -5°C to -33°C HX	-16.0	-30.0	101.9	50.5	5.14	Hot
NG -33°C HX to LNG	-30.0	-160.0	96.9	674.3	65.32	Hot
NG from Frac1 to LNG	-33.5	-160.0	3.3	672.3	2.18	Hot
Cond_Frac1	-0.5	-33.5	16.3	311.6	5.07	Hot
Boiler_Frac1	130.1	140.6	86.6	124.7	10.79	Cold
Cond_Frac2	79.6	73.6	9.1	181.4	1.65	Hot
Boiler_Frac2	130.0	138.4	14.5	101.7	1.48	Cold
Propane	73.6	-16.0	3.0	494.8	1.46	Hot
Cond_Frac3	64.9	59.6	9.0	213.8	1.93	Hot
Boiler_Frac3	141.1	150.4	14.1	155.0	2.18	Cold
Butane	59.6	-2.0	2.9	458.6	1.34	Hot
Pentane Plus	150.4	40.0	5.1	308.8	1.57	Hot

Using Kemp [128] pinch analysis tool at 3 K pinch temperature, the minimum cold and hot utilities are 103.27 MW and 14.21 MW, respectively. The HYSYS model shows that the APCI LNG plant has a cooling capacity of 183.23 MW and requires 14.45 MW of heating. Thus, the APCI LNG plant has an efficiency of

43.63%. The Second Law efficiency was calculated in Chapter 2 to be 45.43%. The difference between the two efficiencies is due to the fact that pinch analysis does not consider losses from pressure drop. The large difference between the APCI LNG plant cooling capacity and the minimum required cooling capacity for natural gas liquefaction is due to that the APCI also cools the mixed refrigerants of the MCR cycle before it uses it in natural gas liquefaction.

The hot and cold composite curves for the APCI LNG plant are shown in Figure 54. The overlap between the cold and hot composite curves shows only 0.3 MW of heat can be exchanged between the cold and hot composite curves at a pinch occurred at 131^{o}C. The rest of the heating and cooling comes from the utility. To utilize the 0.3 MW, the Pentane Plus stream could be used to heat the natural gas in the first fractionation column boiler which would result in 2.78% savings in the first fractionation column boiler heat.

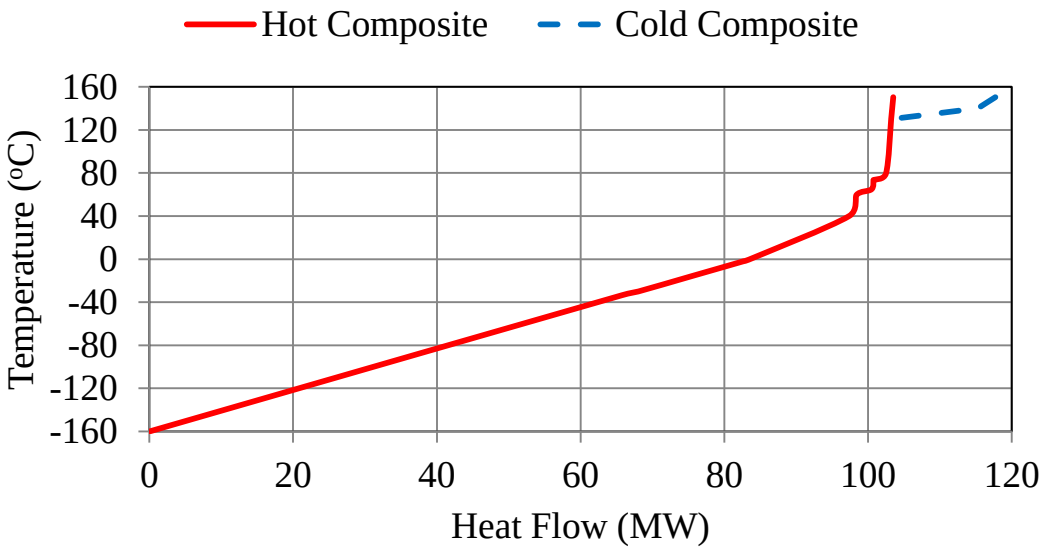

Figure: 54 Hot and cold composite curves in the APCI LNG plant.

3.9.2 Pinch Analysis on the Conventional CCS Configuration

The conventional CCS configuration includes the LNG Plant, the CO_2 removal plant and the multi-stage CO_2 compression cycle as shown in Figure 21. There are three streams to be considered, namely the natural gas, the flue gas and the CO_2 streams. The problem table algorithm for the conventional CCS configuration is shown in Table 36.

The minimum cold and hot utilities were calculated at 3 K pinch temperature to be 189.86 MW and 74.64 MW, respectively. The HYSYS models show that the conventional CCS configuration uses 271 MW of cooling and requires 84.87 MW of heating as shown in Table 37. The cooling demand is high because high amount of cooling is needed for the natural gas liquefaction, CO_2 condensing, flue gas cooling and CO_2 compressors intercooling at temperatures where no other stream could exchange heat with.

Table 36: Streams in the conventional CCS configuration.

Stream Name	Supply Temp. (°C)	Target Temp. (°C)	Mass Flow Rate (kg/s)	Enthalpy Change (kJ/kg)	Heat Flow (MW)	Stream Type
NG feed to -5^{o}C HX	40.0	-2.0	111.11	-116.04	12.89	Hot
NG -5^{o}C to -19^{o}C HX	-2.0	-16.0	106.23	46.43	4.93	Hot
NG -5^{o}C to -33^{o}C HX	-16.0	-30.00	101.95	50.47	5.15	Hot
NG -33^{o}C HX to LNG	-30.0	-160.0	96.87	674.31	65.32	Hot
NG from Frac1 to LNG	-33.53	-160.0	3.25	672.27	2.18	Hot
Cond_Frac1	-0.52	-33.53	16.27	311.57	5.07	Hot
Boiler_Frac1	130.1	140.6	86.57	124.69	10.79	Cold
Cond_Frac2	79.58	73.59	9.14	181.40	1.66	Hot
Boiler_Frac2	129.97	138.39	14.55	101.73	1.48	Cold
Propane	73.59	-16.0	2.95	494.77	1.46	Hot
Cond_Frac3	64.9	59.6	9.05	213.84	1.93	Hot
Boiler_Frac3	141.1	150.4	14.12	154.97	2.19	Cold
Butane	59.6	-2.0	2.93	458.63	1.34	Hot
Pentane Plus	150.4	40.0	5.11	308.79	1.58	Hot
FG Cooler	140.0	40.0	421.0	108.07	45.5	Hot
Rich In	40.9	106.0	424.6	262.42	111.4	Cold
To Reboiler	115.5	117.6	435.1	161.86	70.42	Cold
CO_2 Condenser	104.40	75.92	32.42	825.46	26.76	Hot
Lean Out	117.6	40.0	403.3	-298.2	120.2	Hot
CO_2 to Compressors	75.92	40.0	21.38	237.90	5.09	Hot
Comp. 1 Intercooler	89.75	40.0	19.58	63.38	1.24	Hot
Comp. 2 Intercooler	89.5	40.0	19.44	56.02	1.09	Hot
Comp. 3 Intercooler	89.5	40.0	19.36	52.34	1.01	Hot
Comp. 4 Intercooler	89.5	40.0	19.31	51.26	0.99	Hot
Comp. 5 Intercooler	89.5	40.0	19.29	52.92	1.02	Hot
Comp. 6 Intercooler	89.7	40.0	19.27	60.15	1.16	Hot
Comp. 7 Intercooler	89.5	40.0	19.27	96.76	1.86	Hot
Comp. 8 Intercooler	89.69	54.0	19.27	106.07	2.04	Hot

Table 37: Hot and cold utilities demand from the HYSYS models for the conventional CCS configuration

Utility	Demand in APCI (MW)	Demand in FG (MW)	Demand in CO_2 Removal (MW)	Demand in CO_2 Compression (MW)	Total Demand (MW)
Hot	14.45		70.42		84.87
Cold	183.23	45.5	31.85	10.42	271

The hot and cold composite curves for the conventional CCS configuration are shown in Figure 55. The overlap between the cold and hot composite curves shows 122 MW of heat can be exchanged between the cold and hot composite curves at a pinch occurred at 117^{o}C. To utilize the 122 MW, the "Lean Out" stream in the CO_2 removal plant is used to preheat the "Rich In" stream in addition to using the Pentane Plus stream to heat the natural gas in the first fractionation column boiler.

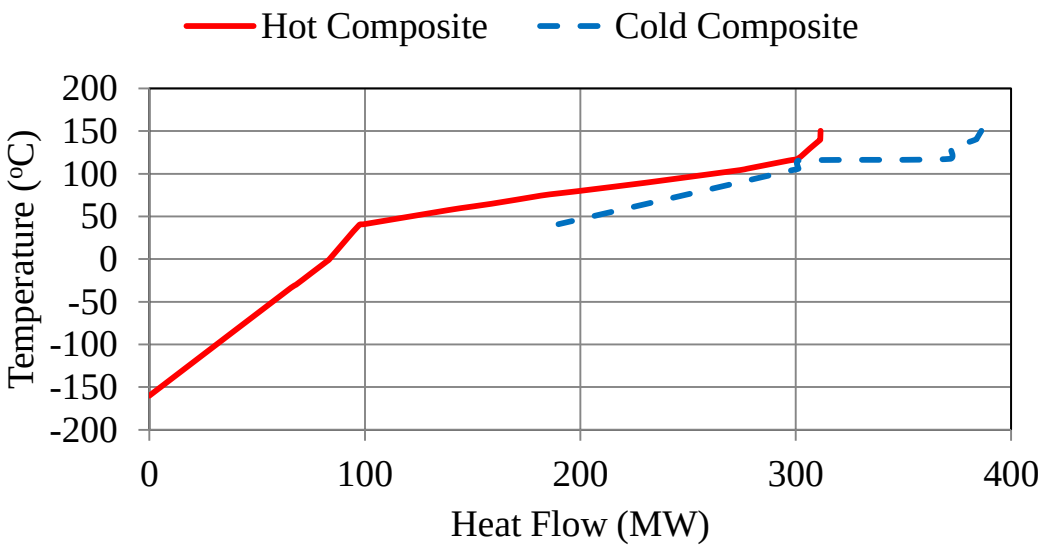

Figure 55: Hot and cold composite curves in the conventional CCS configuration.

3.9.3 Pinch Analysis on the Proposed CCS Configuration

The proposed CCS configuration includes the LNG Plant, the CO_2 removal plant, the multi-stage CO_2 compression and CO_2 liquefaction plant as shown in Figure 24. There are three streams to be considered, namely the natural gas, the flue gas and the CO_2 streams. The problem table algorithm for the proposed CCS configuration is shown in Table 38.

The minimum cold and hot utilities were calculated at 3^oC pinch temperature to be 144.55 MW and 84.43 MW, respectively. The HYSYS models show that the proposed CCS configuration uses 192.71 MW of cooling and requires 85.14 MW of heating as shown in Table 39.

Table 38 Streams in the proposed CCS configuration

Stream Name	Supply Temp. (°C)	Target Temp. (°C)	Mass Flow Rate (kg/s)	Enthalpy Change (kJ/kg)	Heat Flow (MW)	Stream Type
NG feed to -5°C HX	40	-2	111.11	-116.04	12.89	Hot
NG -5°C to -19°C HX	-2	-16	106.23	46.43	4.93	Hot
NG -5°C to -33°C HX	-16	-30	101.95	50.47	5.15	Hot
NG -33°C HX to LNG	-30	-160	96.87	674.31	65.32	Hot
NG from Frac1 to LNG	-33.5	-160	3.25	672.27	2.18	Hot
Cond_Frac1	-0.5	-33.5	16.27	311.57	5.07	Hot
Boiler_Frac1	130.1	140.6	86.57	124.69	10.79	Cold
Cond_Frac2	79.6	73.6	9.14	181.40	1.66	Hot
Boiler_Frac2	130.0	138.4	14.55	101.73	1.48	Cold
Propane	73.6	-16.0	2.95	494.77	1.46	Hot
Cond_Frac3	64.9	59.6	9.05	213.84	1.93	Hot
Boiler_Frac3	141.1	150.4	14.12	154.97	2.19	Cold
Butane	59.6	-2.0	2.93	458.63	1.34	Hot
Pentane Plus	150.4	40.0	5.11	308.79	1.58	Hot
FG Cooler	80.0	40.0	421.00	44.70	18.82	Hot
Rich In	31.0	105.0	393.12	298.25	117.25	Cold
To Reboiler	115.9	117.9	402.65	174.90	70.42	Cold
CO_2 Condenser	80.0	75.9	33.38	149.80	5.00	Hot
Lean Out	117.9	35.3	370.77	-316.04	117.18	Hot
CO_2 to Compressors	75.9	40.0	22.36	237.71	5.31	Hot
Comp. 1 Intercooler	99.0	40.0	20.48	74.57	1.53	Hot
Comp. 2 Intercooler	99.0	40.0	20.31	65.46	1.33	Hot
Comp. 3 Intercooler	99.0	40.0	20.24	51.88	1.05	Hot
Comp. 4 Intercooler	99.0	40.0	20.22	61.71	1.25	Hot
Comp. 5 Intercooler	99.0	40.0	20.18	62.32	1.26	Hot
Comp. 6 Intercooler	110.4	40.0	20.14	86.34	1.74	Hot
CO_2 Precooler HX	40.0	35.6	20.14	-6.65	0.13	Hot
CO_2 Liquefaction HX	35.6	14.3	20.14	218.71	4.40	Hot
CO_2 Subcooler HX	30.1	32.6	20.14	6.80	0.14	Cold
CO_2 Precooler HX	32.6	35.0	20.17	6.65	0.13	Cold

Table 39: Hot and cold utilities demand from the HYSYS models for the proposed CCS configuration

Utility	Demand in APCI (MW)	Demand in FG (MW)	Demand in CO_2 Removal (MW)	Demand in CO_2 Compression and Liquefaction (MW)	Total Demand (MW)
Hot	14.45		70.42	0.27	85.14
Cold	150.89	18.82	10.31	12.69	192.71

The hot and cold composite curves for the proposed CCS configuration are shown in Figure 56. The overlap between the cold and hot composite curves shows 117 MW of heat can be exchanged between the cold and hot composite curves at a pinch occurred at 117^{o}C. To utilize the 117 MW, the "Lean Out" stream in the CO_2 removal plant is used to preheat the "Rich In" stream in addition to using the Pentane Plus stream to heat the natural gas in the first fractionation column boiler and the pressurized CO_2 in precooling the CO_2 stream.

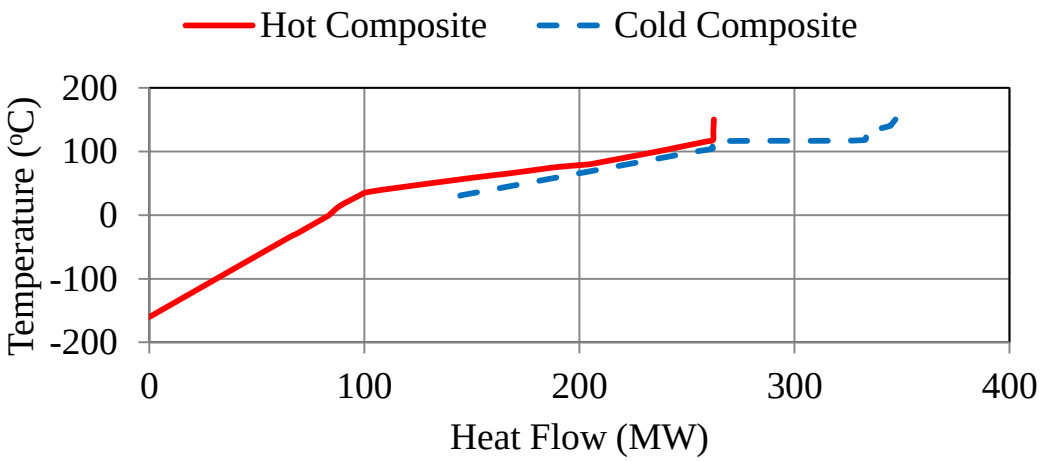

Figure 56: Hot and cold composite curves in the proposed CCS configuration.

Table 40 compares the utility cooling and heating between the proposed CCS configuration and the conventional CCS configuration. The proposed CCS configuration uses 23.86% less utility cooling than the conventional CCS configuration because the improved heat integration and waste heat utilization. For example, less utility cooling is needed in flue gas cooling and CO_2 removal plant since part of its cooling is utilized in absorption chillers. Also, smaller APCI capacity is needed because of the replacement of the 22^oC and 9^oC Evaporators by absorption chillers and subcooling the Propane Cycle to 5^oC. However, 13.11% higher utility heating is required in the proposed configuration due to the required heat to heat up the liquefied and pressurized CO_2. This heat was recovered in CO_2 liquefaction process. The main reason why the proposed CCS requires higher heating than the conventional CCS is that the flue gas heat (e.g. 140^oC to 80^oC) was not included in the proposed CCS problem algorithm table because it was utilized in running an ORC or absorption chillers. If the flue gas heat were to be included in the proposed CCS problem algorithm table, the difference between the utility heating becomes only 0.6%. In this case, portion of the flue gas heat can be used to regenerate the CO_2 or heat the natural gas in the fractionation column.

Table 40: Utility cooling and heating in conventional CCS configuration vs. proposed CCS configuration

Conf-iguration	Utility	Demand in APCI (MW)	Demand in FG (MW)	Demand in CO_2 Removal (MW)	Demand in CO_2 Comp. and Liq-uefaction (MW)	Total Demand from HYSYS Models (MW)	Minimum Demand from Pinch Analysis (MW)
Conv-ential CCS	Hot	14.45		70.42		84.87	74.64
	Cold	183.23	45.5	31.85	10.42	271	189.86
Prop-osed CCS	Hot	14.45		70.42	0.27	85.14	84.43
	Cold	150.89	18.82	10.31	12.69	192.71	144.55

3.10 Conclusions

Comprehensive investigation was conducted on reducing the power loss from implementing a CCS on an LNG plant. Several waste heat sources were identified and potential uses were proposed and evaluated through modeling in HYSYS software with models validation against experimental data. Several steam cycles with steam extractions were modeled and optimized. A steam cycle without steam extraction that provides the CO_2 regeneration heat via high temperature condenser with excess waste heat provided more net available power than steam cycles with steam extractions. One of the proposed CCS configurations that utilize the waste heat in inlet air cooling and in ORC resulted in 187.61 MW, which is 16.31% more power than the conventional CCS as well as 97.87% CO_2 capture efficiency which is 4.57% enhancement or 4.3 tons of CO_2/hr more capturing. In order to compare different waste heat utilization options, the power gain from waste heat ratio was defined. The highest power gain from waste heat ratio was for using the waste heat for inlet-air cooling but it was shown that the power savings from inlet air cooling is highly dependent on the inlet air cooler pressure drop. Pinch Analysis method was used to

compare the utility cooling and utility heating of the proposed and conventional CCS. The result of the Pinch Analysis shows that the proposed CCS configuration requires 23.86% less utility cooling than the conventional CCS configuration because of the improved heat integration and waste heat utilization.

Chapter 4: Development of CO_2 Liquefaction Cycles for CO_2 Sequestration

4.1 Introduction

Carbon capture and sequestration consists of three processes: capture which is typically done by amine absorption, transport which is done by either pipeline or ships, and storage which can be done in underground geological formation such as oil well for EOR. Among the three processes, CO_2 capture has attracted most attention in the literature (literature review section) since it is more technically challenging. Since CO_2 captured in post-combustion capturing method using amine absorption is at atmospheric pressure, CO_2 needs to be pressurized to a supercritical pressure, e.g. 150 bar, before injection in oil well for EOR. As for storage or shipping in tankers, the captured CO_2 is liquefied at a pressure about 6 bar so that its volume is reduced.

Conventionally, CO_2 pressurization is done using multi-stage compression with intercooling. CO_2 compression consumes about 100 kWh/ton CO_2 [65] whereas the energy efficiency of a power plant can be decreased by 3 - 4% points [19]. The other pressurization approach is to liquefy the CO_2 and pump it to the target injection pressure, and then the pressurized CO_2 is evaporated so that phase change does not occur inside the well. The two approaches are shown in Figure 57.

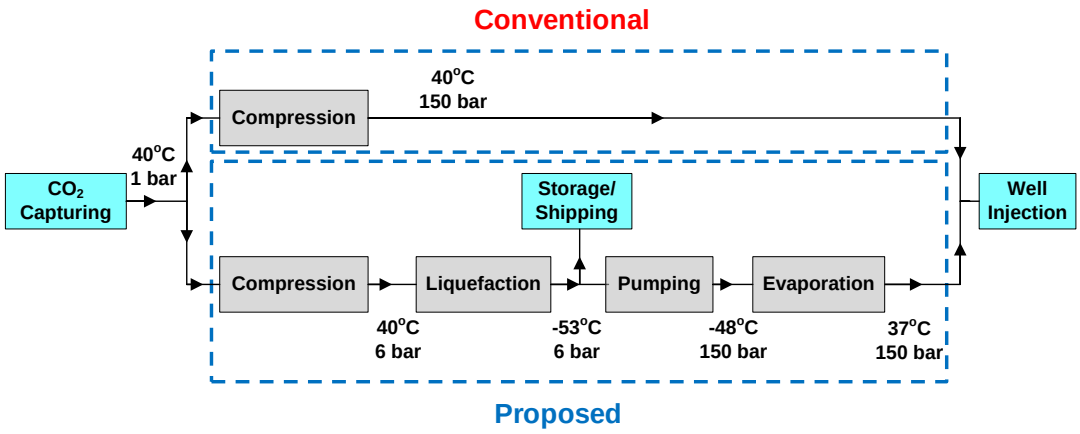

Figure 57: Conventional and proposed CO_2 pressurization approaches.

The objectives of this chapter are (1) to carry out a comprehensive comparison between CO_2 compression and CO_2 liquefaction and pumping processes for EOR application by developing several CO_2 liquefaction cycles and validating or verifying the developed models, (2) to optimize the CO_2 liquefaction pressure, and (3) to evaluate the performance of the open CO_2 liquefaction cycle.

4.2 CO_2 Compression Cycle

In order to inject the captured CO_2 into an oil well for EOR, it needs to be pressurized to a high pressure. The injected CO_2 is in supercritical state. The injection pressure used in this work is 150 bar, which is typical for an EOR project. Pressurizing CO_2 is done using multistage centrifugal compressors with intercooling so that it approaches isothermal compression. Two compression stages of the HYSYS model for the compression plant are shown in Figure 58. It consists of 8 compressor stages, with seawater intercooling to 40°C. Each compressor has isentropic efficiency of 80%.

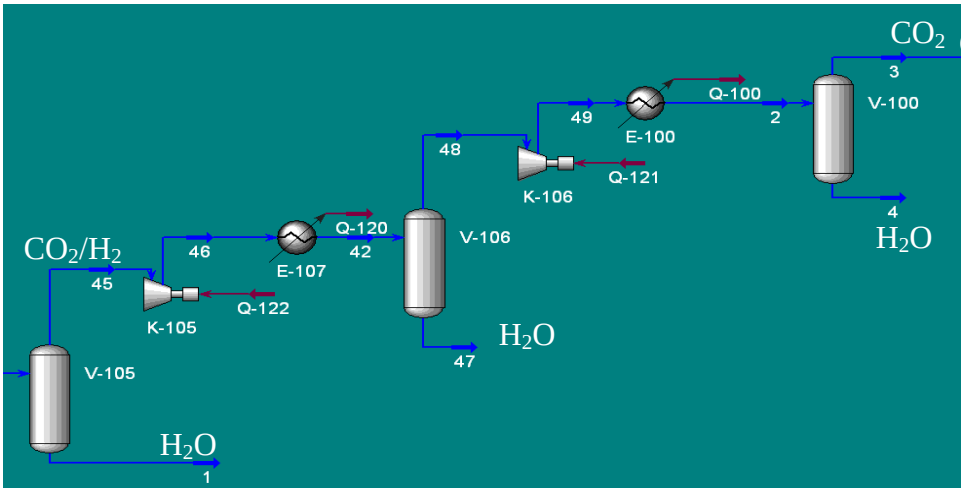

Figure 58: HYSYS model for the CO_2 compression plant (2 stages only shown here out of 8 stages).

The developed model was validated against vendor's data for two CO_2 centrifugal compressors, each having 8 stages with intercooling and different mass flow rate and outlet pressure [129]. The model matched the vendor's data adequately as shown in Table 41.

Table 41: HYSYS CO_2 compressor model validation against vendor's data.

	HYSYS Model	Vendor's data	HYSYS Model	Vendor's data
No. of stages	8		8	
Isentropic efficiency (%)	80		80	
Pin (bar)	1.1		1.1	
Pout (bar)	140		200	
CO_2 flow rate (m^3/hr)	27000		70000	
Power (MW)	4.95	5	13.21	14
Discrepancy (%)	1		5.64	

For the developed CO_2 capturing plant model, the regenerated CO_2 after the stripper contains about 90% CO_2 and 10% water by mass. Their mass flow rate for the conventional case, a 40°C absorption temperature, and the proposed case, a 27°C

absorption temperature, is shown in Table 42. CO_2 is dehydrated after each compression stage. In the final stage, the CO_2 purity is 99.6%.

Table 42: Captured CO_2 composition for the conventional and proposed case.

	Conventional Case	Proposed Case
CO_2 mass flow rate (Ton/hr)	69.26	72.42
H_2O mass flow rate (Ton/hr)	7.7	8.04
Total mass flow rate (Ton/hr)	76.96	80.46

The total compression power for compressing the captured gas from 1.8 bar to 150 bar is 6 MW for the conventional case, and 6.25 MW for the proposed case. The difference in power is due to the difference in the mass flow rate, where the proposed case has higher CO_2 removal efficiency than the conventional case. The P-h diagram for the compression process is shown in Figure 59.

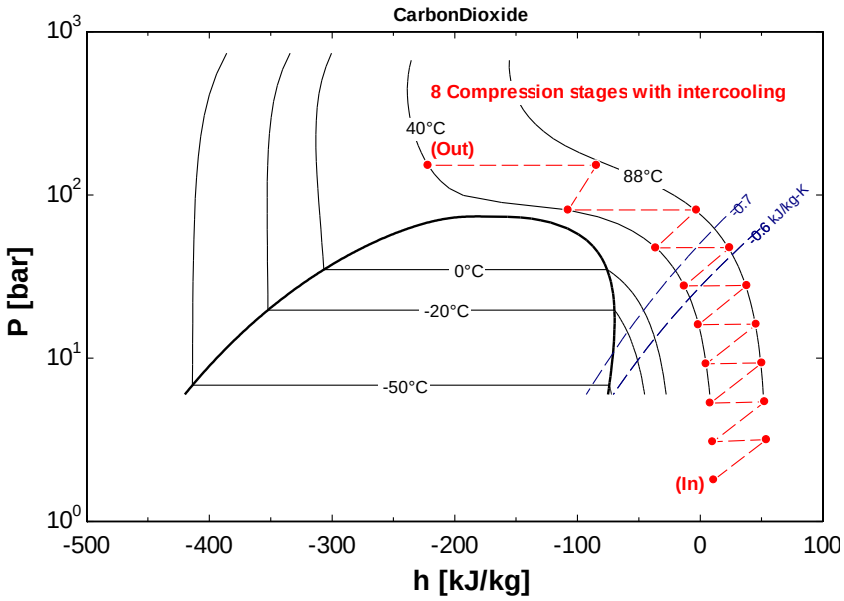

Figure 59: P-h diagram for CO_2 compression process.

4.3 CO_2 Liquefaction Cycle

4.3.1 Introduction

CO_2 can be pressurized with the use of pumps after liquefaction. Pumps are less energy intensive than compressors because the specific volume of the liquid CO_2 is less than the vapor CO_2 as shown in Equ. 9. However, liquefying the CO_2 requires a considerable amount of energy.

$$w = \int_{P_i}^{P_o} v \, dP \tag{9}$$

Since the captured CO_2 from the stripper of the CO_2 removal plant is at 1.8 bar, CO_2 needs to be compressed to a pressure that is higher than the triple point pressure (5.17 bar) before liquefaction takes place. Otherwise, solid CO_2 will be formed with cooling as shown in the CO_2 phase diagram in Figure 60. Therefore, multistage CO_2 compressors are introduced upstream of the liquefaction cycle.

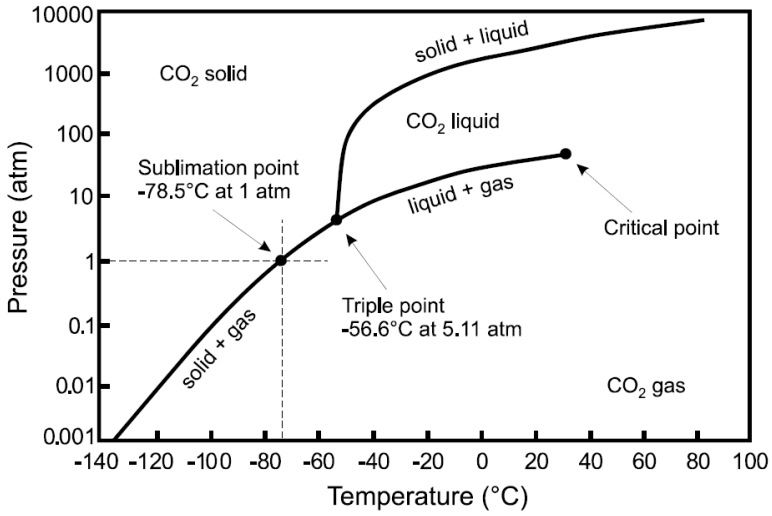

Figure 60: CO_2 phase diagram [130].

4.3.2 CO_2 Liquefaction Cycles

There is no CO_2 liquefaction cycle design available in the open literature. Thus, new designs were explored, which are based on single-refrigerant as well as cascade configuration for liquefying the CO_2. Four common refrigerants were investigated. The refrigerants are NH_3, CO_2, propane and R134a.

A HYSYS model for a cascade refrigeration system using CO_2 and NH_3 refrigerants was developed and validated against experimental data from Dopazo *et al.* [131]. Dopazo *et al.*'s experiment was on 9 kW refrigeration capacity system at -50^{o}C evaporation temperature. The NH_3 was the top vapor compression cycle (VCC) refrigerant whereas the CO_2 was the bottom VCC refrigerant. Their experimental prototype and experiment schematic diagram are shown in Figure 62 and Figure 61, respectively.

Figure 61: Photograph of the experimental prototype of the cascade refrigeration system with CO_2 and NH_3 refrigerant [131].

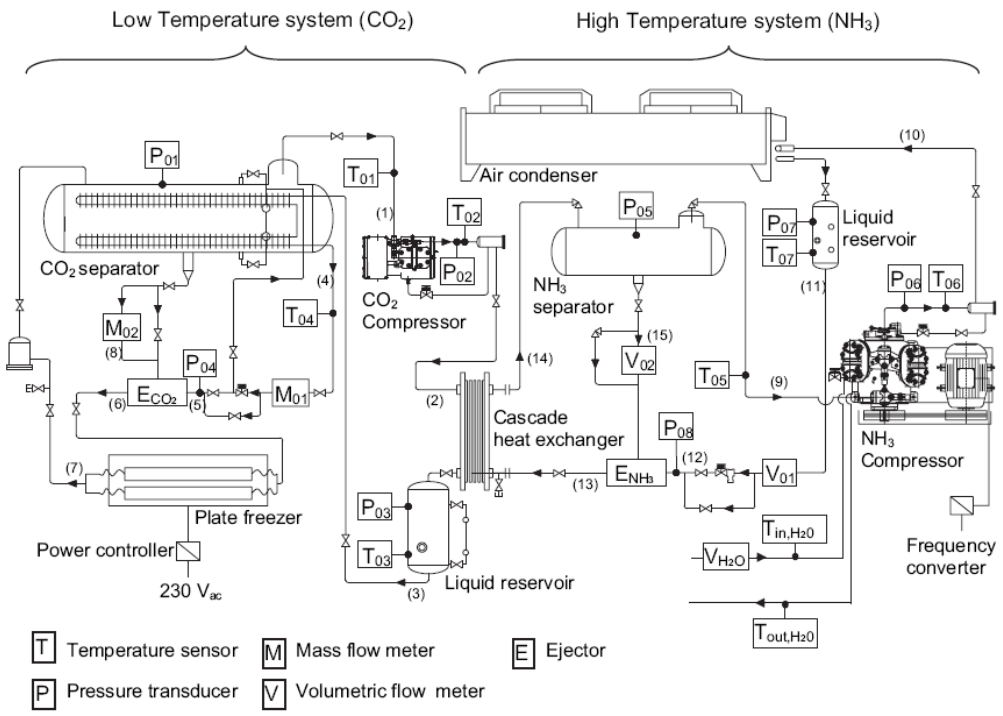

Figure 62: Schematic diagram of the CO_2/NH_3 cascade refrigeration system [131].

The developed HYSYS model that depicts Dopazo *et al.*'s prototype is shown in Figure 63. The model uses same operating parameters as the experiments. The equation of state used in this model is also the Peng-Robinson equation of state that is used in all models in this work. The model has a cooling capacity of 9.45 kW at a cooling temperature of -50^{o}C. The validation results,

Table **43**, matched the experimental data adequately for the top cycle (NH_3 VCC) as well as the bottom cycle (CO_2 VCC). The input parameters for the HYSYS model are the parameters without discrepancy values in Table 43. The maximum discrepancy is in the calculated NH_3 refrigerant volume flow rate. This could be due to the accuracy of the equation of state in predicting the specific volume of the NH_3. However, the power consumption and the overall COP were predicted pretty well.

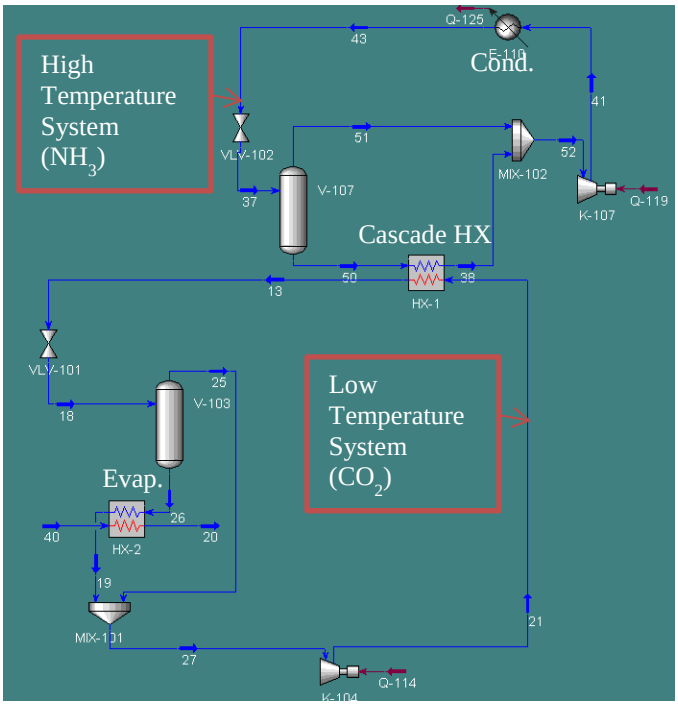

Figure 63: HYSYS model for CO_2/NH_3 cascade refrigeration system that depicts Dopazo *et al.*'s experiment.

Table 43: Validation of the HYSYS model against the Dopazo *et al.*'s experiment

VCC	Bottom (CO_2)			Top (NH_3)		
Parameter	Measurement	HYSYS Model	Discrepancy	Measurement	HYSYS Model	Discrepancy
T_{evap} (^oC)	-50	-50	-	-20.96	-20.96	-
T_{cond} (^oC)	-17.48	-17.48	-	29.72	29.72	-
P_{evap} (kPa)	682	658.6	3.4 %	182	179.5	1.4 %
P_{cond} (kPa)	2127	2127	-	1158	1158	-
ΔT_{sh}	15	14.94	0.4 (^oC)	15	15.02	-0.02 (^oC)
ΔT_{sc}	0.34	0.54	0.2 (^oC)	4.74	0.29	-4.5 (^oC)
Q_{evap} (kW)	9.45	9.45	-	13.5	12.55	7 %
Q_{cond} (kW)	13.2	12.55	4.9 %	17.2	18.03	-4.8 %
W_{ele} (kW)	3.93	3.67	6.6 %	6.32	6.68	-5.8 %
Comp. isen. eff. (%)	57.9	57.9	-	58.8	58.8	-
Ref. flow	124.4 (kg/h)	118.1 (kg/h)	5.1 %	1.28 L/m	1.12 L/m	12.5 %
COP	2.4	2.57	-7.3 %	2.14	1.87	12.3 %
Total	CO_2/NH_3					
$\Delta T_{cascade}$ (^oC)	3.48	3.48	-			
COP CO_2/NH_3	0.92	0.91	0.83 %			

4.3.2.1 Single-Refrigerant CO_2 Liquefaction Cycles

Figure 64 shows a single-refrigerant configuration. The cycle has two cooling stages; one is for dehydration and sensible cooling at 1^{o}C and the other one is for liquefaction at -57^{o}C (at liquefaction pressure of 6 bar). The cycle has two flash tanks at each stage and intercooling to 40^{o}C between compression stages.

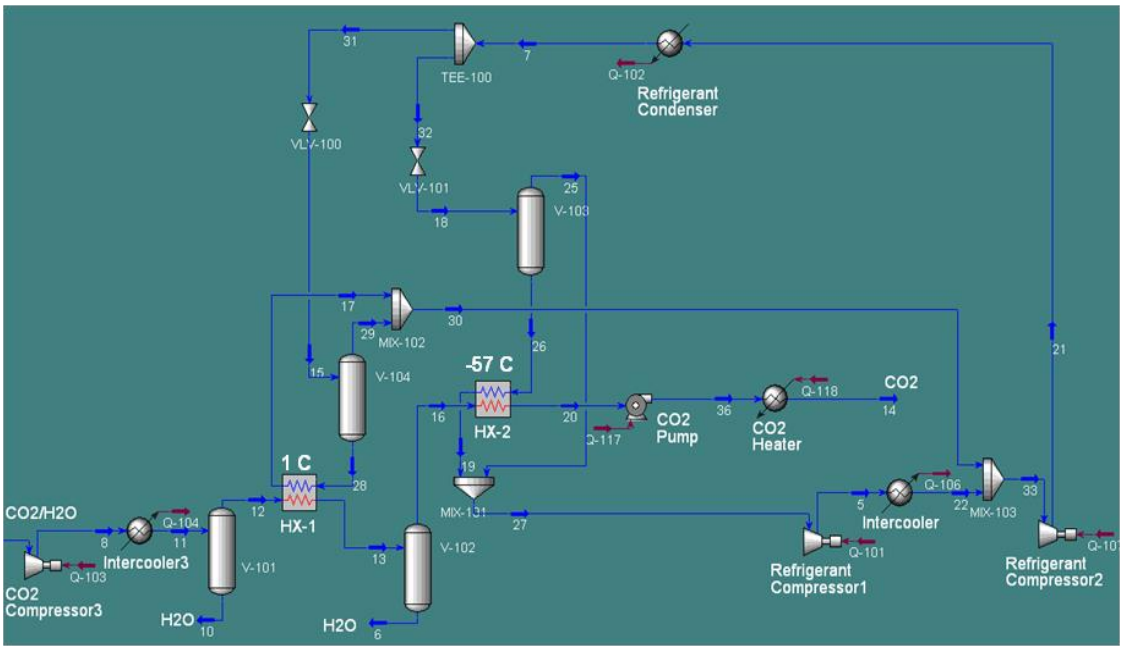

Figure 64: Single-refrigerant liquefaction cycle at 6 bar liquefaction pressure with two compression stages and intercooling.

The condensing temperature for all cycles is 40°C. The condensing pressure is determined from the enthalpy after the expansion valve, which is an isenthalpic process. The enthalpy after the expansion valve is determined to provide the CO_2 liquefaction load for a given flow rate. The P-h diagrams for the three cycles are shown in Figure 65.

The number of compression stages is set based on a maximum stage pressure ratio of 5 as well as the outlet temperature at a compressor outlet pressure. To prevent

excessive heat, the maximum outlet temperature from a compressor stage was set to be less than 90^{o}C. According to the P-h diagrams in Figure 65, the temperature lines in the superheated region in ammonia refrigerant are closer than the ones in R134a and propane refrigerants. Therefore, 7 compression stages were used in the ammonia cycle and 2 compression stages were used in the R134a and propane cycles.

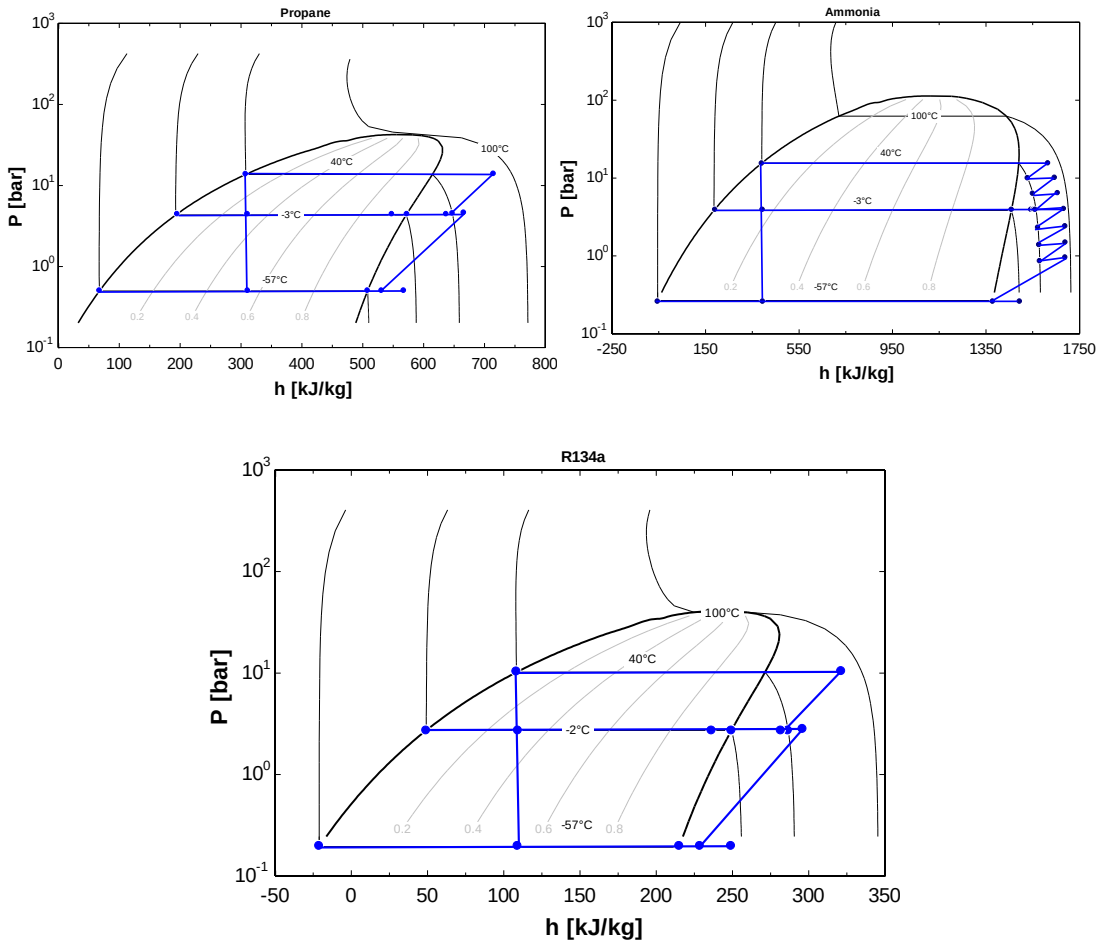

Figure 65: P-h diagrams for single-refrigerant liquefaction cycle at 6 bar liquefaction pressure.

The liquefaction cycles power consumption and the CO_2 compressors power consumption are tabulated in Table 44. The least power consumption is for the ammonia cycle. Since the required VCC load is 9.01 MW, the COP of the ammonia cycle, Eq. 10, is 1.42.

$$COP\ of\ VCC\ = \frac{VCC\ cooling\ load}{VCC\ power\ input} \quad (10)$$

Table 44: Single-refrigerant liquefaction cycles power consumption at 6 bar liquefaction pressure

Refrigerant	VCC Power (MW)	CO_2 Compressors Power (MW)	COP	Critical Point Temperature (^oC)
Propane	7.95	1.98	1.13	96.86
Ammonia	6.34	1.98	1.42	132.3
R134a	7.78	1.98	1.15	101
CO_2	10.46	1.98	0.86	30.98

The highest COP is for the NH_3 cycle. Since NH_3 has the highest critical temperature it was expected to consume the least power according to Mclinden [132] observation that a high critical point refrigerant yields high COP. The COPs of the investigated refrigerants against their critical point temperature are shown in Figure 66.

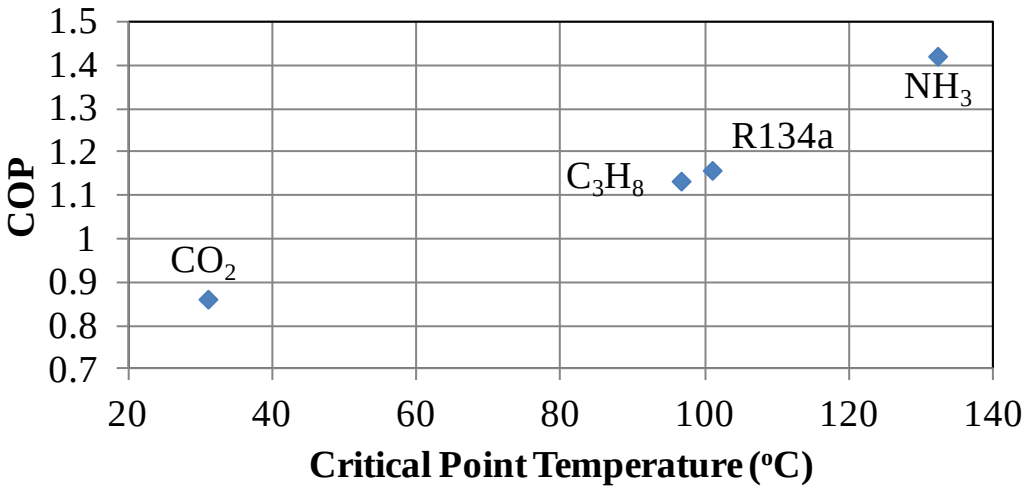

Figure 66: COP of single-refrigerant liquefaction cycle against critical point temperature.

The Carnot cycle is a reversible VCC cycle that has the least possible power consumption. In other words, no actual cycle has the efficiency of Carnot cycle. Hence, the Carnot cycle is used to compare how close the actual cycle to a reversible cycle.

$$Carnot\ COP\ for\ cooling\ cycle = \frac{T_{evap}}{T_{cond} - T_{evap}} \quad (11)$$

$$Reversible\ compression\ power, W_{rev} = \frac{Cooling\ load, Q}{Carnot\ COP} \quad (12)$$

$$Second\ Law\ efficiency, \eta_{II} = \frac{Reversible\ compression\ power, W_{rev}}{Actual\ compression\ power, W_{vcc}} \quad (13)$$

The Carnot cycle COP is calculated for the CO_2 sensible cooling evaporator, 0.962 MW at -2^{o}C, and the CO_2 liquefaction evaporator, 8.05 MW at -57^{o}C, to be 2.39. Therefore, the Second Law efficiency for the ammonia cycle is 59.34%. The liquefied CO_2 is pumped to 150 bar. After pumping, it has a temperature of -48^{o}C. This liquid CO_2 needs to be evaporated above the critical point temperature so that it is vapor in the supercritical state before injection. This heating process is proposed to be recovered in cooling another stream. The available recoverable heat at 6 bar liquefaction pressure is 3.69 MW. Total power consumption of ammonia single-refrigerant liquefaction cycle is shown in Table 45. The total power consumption, 8.65 MW, is 38.4% higher than 8-stages compression with intercooling for the proposed system.

Table 45: Total power consumption and efficiency of liquefying CO_2 at 6 bar using ammonia as a refrigerant

Liquefaction load (MW) to -53^{o}C	9.01
Pumping power (MW) to 150 bar	0.33
Recoverable Heat (MW) to -47 to 37^{o}C	3.69
Ammonia liquefaction cycle power (MW)	6.34
Minimum reversible liquefaction power (MW)	3.76
Liquefaction cycle COP	1.42
Liquefaction cycle Second Law efficiency (%)	59.34
CO_2 compressors power (MW) (from 1.8 bar to 6 bar)	1.98
Total power (MW)	8.65

4.3.2.2 Cascade CO_2 Liquefaction Cycles

According to Carnot COP Eq. 9, the COP of a VCC decreases when the ratio between the condensing temperature and evaporation temperature increases. In addition, the evaporation pressure in the single-refrigerant cycles was below atmospheric pressure which can cause air leak to the heat exchangers.

Cascade configuration employs two vapor compression cycles where the top VCC serves as the condensing cycle for the bottom VCC. The bottom VCC is the cooling cycle. Figure 67 shows the T-s diagram for ideal single-fluid VCC (AJGIA) and ideal cascade VCCs [133]. In the cascade configuration, the bottom VCC is indented by the corner states ABCDA and the top VCC by EFGHE. According to the T-s diagram, the improvements in the cascade configuration are less superheat (J-F line) in the condenser which results in less entropy generation in the condenser due to smaller temperature difference between the condenser and the ambient temperature. Also, there is improvement in the evaporator capacity (D-I line).

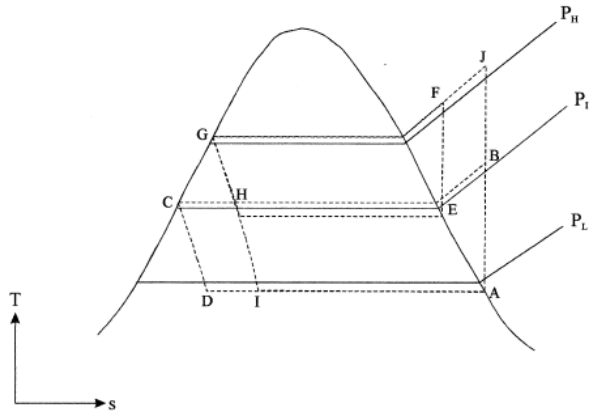

Figure 67: Two-stage, single-fluid vapor compression refrigeration cycle [133].

Different CO_2 liquefaction cascade cycles were designed and modeled using HYSYS software. One cascade model for CO_2 liquefaction at 8 bar liquefaction pressure with NH_3 refrigerant in the top VCC and CO_2 refrigerant in the bottom VCC is shown in Figure 68. The top VCC is designed to have two cooling levels: one for dehydrating and sensible cooling the CO_2 to 1^oC and one for liquefying the CO_2 refrigerant in the bottom VCC from 40^oC to -15^oC. The bottom VCC has one cooling level at -50^oC where liquefaction occurs. In both cycles, the refrigerants have a pressure higher than the atmospheric pressure. Therefore, the possibility of air leaks into heat exchangers is avoided in the cascade configuration.

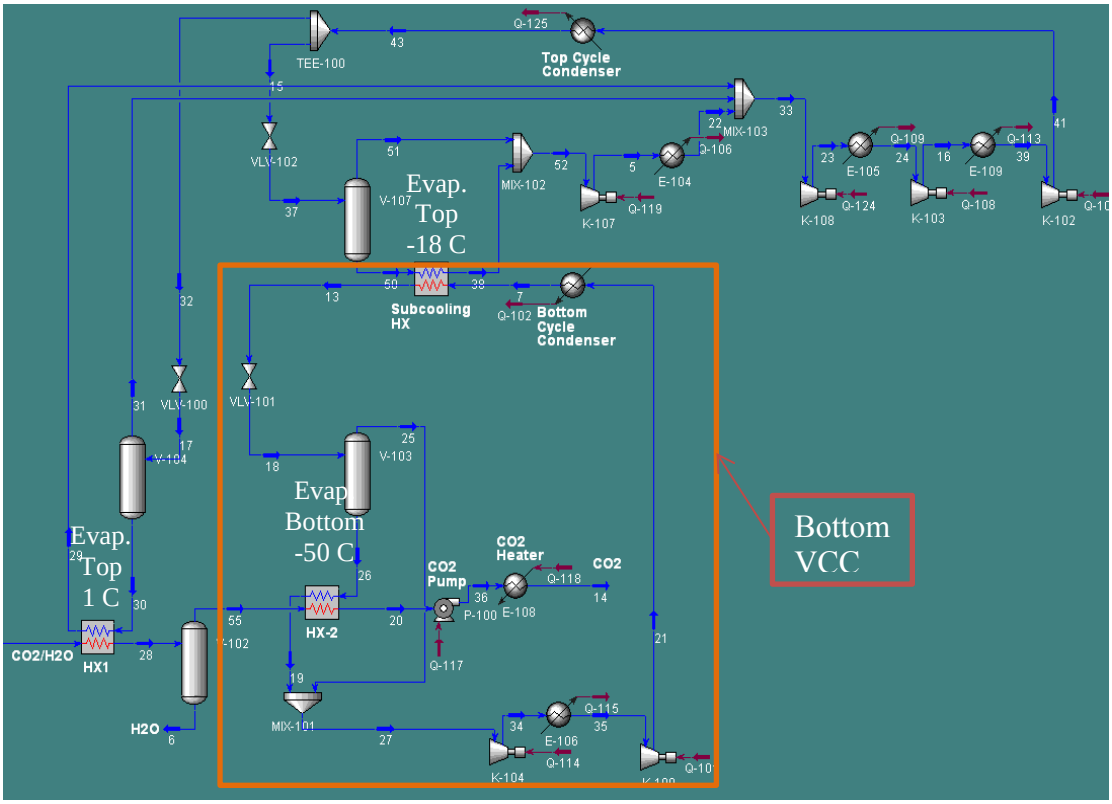

Figure 68: Cascade CO_2 liquefaction cycle using ammonia in the top cycle and CO_2 in the bottom cycle at 8 bar liquefaction pressure.

The performance of the cascade cycle is a function of the subcooling temperature. Optimization studies were done to find the optimum subcooling temperature using exergy minimization. For the CO_2/NH_3 configuration, a correlation was developed for finding the optimum subcooling temperature by Lee *et al.* [134]. Their correlation is as follows:

$$T_{opt,\,sc} = 40.63 + 0.4\,T_{cond} + 0.4\,T_{evap} + \Delta T_{cascade} \qquad (14)$$

Where, T is in K

At 40°C condensing temperature, -50°C evaporation temperature and 3 K approach temperature in the subcooling heat exchanger, the optimum subcooling

temperature using Lee *et al.*'s correlation is -15^{o}C. The total cascade VCC power consumption including the CO_2 compressor power at these conditions is 7.52 MW.

For further investigating CO_2 liquefaction cycle power consumption, four different refrigerants for CO_2 liquefaction at 6 bar liquefaction pressure using cascade configuration were also modeled using HYSYS software. The refrigerants are R134a, CO_2, NH_3 and propane. The modeled cycles have 5^{o}C cascade subcooling temperature and -55^{o}C CO_2 sensible cooling temperature. Their power consumption is shown in Table 46, where the lowest power consumption is for the C3-NH_3 cascade cycle.

Table 46: Power consumption of different cascade liquefaction cycles

Refrigerants (Top-Bottom)	NH_3-CO_2	NH_3-CO_2	C3-NH_3	C3-CO_2	R134a-NH_3
Liquefaction Pressure (bar)	6	8	6	6	6
Top VCC Power Consumption (MW)	2.37	3.04	3	3	3.15
Bottom VCC Power Consumption (MW)	4.8	2.06	3.31	4.69	3.29
Total VCC Power Consumption (MW)	7.17	5.10	6.31	7.67	6.44
CO_2 Compressor Power (MW)	1.98	2.13	1.98	1.98	1.98
Pump Power (MW)	0.34	0.29	0.34	0.34	0.34
Total Power Consumption (MW)	9.49	7.52	8.63	9.99	8.76

Since C3-NH_3 cascade cycle has the lowest power consumption, the optimum cascade subcooling temperature for it was investigated. The effect of the subcooling temperature is shown in Table 47. When the cascade subcooling temperature

decreased, the power consumption of the top cycle increased but the power consumption of the bottom cycle decreased. The table shows the lowest power consumption is at a 5 K cascade subcooling temperature.

Table 47: Effect of cascade subcooling temperature on the C3-NH_3 cycle at 6 bar liquefaction pressure

Cascade subcooling temperature (K)	Total C3-NH3Cascade Power (MW)
-33	8.14
-23	7.52
-13	6.96
-3	6.47
2	6.4
5	6.31
7	6.34
12	6.4
17	6.38
22	6.47
27	6.48
32	6.64

4.3.2.3 CO_2 Liquefaction Using Cold Seawater

Deep seawater is cooler than seawater at the surface. The temperature of the seawater can be as cold as 4°C depending on the depth of the sea. The assumed surface seawater temperature is 35°C. If seawater was extracted below the surface level, with a temperature of 4°C, it could be used to liquefy the CO_2 at the 6^{th} compression stage pressure (44.52 bar). A HYSYS model was developed that is similar to the 8-compression stage model except that it has a pump instead of the last two compression stages. Deep seawater is used to liquefy the CO_2 at 9°C. The resulting total power consumption with this configuration is 4.68 MW, which is 1.57 MW or 25.12% power savings as compared to the 8-compression stage case.

4.4 Optimization of CO_2 Liquefaction Pressure

CO_2 liquefaction is done by vapor compression cycles where the CO_2 is liquefied from 40°C to the liquefaction temperature. The liquefaction temperature is the saturation temperature at the liquefaction pressure (e.g. -53.5°C at 6 bar). As the liquefaction pressure increases, the liquefaction temperature will increase which will increase the Carnot COP of a liquefaction cycle as shown in Figure 69. The graph shows that the Carnot COP of the liquefaction cycle varies from 2.3 at 5.7 bar to 31 at 72 bar as a result of the variation of the liquefaction temperature. However, this will have four consequences. First, it will add more power to the CO_2 compressors that compress the CO_2 to the liquefaction pressure which is above the triple point pressure (5.17 bar). Second, it will reduce the latent liquefaction load as shown in the P-h diagram Figure 72. Third, it will reduce the pumping power of the liquefied CO_2 from the liquefaction pressure to the injection pressure (150 bar). Fourth, it will make the pressurized liquid CO_2 warmer which will make it not suitable for cold energy recovery. As a result, the recoverable cooling in the liquefied and pressurized CO_2 decreases as shown in Figure 70.

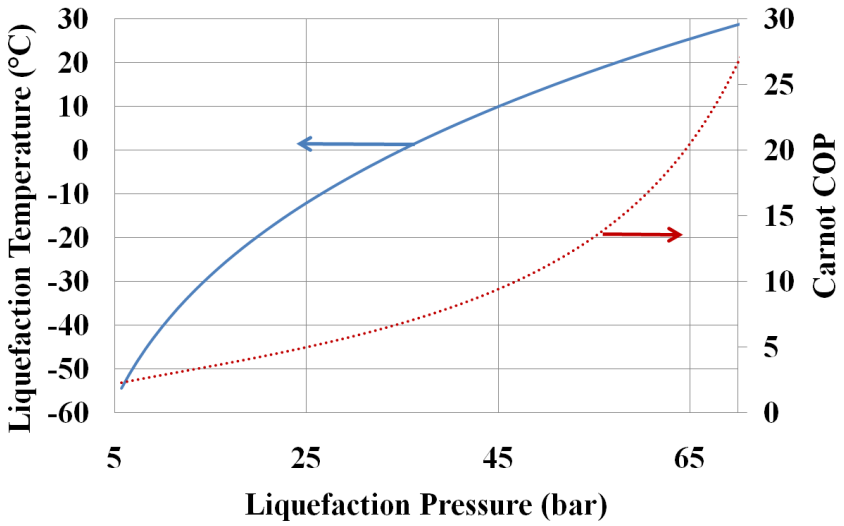

Figure 69: Liquefaction pressure versus liquefaction temperature and Carnot cooling cycle COP.

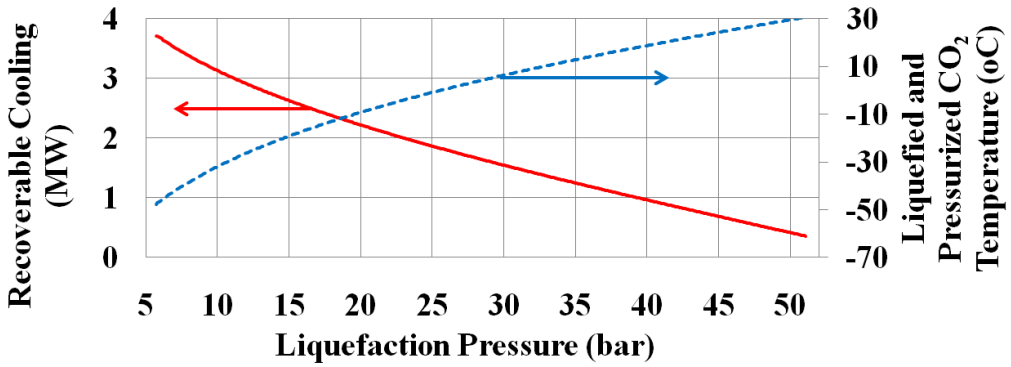

Figure 70: Recoverable cooling in the liquefied and pressurized CO_2 variation with liquefaction pressure.

Since there are two conflicting objectives (i.e., CO_2 compressor power and CO_2 liquefaction cycle power), an optimum liquefaction pressure can be investigated. Thus, a Matlab code was written to find the optimum liquefaction pressure with has the lowest power consumption. The code is coupled with a generic HYSYS model that was developed for this purpose. The generic HYSYS model, shown in Figure 71, calculates the CO_2 compressors and a pump power. It also calculates the liquefaction

latent load and the available cold energy in the liquefied and pressurized CO_2 (e.g. -46.3°C at 150 bar that was liquefied at 6 bar). This cold energy is recovered in a recovery heat exchanger. The P-h and T-s diagrams for the liquefaction process against compression process are shown in Figure 72.

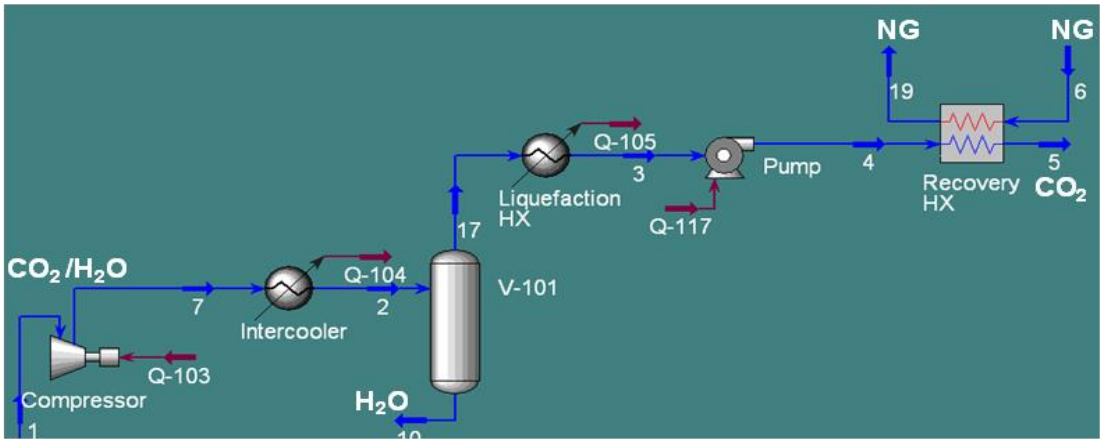

Figure 71: Generic HYSYS model for finding the optimum liquefaction power.

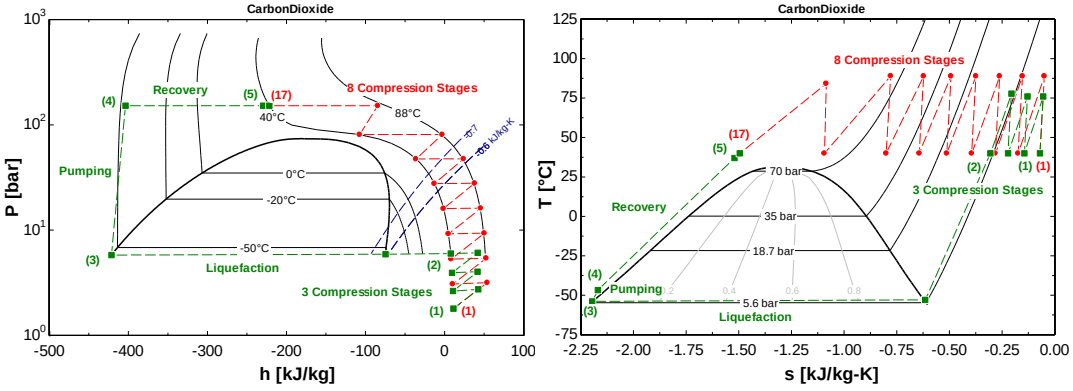

Figure 72: CO_2 P-h and T-s diagrams showing two pressurizing processes. liquefaction and pumping with cold CO_2 recovery (Green). Multistage compression with intercooling (Red).

The optimization technique was based on the exhaustive search technique because all designs are considered in finding the optimum solution. Further, the

design space is not large and the generic HYSYS model is computationally simple. The Matlab-HYSYS interface code structure is shown in Figure 73. The liquefaction pressure was the only variable and it was varied from 5.7 bar to 72 bar with a step value, ΔP, of 0.1 bar. Thus, 663 designs were considered.

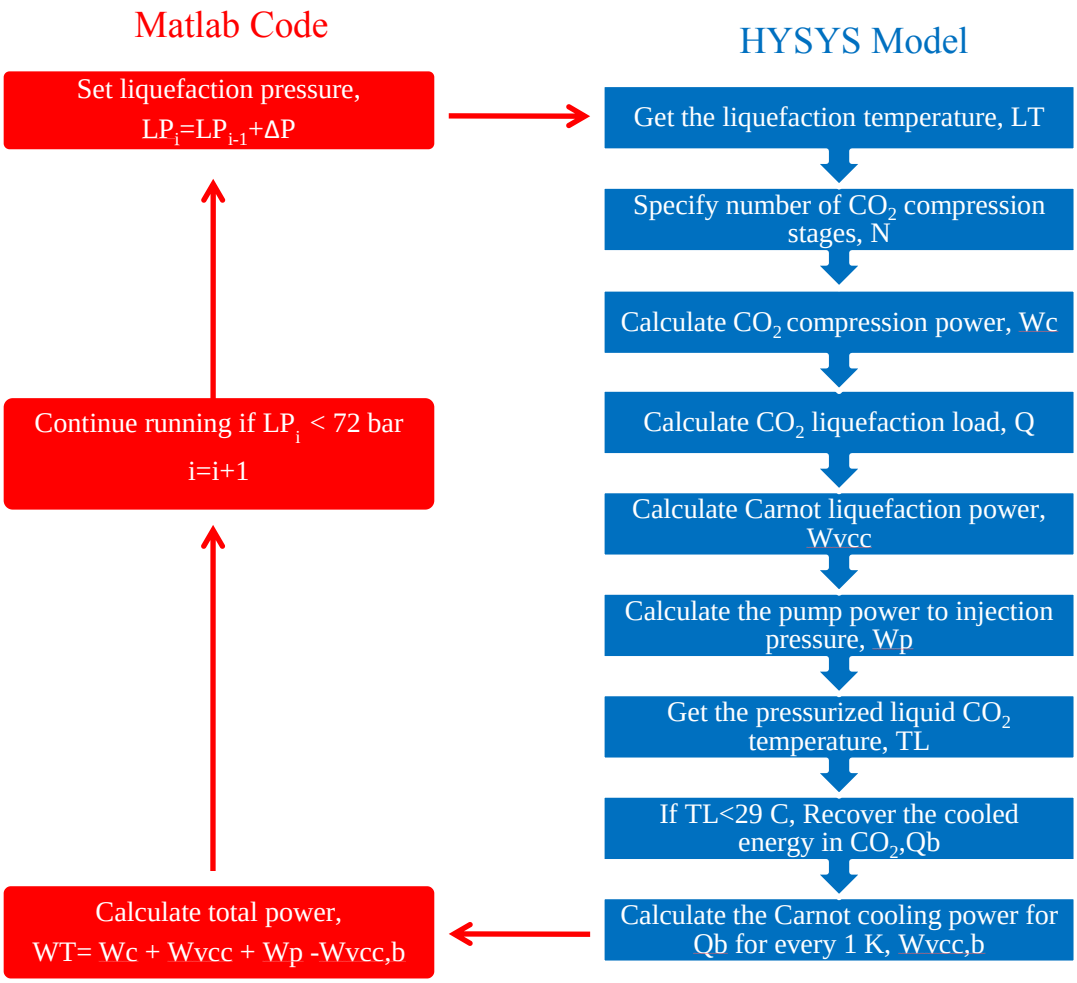

Figure 73: Matlab-HYSYS interface code structure.

The vapor compression cycle liquefaction power, Wvcc, was calculated using following equation:

$$\text{Wvcc} = \frac{Q}{Carnot\ COP * \eta_{II}} \qquad (15)$$

Where,

T_{evap} is the liquefaction temperature

T_{cond} is the condensing temperature

Q is the latent liquefaction load

η_{II} is the Second Law efficiency

Since the pressurized liquid CO_2 is sensibly heated when it cools the natural gas stream (the temperature of the pressurized liquid CO_2 is not constant here), the Carnot COP needs to be discretized for more accurate calculation of the vapor compression cycle power that will be required to provide an equivalent cooling to the recoverable cold energy. Thus, the Carnot COP calculation for the Recovery HX, Figure 71, was discretized for every 1 K.

The results from the exhaustive search are shown in Figure 74. Total power for different cooling cycles' Second Law efficiencies are plotted to show where the optimum solution is located based on the efficiency of the vapor compression cycle. The Second Law efficiency describes how close a real cycle is to an ideal cycle. Thus, by using Carnot cycle and assuming the Second Law efficiency we can find the optimal solution.

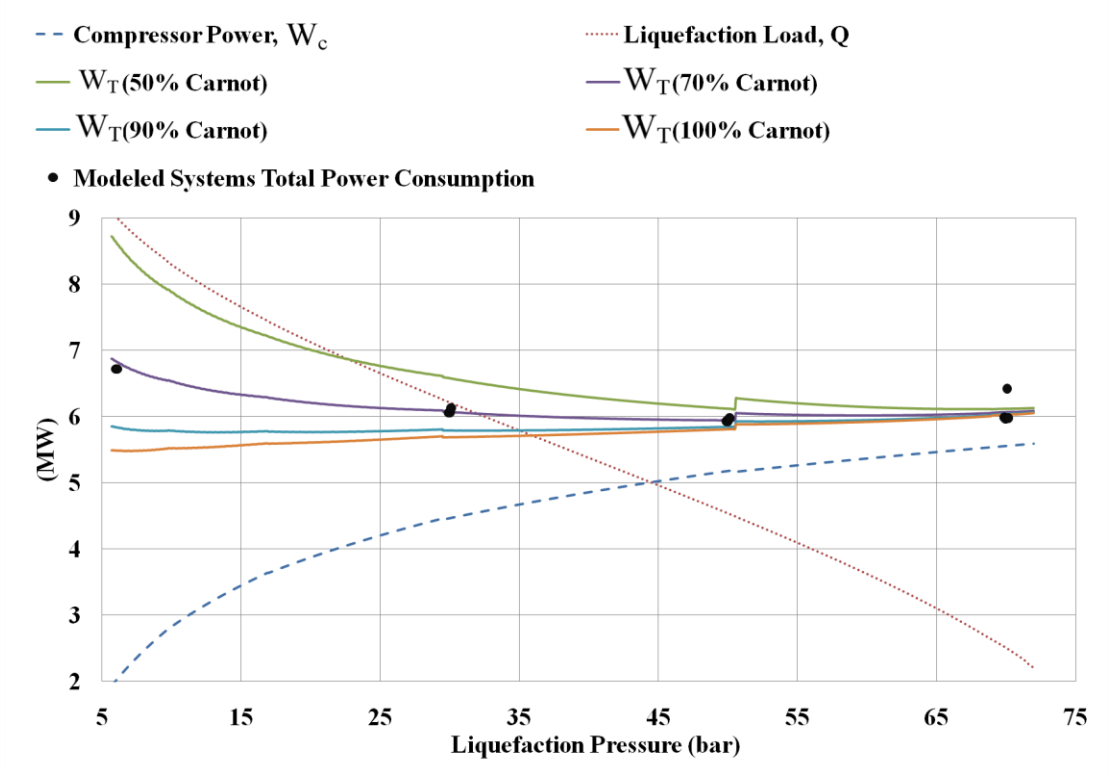

Figure 74: Total power consumption for CO_2 liquefaction and pressurization at different liquefaction pressures.

Figure 74 shows that for efficient cycles (η_{II} of 100% and 90% cases), the optimal solution is at the lowest liquefaction pressure. However, no real vapor compression cycle has such efficiency. For η_{II} of 70% and 50% cases, the optimum is located at 50 bar liquefaction pressure. The small jump in the total power curves at 51 bar is because the temperature of the liquid CO_2 is greater than 29^{o}C, so it was not utilized in cooling another stream.

The modeled systems in the graph are complete HYSYS models for CO_2 liquefaction cycle with cold energy recovery (Details in Section 4.5). They are superimposed in the graph to verify the code and the generic HYSYS model.

Furthermore, their location on the graph indicates that they all have 70% Second Law efficiency.

4.5 CO_2 Liquefaction Cycles with Waste Heat Recovery

In this section, some of the waste heat sources and their uses that were proposed in Figure 28 are modeled.

4.5.1 Using Cold CO_2 for Cooling the CO_2 and Refrigerant

4.5.1.1 Single-Refrigerant CO_2 Liquefaction Cycles with Cold CO_2 Recovery in CO_2 Liquefaction Cycle

The proposed idea of using the cold CO_2 to subcool the refrigerant after the condenser, and to precool the CO_2 before liquefaction was also investigated and modeled using HYSYS software as shown in Figure 75. As stated earlier, the available cooling capacity in the liquefied CO_2 at 6 bar liquefaction pressure is 3.69 MW. Subcooling the refrigerant using the cold CO_2 will make the refrigerant cooler than 40°C after the refrigerant condenser and before its expansion valve. Therefore, lower refrigerant quality or more cooling capacity is available for liquefying the CO_2. HX-1, Figure 64, was replaced by a precooling heat exchanger for the CO_2/H_2O stream using the cold CO_2 in Figure 75. Thus, lower cooling load is required from the VCC.

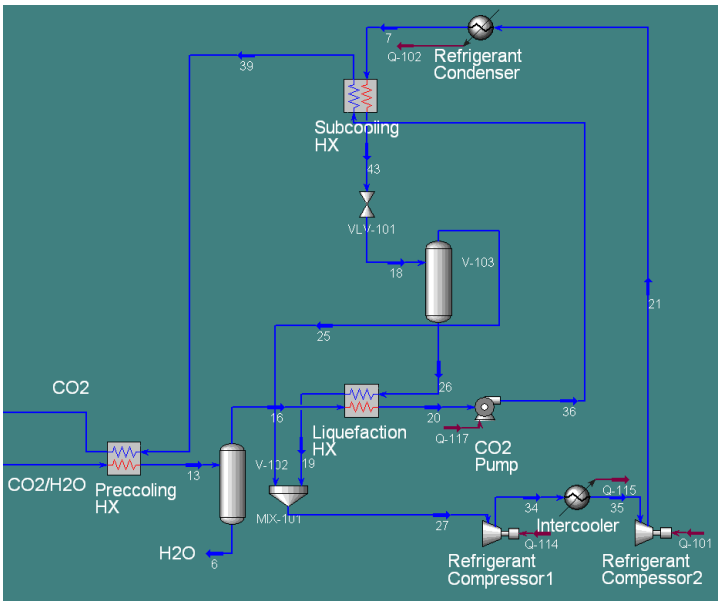

Figure 75: Single-refrigerant CO_2 liquefaction cycle with cold CO_2 recovery.

The P-h diagram for ammonia refrigerant with cold CO_2 recovery at 6 bar liquefaction pressure is shown in Figure 76. In comparison to the cycle without cold CO_2 recovery (Figure 64), the subcooling temperature is -10°C instead of 40°C. Further, the VCC cooling load is 7.23 MW instead of 9.01 MW. The resulting VCC power consumption is 4.39 MW, which is 30.75% less than the cycle without cold CO_2 recovery.

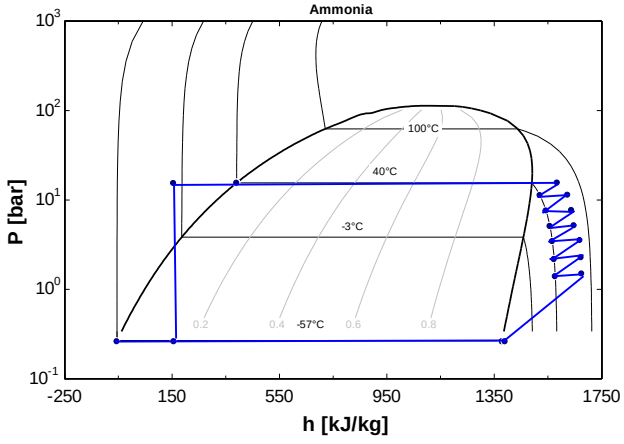

Figure 76: P-h diagram for ammonia in single-refrigerant CO_2 liquefaction cycle at 6 bar with cold CO_2 recovery.

Since liquefaction pressure effects liquefaction load and CO_2 compressors power, eight liquefaction cycles with cold CO_2 recovery were modeled using HYSYS software that has different refrigerants at randomly chosen liquefaction pressure. The results, Table 48, show that the lowest total power consumption is at 50 bar liquefaction pressure using ammonia refrigerant. Moreover, Table 48 shows that at different liquefaction pressures, different refrigerants other than ammonia can be used with close power consumption. In comparison to CO_2 compression only (conventional configuration), the savings in power consumption for the ammonia cycle at 50 bar is 5.12%. On the other hand, the savings against ammonia liquefaction cycle at 6 bar liquefaction pressure without cold CO_2 energy recovery is 31.44%.

Table 48: Results from HYSYS models for different CO_2 liquefaction cycles.

Refrigerant	R134a	NH_3	NH_3	NH_3	R134a	CO_2	Propane
Liquefaction Press. (bar)	30	30	6	70	70	70	70
Pump (MW)	0.34	0.34	0.34	0.38	0.38	0.38	0.38
VCC Power (MW)	1.43	1.37	4.39	0.15	0.15	0.6	0.16
CO_2 Comp. Power (MW)	4.36	4.36	1.98	5.44	5.44	5.44	5.44
Total Power (MW)	6.13	6.06	6.72	5.97	5.98	6.42	5.99
Refrigerant	NH_3	R141b	R142b	CO_2	Propane	R22	R134a
Liquefaction Press. (bar)	50	50	50	50	50	50	50
Pump (MW)	0.33	0.33	0.33	0.33	0.33	0.33	0.33
VCC Power (MW)	0.59	0.61	0.61	1.27	0.63	0.64	0.62
CO_2 Comp. Power (MW)	5.01	5.01	5.01	5.01	5.01	5.01	5.01
Total Power (MW)	5.93	5.95	5.95	6.61	5.97	5.98	5.96

Alefeld and Radermacher [135] derived a dimensionless parameter that can be used to evaluate the performance of vapor compression cycles with different refrigerants. The parameter, shown in Equ. 16, represents the ratio of the liquid specific heat multiplied by the temperature difference over the refrigerant latent heat

at the evaporator temperature. The COP of a vapor compression cycle improves with refrigerants having low cT/r because these refrigerants will have less superheating and less expansion loss. The investigated refrigerants for the heat pump that have low cT/r values resulted in less power consumption than refrigerants with large cT/r as shown in Figure 77.

$$cT/r = \frac{Cp*(T_{Cond.}-T_{Evap.})}{hfg_{Evap.\ Temp.}} \quad (16)$$

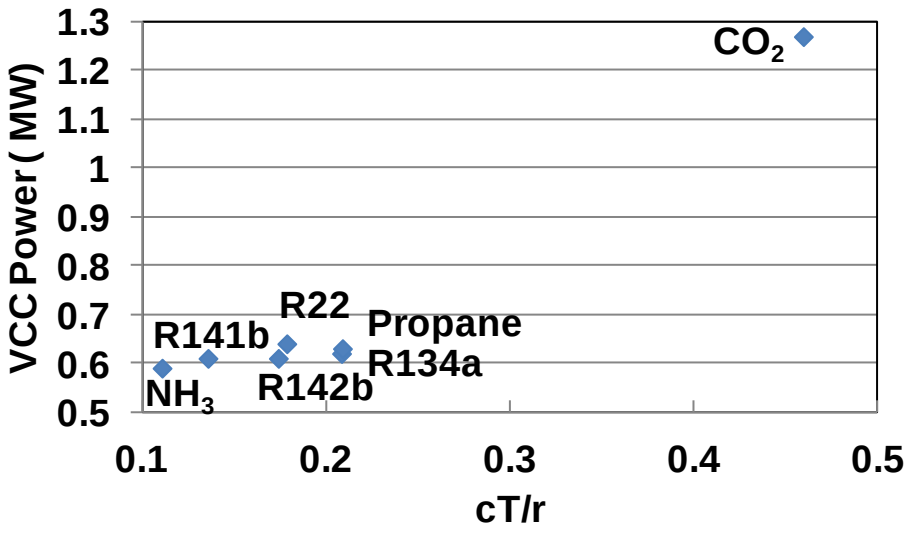

Figure 77: Alefeld and Radermacher dimensionless parameter for the investigated refrigerants at 50 bar liquefaction pressure.

4.5.1.2 Cascade CO_2 Liquefaction Cycles with Cold CO_2 Recovery in CO_2 Liquefaction Cycle

The proposed idea of using the cold CO_2 to subcool the refrigerant after the condenser and to precool the CO_2 before liquefaction was also investigated and modeled for the cascade configuration using HYSYS software as shown in Figure 78. The available cooling capacity in the liquefied CO_2 at 8 bar liquefaction pressure is 3.38 MW.

HX-1, Figure 68, was replaced by two precooling heat exchangers for the CO_2/H_2O stream using the cold CO_2 in Figure 78. These two heat exchangers precool the CO_2 to -37^oC. Further, a subcooling heat exchanger was introduced to subcool the NH_3 refrigerant to 0^oC in the Top VCC using the cold CO_2. As a result, the total cascade power consumption was reduced from 7.52 MW to 6.69 MW, which is 0.82 MW or 11.03% power savings.

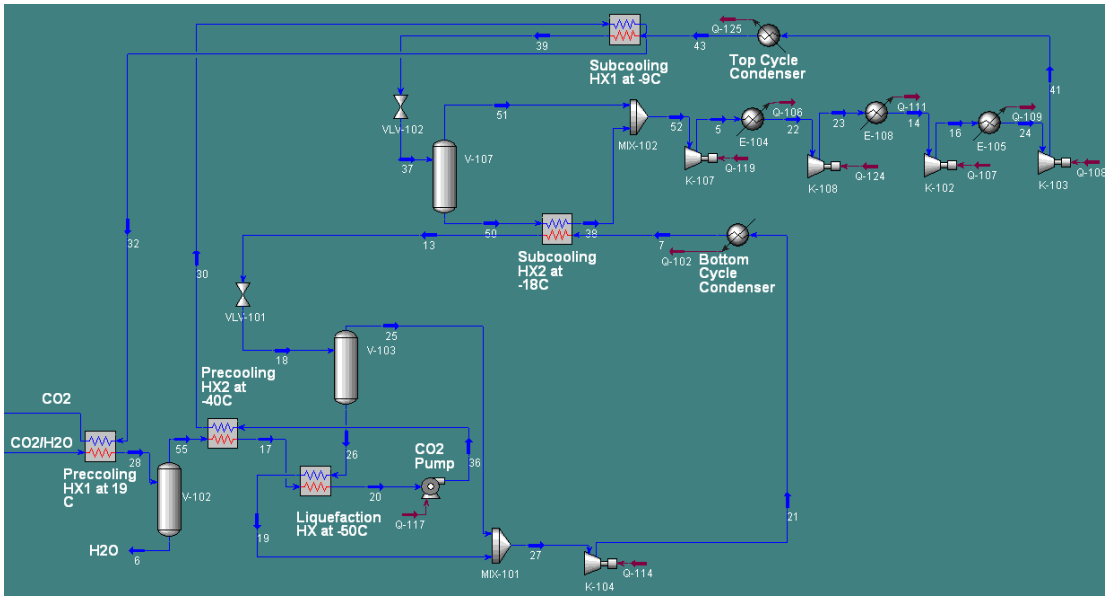

Figure 78: Cascade CO_2 liquefaction cycle using ammonia in the top cycle and CO_2 in the bottom cycle at 8 bar liquefaction pressure with cold CO_2 recovery.

4.5.2 Using Flue Gas Waste Heat for CO_2 Liquefaction

The available waste heat in the Combined Cycle with a High Temperature Condenser configuration (Figure 30) that also utilizes the waste heat in the flue gas from 140^oC to 80^oC is 116.6 MW. Part of this waste heat, 26.68 MW, is used to cool the flue gas to 27^oC. Other part, 13.35 MW, is used to replace the VCC with ammonia absorption chillers for liquefying the CO_2 at -12^oC or 25 bar liquefaction pressure. The liquefaction load is 5.84 MW. The total power consumption (CO_2 compressors

and pump) for this option is 4.37 MW, which is the lowest power consumption for preparing the captured CO_2 for injection (1.88 MW or 30.08% power savings as compared to the multi-stage compression).

4.6 Open CO_2 Liquefaction Cycle

4.6.1 Conventional Open CO_2 Liquefaction Cycle

The second way to pressurize CO_2 is to liquefy it and then pump it to the desired pressure. The open CO_2 liquefaction cycle is a patented cycle for liquefying the CO_2 from a stationary source by Aspelund *et al.* [89]. According to Aspelund *et al.*, the liquefaction of CO_2 is best achieved using their open CO_2 liquefaction cycle. The purpose here is to model the open CO_2 liquefaction cycle at equivalent ambient conditions as the previous models.

The working principle of the cycle is that it uses the captured CO_2 to liquefy itself. As shown in the developed HYSYS model for the open CO_2 liquefaction cycle (Figure 79), the cycle consists of three compression stages, three intercoolers and two multi-stream heat exchangers. Portion of the compressed CO_2 is re-circulated and expanded through an expansion valve. Due to CO_2 expansion, its temperature will be reduced and then it can be used to cool another incoming CO_2 stream. Then, the CO_2 that was used to cool the incoming CO_2 stream is sent back in a vapor state to an intermediate compressor. A final expansion valve is used to expand the compressed and cooled CO_2 to a low pressure at a saturation state where the vapor and liquid are separated. The vapor is used in cooling the incoming CO_2 stream while the liquid is sent to storage or pumping.

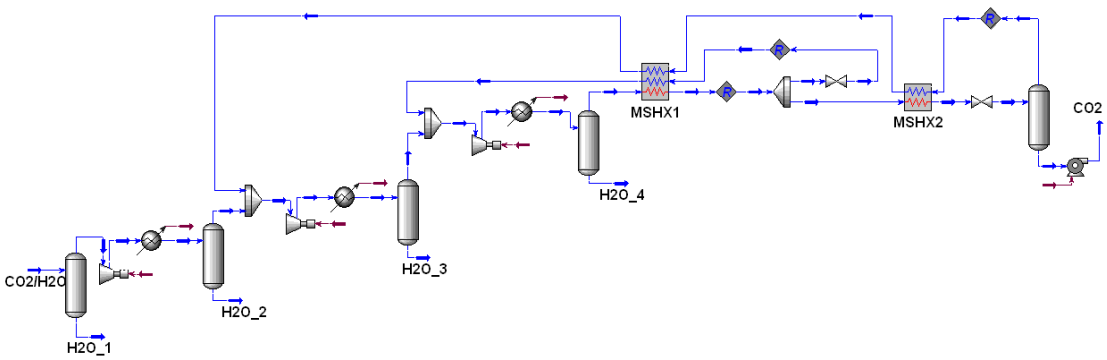

Figure 79: Open CO_2 liquefaction cycle HYSYS model.

The open CO_2 liquefaction cycle power consumption is function of the available seawater temperature, the mass recirculation ratio and three pressure levels (i.e., the high side and the two expansion pressures). Due to mass flow rate recirculation, the convergence of the model was not simple. So in order to understand the performance of this cycle, a simplified exhaustive search was done by varying the seawater temperature from 28°C to 40°C and the high side pressure from 43 bar to 70 bar at 0.35 mass flow rate recirculation ratio. It was observed that the power consumption was not a strong function of the mass flow recirculation ratio because the model kept re-circulating the required amount of CO_2 until it liquefied the desired amount of CO_2 so that mass balance is satisfied.

Twenty four cycles were resulted from the exhaustive search for liquefying the same feed gas (Table 42). Their power consumption values varied from 14 MW to 34 MW. The power consumption decreased with lower seawater temperature and higher high side pressure as shown in Figure 80. The figure also shows for a given seawater temperature, the high side pressure needs to be increased in order to reduce the compression power. The reason for this reduction in power consumption although

the pressure is higher is that at high pressure case the re-circulated and expanded mass flow rate is reduced and it is in the two-phase region which has lower temperature and lower enthalpy.

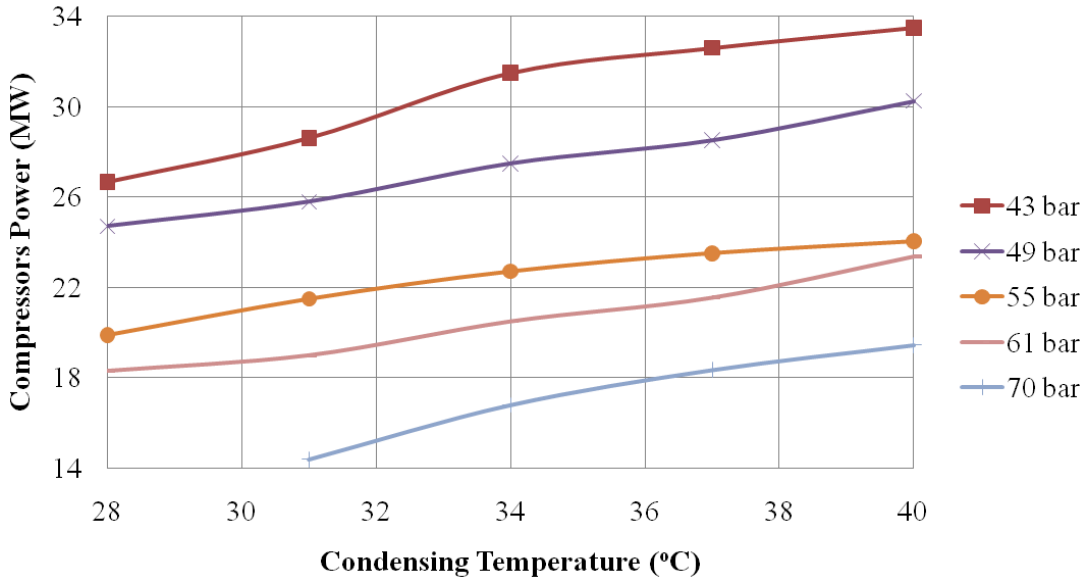

Figure 80: Exhaustive search results for varying the condensing temperature and the high side pressure of the open CO_2 liquefaction cycle.

Two open cycles at two different high side pressures are plotted in P-h diagrams as shown in Figure 81. Although they are both cooled by an equivalent condensing temperature (40^oC), they have different power consumptions for liquefying 72.42 Ton/hr of CO_2 feed gas. In order to simplify plotting the cycles in P-h diagram, the water content was ignored here since it is only a small percentage and most of it would condense during the first compression stage. The highest pressure side for the low pressure one, Figure 81(a), is 50 bar and its power consumption is 28.7 MW. The highest pressure of the high pressure cycle, Figure 81(b), is 93 bar and its power consumption is 8.014 MW. As explained, the reason for this difference is that the high pressure one uses two-phase CO_2 which has more cooling capacity than

the low pressure one which uses vapor CO_2. This resulted in three times more re-circulated CO_2 mass flow rate for the low pressure cycle than the high pressure cycle.

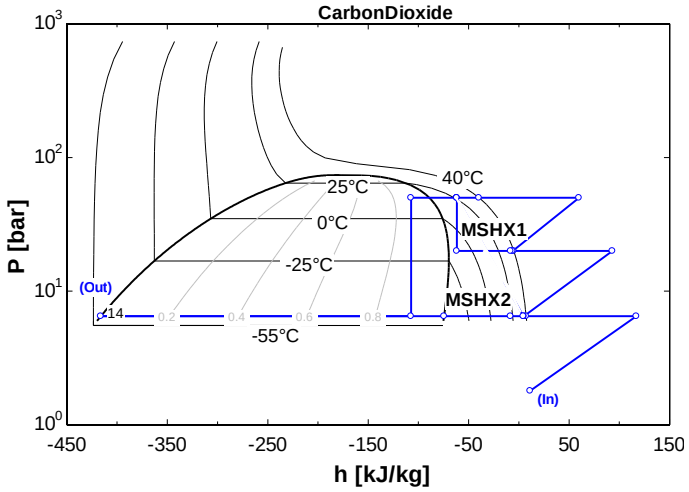

(a)

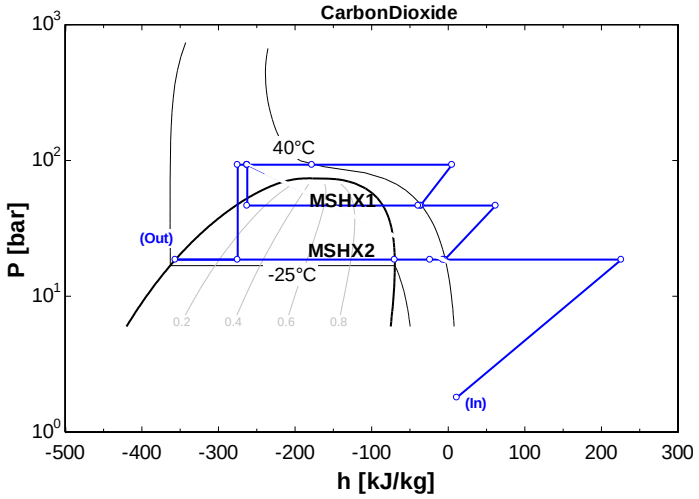

(b)

Figure 81: (a) P-h diagram for the low pressure open CO_2 liquefaction cycle. (b) P-h diagram for the high pressure open CO_2 liquefaction cycle.

4.6.2 Open CO_2 Liquefaction Cycle Model Verification

Since there is no available experimental data for the open CO_2 liquefaction cycle, the developed HYSYS model was verified against EES model for two different

high side pressures. The verification results show good agreement as tabulated in Table 49.

Table 49: Open CO_2 liquefaction cycle model verification

Power Consumption	HYSYS Model	EES Model	Discrepancy (%)
Power Consumption (HP=93 bar) (MW)	8.014	7.71	-3.79
Power Consumption (HP=50 bar) (MW)	28.7	28.38	-1.11

4.6.3 Modified Open CO_2 Liquefaction Cycle

The least power consumption using open CO_2 liquefaction cycle, Figure 79, for liquefying the feed gas showing in Table 42 was found to be 8.2 MW. The liquefied CO_2 after pumping to 150 bar is at a temperature of -43^oC. A simple modification would be to use this stream in the multi-steam heat exchangers to liquefy the incoming gas stream. Thus, less mass flow rate needs to be re-circulated. This modification resulted in reducing the power consumption to 7.33 MW or 11.87% savings.

4.7 Comparison

Table 50 lists the least power consumption for all explored options. It shows that the developed VCC that uses NH_3 as a refrigerant and recovers the cold energy in the liquefied CO_2 at the optimum liquefaction pressure consumes less energy than the conventional multi-stage compression with intercooling by 5.12%. Further, the NH_3-CO_2 cascade cycle consumes less power than the single refrigerant cycle if the cold CO_2 energy were not recovered. The open CO_2 liquefaction cycle consumes the highest power due to the large recirculated mass flow rate (31.2% more power than conventional compression at 40^oC condensing temperature).

Table 50: Summary of the least power consuming options for pressurizing the CO_2 to 150 bar.

Option	Total Power Consumption (MW)	Note
Compression	6.25	Baseline
Single refrigerant	8.65	NH_3 VCC at 6 bar liquefaction pressure
Single refrigerant w/ energy recovery	5.93	NH_3 VCC at 50 bar liquefaction pressure
Cascade cycle	7.52	NH_3-CO_2 VCCs at 8 bar liquefaction pressure
Cascade cycle w/ energy recovery	6.69	NH_3-CO_2 VCCs at 8 bar liquefaction pressure
Open cycle	8.2	93 bar high side pressure
Modified open cycle w/ energy recovery	7.33	93 bar high side pressure
NH_3 absorption chillers	4.37	Subjected to the availability of waste heat
Liquefaction using seawater	4.68	Subjected to the availability of seawater at 4^oC

4.8 Sensitivity Analysis

Since the developed vapor compression CO_2 liquefaction cycles that use NH_3 as a refrigerant at an optimized liquefaction pressure resulted in less power consumption than the conventional multi-stage compression cycle, sensitivity analysis needs to be conducted to explore the change in the power savings if different heat exchangers' pressure drop and compressors' isentropic efficiency were used than the one used in Table 19. In the sensitivity analysis, the heat exchangers pressure drop was varied from 0 to 50 kPa with an increment of 2.5 kPa and the CO_2 compressors and the refrigerant compressors isentropic efficiency was varied from 50 to 95% with an increment of 4%. Thus, 231 cases were compared. The power consumption of both cycles increases with increasing the heat exchangers pressure and with decreasing the compressors isentropic efficiency.

The savings in power consumption, which is the difference between the two cycles' total power consumption, increases with increasing the heat exchangers pressure drop and with decreasing the compressors isentropic efficiency as shown in Figure 82. This means that the developed cycle outperforms the conventional cycle especially when using compressors with low efficiency and heat exchangers with high pressure drop. The developed cycle resulted in power savings as much as 12.24%, which is 1.59 MW. The power savings decreases with high compressors' efficiency since the compression process approaches the isentropic compression process. On the other hand, further power savings could be achieved in the liquefaction and pumping approach since there are more variable to optimize (e.g., refrigerant, mass flow rates, pressure) than the multi-stage compression approach.

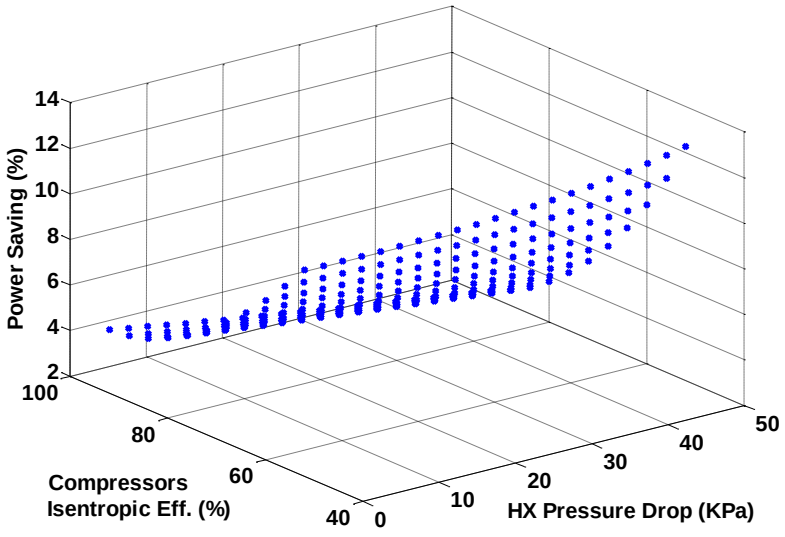

Figure 82: Percent of power savings in the developed liquefaction cycles changes with heat exchangers pressure drop, compressors isentropic efficiency and seawater temperature.

4.9 Effect of the Condensing Temperature

The condensing temperature has a significant effect on the performance of the conventional multi-stage compression cycle as well as the liquefaction cycle. Investigating the effect of the condensing temperature is important when implementing the developed cycles in cold regions or warm regions or when the available seawater temperature changes significantly during a year. The effect of the condensing temperature on the performance of the multi-stage compression cycle and the liquefaction cycle was investigated as shown in Figure 83. The condensing temperature was varied from 5^{o}C to 43^{o}C which represents having seawater with temperature as low as 1^{o}C and as high as 38^{o}C.

The multi-stage compressor model has 8 stages. The outlet pressure of each stage is shown in Table 51. The compression power decreases with decreasing the condensing temperature because of the increase in the gas density. As the condensing temperature reduces below 29^{o}C, supercritical liquid is formed in the last intercooler. Therefore, the last compressor stage was replaced by a pump. Further reduction in the condensing temperature makes liquid formed after the 6^{th} compressor intercooler. Thus, six compressors and a pump were used in a condensing temperature of less than 9^{o}C.

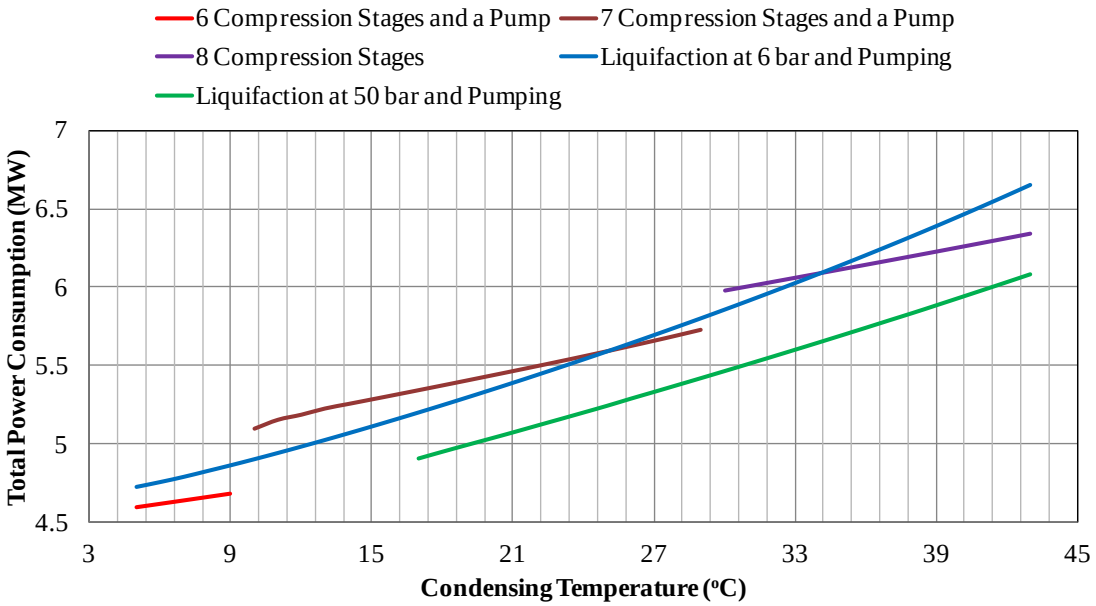

Figure 83: Total power consumption change with condensing temperature for several pressurization options for pressurizing the captured gases from atmospheric pressure to 150 bar.

Table 51: Outlet pressure in the multi-compression stage model.

Compression Stage	Outlet Pressure (bar)
1st stage	3.13
2nd stage	5.28
3rd stage	8.99
4th stage	15.38
5th stage	26.26
6th stage	44.52
7th stage	81.00
8th stage	150.00

At the optimized CO_2 liquefaction pressure (50 bar), CO_2 liquefaction using vapor compression cycle resulted in less power than multi-stage compression for all condensing temperature which confirms the superiority of the developed cycle. The total power consumption was calculated using the generic HYSYS model shown in Figure 71. The condensing temperature was limited to 17°C so that no liquid is

formed in the CO_2 compressors. As the condensing temperature is reduced, the liquefaction cycle power is reduced due to the increase of the liquefaction cycle COP.

Nonetheless, CO_2 liquefaction and pumping at 6 bar liquefaction pressure consumed more power than multi-stage compression in high condensing temperature (above 34^{o}C) and low condensing temperature (below 9^{o}C where CO_2 is liquefied using seawater). The reason is that at high condensing temperature and low liquefaction temperature (-53.5^{o}C at 6 bar) the vapor compression cycle COP is small. The investigation here shows the importance of using optimization which resulted in developing a liquefaction cycle that outperformed a multi-stage compression in all condensing temperatures.

4.10 Effect of the Injection Pressure

The injection pressure is a function of several variables such as the well pressure and piping length. It was assumed to be 150 bar. The effect of changing the injection pressure from 80 bar to 200 bar was investigated on the multi-stage compression cycle as well as the CO_2 liquefaction cycle at the optimized CO_2 liquefaction pressure. The results, shown in Figure 84, show that the power savings in using CO_2 liquefaction and pumping increase with increasing the injection pressure. At 200 bar injection pressure, the power savings reaches to 7% although the CO_2 liquefaction cycle was optimized for 150 bar injection pressure. However, the two options consume equivalent amount of power at 80 bar injection pressure. The reason for the variation in power savings with the injection pressure is due to the gain from increasing the CO_2 density becomes more significant at higher injection pressure. It

should be noted that more power savings could be achieved when using a CO_2 liquefaction cycle which was optimized for the required injection pressure.

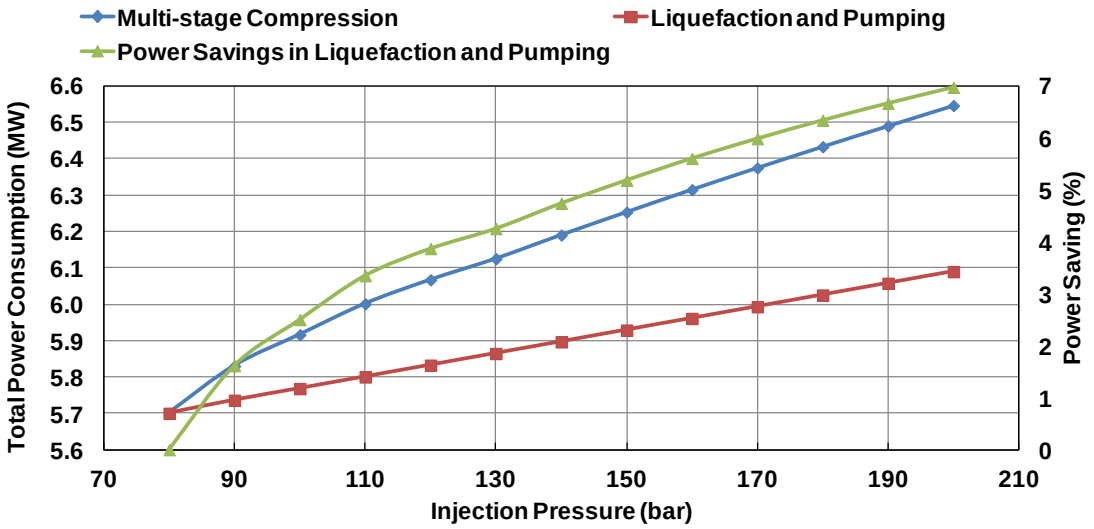

Figure 84: Effect of injection pressure on the power savings from using the NH_3 liquefaction cycle against the multi-stage compression.

4.11 Conclusions

Five options were investigated for pressurizing the captured CO_2 gas for EOR applications. The investigation was carried out through development of HYSYS models with models validation against experimental data with good agreements. The liquefaction of CO_2 was optimized using generic HYSYS model coupled with Matlab optimization tool that considers all power consumption and all recoverable cooling. The results show, for a liquefaction cycle that has 70% Second Law efficiency, the optimum liquefaction pressure is 50 bar where CO_2 liquefaction and pumping consumes less power than compression.

Sensitivity analysis was carried out to explore the effect of heat exchangers pressure drop and compressors isentropic efficiency on the power savings. The results show that the developed liquefaction cycle outperforms the conventional multi-stage

compression cycle in all cases explored. The regions where CO_2 liquefaction and pumping outperforms multi-stage compression with different seawater temperatures and injection pressures were identified. An open CO_2 liquefaction cycle model was developed and its performance was investigated. An improvement was made on the conventional open CO_2 liquefaction cycle that resulted in 10.61% power savings that the conventional open CO_2 liquefaction cycle.

Chapter 5: Proposed Regeneration Heat Source

5.1 Proposed Concept

In a typical CO_2 removal cycle, the regeneration heat is provided by low pressure steam at a temperature about 125^{o}C. This steam is extracted from the steam turbine as shown in Figure 85. As discussed previously, the steam extraction results in a significant power loss in the steam cycle. The power loss in the modeled conventional CCS configuration was calculated to be 29.06 MW (15.18% reductions in power). Out of the 29.06 MW, 23.06 MW power loss (79.35%) was due to the steam extraction for providing the 70.42 MW CO_2 regeneration heat. This huge power demand for providing the CO_2 regeneration heat limits the feasibility of implementing CO_2 capturing and sequestration. The power loss breakdown for the conventional system is plotted in Figure 22.

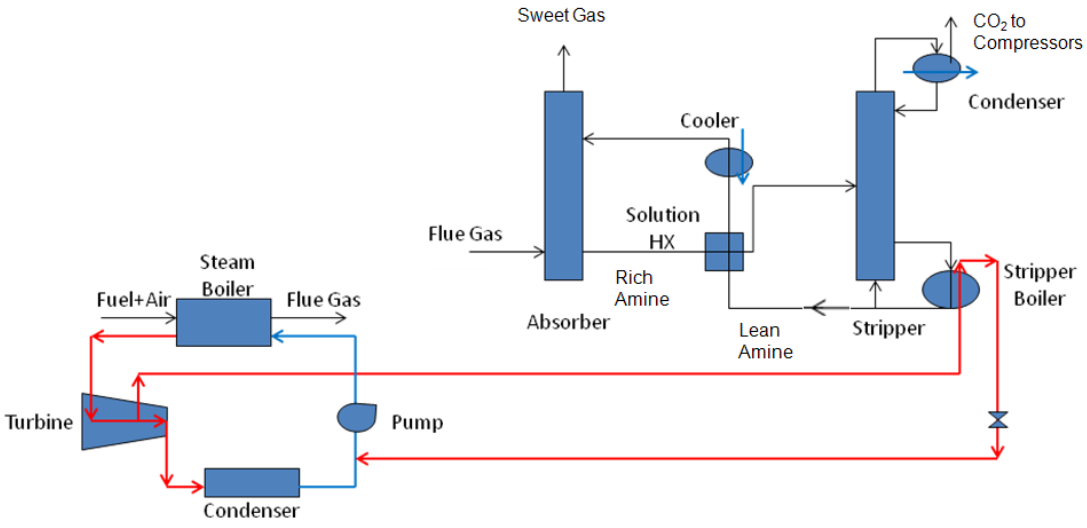

Figure 85: Schematic of steam power plant and CO_2 removal plant

To reduce the power drop from steam extraction, few innovative methods were proposed in the literature (refer to literature review section, Figure 6 to Figure 8). A new method is proposed here. The proposed method is to regenerate the CO_2 using heat from a heat pump condenser.

Heat pump based on vapor compression cycle is shown in Figure 86. The major components are compressor, evaporator, condenser and expansion valve. Power input is provided to the compressor to compress the refrigerant which makes the refrigerant's temperature to increase. In the condenser, heat is extracted from the refrigerant at high temperature and pressure until the refrigerant condenses. The refrigerant expands in the expansion valve which lowers its temperature and pressure. In the evaporator, heat is absorbed from the refrigerant at low temperature until the refrigerant evaporates.

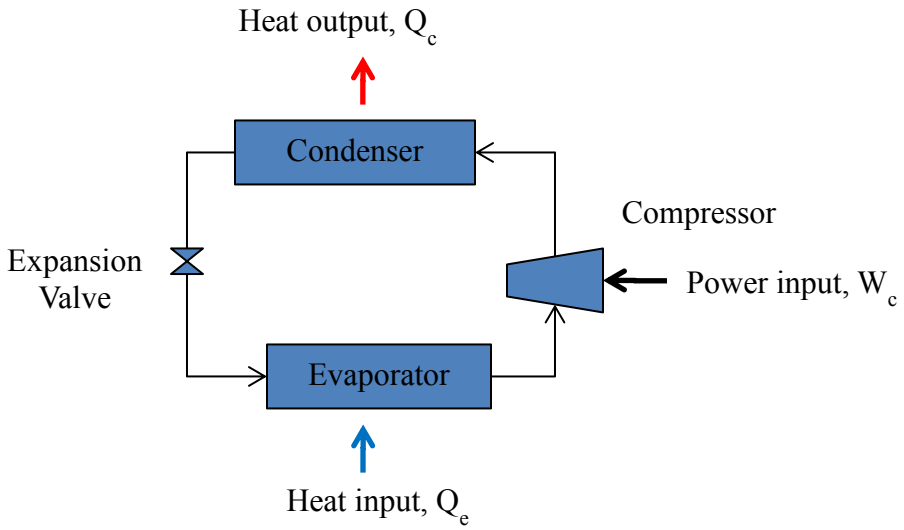

Figure 86: Schematic diagram of heat pump.

Energy balance of the heat pump shows that condenser heat, which is at high temperature, is the sum of the evaporator heat, which is at low temperature, and the compressor power, that is $Q_c=W_c+Q_e$. The condenser heat can be used to supply heat at high temperature, such as space heating, whereas the evaporator heat can be used to extract heat at low temperature, such as space cooling.

In addition to the CO_2 regeneration heat, cooling is needed in power plants with and without CCS. The cooling demands are usually met by using either seawater or ambient air. Sea water has a limited temperature that is a function of the environment and the location. Cooler temperature, which will increase the efficiency of the power plant, cannot be obtained without cooling devices which consume intensive energy. Similarly, heating is needed in any processes such as heating the condensed water in steam cycles or providing heat for an absorption chiller's desorber. Providing this heat also requires energy.

The proposed concept addresses the three requirements (i.e., providing the CO_2 regeneration energy, providing the cooling needs at lower temperature than the ambient temperature, and providing the process heating needs). The concept is using heat pump(s) with condenser that has three heat exchangers working at different temperature levels. The high temperature heat exchanger provides the CO_2 regeneration heat instead of steam extraction. The medium temperature heat exchanger provides heating for different processes such as condensed water preheating or desorber of absorption chiller's heating. The low temperature condenser dumps the remaining low grade heat to the ambient or could be used with adsorption cycle or dehumidification technologies. The heat pump evaporator will provide

cooling for different processes (such as cooling the flue gas before the absorber, cooling inlet air before the gas turbine, natural gas precooling in the APCI cycle or providing compressors intercooling need). The proposed heat pump is shown in Figure 87.

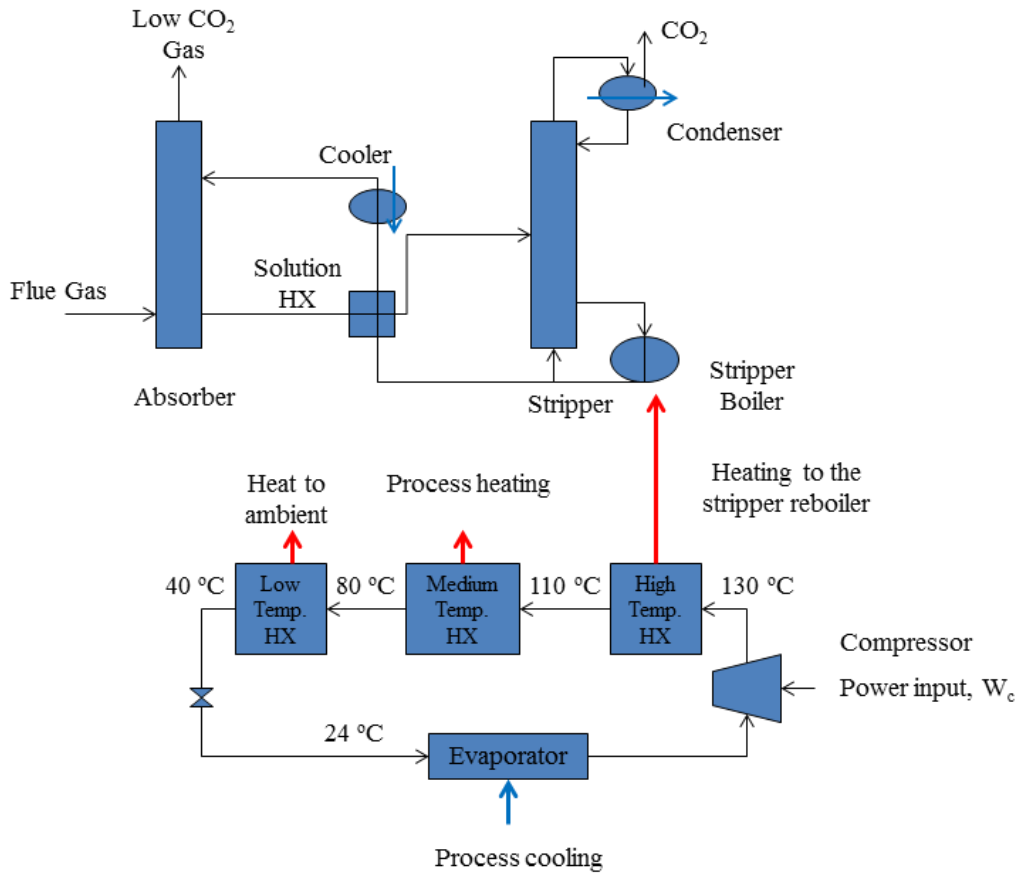

Figure 87: Proposed heat pump cycle with CO_2 regeneration.

5.2 Justification of the Heat Pump Concept Using Pinch Analysis

Pinch Analysis can be used to investigate the applicability of placing a heat pump using the grand composite curve. The grand composite curve represents the net

difference between the heat flow between the cold composite curve and the hot composite curve shifted at the pinch temperature [128]. Thus, no heat flows at the pinch point.

The grand composite curve of the CO_2 removal plant and flue gas cooling is shown in Figure 88. The pinch point occurred at 117^{o}C. CO_2 regeneration heat is needed above the pinch point and CO_2 and flue gas cooling is needed below the pinch point. According to Linnhoff's theory, a heat pump can be appropriately integrated across the pinch point to provide the cooling and heating needs. Thus, provide savings in cold utility as well as hot utility.

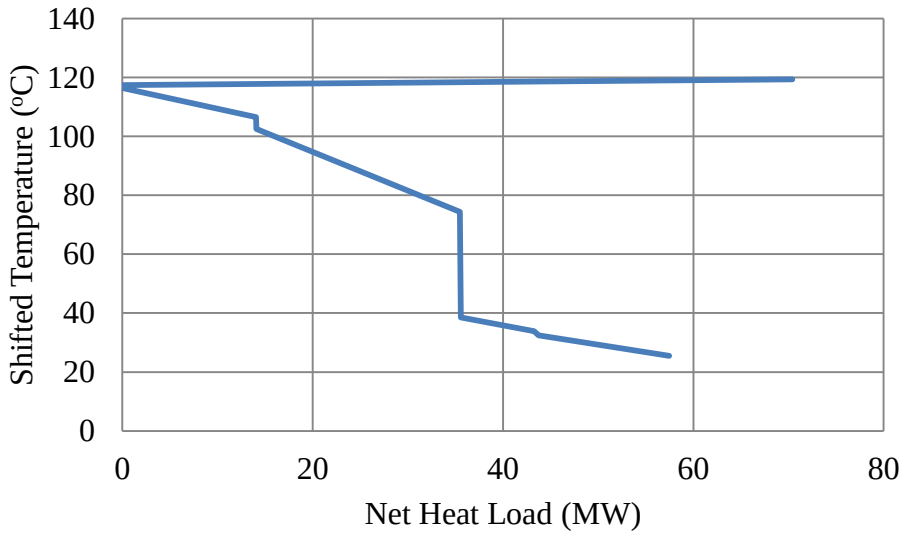

Figure 88: Grand composite curve of the CO_2 removal plant and flue gas cooling.

5.3 Heat Pump Model

A heat pump model was developed using HYSYS software as shown in Figure 89. The refrigerant is compressed to high temperature, e.g., 130^{o}C, and then cooled in three heat exchangers. The first heat exchanger represents the stripper

boiler, which has heat rate of 70.42 MW, and its outlet temperature is 110°C. The second heat exchanger cools the refrigerant to 80°C. According to the developed waste heat utilization graph, this heat exchanger can be used to provide heating for absorption chillers or other sources of heating such as heating the condensed steam in the steam power cycle. The third heat exchanger cools the refrigerant to the environment temperature, e.g. 40°C.

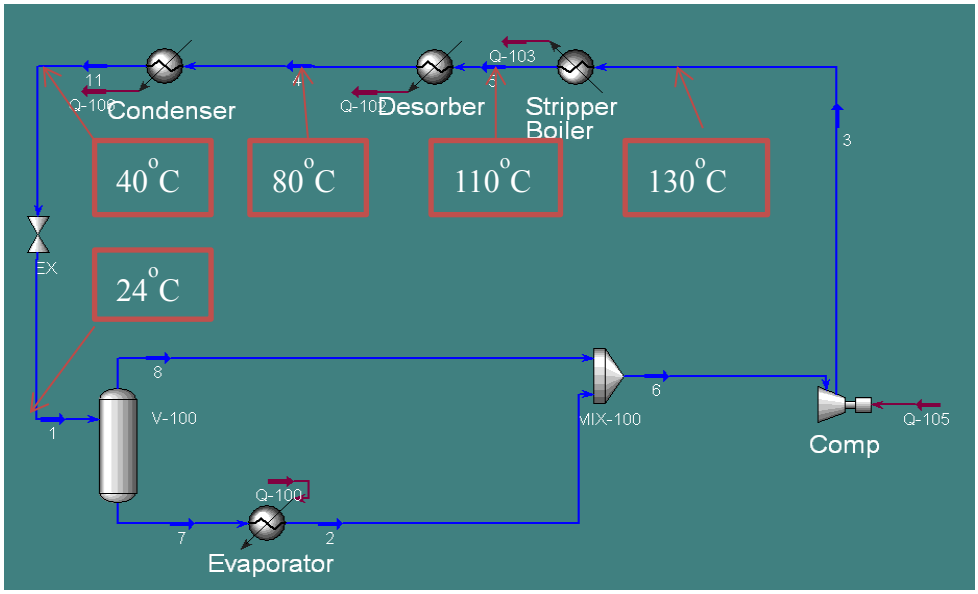

Figure 89: Proposed heat pump for providing CO_2 regeneration and additional cooling.

The proposed expansion temperature is 24°C. Thus, the expanded refrigerant can be used to cool the flue gas before it enters the CO_2 removal plant or other cooling options, e.g. APCI cycle or inlet air cooling to the gas turbine. The benefit ratio and the equivalent power gain were defined as follows:

$$\text{Benefit ratio} = \frac{(Q_{Evaporator}+Q_{Desorber}+Q_{Boiler})}{P_{Comp.}} \quad (17)$$

$$\text{Equivalent power gain} = \frac{Q_{Evaporator}}{COP_{VCC}} + \frac{Q_{Desorber}\, COP_{Abs.Chillers}}{COP_{VCC}} + PP_{NGCC} - P_{Comp.} \quad (18)$$

Where, $COP_{VCC} = 4$

$COP_{Abs.\ Chillers} = 0.37$

Prevented power loss due to not extracting the steam, $PP_{NGCC} = 24.4$ MW

The equivalent power gain represents the power needed to provide an equivalent cooling from the evaporator and the absorption chillers, and the power saved from not extracting steam in the steam cycle minus the required compressor power of the heat pump.

5.4 Heat Pump Model Verification

The heat pump model was developed using C# code which calls xProps refrigerants property calculations [145]. The C# code was verified against HYSYS model. The models verification resulted in good agreements as shown in Table 52.

Table 52: Heat pump model verification.

Model	Compressor Power (MW)	Evaporator Capacity (MW)	Desorber Capacity (MW)	Discrepancy in Compressor Power (%)
R141b using C# code	23.98	77.54	13.80	-1.24
R141b using HYSYS	23.69	77.00	13.62	-

The P-h diagram of the developed heat pump using R141b is shown in Figure 90. The power consumption is only 23.98 MW and the equivalent power gain is 29.13 MW.

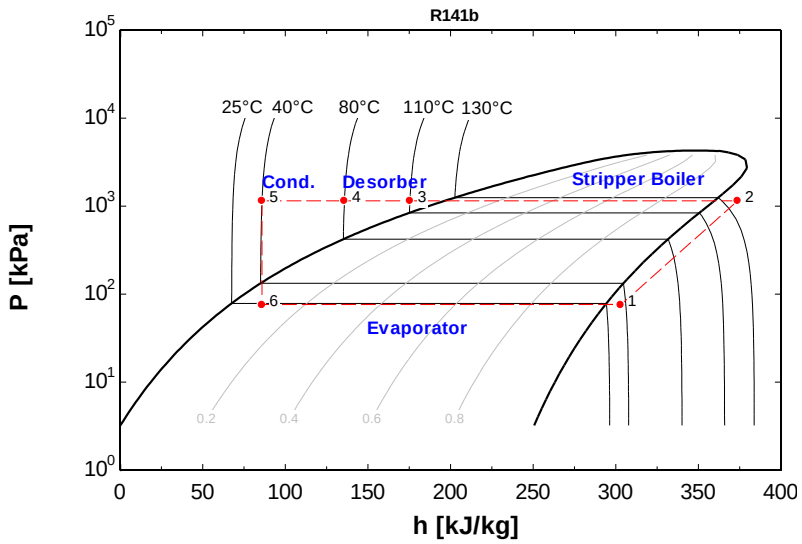

Figure 90: P-h diagram for the proposed heat pump using R141b refrigerant.

5.5 Heat Pump Refrigerant Investigation

Forty two refrigerants were investigated using the C# code and their performances are listed in Table 53 and plotted in Figure 91. Although some of the refrigerants are phased out in many countries and some have vacuum suction pressure, they are included here for more comprehensive investigation. The final design should consider practical design factors in the final selection.

Table 53: Performance of the proposed heat pump with different refrigerants.

Refrigerant	Compressor Power (MW)	Evaporator Capacity (MW)	Desorber Capacity (MW)	Equivalent Power Gain (MW)	Benefit Ratio	T_{cr} (^oC)	α (^oC/Pa)	CT/r
C_7H_8	22.52	70.40	10.11	20.42	6.70	318.8	7.75E-04	6.47E-02
R11	22.68	76.37	12.86	22.00	7.04	198.1	1.10E-04	7.62E-02
R141b	23.98	77.54	13.80	21.08	6.74	204.5	1.05E-04	8.29E-02
Ammonia	26.59	72.51	14.61	17.29	5.97	132.4	3.12E-05	6.75E-02
R142b	28.17	94.23	24.15	22.02	6.70	137.3	3.92E-05	1.06E-01
R245ca	28.69	90.33	21.74	20.30	6.36	174.6	5.66E-05	1.08E-01
R365mfc	29.33	94.74	23.85	20.96	6.44	187.0	8.62E-05	1.15E-01
R245fa	29.75	94.41	24.25	20.50	6.36	154.2	4.33E-05	1.13E-01
Isobutane	32.67	105.03	31.29	20.88	6.33	134.8	3.32E-05	1.21E-01

R124	33.42	111.55	35.18	22.12	6.50	122.4	3.05E-05	1.25E-01
R236ea	33.53	110.44	33.27	21.56	6.39	139.4	3.55E-05	1.31E-01
Care30	36.66	114.61	39.98	20.09	6.14	118.3	2.70E-05	1.24E-01
R236fa	37.21	126.92	43.29	22.92	6.47	125.1	3.12E-05	1.40E-01
R1234ze	38.14	129.59	47.67	23.07	6.49	109.5	2.54E-05	1.34E-01
R423A	45.48	154.98	64.78	23.66	6.38	99.3	2.15E-05	1.46E-01
R1234yf	49.28	167.34	71.51	23.57	6.28	94.9	2.04E-05	1.54E-01
Propane	51.25	172.39	87.09	24.30	6.44	96.9	2.17E-05	1.30E-01
R413A	52.74	178.93	88.78	24.60	6.41	96.7	2.13E-05	1.39E-01
RC318	52.86	189.60	78.58	26.21	6.40	115.4	2.51E-05	1.72E-01
R227ea	53.46	185.35	78.23	24.51	6.25	101.9	2.05E-05	1.69E-01
R426A	53.68	185.60	97.57	26.15	6.59	100.0	2.27E-05	1.32E-01
R134a	55.28	192.94	105.73	27.14	6.68	101.2	2.35E-05	1.29E-01
R420A	56.37	194.73	109.74	26.86	6.65	104.9	2.50E-05	1.26E-01
R417A	58.18	193.31	94.52	23.29	6.16	87.3	1.80E-05	1.52E-01
R424A	58.85	194.55	95.03	22.98	6.12	86.0	1.77E-05	1.53E-01
R422B	59.76	196.55	94.84	22.55	6.05	83.4	1.69E-05	1.57E-01
R421A	59.92	197.78	96.49	22.85	6.09	82.9	1.70E-05	1.56E-01
R422D	61.34	199.62	94.61	21.72	5.94	79.7	1.56E-05	1.64E-01
R419A	61.43	198.37	97.84	21.61	5.97	82.2	1.69E-05	1.56E-01
R404A	62.94	207.48	98.74	22.46	5.98	72.2	1.51E-05	1.67E-01
R143a	62.98	211.38	104.04	23.89	6.13	72.9	1.63E-05	1.60E-01
R507A	63.44	208.02	98.08	22.04	5.94	70.8	1.45E-05	1.70E-01
R115	63.94	202.60	90.68	19.50	5.69	80.1	1.46E-05	1.81E-01
R502	64.23	218.91	117.04	25.72	6.33	81.7	1.89E-05	1.47E-01
R421B	64.38	205.96	95.89	20.38	5.78	72.6	1.37E-05	1.74E-01
R422C	64.52	205.48	95.33	20.07	5.75	73.2	1.36E-05	1.75E-01
R422A	65.32	206.62	95.47	19.57	5.70	71.9	1.32E-05	1.77E-01
R407B	65.68	216.02	108.61	22.77	6.01	75.1	1.53E-05	1.60E-01
R428A	65.96	208.85	96.51	19.58	5.70	69.2	1.29E-05	1.79E-01
R402A	66.24	221.94	114.32	24.22	6.14	76.0	1.63E-05	1.56E-01
R509A	66.42	208.00	95.95	18.86	5.64	68.6	1.33E-05	1.81E-01
R125	68.17	210.97	96.71	17.92	5.55	66.2	1.16E-05	1.86E-01

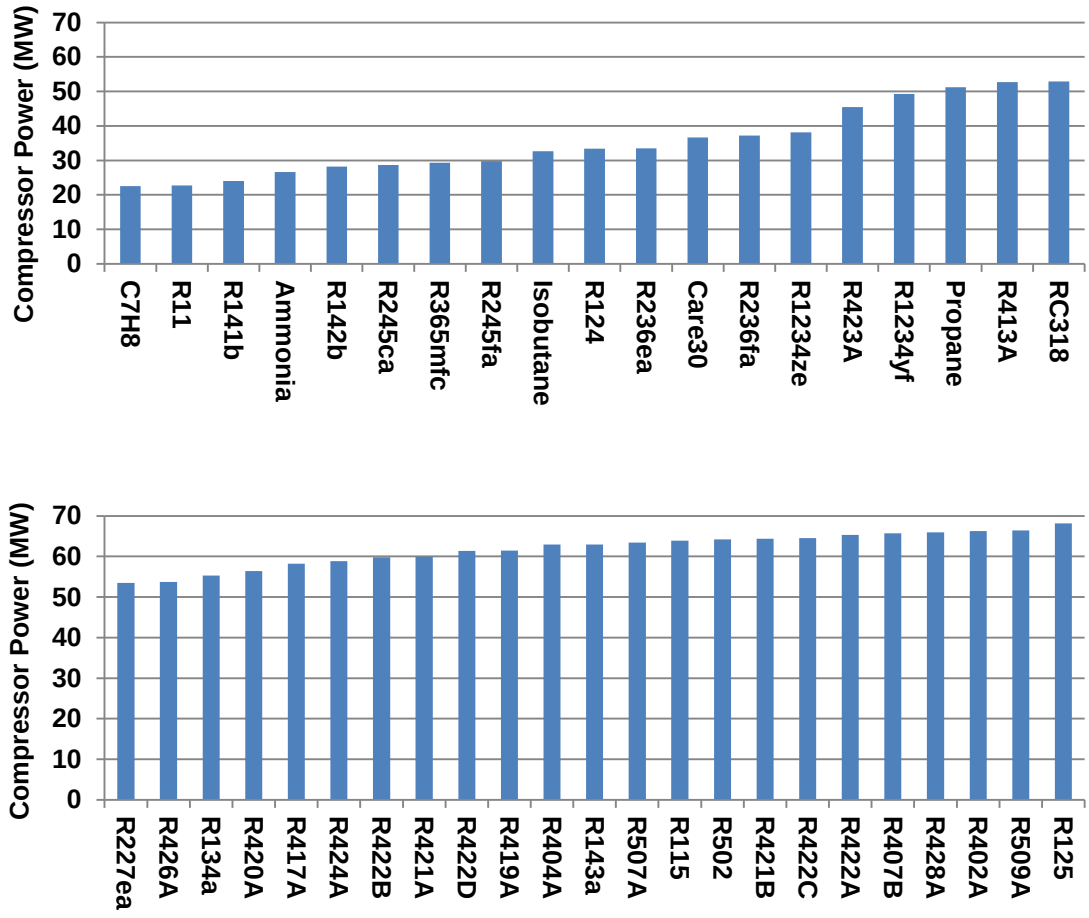

Figure 91: Compressor power of the proposed heat pump with different refrigerants.

The desired refrigerants are characterized by having two-phase region inside the stripper boiler so that less mass flow rate is needed to provide the stripper's heat. Further, the desired refrigerants need to have high temperature increase in the compression process for a given pressure ratio so that they achieve the stripper temperature for low pressure ratio.

A new thermodynamic parameter, α, is introduced here that describes the increase in a refrigerant temperature after an isentropic compression process. That is,

the unit is 1 degree Celsius over 1 bar. This parameter can be used as a tool to predict the refrigerant performance for the heat pump. Refrigerants with high value of α should be investigated because they achieve the desired temperature for small pressure increase, thus, less compressor power. As shown in Figure 92, the compressor power reduces when α of a refrigerant increases and vice versa. The figure shows the trend that the power reduces with increasing α except in limited cases the power increases with α. This is due to the fact that α does not consider some important parameters which will affect the power consumption such as the mass flow rate and the latent heat.

Temperature increase in isentropic compression process, $\alpha = \left(\frac{dT}{dP}\right)_s$ (19)

Where,

$dT=T_o-T_i$

To: Compressor outlet temperature

Ti: Compressor inlet temperature

$dP=P_o-P_i$

P_o: Compressor outlet pressure

P_i: Compressor inlet pressure

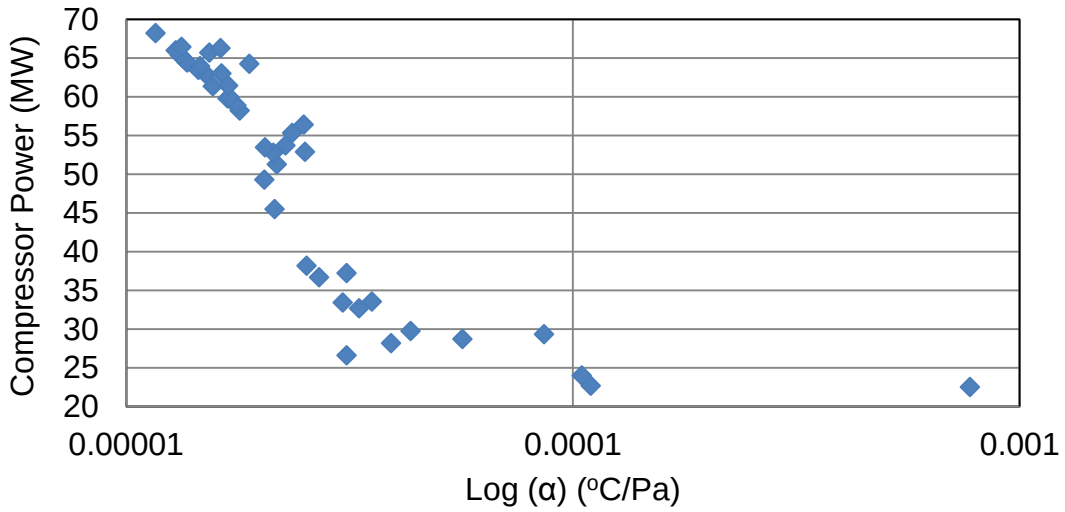

Figure 92: Heat pump compressor power against α parameter for the investigated refrigerants.

McLinden [132] used the principle of corresponding states to compare refrigerant performances. It can be again used here to compare working fluids for the heat pump. The observation was that the COP increases with refrigerants having higher critical point temperature because they have less superheat (thus less irreversibility) in the compressor outlet than refrigerants having low critical point temperature.

The compressor power of the heat pump against refrigerant's critical point temperature was plotted and shown in Figure 93. The heat pump compressor power decreases with refrigerant's critical point temperature. Similar plot but with opposite trend can be obtained using a dimensionless parameter such as the desorber heat over the compressor power.

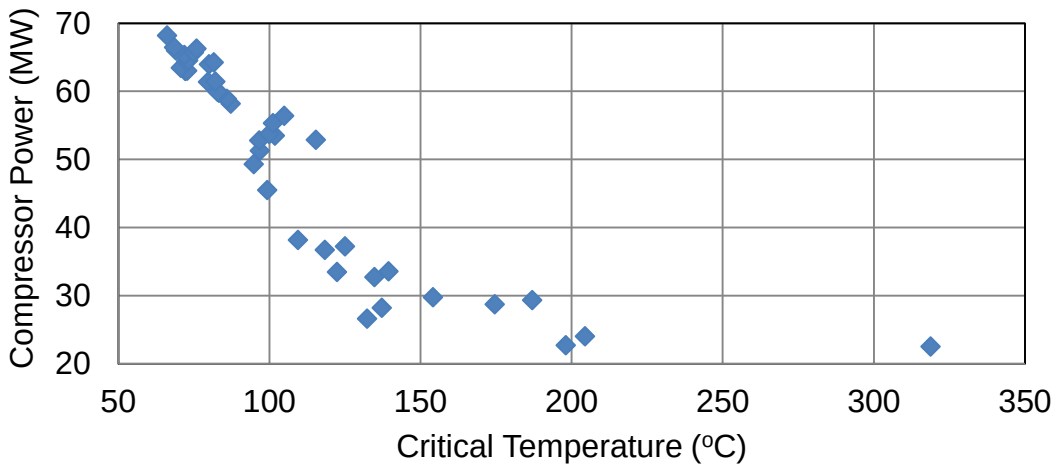

Figure 93: Heat pump compressor power against refrigerants' critical temperature for the investigated refrigerants.

Similarly, Alefeld and Radermacher [135] dimensionless parameter (Equ. 16) can also be used to evaluate the performance of heat pumps with different refrigerants. The investigated refrigerants for the heat pump that have low cT/r values resulted in less power consumption than refrigerants with large cT/r as shown in Figure 94.

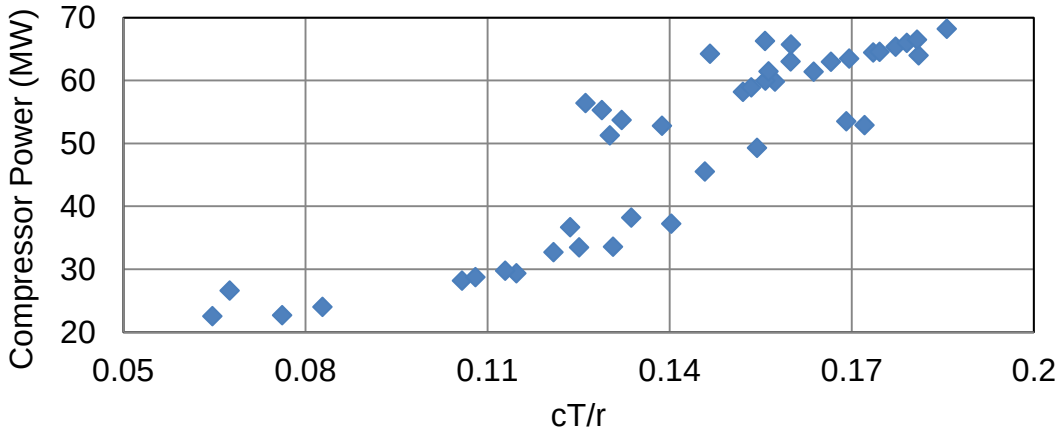

Figure 94: Heat pump compressor power against refrigerants' cT/r value for the investigated refrigerants.

The main design strategy in selecting a refrigerant for the heat pump was that the heat pump high temperature heat exchanger in the condenser meets the required desorber heat at the required temperature. In the LNG plant considered in this thesis, the desired refrigerant is the refrigerant that has the least compressor power. In other application where cooling is needed, refrigerant that has more available cooling (or more equivalent power gain) could be selected although their compressor power is not the least.

In refrigerants where the enthalpy change across the high temperature heat exchanger in the condenser is small, more mass flow rates is needed to provide the heat as can be seen in Equ. 20. High mass flow rate results in higher compressor power, more cooling available in the evaporator, more heat available in the desorber and, thus, higher equivalent power gain in most cases until compressor power of about 55 MW where the power loss from the compressor exceeded the gain from the cooling at the defined COP values as shown in Figure 95.

$$Q_{Stripper} = \dot{m}\,\Delta h \tag{20}$$

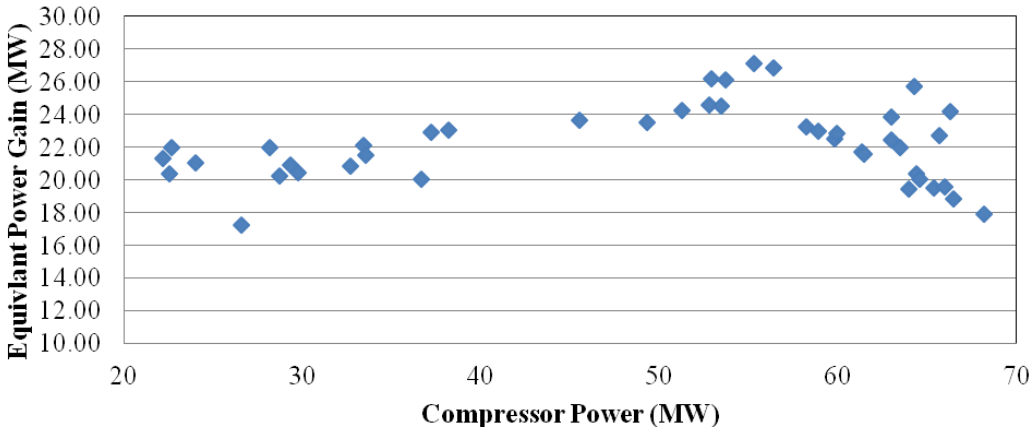

Figure 95: Equivalent heat power gain vs. compressor power.

5.6 Cascade Heat Pump

Since the temperature lift across the compressor in the proposed heat pump is high (24°C to 130°C), the COP is reduced as can be seen from Carnot COP (Eq. 21). Also, some refrigerants have below atmospheric pressure in there evaporator. An alternative heat pump which works on cascade configuration is proposed here as shown in Figure 96. The evaporator temperature and the stripper temperature are similar to the single refrigerant heat pump. The intermediate heat exchanger temperature was taken to be 63°C. A third stage can be added to serve low temperature cooling needs such as CO_2 liquefaction.

$$Carnot\ COP\ for\ heating\ cycle = \frac{T_{cond}}{T_{cond} - T_{evap}} \tag{21}$$

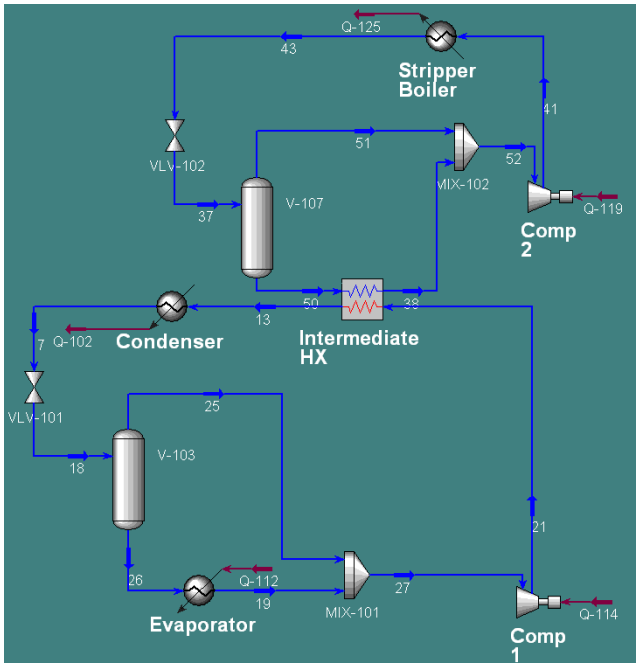

Figure 96: Cascade heat pump cycle.

The intermediate heat exchanger that could run absorption chillers in the single refrigerant heat pump was eliminated in the cascade configuration because it will increase the power consumption of the bottom cycle. The results of few refrigerants investigated are shown in Table 54. Water was included because of its known stability although the evaporation pressure was 0.2 bar. Four out of the six investigated cascade heat pump cycles consumed less power than the power resulted from steam extraction (24.4 MW) which resulted in power savings as well as large amount of "free" cooling in the evaporator.

Table 54: Cascade heat pump power consumption of different refrigerants.

Bottom Refrigerant	Top Refrigerant	Bottom HP Power (MW)	Top HP Power (MW)	Total Comp. Power (MW)	Q_{evap} (MW)	Equiv. Power Gain (MW)	Benefit Ratio
Propane	R141b	11.06	15.22	26.28	58.38	12.72	4.90
Propane	Benzene	10.52	13.75	24.27	61.03	15.39	5.42
Propane	R141b	10.53	15.27	25.8	58.91	13.33	5.01
Propane	Water	10.06	12.53	22.59	63.48	17.68	5.93
R11	Water	9.40	12.53	21.93	54.89	16.19	5.71
R141b	Water	9.01	12.59	21.60	55.59	16.70	5.83

5.7 Heat Pump with Expander

Another enhancement on the proposed heat pump is to use a liquid expander instead of expansion valve. Liquid expanders recover some of the expansion loss and increase the evaporator capacity. Refrigerants that have high specific heat will have higher loss (more vapor) in the expansion process [132].

Table **55** lists the power consumption of three refrigerants with expanders that have an efficiency of 75%.

Table 55: Performance of heat pump with expanders.

	Without Liquid Expanders		With Liquid Expanders			Enhancements	
Fluid	Comp. Power (MW)	Evap. Capacity (MW)	Comp. Power (MW)	Expander Power (MW)	Evap. Capacity (MW)	Power Consumption (%)	Evaporator Capacity (%)
R141b	23.67	76.93	23.67	0.217	77.14	-0.92	0.27
NH_3	26.59	72.51	26.59	0.567	73.09	-2.13	0.80
R123	26.53	81.48	26.53	0.3379	81.81	-1.27	0.41

5.8 Heat Pump with CO_2 Liquefaction

The proposed heat pump concept could be improved by including multi-evaporators with different evaporation temperatures so that different cooling needs can be served as shown in Figure 97. The high pressure evaporator could be used to cool the flue gas which would eliminate the absorption chillers that cool the flue gas. Therefore, the proposed heat pump is suitable for high sulfur fuel where the flue gas energy utilization temperature is high. Also, the high pressure evaporator could be used to precool the NG and the MCR refrigerant in the APCI cycle which would lower its power consumption.

The low pressure evaporator could be used for CO_2 liquefaction which would eliminate the need for CO_2 liquefaction cycle. Figure 97 shows the proposed concept where a heat pump is used in flue gas cooling to 27^oC, CO_2 liquefaction at the optimum liquefaction pressure, 50 bar, as well as providing the CO_2 regeneration and additional heat for feed water preheating or for absorption chillers.

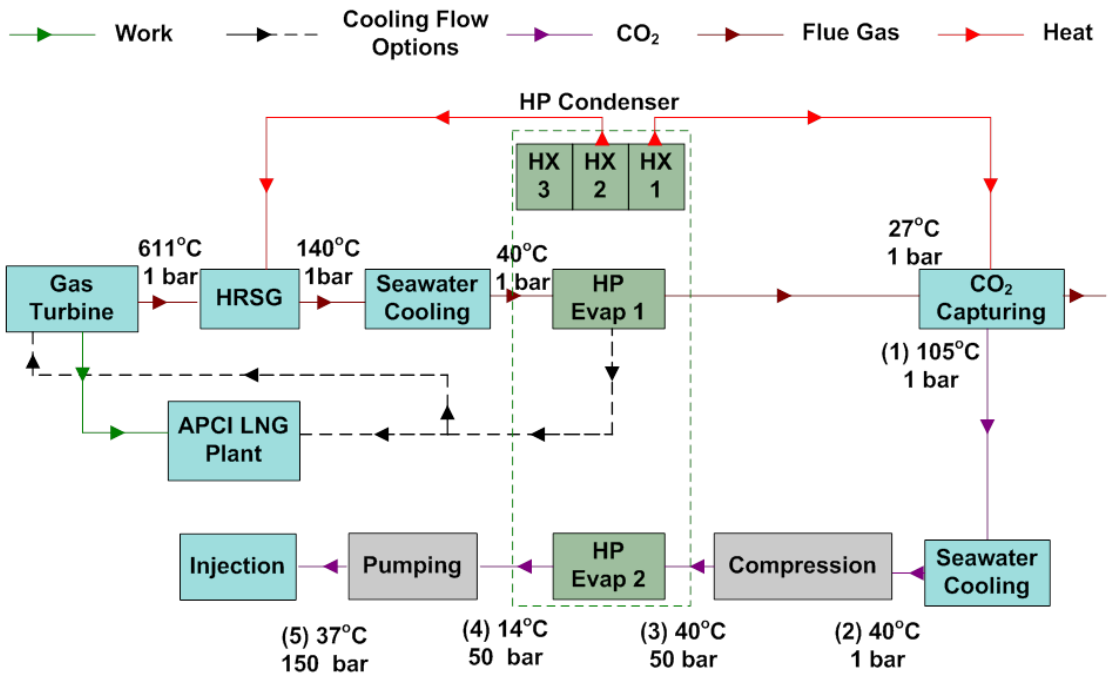

Figure 97: Proposed heat pump (HP) with two evaporators integrated with the CCS and LNG plant.

A heat pump model with two evaporators was developed in HYSYS software as shown in Figure 98. The first evaporator is used to cool the flue gas and NG. The second evaporator is used to liquefy the captured CO_2. The performance of this heat pump with different refrigerants and different CO_2 liquefaction pressure are shown in Table 56. The equivalent power gain varied from 15.67 MW to 19.79 MW.

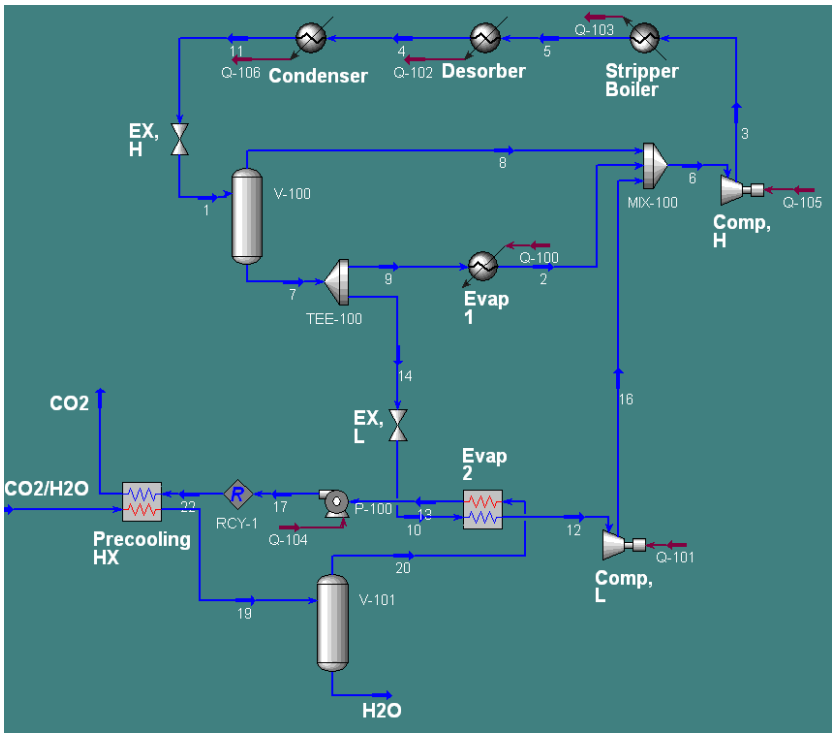

Figure 98: HYSYS model for the two evaporators heat pump.

Table 56: Performance of the two evaporators heat pump.

CO_2 Liq. Press. (bar)	Refrig-erant	Heat Pump Comp. Power (MW)	Evap. 1 Heat (MW)	Evap. 2 Heat (MW)	Desorber Heat (MW)	CO_2 Comp. and Pump Power (MW)	Benefit Ratio	Equiv-alent Power Gain (MW)
50	R123	26.76	76.84	4.31	16.94	5.34	6.30	19.02
50	NH_3	26.86	67.82	4.31	14.54	5.34	5.85	16.44
50	R141b	25.15	70.15	4.31	13.13	5.34	6.28	18.59
50	C_7H_8	22.60	65.84	4.31	10.07	5.34	6.67	19.79
6	NH_3	30.45	63.99	7.21	14.31	2.32	5.12	15.67

5.9 Heat Pump across the Stripper Column Only

One modification on the heat pump concept is to apply the heat pump across the stripper column only without process cooling or flue gas cooling. Therefore, the heat pump is applied on a smaller scale. This heat pump takes the heat from the CO_2 condenser and pumps the heat to the CO_2 boiler. Since the CO_2 condenser is at a

temperature of 75°C, the temperature lift in this case is less than the case where the flue gas heat was utilized. The concept is shown in Figure 99.

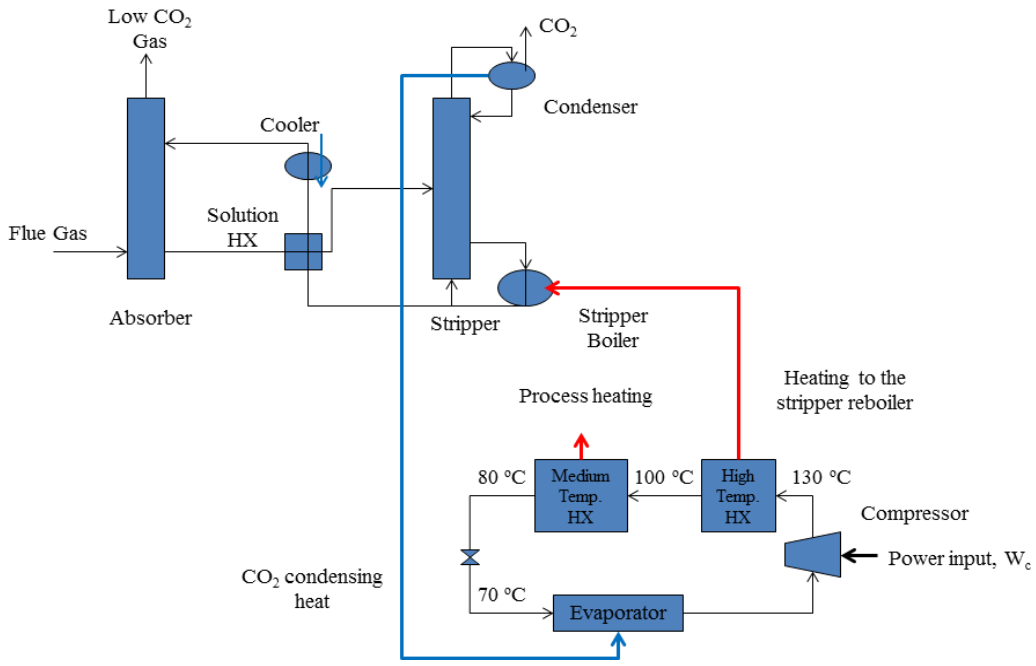

Figure 99: Heat pump across the stripper column only schematic.

HYSYS model was developed to evaluate the performance of this concept. The previous heat pumps were designed to supply the entire stripper heat that is required for CO_2 regeneration (i.e., 70.42 MW). It was possible to provide this high amount of heat because the heat utilized in the flue gas or process cooling was larger than the CO_2 regeneration heat. In the heat pump across the stripper column concept, the heat pumps were designed to take the CO_2 condenser heat (26.75 MW at 75°C) in the heat pump evaporator. Thus, the heat pump evaporator was sized to have 26.75 MW at 70°C. At this conditions, some steam needs to be extracted from the steam cycle to provide part of the 70.42 MW (the CO_2 regeneration heat) that is not provided by the high temperature condenser of the heat pump. To estimate the power

loss from steam extraction, the previous result shows that 24.4 MW power loss in the steam cycle is experienced when 70.42 MW of heat is extracted. Therefore, at different amount of heat should be used to estimate the power loss.

$$\text{Estimated Power Loss from Steam Extraction, EPL, (MW)} = \frac{24.4}{70.42} * \text{Heat in Extracted Steam (MW)} \quad (22)$$

The evaporator cooling is not considered in the calculation of the equivalent power gain as in the previous sections because the CO_2 condenser was provided by seawater in the previous concept.

$$\text{Equivalent power gain} = \frac{Q_{Desorber}\, COP_{Abs.Chillers}}{COP_{VCC}} + PP_{NGCC} - EPL - P_{Comp.} \quad (23)$$

Several refrigerants were investigated as shown in Table 57. The benefit ratio is higher than the previous heat pumps due to less compressor power. The equivalent power gain is lower than the previous heat pumps due to less free associated cooling.

Table 57: Heat pump across the stripper column performance with estimated power loss in the steam cycle.

Ref-rigerant	Evap. Heat (MW)	Heat to the Stripper (MW)	Desorber Heat (MW)	Comp. Power (MW)	Benefit Ratio	Equivalent Power Gain (MW)	Required Heat from Steam Extraction (MW)	Estimated Power Loss from Steam Extraction (MW)
C_7H_8	26.75	26.45	4.08	3.78	15.15	5.76	43.97	15.24
R11	26.75	25.25	5.00	3.51	16.23	5.70	45.17	15.65
NH_3	26.75	23.87	6.72	3.83	14.97	5.06	46.55	16.13
R141b	26.75	27.97	5.93	5.22	11.63	5.02	42.45	14.71
R123	26.75	27.1	7.08	5.26	11.58	4.78	43.32	15.01
R142b	26.75	25.15	9.10	4.97	12.28	4.59	45.27	15.69
Water	26.75	29.05	1.52	3.82	15.01	6.39	41.37	14.33

5.10 Heat Pump with the Ultimate Heat Exchange

This concept combines the concepts in Section 5.9 and Section 5.8. In other words, this heat pump uses the CO_2 condensing heat, the flue gas cooling heat, CO_2 liquefaction heat to supply the CO_2 regeneration heat. From the energy balance, the heat pump compressor power will be lower than in Section 4.9 and Section 4.8 because more heat is used in the evaporator. The heat pump model in HYSYS is shown in Figure 100. The evaporator 1 condenses the water and CO_2 in the stripper column. The evaporator 2 cools the flue gas or process cooling. The evaporator 3 liquefies the captured CO_2. The results of two refrigerants are shown in Table 58.

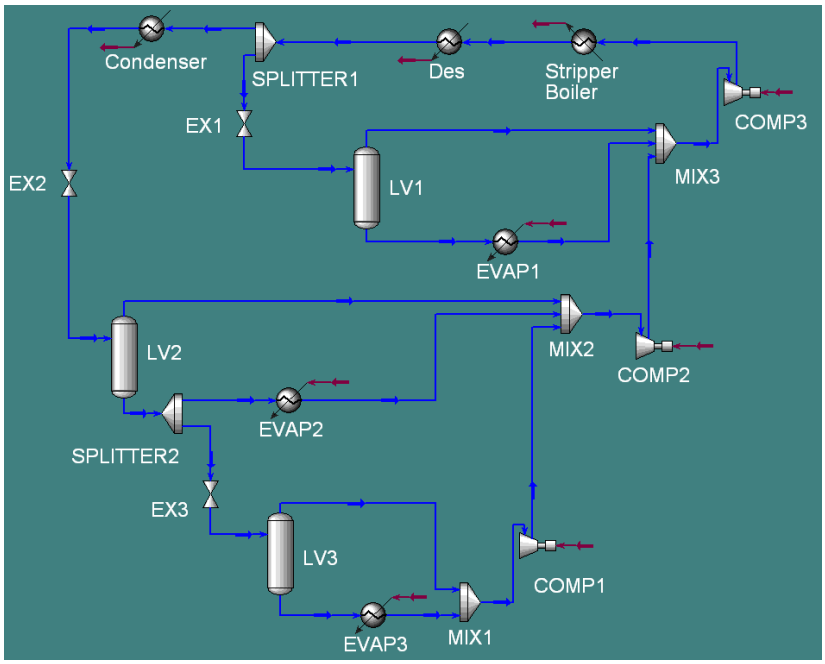

Figure 100: Heat pump with three evaporators model in HYSYS.

Table 58: Result from the heat pump with three evaporators model using HYSYS software.

CO_2 Liq. Press. (bar)	Refrig-erant	Heat Pump Comp. Power (MW)	Evap. 1 Heat (MW)	Evap. 2 Heat (MW)	Evap. 3 Heat (MW)	Desorber Heat (MW)	CO_2 Comp. and Pump Power (MW)	Benefit Ratio	Equiv-alent Power Gain (MW)
50	NH_3	21.52	26.75	44.08	4.31	16.79	5.34	3.49	15.46
50	C_7H_8	18.04	26.75	39.37	4.31	10.36	5.34	3.90	17.16
6	NH_3	25.89	26.75	35.53	7.21	15.84	2.32	2.68	8.86

5.11 Heat Pump using Absorption Cycle

Absorption heat pumps can be used to provide the CO_2 regeneration heat. In an absorption heat pump, the heat provided is from the condenser and absorber. Low grade heat is provided in the evaporator and high grade heat is provided in the desorber. In order to estimate the performance of this system with CO_2 regeneration heat of 70.42 MW at 130^{o}C, the following assumptions were made

1- Desorber heat: 43.67 MW of steam extracted from steam cycle at 220^{o}C
2- Evaporator heat: 26.75 MW of heat from CO_2 and water condenser in the stripper column at 72^{o}C

Where, the evaporator heat was assumed to be 61% of the desorber heat (cooling COP of 0.61) and the regeneration heat equals the sum of the desorber heat and the evaporator heat.

Using the steam cycle with parallel steam turbine configurations, the power loss in the steam cycle due to steam extraction was estimated to be 23.29 MW which is only 1.11 MW less power loss than extracting conventional steam extraction (70.42 MW at

130^{o}C) due to the fact that the quality (temperature) of the steam needed to be extracted in this option is higher (220^{o}C).

5.12 Conclusions

The proposed heat pump utilizes the evaporator heat which could be used in a flue gas cooler, a steam cycle condenser, or a subcooler for the propane cycle or a precooler for the NG and MCR refrigerant in the APCI LNG plant to provide the CO_2 regeneration heat which would otherwise require steam extraction from the steam cycle, resulting in 24.4 MW power loss. Several refrigerants were investigated and their performances were justified based on three parameters.

The use of expanders which recover the expansion loss was investigated. Cascade heat pump configuration was also developed which allowed the use of water in the top cycle. Two evaporators heat pump concept was also developed which made the CO_2 regeneration, liquefaction as well as process cooling possible in one unit, eliminating the need for steam extraction and CO_2 liquefaction cycle.

The performances of different heat pump concepts against the developed CO_2 liquefaction cycles and the conventional multi-stage compression cycle are listed in Table 59 and plotted in Figure 101. Some of the developed heat pump concepts consumed less total power for CO_2 regeneration and pressurization than the conventional steam extraction with CO_2 multi-stage compression. For example, the cascade two evaporators heat pump using R141b-Water as a refrigerant and heat pump using C_7H_8 or R141b with the developed CO_2 liquefaction cycle consumed less

total power than the conventional steam extraction with CO_2 multi-stage compression.

The heat pump with three evaporators concept has the least power consumption because it utilizes more heat in the evaporators, thus requiring less compressor power. The total power demand with C_7H_8 working fluid is 23.28 MW which is 7.37 MW or 24.04% less than the conventional case. The additional cooling is 43.17 MW.

The equivalent power demand which considers the additional cooling (extra cooling available which is not used for CO_2 liquefaction or condensation) shows the superiority of the developed heat pump concepts with saving in equivalent power demand from 17.41% to 69%.

Last, a new thermodynamic parameter, α, was introduced that can determine the temperature increase during isentropic compression process. This parameter can help in choosing refrigerants for the heat pump with low compressor power.

Table 59: Power demand and available cooling with different CO_2 regeneration and pressurization approaches.

Case	CO_2 Re-generation Heat Source	CO_2 Re-generation Power Demand (MW)	CO_2 Pressurization Approach	CO_2 Press-urization Power Demand (MW)	Available Additional Cooling (MW)	Total Power Demand (MW)	Equiv. Power Demand (MW)	Saving in Equiv. Power Demand (%)
1	Steam Extraction	24.4	Multi-Stage Compression	6.25	N/A	30.65	30.65	N/A
2	Steam Extraction	24.4	Developed Liquefaction Cycle	5.93	N/A	30.33	30.33	1.04
3	Heat Pump using R141b	23.98	Developed Liquefaction Cycle	5.93	82.65	29.91	9.25	69.83
4	Heat Pump using C_7H_8	22.5	Developed Liquefaction Cycle	5.93	74.14	28.43	9.89	67.72
5	Heat Pump using NH_3	26.59	Developed Liquefaction Cycle	5.93	77.91	32.52	13.04	57.45
6	Steam Extraction & Heat pump across the Stripper Column using R141b	19.93	Developed Liquefaction Cycle	5.93	2.19	25.86	25.31	17.41
7	Two Evaporators Heat Pump using R141b	25.15	Two Evaporators Heat Pump using R141b	5.34	75	30.49	11.74	61.7
8	Two Evaporators Heat Pump using C_7H_8	22.6	Two Evaporators Heat Pump using C_7H_8	5.34	69.57	27.94	10.55	65.58

9	Two Evaporators Heat Pump using NH_3	26.86	Two Evaporators Heat Pump using NH_3	5.34	73.2	32.2	13.9	54.65
10	Cascade Heat Pump using R141b-Water	21.6	Developed Liquefaction Cycle	5.93	55.59	27.53	13.63	55.52
11	Cascade Two Evaporator Heat Pump using R141b-Water	21.82	Cascade Two Evaporator Heat Pump using R141b-Water	5.34	51.07	27.16	14.39	53.04
12	Heat Pump with three Evaporators using C_7H_8	18.04	Heat Pump with three Evaporators using C_7H_8	5.34	43.17	23.28	12.59	58.93
13	Heat Pump with three Evaporators using NH_3	21.52	Heat Pump with three Evaporators using NH_3	5.34	50.29	26.86	14.28	53.38
14	Absorption Heat Pump	23.29	Developed Liquefaction Cycle	5.93	-	29.22	29.22	4.67

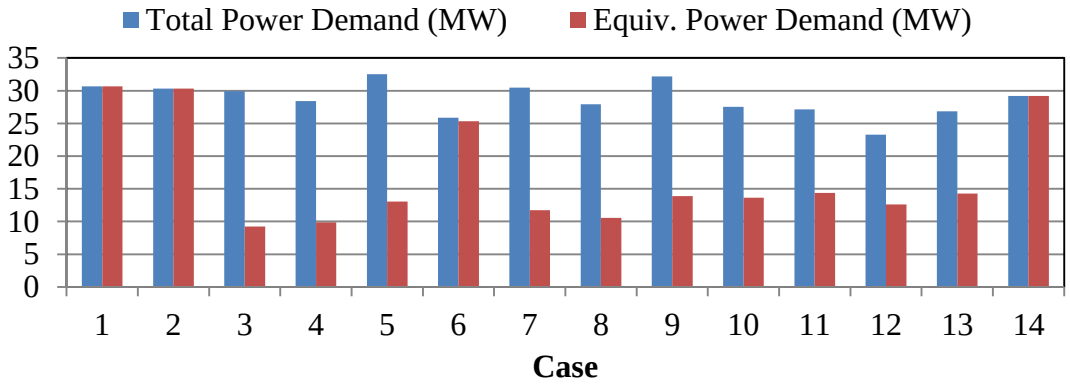

Figure 101: Power demand and equivalent power demand for the different CO_2 regeneration and pressurization approaches. Case 1 represents the baseline or the conventional approach.

Chapter 6: Research Contributions and Future Work

6.1 Introduction

The thesis fulfilled five gaps in the literature in the area of CCS integration with LNG plants. The gaps are summarized as in the following:

1. None of the previous studies applied global optimization on detailed C3-MR model and investigated the effect of cryogenic heat exchanger performance.
2. None of the previous studies considered the effect of uncertainty in feed gas compositions on the performance of C3-MR cycle and developed a refrigerant which can handle a range of natural gas feeds.
3. No research done on integrating an LNG plant with power cycle and CCS, with comprehensive waste heat evaluation, along with uses that will result in power savings with any solvents used to capture the CO_2.
4. No alternative concepts to CO_2 compression other than the open CO_2 liquefaction cycle were explored in the literature.
5. No other regeneration heat concepts other than steam extraction or compressed CO_2 were proposed in the literature.

This chapter highlights the summary from the thesis chapters, contributions, lists the publication from this work, and summarizes the proposed future work.

6.2 Chapters Summary

6.2.1 Chapter 2: Optimization of LNG Plants

An APCI LNG plant was modeled in HYSYS and verified with Mortazavi *et al.*[1]'s ASPEN Plus model, with good agreements. Although the approach of coupling a comprehensive modeling software, HYSYS, with a powerful optimization software tool, GA in Matlab, is time consuming, it provides greater confidence in reaching a global optimal. Optimized refrigerant mixture and system variables were obtained. Total power consumption was reduced by 9.1%. The effect of the pinch temperatures on power consumption was also investigated. The savings in power consumption from using heat exchangers with 1 K pinch temperature in the cryogenic column is 17% lower than using heat exchangers with 5 K pinch temperature. The obtained optimum composition of refrigerant mixtures for this work was compared with two optimized compositions of refrigerant mixtures from the open literature. Results show that the current work has achieved better refrigerant compositions than the literature ones. The method used in this work can be implemented in optimizing any processes modeled with HYSYS software. The effect of uncertainty in natural gas feed was identified, and a robust refrigerant was developed. The natural gas liquefaction load and temperature changes with the natural gas feed compositions. The robust refrigerant can handle several natural gas feeds consumes 35.2 MW more than the refrigerant that was developed using deterministic optimization. However, this refrigerant was very sensitive to variation in natural gas feeds.

6.2.2 Chapter 3: Energy Consumption Reduction in CCS of an LNG Plant through Process Integration and Waste Heat Utilization

Comprehensive investigation was conducted on reducing the power loss from implementing a CCS on an LNG plant. Several waste heat sources were identified and potential uses were proposed and evaluated through modeling in HYSYS software with models validation against experimental data. Several steam cycles with steam extractions were modeled and optimized. A steam cycle without steam extraction that provide the CO_2 regeneration heat via high temperature condenser with excess waste heat provided more net available power than steam cycles with steam extractions. One of the proposed CCS configurations that utilize the waste heat in inlet air cooling and in ORC resulted in 187.6 MW, which is 16.3% more power than the conventional CCS configuration as well as 97.9% CO_2 capture efficiency which is 4.6% enhancement or 4.3 tons of CO_2/hr more capturing. In order to compare different waste heat utilization options, the power gain from waste heat ratio was defined. The highest power gain from waste heat ratio was for using the waste heat for inlet-air cooling but it was shown that the power savings from inlet air cooling is highly dependent on the inlet air cooler pressure drop. Pinch Analysis method was used to compare the utility cooling and utility heating of the proposed and conventional CCS. The result of the Pinch Analysis shows that the proposed CCS configuration requires 23.9% less utility cooling than the conventional CCS configuration because of the improved heat integration and waste heat utilization.

6.2.3 Chapter 4: Development of CO_2 Liquefaction Cycles for CO_2 Sequestration

Five options were investigated for pressurizing the captured CO_2 gas for EOR applications. The investigation was carried out through development of HYSYS models with models validation against experimental data with good agreements. The liquefaction of CO_2 was optimized using generic HYSYS model coupled with Matlab optimization tool that considers all power consumption and all recoverable cooling. The results show for a liquefaction cycle that has 70% Second Law efficiency the optimum liquefaction pressure is 50 bar where CO_2 liquefaction and pumping consumes less power than compression. Sensitivity analysis was carried out to explore the effect of heat exchangers pressure drop and compressors isentropic efficiency on the power savings. The results show that the developed liquefaction cycle outperforms the conventional multi-stage compression cycle in all cases explored. The regions where CO_2 liquefaction and pumping outperforms multi-stage compression with different seawater temperatures and injection pressures were identified. An open CO_2 liquefaction cycle model was developed and its performance was investigated. An improvement was made on the conventional open CO_2 liquefaction cycle that resulted in 10.6% power savings than the conventional open CO_2 liquefaction cycle.

6.2.4 Chapter 5: Proposed Regeneration Heat Source

Any CCS system requires heat to regenerate the CO_2 as well as cooling to cool the flue gas. Instead of extraction steam which resulted in 24.4 MW of power loss from the steam cycle, novel heat pump systems were proposed to regenerate the CO_2 instead of steam extraction. The proposed heat pump concept addresses three

common requirements in any CCS system using one unit (providing the CO_2 regeneration energy, providing cooling needs, and providing process heating needs). Forty-two refrigerants were investigated and their performances were justified based on three thermodynamic parameters in which one of the parameter was proposed in this thesis. The introduced parameter can help in choosing refrigerants for the heat pump with low compressor power. Seven configurations of different heat pump concepts were proposed and their performances were compared against the conventional system. Some of the developed heat pump concepts consumed less total power for CO_2 regeneration and pressurization than the conventional steam extraction with CO_2 multi-stage compression. For example, the total power demand in one of the heat pump is 23.3 MW which is 7.4 MW or 24 % less than the conventional case which is CCS with steam extraction and multi-stage compression. The equivalent power demand which considers the additional cooling shows the superiority of the developed heat pump concepts with saving in equivalent power demand varying from 17.4% to 69%.

6.3 Research Contributions

Major contributions that resulted in number of benefits were achieved in this work. They are summarized as follows:

- *Research Thrust #1 (LNG Plants Power Demand)*
    - Improved the process of natural gas liquefaction

1. Developed an optimization platform coupling Matlab-HYSYS software. Thus, Matlab can be used to optimize any process simulated with HYSYS software.

2. Developed refrigerant mixture compositions which outperformed literature published refrigerant mixture compositions by as much as 14% power savings.

3. Developed a correlation which can be used to estimate the MCR power consumption for different cryogenic heat exchanger performances.

4. Identified the challenges and proposed a solution to LNG plants optimization with uncertainty in natural gas feed compositions. In collaboration with Design Decision Support Lab (DDSL), developed a robust refrigerant which is capable to liquefy a range of natural gas feeds.

- *Research Thrust #2 (Waste Heat Utilization and Process Integration)*

  – Developed new integrated CCS configurations

1. Proposed a novel power cycle (NGCC with ORC and inlet air cooling to gas turbine) which resulted in highest net power.
2. Process integration and waste heat utilization revealed up to 16.3% power gain and 4.6% enhancement in the CO_2 capturing efficiency compared to conventional CCS.

3. Developed models in HYSYS for LNG plant, steam power cycles, CO_2 capturing, CO_2 liquefaction, CO_2 compression, ORC and heat pumps. The categories of the developed models and their validation against experimental data are shown in Figure 102.

- *Research Thrust #3 (CO_2 Pressurization Concepts)*
  - Developed new CO_2 liquefaction cycles
    1. Optimized CO_2 liquefaction pressure irrespective of the liquefaction cycle.
    2. Developed a CO_2 liquefaction cycle which consumes 5.1% less total power than multistage CO_2 compression.
    3. Investigated the effect of four operating parameters on the power savings of the developed liquefaction cycles compared to the multistage CO_2 compression cycle.
- *Research Thrust #4 (New Concept of Regeneration Heat Source)*
  - Developed Heat Pump Systems for CCS
    1. Proposed seven novel heat pump systems which can regenerate, liquefy the CO_2 and provide process heat without steam extraction or a liquefaction cycle.

2. Proposed a new thermodynamic parameter which can help in choosing refrigerants for the proposed heat pump with low compressor power.

3. One of the heat pump systems has 24% less total power demand or 59% less equivalent power demand than conventional CCS with steam extraction and CO_2 compression.

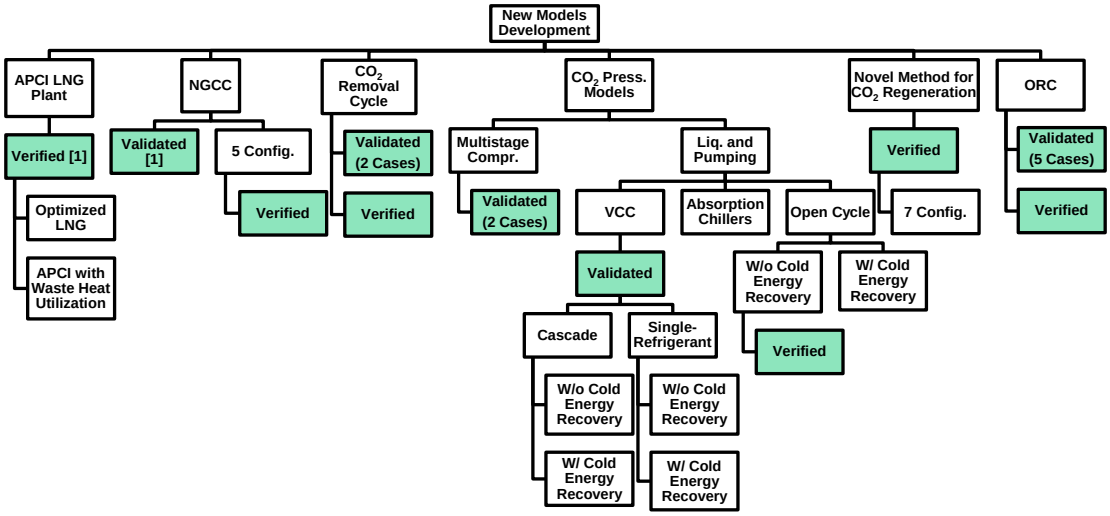

Figure 102: Categories of developed models in HYSYS. White boxes represent developed model categories. Green boxes represent validation or verification was done on the model categories.

6.4 List of Publications

- Journal papers:
    - **Alabdulkarem A.**, Hwang Y., Radermacher R., "Energy Consumption Reduction in CO_2 Capturing and Sequestration of an LNG Plant through Process Integration and Waste Heat Utilization"

International Journal of Greenhouse Gas Control Journal, 10, Sep. 2012, pp. 215-228.

- **Alabdulkarem A.**, Hwang Y., Radermacher R., "Development of CO_2 liquefaction Cycles for CO_2 Sequestration" Applied Thermal Engineering Journal, 33 (34), May 2012, pp. 144-156.
- **Alabdulkarem A.**, Mortazavi A., Hwang Y., Radermacher R., and Rodgers P., "Optimization of Propane Pre-cooled Mixed Refrigerant LNG Plant" Applied Thermal Engineering Journal, 31 (6), May 2011, pp. 1091-1098.
- Mortazavi A., Somers C., **Alabdulkarem A.**, Hwang Y., and Radermacher R., "Enhancement of APCI Cycle Efficiency with Absorption Chillers" Energy Journal, 2010, 35 (9), pp. 3877-3882.
- Mortazavi A., **Alabdulkarem A.**, Radermacher R., Azarm S., and Hwang Y. "Development of a Robust Refrigerant Mixture for APCI LNG Plants" To be submitted to Applied Energy Journal, 2014.
- Mortazavi A., **Alabdulkarem A.**, Hwang Y., Radermacher R., and Azarm S. "Novel Combined Cycle Configurations for APCI Natural Gas Liquefaction Cycle" Applied Energy, 117, March 2014, pp 76-86.
- **Alabdulkarem A.**, Hwang Y., Radermacher R., "Heat Pumps Integration with a CO_2 Removal Plant" to be prepared and submitted to International Journal of Greenhouse Gas Control Journal.

- Conference papers:

- **Alabdulkarem A.**, Hwang Y., Radermacher R., "Efficiency Improvement of Natural Gas Combined Cycle Power Plant with CO_2 Capturing and Sequestration" ASME International Mechanical Engineering Congress & Exposition, Houston, TX. Nov. 2012, IMECE2012-87436.
- **Alabdulkarem A.**, Hwang Y., Radermacher R., "New Energy Efficient CO_2 Pressurization Strategies for Enhanced Oil Recovery Applications" Carbon Management Technology Conference, USA, FL., Feb. 2011. CMTC 151639.

- Book chapters:
  - Hwang Y., **Alabdulkarem A.**, Mortazavi A. and Radermacher R., "Natural Gas Liquefaction Cycle Enhancements and Optimization" in Handbook of Liquefied Natural Gas, Gulf Professional Publishing, Oct. 2013.
- Invention disclosure:
  - **Alabdulkarem A.**, Hwang Y., Radermacher R., "Novel Method for CO_2 Regeneration in CO_2 Removal Plant", PS-2011-005.
  - Horvath C., Leighton D., Gluesenkamp K., **Alabdulkarem A.**, Hwang Y., Radermacher R., "Air-Cooled Absorber Design", PS-2012-013.
- Technical newsletter:
  - **Alabdulkarem A.**, Hwang Y., Radermacher R., "Waste Heat to Cooling using Absorption Chillers: A Showcase on Natural Gas

Liquefaction Facility with CO_2 Capturing Plant" Heat Pump Center Newsletter, March. 2012.

6.5 Future Work

Although this thesis provided new and optimized refrigerants for the LNG plant and new integrated CCS systems with novel concepts in regenerating the CO_2 that resulted in significant energy savings and provided researchers and industry a new frontier in the advancement of CCS systems and refrigerants' optimization, research in following items could also result in significant contributions:

- The cost against the benefit of the additional equipment in the proposed CCS system and the heat pump system. The cost analysis should include the equipment cost, floor area and volume consideration, maintenance cost, operational cost, fuel cost as well as CO_2 cost.
- Developing an optimization map which shows when to capture the CO_2 or emit it to the atmosphere based on the natural gas price, LNG price and CO_2 emission prices.
- Designing new refrigerants for NG liquefaction. Among many available refrigerants, refrigerants selection is a complex process and requires a lengthy trial and error. The difference between this item and the completed optimization work is that the completed optimization work limited the refrigerant components to be identical to the used ones (e.g., C1, C2, C3 and N_2) and varied the mass fractions. This item looks at new components and mass fractions. This item could be applied for NG liquefaction, CO_2 liquefaction and heat pump refrigerants.

- Expanding the optimization of robust refrigerant to include ambient temperature variation in the optimization problem with uncertainty since ambient temperature vary significantly and the performance of liquefaction cycles vary with them as well.
- Development of new refrigerant molecules or new CO_2 solvents molecules. This advancement from item 1 looks at developing new refrigerant molecules or new CO_2 solvents molecules that never existed before using group contribution methods. Some researchers (e.g. [136]) applied this approach in developing refrigerants for specific applications other than the applications considered in this thesis.
- Investigation the benefit of flue gas cooling that enhanced the CO_2 absorption with other CO_2 solvents such as K_2CO_3/PZ.
- Since the developed heat pump concept works at high temperature with multi-temperature levels, validating the heat pump performance experimentally would be important.
- Development of the next generation cryogenic heat exchangers. The most complex and expensive part in the C3MR LNG plant is the SPWH. However, the configuration and the performance of this heat exchanger are unknown. Developing a better cryogenic heat exchanger and conducting an experiment to evaluate its performance would result in significant benefits.

Appendices

Appendix A: Basic Equations Used in HYSYS Models

A.1 Peng-Robinson equation-of-state

Peng-Robinson equation-of-state [137] was used in this thesis because it is one of the most common equation-of-states and it is recommended by HYSYS software for the components used in the simulation work. HYSYS calculates thermodynamic properties based on the equation of states. Then based on the energy balance and mass balance across each unit (e.g., heat exchangers or compressors), HYSYS calculates the power needed or the heat load of such units. In case the heat balance or the mass balance did not converge to the specified tolerance, the solver will not display any results.

This section presents the Peng-Robinson equation-of-state as well as the equations used to calculate the power or heat demand of some units used in this thesis.

The Peng-Robinson equation-of-state is as follows:

$$P = \frac{RT}{v-b} - \frac{a(T)}{v(v+b)+b(v-b)} \quad (24)$$

Where, P is the pressure, T is the temperature, v is the specific volume and R is the gas constant

Equation (24) can be written as:

$$Z^3 - (1-B)Z^2 + (A - 3B^2 - 2B)Z - (AB - B^2 - B^3) = 0 \quad (25)$$

Where, Z is the compressibility factor. The other variables are defined as:

$$A = \frac{aP}{R^2T^2} \tag{26}$$

$$B = \frac{bP}{RT} \tag{27}$$

$$Z = \frac{Pv}{RT} \tag{28}$$

The variables are defined as:

$$b = \sum_{i=1}^{N} x_i b_i \tag{29}$$

$$a = \sum_{i=1}^{N} \sum_{j=1}^{N} x_i\, x_j (a_i a_j)^{0.5} (1 - k_{ij}) \tag{30}$$

$$a_i = a_{ci}\alpha_i \tag{31}$$

$$a_{ci} = 0.457235 \frac{(RT_{ci})^2}{P_{ci}} \tag{32}$$

$$\alpha_i = 1 + m_i(1 - {T_{ri}}^{0.5}) \tag{33}$$

$$m_i = 0.37464 + 1.54226\omega_i - 0.26992\omega_i^2 \tag{34}$$

$$\omega_i = -\log(P_{Sat})_{T_r=0.7} - 1 \tag{35}$$

Where, x is the mole fraction, k_{ij} is the binary interaction coefficients, i and j are component identifiers, N is total number of components, m_i is the characteristic constant, ω is the acentric factor. The subscripts c and r represent the critical and reduced properties, respectively.

The enthalpy (H) and entropy (S) departure are calculated in HYSYS by integrating the equation of states as following:

$$\frac{H-H_{Ideal}}{RT} = Z - 1 + \frac{1}{RT}\int_{\infty}^{V}[T(\frac{\partial P}{\partial T})_V - P]\, dV \quad (36)$$

$$\frac{S-S_{o\,Ideal}}{RT} = \ln(Z) - ln\frac{P}{P^O} + \int_{\infty}^{V}[\frac{1}{R}(\frac{\partial P}{\partial T})_V - \frac{1}{V}]\, dV \quad (37)$$

A.2 Components Equations

HYSYS uses the enthalpy and entropy values to calculate the power consumption for power consuming devices such as pumps or compressors as following:

$$w_{\dot{C}onsumed} = \frac{m^{\cdot}(h_{out,s}-h_{in})}{\eta_{isentropic}} \quad (38)$$

Where, $h_{out,s}$ is the enthalpy at the outlet conditions per unit mass calculated at constant entropy line from the inlet conditions.

Similarly, for power producing devices such as expanders or turbines, the power produced is calculated as following:

$$w_{Produced} = m^{\cdot}(h_{in} - h_{out,s})\eta_{isentropic} \quad (39)$$

For heat exchangers such as condensers or evaporators, the energy balance is used to calculate the required heat load as following:

$$Q^{\cdot} = m^{\cdot}(h_{out} - h_{in}) \quad (40)$$

The UA values is calculated in HYSYS using the weighted model where the heating/cooling curves are broken into intervals, and an energy balance is performed

along each interval. The LMTD and UA are calculated for each interval in the heat curve, and summed to calculate the overall exchanger UA.

$$Q^{\cdot} = UA\ LMTD\ F \tag{41}$$

Where F is a correction factor

$$LMTD = \frac{\Delta T_1 - \Delta T_2}{\mathrm{LN}(\frac{\Delta T_1}{\Delta T_2})} \tag{42}$$

$$\Delta T_1 = T_{Hot,out} - T_{Cold,in} \tag{43}$$

$$\Delta T_2 = T_{Hot,in} - T_{Cold,out} \tag{44}$$

Appendix B: Introduction to Optimization

B.1 Overview

Design of a system involves selecting variables that meet system requirements which are defined beforehand by a customer. For example, a heat exchanger designer needs to know the required heating load and other product requirements specified by the customer. Then the designer would select design variables such as the heat exchanger material, dimensions and so on that meet the heat exchanger requirements. Several heat exchanger designs could be developed that meet the same heat load requirements. However, the heat exchanger's performance and cost depend on the selected variables. The optimal design represents the design that has the most desired objectives, such as minimum cost or highest performance.

In conventional design approach, the process of selecting "design variables" is

based on a designer's intuition and experience. A designer could achieve optimal design with the conventional design approach when designing simple products where only a limited number of design variables (less than 3 variables) are varied. On the other hand, it is difficult and could be impossible to achieve optimal design when designing complex systems with many variables when using the conventional design approach.

The process of finding the optimal design is called optimization. Optimization uses mathematical techniques to achieve the optimum design. In this approach, the designer identifies an objective function to be optimized; design variables to be varied, design parameters that are assumed to be non-variable by the designer and constraints to be satisfied. There are two types of optimization problems namely deterministic (conventional) and stochastic (Lee, [143]). In the deterministic optimization it is assumed there is no uncertainty in the design variables and parameters. However in the stochastic optimization problems the uncertainties in the design variables and parameters are considered. One class of stochastic optimization problems is robust optimization. In robust optimization the solutions should be feasible for all variations of the uncertain variables and parameters. In deterministic optimization, design parameters are fixed but design variables are varied. Mathematically the deterministic optimization problems are stated as follows:

$\min_{\mathbf{x}} f(\mathrm{x}) = f(x_1, x_2, \ldots, x_n)$

Subject to the p equality constraints:

$h_j(\mathrm{x}) = h_j(x_1, x_2, \ldots, x_n) = 0; \quad j = 1 \; to \; p$

and the m inequality constraints:

$g_i(\mathrm{x}) = g_i(x_1, x_2, \ldots., x_n) \leq 0; \quad i = 1\ to\ m$

With variables bounds

$x_{il} \leq x_i \leq x_{iu}$

B.2 Conventional Optimization Methods

Generally optimization methods can be classified into general methods and methods tailored for specific class of problems. Specific methods such as linear programming and quadratic programming are more efficient in solving the problems as they are tailored for than the general methods. However, they are not applicable to general problems. General methods can be divided to local optimization methods and global optimization methods. Except for specific problems local optimization methods only provide results that are locally optimal. However, their computational cost is lower than those of global search methods. Newton method and sequential quadratic programming are examples of local optimization methods. Global optimization methods are heuristic based methods. This means that there is no guarantee for their result to be globally optimal. Genetic algorithm (GA) is an example of methods that do not have any restriction in the type of functions that are used in stating the objective and constraint functions. GA optimization method will be explained briefly in the next section because it was used in the LNG plant refrigerant and steam cycles optimization sections.

B.2.1 Genetic Algorithm

GA is a class of heuristic optimization methods. GA mimics the process of natural evolution by modifying a population of individual solutions. Design points,

x’s, are represented by chromosomes. The method randomly selects individuals from the current population to be parents and uses them to produce the children for the next generation. Over consecutive generations, the population approaches an optimal solution because “good” parents produce “good” children. The “bad” points are eliminated from the generation. GA can be applied to solve a variety of optimization problems in many applications that are not suited for conventional optimization methods, including problems in which the objective function is discontinuous, non-differentiable, or non-linear. GA has the potential to reach to the global optimal solution if it did not stick at a local optimal solution. Since GA is a probabilistic approach, different solutions could be generated by different runs. Therefore, multiple runs are required to verify the optimal solution. GA flowchart is showing in

Figure **103**. The steps involved in using GA are described in the following sections, using a simple refrigerant compositions optimization problem illustrated below. Further information can be found in GA books such as Deb [144].

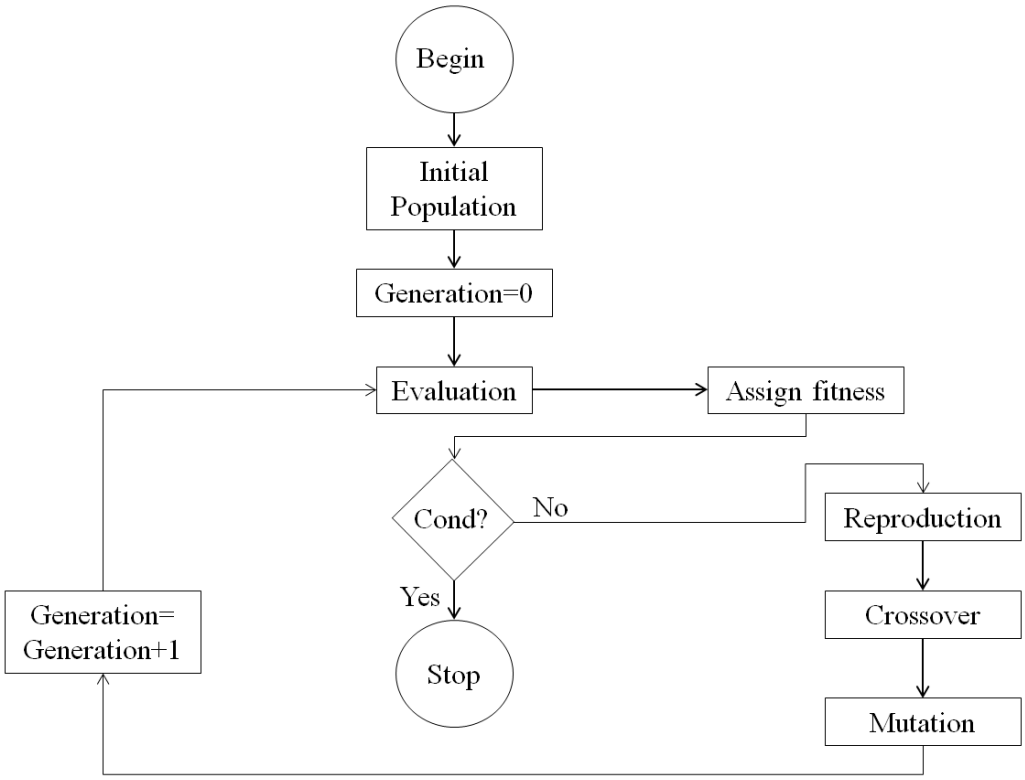

Figure 103: GA flowchart

B.2.2 Example of GA

Finding the optimal refrigerant composition is difficult without optimization. Suppose we would like to find the optimal refrigerant composition of mixture for a vapor compression cycle that has a given cooling load. The optimal refrigerant would require less compression power for the same cooling. The formulation of the optimization problem is as follow:

Objective function,

Minimize compressor power (x_1, x_2, x_3, x_5, x_6)

where

x_1, x_2, x_3, x_4 are mass fractions of constituents

x_5 total refrigerant mass flow rate

x_6 *refrigerant condensing pressure*

Subjected to:

Evaporator cooling capacity = Baseline value

Evaporator cooling temperature = Baseline value

$x_4 = 1 - (x_1 + x_2 + x_3)$

$0 \leq x_1, x_2, x_3, x_4 \leq 1$

$80\%\ x_{5,\ Baseline} \leq x_5 \leq 120\%\ x_{5,\ Baseline}$

$80\%\ x_{6,\ Baseline} \leq x_6 \leq 120\%\ x_{6,\ Baseline}$

x_5 and x_6 were assumed to be limited by 20% range from the baseline values so that we have a limited design space.

B.2.2.1 Representing a solution

GA represents the variables as binary strings. In the example, we have five variables because x_4 is not an independent variable. Each variable is coded in 4 bits. The more bits we have, the more precise the variables would be. Since we assumed 4 bits, each variable can have 2^4 possible values. One 20-bit string (or chromosome) which represents one solution is as follow:

x_1, x_2, x_3, x_5, x_6 = 0110 1100 0101 1110 0001

For example, x_6 is represented in this string as 0001 which represents a certain value for the refrigerant condensing pressure within the specified lower and upper limits. The same thing is true for the other variables. Thus, this chromosome represents a design that has a corresponding compressor power as well as values for meeting or violating the constraints. In the beginning of the GA, a population of chromosomes is randomly generated to be evaluated in the next steps. The number of

the generated chromosomes can be taken to be 20 times the number of the decision variables.

B.2.2.2 Assigning a fitness to a solution

Once the initial population was generated, a fitness function is assigned to evaluate the "goodness" or "badness" of a solution or a chromosome. In minimization problem, the good solution has small fitness function value and the bad solution has high fitness function value. The generated solutions are evaluated based on the objective function value and constraints violation. In our example, the objective function is the minimization of the compressor power and the constraints are the evaporator capacity and temperature. Following fitness assignment, the GA checks for termination conditions and, if not met, new population is generated based on three genetic operators which are the reproduction, crossover, and mutation operators.

B.2.2.3 Reproduction operator

The reproduction operator duplicates "good" solutions and eliminates "bad" solutions in the population. Different methods exist in the reproduction operator such as tournament selection or ranking selection (Deb, 2001). Tournament selection method, for example, compares two solutions and the best one survives in the mating pool. Ranking selection method lists the population based on individual solutions' fitness values. As the GA runs, only "good" solutions survive in the population.

B.2.2.4 Crossover operator

The reproduction operator does not generate new solution. It just duplicates "good" solutions and eliminates "bad" solutions. The crossover operator is used to

generate new solutions. It selects two chromosomes, called parents, from the mating pool and exchanges bits at certain point to generate a new solution, called offspring, as shown in Figure 104. The “good” parents hopefully will produce “good” offspring.

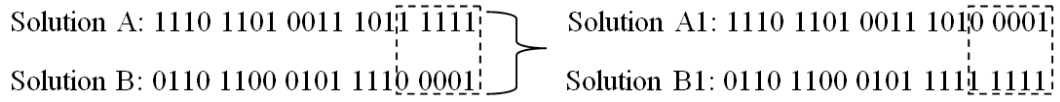

Figure 104: Crossover operator (Solution A and B are called parent solution while A1 and B1 are called offspring.)

B.2.2.5 Mutation operator

The mutation operator has the same objective as the crossover operator which is to generate new solutions and possibly jump out from a local optimum. It works by exchanging a string in the mating pool from 0 to 1 or vice versa as shown in

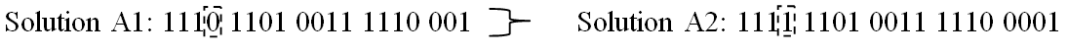

Figure 105Figure 105.

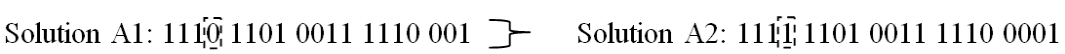

Figure 105: Mutation operator (Solution A1 is old solution and Solution A2 is the new solution.)

B.2.2.6 Stopping criteria

Different stop criteria can be implemented in GA. Common stop criteria are reaching maximum number of generation, tolerance in objective function or minimum fitness value.

Nomenclature

Abbreviations

P	Pressure (kPa)
$\dot{m}$	Mass flow rate (kg/s)
H	Enthalpy (kg/MJ)
S	Entropy(kg/MJ-K)
$\dot{W}$	Power (MW)
Ex	Exergy (MJ/kg)
Ref	Refrigerant
LMTD	Log mean temperature difference (K)
X	Mass fraction
HP	High pressure
LP	Low pressure
FG	Flue gas
GT	Gas turbine
ST	Steam turbine
NG	Natural gas
LNG	Liquefied natural gas
LPG	Liquefied petroleum gas
C3-MR	Propane pre-cooled mixed refrigerant
MCR	Multi-component refrigerant cycle
SPWH	Spiral-wound heat exchanger
C1	Methane
C2	Ethane
C3	Propane
C4	Butane
TP	Pinch Temperature (K)
HX	Heat exchanger
MEA	Monoethanolamine
PZ	Piperazine
DEA	Diethanolamine
MDEA	Methyldiethanolamine
AMP	2-amino-2-methyl-1-propanolamine
VCC	Vapor compression cycle
HRSG	Heat recovery steam generator
NGCC	Natural gas combined cycle
CCS	CO_2 capture and sequestration
EOR	Enhanced oil recovery
COP	Coefficient of performance
ORC	Organic Rankine cycle

Greek symbols

η	Efficiency

Subscripts

I	Intermediate
H	High
Ex	Expansion
L	Low
g	Gas
f	Liquid
sc	Subcooling
sh	Superheating

References

[1] Mortazavi A., Somers C., Alabdulkarem A., Hwang Y., and Radermacher R., 2010, "Enhancement of APCI cycle efficiency with absorption chillers," Energy, 35(9), pp. 3877-3882.

[2] Liu M., Lior N., Zhang N., and Han W., 2009, "Thermoeconomic analysis of a novel zero-CO_2-emission high-efficiency power cycle using LNG coldness," Energy Conversion and Management, 50(11), pp. 2768-2781.

[3] IEA, 2004, Security of Gas Supply in Open Markets, LNG And Power at a Turning Point.

[4] Hasan M. M. F., Karimi I. A., and Alfadala H. E., 2009, "Optimizing Compressor Operations in an LNG Plant," Proceedings of the 1st Annual Gas Processing Symposium. Elsevier B.V., pp. 1-6.

[5] Coyle D., Vega F. F. D. L., and Durr C., 2007, "Natural Gas Specification Challenges in the LNG Industry," 15th international conference and exhibition on liquefied natural gas, Barcelona, Spain, pp. 1-21.

[6] Climate Change 2007: An Assessment of the Intergovernmental Panel on Climate Change.

[7] "World Resources Institute, http://pdf.wri.org/world_greenhouse_gas_emissions_2005_chart.pdf."

[8] IEA, 2010, CO_2 emissions from fuel combustion.

[9] "Woods Hole Research Center, http://www.whrc.org/resources/primer_fundamentals.html."

[10] Herzog H. J., and Drake E. M., 1996, "Carbon Dioxide Recovery and Disposal From Large Energy Systems," Annual Review of Energy and the Environment, 21(1), pp. 145-166.

[11] White C. M., Strazisar B. R., Granite E. J., Hoffman J. S., and Pennline H. W., 2003, "Separation and Capture of CO_2 from Large Stationary Sources and Sequestration in Geological Formations—Coalbeds and Deep Saline Aquifers," Journal of the Air & Waste Management Association, 53, pp. 645–715.

[12] Figueroa J., Fout T., Plasynski S., Mcilvried H., and Srivastava R., 2008, "Advances in CO_2 capture technology—The U.S. Department of Energy's Carbon Sequestration Program," International Journal of Greenhouse Gas Control, 2(1), pp. 9-20.

[13] Steeneveldt R., Berger B., and Torp T., 2006, "CO_2 Capture and Storage Closing the Knowing–Doing Gap," Chemical Engineering Research and Design, 84(9), pp. 739-763.

[14] Oyenekan B. A., and Rochelle G. T., 2006, "Energy performance of stripper configurations for CO_2 capture by aqueous amines," Ind. Eng. Chem. Res, 45(8), pp. 2457–2464.

[15] Oexmann J., and Kather A., 2010, "Minimising the regeneration heat duty of post-combustion CO_2 capture by wet chemical absorption: The misguided focus on low heat of absorption solvents," International Journal of Greenhouse Gas Control, 4(1), pp. 36-43.

[16] Kucka L., Müller I., Kenig E. Y., and Górak A., 2003, "On the modelling and simulation of sour gas absorption by aqueous amine solutions," Chemical Engineering Science, 58(16), pp. 3571-3578.

[17] Knudsen J. N., Jensen J. N., and Vilhelmsen P.-jacob, 2007, "First year operation experience with a 1 t/h CO_2 absorption pilot plant at Esbjerg coal-fired power plant," Proceedings of European Congress of Chemical Engineering, (September), pp. 16-20.

[18] Desideri U., and Paolucci A., 1999, "Performance modelling of a carbon dioxide removal system for power plants," Energy Conversion and Management, 40(18), pp. 1899-1915.

[19] Cifre P. G., Brechtel K., Hoch S., García H., Asprion N., Hasse H., and Scheffknecht G., 2009, "Integration of a chemical process model in a power plant modelling tool for the simulation of an amine based CO_2 scrubber," Fuel, 88(12), pp. 2481-2488.

[20] Rao A. B., Rubin E. S., Keith D. W., and Granger Morgan M., 2006, "Evaluation of potential cost reductions from improved amine-based CO_2 capture systems," Energy Policy, 34(18), pp. 3765-3772.

[21] Salem G., 2006, "Carbon Dioxide Capture Technology for the Coal-Powered Electricity Industry: A Systematic Prioritization of Research Needs. Massachusetts Institute of Technology, MS Thesis.," Massachusetts Institute of Technology.

[22] Gibbins J. R., and Crane R. I., 2004, “Scope for reductions in the cost of CO2 capture using flue gas scrubbing with amine solvents,” Journal of Power and Energy, 218, pp. 231-239.

[23] Dugas R. E., 2006, “Pilot Plant Study of Carbon Dioxide Capture by Aqueous Monoethanolamine,” M.S. Thesis, University of Texas at Austin.

[24] Dugas R., and Rochelle G., 2009, “Absorption and desorption rates of carbon dioxide with monoethanolamine and piperazine,” Energy Procedia, 1(1), pp. 1163-1169.

[25] Idem R., Wilson M., Tontiwachwuthikul P., Chakma A., Veawab A., Aroonwilas A., and Gelowitz D., 2006, “Pilot Plant Studies of the CO_2 Capture Performance of Aqueous MEA and Mixed MEA/MDEA Solvents at the University of Regina CO_2 Capture Technology Development Plant and the Boundary Dam CO_2 Capture Demonstration Plant,” Industrial & Engineering Chemistry Research, 45(8), pp. 2414-2420.

[26] Choi W.-J., Seo J.-B., Jang S.-Y., Jung J.-H., and Oh K.-J., 2009, “Removal characteristics of CO_2 using aqueous MEA/AMP solutions in the absorption and regeneration process,” Journal of Environmental Sciences, 21(7), pp. 907-913.

[27] Mangalapally H. P., Notz R., Hoch S., Asprion N., Sieder G., Garcia H., and Hasse H., 2009, “Pilot plant experimental studies of post combustion CO_2 capture by reactive absorption with MEA and new solvents,” Energy Procedia, 1(1), pp. 963-970.

[28] Ogawa T., Ohashi Y., Yamanaka S. U., and Miyaike K., 2009, "Development of Carbon dioxide removal system from the flue gas of coal fired power plant," Energy Procedia, 1(1), pp. 721-724.

[29] Yeh A., and Bai H., 1999, "Comparison of ammonia and monoethanolamine solvents to reduce CO_2 greenhouse gas emissions," The Science of The Total Environment, 228(2-3), pp. 121-133.

[30] Puxty G., Rowland R., and Attalla M., 2010, "Comparison of the rate of CO_2 absorption into aqueous ammonia and monoethanolamine," Chemical Engineering Science, 65(2), pp. 915-922.

[31] Yeh J. T., Resnik K. P., Rygle K., and Pennline H. W., 2005, "Semi-batch absorption and regeneration studies for CO_2 capture by aqueous ammonia," Fuel Processing Technology, 86(14-15), pp. 1533-1546.

[32] Darde V., Thomsen K., Well W. J. M. van, and Stenby E. H., 2009, "Chilled ammonia process for CO_2 capture," Energy Procedia, 1(1), pp. 1035-1042.

[33] Choi W.-J., Min B.-M., Shon B.-H., Seo J.-B., and Oh K.-J., 2009, "Characteristics of absorption/regeneration of CO_2–SO_2 binary systems into aqueous AMP+ammonia solutions," Journal of Industrial and Engineering Chemistry, 15(5), pp. 635-640.

[34] Gabrielsen J., Svendsen H. F., Michelsen M. L., Stenby E. H., and Kontogeorgis G. M., 2007, "Experimental validation of a rate-based model for CO_2 capture using an AMP solution," 62, pp. 2397 - 2413.

[35] Cullinane J., and Rochelle G., 2004, "Carbon dioxide absorption with aqueous potassium carbonate promoted by piperazine," Chemical Engineering Science, 59(17), pp. 3619-3630.

[36] Chen E., 2007, "Carbon Dioxide Absorption into Piperazine Promoted Potassium Carbonate using Structured Packing, PhD Thesis, The University of Texas at Austin," PhD Thesis, The University of Texas at Austin.

[37] Bryngelsson M., and Westermark M., 2009, "CO_2 capture pilot test at a pressurized coal fired CHP plant," Energy Procedia, 1(1), pp. 1403-1410.

[38] Lee S., Maken S., Park J.-won, Song H.-jun, Jin J., Shim J.-goo, Kim J.-han, and Eum H.-moon, 2008, "A study on the carbon dioxide recovery from 2 ton-CO_2/day pilot plant at LNG based power plant," Fuel, 87, pp. 1734-1739.

[39] Feron P. H. M., 2010, "Exploring the potential for improvement of the energy performance of coal fired power plants with post-combustion capture of carbon dioxide," International Journal of Greenhouse Gas Control, 4(2), pp. 152-160.

[40] Zhang Y., Chen H., Chen C.-C., Plaza J. M., Dugas R., and Rochelle G. T., 2009, "Rate-Based Process Modeling Study of CO_2 Capture with Aqueous Monoethanolamine Solution," Industrial & Engineering Chemistry Research, 48(20), pp. 9233-9246.

[41] Mores P., Scenna N., and Mussati S., 2010, "Post-combustion CO_2 capture process: Equilibrium stage mathematical model of the chemical absorption of CO_2 into monoethanolamine (MEA) aqueous solution," Chemical Engineering Research and Design, (May), pp. 1-13.

[42] Pintola T., Tontiwachwuthikul P., and Meisen A., 1993, "Simulation of pilot plant and industrial CO_2-MEA absorbers," Gas Separation & Purification, 7(1), pp. 47-52.

[43] Tobiesen F., Juliussen O., and Svendsen H., 2008, "Experimental validation of a rigorous desorber model for CO_2 post-combustion capture," Chemical Engineering Science, 63(10), pp. 2641-2656.

[44] Kvamsdal H., Jakobsen J., and Hoff K., 2009, "Dynamic modeling and simulation of a CO_2 absorber column for post-combustion CO_2 capture," Chemical Engineering and Processing: Process Intensification, 48(1), pp. 135-144.

[45] Ziaii S., Rochelle G. T., and Edgar T. F., 2009, "Dynamic Modeling to Minimize Energy Use for CO_2 Capture in Power Plants by Aqueous Monoethanolamine," Ind. Eng. Chem. Res., 48, pp. 6105-6111.

[46] Lawal A., Wang M., Stephenson P., Koumpouras G., and Yeung H., 2010, "Dynamic modelling and analysis of post-combustion CO_2 chemical absorption process for coal-fired power plants," Fuel, 89(10), pp. 2791-2801.

[47] Gáspár J., and Cormoş A.-M., 2010, "Dynamic modeling and validation of absorber and desorber columns for post-combustion CO_2 capture," Computers & Chemical Engineering.

[48] Dey A., and Aroonwilas A., 2009, "CO_2 absorption into MEA-AMP blend: Mass transfer and absorber height index," Energy Procedia, 1(1), pp. 211-215.

[49] Aboudheir A., Tontiwachwuthikul P., and Idem R., 2006, "Rigorous Model for Predicting the Behavior of CO_2 Absorption into AMP in Packed-Bed

Absorption Columns," Industrial & Engineering Chemistry Research, 45(8), pp. 2553-2557.

[50] Martin M. Suenson, Christos Georgakis L. B. E., 1985, "Steady-state and dynamic modeling of a gas absorber-stripper system," Ind. Eng. Chem. Fundamen., 24(3), pp. 288-295.

[51] Mathias P. M., Reddy S., and O'Connell J. P., 2010, "Quantitative evaluation of the chilled-ammonia process for CO_2 capture using thermodynamic analysis and process simulation," International Journal of Greenhouse Gas Control, 4(2), pp. 174-179.

[52] Cullinane J. T., and Rochelle G. T., 2005, "Thermodynamics of aqueous potassium carbonate, piperazine, and carbon dioxide," Fluid Phase Equilibria, 227(2), pp. 197-213.

[53] Oyenekan B., and Rochelle G., 2009, "Rate modeling of CO_2 stripping from potassium carbonate promoted by piperazine," International Journal of Greenhouse Gas Control, 3(2), pp. 121-132.

[54] Sanyal D., Vasishtha N., and Saraf D. N., 1988, "Modeling of carbon dioxide absorber using hot carbonate process," Industrial & Engineering Chemistry Research, 27(11), pp. 2149-2156.

[55] Thiele R., Faber R., Repke J., Thielert H., and Wozny G., 2007, "Design of Industrial Reactive Absorption Processes in Sour Gas Treatment Using Rigorous Modelling and Accurate Experimentation," Chemical Engineering Research and Design, 85(1), pp. 74-87.

[56] Aboudheir A., and ElMoudir W., 2009, "Performance of formulated solvent in handling of enriched CO_2 flue gas stream," Energy Procedia, 1(1), pp. 195-204.

[57] Bernier E., Maréchal F., and Samson R., 2010, "Multi-objective design optimization of a natural gas-combined cycle with carbon dioxide capture in a life cycle perspective," Energy, 35(2), pp. 1121-1128.

[58] Dugas R., Alix P., Lemaire E., Broutin P., and Rochelle G., 2009, "Absorber model for CO_2 capture by monoethanolamine — application to CASTOR pilot results," Energy Procedia, 1(1), pp. 103-107.

[59] Khan F. M., Krishnamoorthi V., and Mahmud T., 2010, "Modelling Reactive Absorption of CO_2 in Packed Columns for Post-Combustion Carbon Capture Applications," Chemical Engineering Research and Design.

[60] Aliabad Z., 2009, "Removal of CO_2 and H_2S using Aqueous Alkanolamine Solutions," Engineering and Technology, pp. 194-203.

[61] Kim S., Kim H., and Chi B., 2004, "Optimization of CO_2 Absorption Process with MEA Solution," Studies in surface science and ctalysis, 153, pp. 429-434.

[62] Abuzahra M., Schneiders L., Niederer J., Feron P., and Versteeg G., 2007, "CO_2 capture from power plants Part I. A parametric study of the technical performance based on monoethanolamine," International Journal of Greenhouse Gas Control, 1(1), pp. 37-46.

[63] Luo X., Knudsen J. N., Montigny D. de, Sanpasertparnich T., Idem R., Gelowitz D., Notz R., Hoch S., Hasse H., and Lemaire E., 2009, "Comparison

and validation of simulation codes against sixteen sets of data from four different pilot plants," Energy Procedia, 1(1), pp. 1249-1256.

[64] Sanpasertparnich T., Idem R., Bolea I., deMontigny D., and Tontiwachwuthikul P., 2010, "Integration of post-combustion capture and storage into a pulverized coal-fired power plant," International Journal of Greenhouse Gas Control, 4(3), pp. 499-510.

[65] Moller B., Genrup M., and Assadi M., 2007, "On the off-design of a natural gas-fired combined cycle with CO_2 capture," Energy, 32(4), pp. 353-359.

[66] Amrollahi Z., Ertesvåg I. S., and Bolland O., 2010, "Thermodynamic analysis on post-combustion CO_2 capture of natural-gas-fired power plant," International Journal of Greenhouse Gas Control, pp. 422-426.

[67] Erik L., 2007, "Aspen HYSYS Simulation of CO_2 Removal by Amine Absorption from a Gas Based Power Plant," SIMS2007 Conference, Geoteborg, pp. 73-81.

[68] Genova M., Rossi L. D., Protti A., and Usai G., 2009, "Retrofitting study for a 120 MW NGCC plant with post- combustion : a particular case to optimize the CO_2 capture process," 1st International Conference on Sustainable Fossil Fuels for Future Energy, pp. 1-17.

[69] Oexmann J., Hensel C., and Kather A., 2008, "Post-combustion CO_2-capture from coal-fired power plants: Preliminary evaluation of an integrated chemical absorption process with piperazine-promoted potassium carbonate," International Journal of Greenhouse Gas Control, 2(4), pp. 539-552.

[70] Oyenekan B. A., and Rochelle G. T., 2007, "Alternative Stripper Configurations for CO_2 Capture by Aqueous Amines," American Institute of Chemical Engineers Journal, 53(12).

[71] Rahimpour M., and Kashkooli a, 2004, "Enhanced carbon dioxide removal by promoted hot potassium carbonate in a split-flow absorber," Chemical Engineering and Processing, 43(7), pp. 857-865.

[72] Chang H., and Shih C.-M., 2005, "Simulation and Optimization for Power Plant Flue Gas CO_2 Absorption-Stripping Systems," Separation Science and Technology, (915429163).

[73] Fisher K. S., Investigator P., Street S. A., Rochelle G., and Figueroa J. D., 2005, "Integrating MEA regeneration with CO_2 compression to reduce CO_2 capture costs," Fourth annual conference on carbon capture and sequestration DOE/NETL.

[74] Romeo L. M., Bolea I., Lara Y., and Escosa J. M., 2009, "Optimization of intercooling compression in CO_2 capture systems," Applied Thermal Engineering, 29(8-9), pp. 1744-1751.

[75] Nagashima, S, Miyagawa, T, Matsumotoa, M, Suzuki, S, Komaki, H, Takagi, M, Murai, S "Life cycle assessment performed on a CCS model case in Japan and evaluation of improvement facilitated by heat integration" Energy Procedia Volume 4, 2011, Pages 2457–2464.

[76] Pellegrini L. a., Moioli S., and Gamba S., 2010, "Energy saving in a CO_2 capture plant by MEA scrubbing," Chemical Engineering Research and Design.

[77] Chinn D., Choi G. N., Chu R., Degen B., Energy C., Company T., and Francisco S., "Cost efficient amine plant design for post combustion CO_2 capture from power plant flue gas," http://uregina.ca/ghgt7/PDF/papers/nonpeer/379.pdf, pp. 1-5.

[78] Johnson, Dennis, Reddy, Satish, Gilmartin J., 2008, "Fluor's Econamine FG Plus SM Technology for CO_2 Capture at Coal-fired Power Plants," Power Plant Air Pollutant Control "Mega" Symposium, Baltimore.

[79] Pfaff I., Oexmann J., and Kather a., 2010, "Optimised integration of post-combustion CO_2 capture process in greenfield power plants," Energy, 35(10), pp. 4030-4041.

[80] Moser P., Schmidt S., Sieder G., Garcia H., Ciattaglia I., and Klein H., 2009, "Enabling post combustion capture optimization–The pilot plant project at Niederaussem," Energy Procedia, 1(1), pp. 807-814.

[81] Shooshtari A., Kuzmicki R., Dessiatoun S., Alshehhi M., Al-Hajri E., and Ohadi M., 2012, "Enhancement of CO_2 Absorption in Aqueous Diethanolamine Amine Using Microchannel Contactors," Carbon Management Technology Conference, Orlando, FL, p. 151732.

[82] Harkin T., Hoadley A., and Hooper B., 2009, "Process integration analysis of a brown coal-fired power station with CO_2 capture and storage and lignite drying," Energy Procedia, 1(1), pp. 3817-3825.

[83] Harkin T., Hoadley A., and Hooper B., 2010, "Reducing the energy penalty of CO_2 capture and compression using pinch analysis," Journal of Cleaner Production, 18(9), pp. 857-866.

[84] Romeo L., Bolea I., and Escosa J., 2008, "Integration of power plant and amine scrubbing to reduce CO_2 capture costs," Applied Thermal Engineering, 28(8-9), pp. 1039-1046.

[85] Aroonwilas A., and Veawab A., 2007, "Integration of CO_2 capture unit using single- and blended-amines into supercritical coal-fired power plants: Implications for emission and energy management," International Journal of Greenhouse Gas Control, 1(2), pp. 143-150.

[86] Aroonwilas A., and Veawab A., 2009, "Integration of CO_2 capture unit using blended MEA–AMP solution into coal-fired power plants," Energy Procedia, 1(1), pp. 4315-4321.

[87] Botero C., Finkenrath M., Bartlett M., Chu R., Choi G., and Chinn D., 2009, "Redesign, Optimization, and Economic Evaluation of a Natural Gas Combined Cycle with the Best Integrated Technology CO_2 Capture," Energy Procedia, 1(1), pp. 3835-3842.

[88] Jonshagen K., Sipöcz N., and Genrup M., 2011, "A Novel Approach of Retrofitting a Combined Cycle with Post Combustion CO_2 Capture," Journal of Engineering for Gas Turbines and Power, 133(1), p. 011703.

[89] Aspelund A., MØLNVIK M. J., and Koeijer G. D. E., 2006, "Ship Transport of CO_2 Technical Solutions and Analysis of Costs, Energy Utilization, Exergy Efficiency and CO_2 Emissions," Chemical Engineering Research and Design, 84(September), pp. 847-855.

[90] Aspelund A., and Jordal K., 2007, "Gas conditioning—The interface between CO_2 capture and transport," International Journal of Greenhouse Gas Control, 1(3), pp. 343-354.

[91] Aspelund A., MØLNVIK M. J., and Koeijer G. D. E., 2007, Novel Concepts for The Compression of Large Volumes of Carbon Dioxide.

[92] Botero C., Finkenrath M., Belloni C., Bertolo S., DErcole M., and Gor E., 2009, "Thermoeconomic Evaluation of CO_2 Compression Strategies for Post-Combustion CO_2 Capture Applications," Proceedings of ASME Turbo Exp, Orlando, FL.

[93] Gluesenkamp K., Radermacher R., and Hwang Y., 2011, "Trends in absorption machines," ISHPC, Padova Italy.

[94] Townsend D. W., and Linnhoff B., 1983, "Heat and power networks in process design," AIChE Journal, 29, pp. 2500-2500.

[95] Lee G. C., Smith R., and Zhu X. X., 2002, "Optimal Synthesis of Mixed-Refrigerant Systems for Low-Temperature Processes," Ind. Eng. Chem. Res., 41, pp. 5016-5028.

[96] Alffev V. N., Yagodin V. M., and Nikol'skii V. A., "Cooling articles to cryogenic temperatures, Patent No. 362978, S.U., 1972."

[97] Boyarsky M., Mogorychny V. L., Klusmier L., and Yudin B., 1995, "Cryogenic mixed gas refrigerant for operation within temperature ranges of 80 K - 100 K. Patent No. 5441658 U.S."

[98] Paradowski H., Bamba M. O., and Bladanet C., 2004, "Propane Precooling Cycles for Increased LNG Train Capacity," 14th International Conference and Exhibition on Liquefied Natural Gas, pp. 1-18.

[99] Mortazavi A., Hwang Y., Radermacher R., Al-Hashimi S., and Rodgers P., "Enhancement of LNG Propane Cycle through Waste Heat Powered Absorption Cooling," Energy 2030 conference, Abu Dhabi, UAE, Nov. 2008.

[100] Remeljej C., and Hoadley a, 2006, "An exergy analysis of small-scale liquefied natural gas (LNG) liquefaction processes," Energy, 31(12), pp. 2005-2019.

[101] Arora J., Introduction to Optimum Design. 2nd edition., Elsevier.

[102] Shukri T., 2004, "LNG Technology Selection," Hydrocarbon Engineering, (February).

[103] Aspelund a., Gundersen T., Myklebust J., Nowak M. P., and Tomasgard a., 2010, "An optimization-simulation model for a simple LNG process," Computers & Chemical Engineering, 34(10), pp. 1606-1617.

[104] Chelouah R., and Siarry P., 2005, "A hybrid method combining continuous tabu search and Nelder Mead simplex algorithms for the global optimization of multiminima functions," European Journal of Operational Research, 161(3), pp. 636-654.

[105] Nogal F. D., Kim J.-K., Perry S., and Smith R., 2008, "Optimal Design of Mixed Refrigerant Cycles," Industrial & Engineering Chemistry Research, 47(22), pp. 8724-8740.

[106] Jensen J., and Sigurd S., 2006, "Optimal operation of a mixed fluid cascade LNG plant," 6th European Symposium on Computer Aided Process

Engineering and 9th International Symposium on Process Systems Engineering.

[107] "Process Systems Enterprise Limited, gproms software. http://www.psenterprise.com/gproms/index.html."

[108] Vaidyaraman S., and Maranas C., 2002, "Synthesis of Mixed Refrigerant Cascade Cycles," Chemical Engineering Communications, 189(8), pp. 1057-1078.

[109] Venkatarathnam G., 2008, Cryogenic Mixed Refrigerant Processes, Springer-Verlag New York, LLC,.

[110] "Aspen Technology, Inc. Aspen and Hysys software. www.aspentech.com."

[111] "MathWorks. Matlab software. www.mathworks.com," Materials Today, 4(2).

[112] Finn A., Johnson G., and Tomlinson T., 1999, "Developments in Natural Gas Liquefaction. Hydrocarbon Processing," Hydrocarbon Processing,, (April), pp. 47-59.

[113] Hasan, M., Karimi, I., Alfadala H., and Grootjans H., 2009, "Operational Modeling of Multistream Heat Exchangers with Phase Changes," AIChE Journal, 55(1).

[114] "The Linde Group. www.linde.com."

[115] Hasan, M., Karimi, I., Alfadala H., and Grootjans H., 2007, "Modeling and simulation of main cryogenic heat exchanger in a base-load liquefied natural gas plant," Process Engineering, pp. 219-224.

[116] Rackley S., 2009, Carbon Capture and Storage, Butterworth-Heinemann.

[117] Somers C., Mortazavi A., Hwang Y., Radermacher R., Al-Hashimi S., and Rodgers P., 2008, "Modeling water/lithium bromide absorption chillers in ASPEN plus," Energy 2030 conference, Abu Dhabi, UAE, Abu Dhabi, UAE.

[118] "GE Inlet Air Cooling 'http://st-www.ge-energy.com/businesses/ge_oilandgas/en/literature/en/downloads/inlet_air_cooling.pdf'," (2).

[119] Quoilin S., Lemort V., and Lebrun J., 2010, "Experimental study and modeling of an Organic Rankine Cycle using scroll expander," Applied Energy, 87(4), pp. 1260-1268.

[120] Bruno J., Lopezvillada J., Letelier E., Romera S., and Coronas a, 2008, "Modelling and optimisation of solar organic rankine cycle engines for reverse osmosis desalination," Applied Thermal Engineering, 28(17-18), pp. 2212-2226.

[121] Saleh B., Koglbauer G., Wendland M., and Fischer J., 2007, "Working fluids for low-temperature organic Rankine cycles," Energy, 32(7), pp. 1210-1221.

[122] Desai N. B., and Bandyopadhyay S., 2009, "Process integration of organic Rankine cycle," Energy, 34(10), pp. 1674-1686.

[123] Calm J., and Didion D., 1998, "Trade-offs in refrigerant selections: past , present , and future," International Journal of Refrigeration, 21(4), pp. 308-321.

[124] Kalinowski P., Hwang Y., Radermacher R., Al Hashimi S., and Rodgers P., 2009, "Application of waste heat powered absorption refrigeration system to

the LNG recovery process," International Journal of Refrigeration, 32(4), pp. 687-694.

[125] Linnhoff B., and Hindmarsh E., 1983, "The Pinch Design Method for Networks," Chemical Engineering Science, 38(5), pp. 745-763.

[126] Feng X., and Zhu X. X., 1997, "Combining Pinch and Exergy Analysis Process Modifications," Applied Thermal Engineering, II(3), pp. 249-261.

[127] Aspelund a, Berstad D., and Gundersen T., 2007, "An Extended Pinch Analysis and Design procedure utilizing pressure based exergy for subambient cooling," Applied Thermal Engineering, 27(16), pp. 2633-2649.

[128] Kemp I. C., 2007, Pinch Analysis and Process Integration: A User Guide on Process Integration for the Efficient Use of Energy, Butterworth-Heinemann.

[129] "MAN Diesel & Turbo, www.mandieselturbo.com."

[130] "CO_2 Phase Diagram, http://scifun.chem.wisc.edu/chemweek/pdf/CarbonDioxide.pdf."

[131] Dopazo J. A., and Fernández-Seara J., 2010, "Experimental evaluation of a cascade refrigeration system prototype with CO_2 and NH_3 for freezing process applications," International Journal of Refrigeration, pp. 257-267.

[132] Mclinden M., 1988, "Thermodynamic evaluation of refrigerants in the vapor compression cycle using reduced properties," International Journal of Refrigeration, 11(3), pp. 134-143.

[133] Ratts E. B., and Brown J. S., 2000, "A generalized analysis for cascading single fluid vapor compression refrigeration cycles using an entropy generation minimization method," International Journal of Refrigeration, 23, pp. 353-365.

[134] Lee T., Liu C., and Chen T., 2006, "Thermodynamic analysis of optimal condensing temperature of cascade-condenser in CO_2/NH_3 cascade refrigeration systems," International Journal of Refrigeration, 29(7), pp. 1100-1108.

[135] Alefeld G., and Radermacher R., 1993, Heat Conversion Systems, CRC Press.

[136] Marcoulaki E. C., and Kokossis a. C., 2000, "On the development of novel chemicals using a systematic synthesis approach. Part I. Optimisation framework," Chemical Engineering Science, 55(13), pp. 2529-2546.

[137] Peng D.-Y., and Robinson D. B., 1976, "A New Two-Constant Equation of State," Industrial & Engineering Chemistry Fundamentals, 15(1), pp. 59-64.

[138] Xu X., Liu J., Jiang C., and Cao L., 2012, "The correlation between mixed refrigerant composition and ambient conditions in the PRICO LNG process," Available Online in Applied Energy.

[139] Mokarizadeh Haghighi Shirazi M., and Mowla D., 2010, "Energy optimization for liquefaction process of natural gas in peak shaving plant," Energy, 35(7), pp. 2878–2885.

[140] Wang M., Zhang J., and Xu Q., 2012, "Optimal design and operation of a C3MR refrigeration system for natural gas liquefaction," Computers & Chemical Engineering, 39, pp. 84–95.

[141] Mortazavi, A., Azarm, S., Gabriel, S., 2012, "Adaptive Gradient Assisted Robust Design Optimization under Interval Uncertainty", Engineering Optimization, In Press.

[142] Mortazavi A., Alabdulkarem A., Radermacher R., Azarm S., and Hwang Y. "Development of a Robust Refrigerant Mixture for APCI LNG Plants" To be submitted to Applied Energy Journal, 2013.

[143] Lee K., "Robust Optimization Considering Tolerances of Design Variables", Computers & Structures, 79, 1, 77-86 (2001).

[144] Deb, K., "Multi-objective Optimization Using Evolutionary Algorithms", 1st Edition, John Wiley & Sons Inc., Chichester, UK (2001).

[145] xProps property routine, http://www.optimizedthermalsystems.com.